Characterization of barefoot and shod running



Richard Charles Franzese

Wolfson College

University of Oxford

A thesis submitted for the degree of

Doctor of Philosophy

Trinity 2018

To Christina Jane Franzese.

Abstract

Barefoot (BF) and shod (SD) running mark relevant mechanical boundary conditions for affecting running biomechanics. This thesis studies the variation in foot-strike strategy (FSS), and whilst accounting for this variation provides a description of BF and SD running at different aerobic training velocities in uninjured, highly trained competitive (1500 m personal best: $\mu \pm \sigma$ = 3:59.8 $\pm$10.0) male distance runners (n = 19). At one velocity, BF running for nine uninjured competitive female runners is also studied. Three dimensional (3D) gait analysis was used to measure lower-limb joint angles during treadmill running, and surface electromyography (EMG) was used to measure lower-leg muscle activity. Generalized linear mixed models (GLMMs) were used to account for and quantify between-subject variation and stride-specific foot-strike angle (FSA).

This thesis provides evidence to discourage the general practice of classifying runners in the present population within a FSS group for BF running. Also, a subset of individuals exhibited high FSA variability for BF running, possibly because of discomfort.

The hypothesis that FSA correlates with changes in running kinematics was supported. A larger hip width to femur length ratio found in females was associated with more hip adduction, corroborating previous research.

More plantarflexed FSA was hypothesized for higher velocities, and flatter foot placement was anticipated for BF versus SD running. Flatter foot placement was observed for BF running, but FSA was independent of velocity for BF running and more foot dorsiflexion at foot-strike (FS) was observed for fast velocity for SD running. These adjustments may be motivated by maximal or sub-maximal deformation of the heel pad and the novelty of BF running. Coupled with the observed increase in *gastrocnemius* muscle activity for BF versus SD running, these observations may be cause for caution for the novice BF runner. A different coordinative structure for tibia and rearfoot coupling emerged as velocity increased, possibly in response to an increased functional demand of the talocrural and subtalar joints for BF running as velocity increases.

The hypothesis that coordinative variability changes with FSA during impact phase, to reflect the underlying elevated injury risk for rearfoot-strike runners, was not supported. Coordinative variability was independent of FSA. In addition, coordination was more robust to changes in velocity and differences in FSA for SD running, possibly reflecting habituation.

Running BF may have potential as a diagnostic tool for studying injury etiology, because the limit of no external cushioning may place mechanical demands on the runner sufficient to elicit anomalous running kinematics, which may manifest as high kinematic variability.

Acknowledgements

The work in this thesis was funded by the Engineering and Physical Sciences Research Council (EPSRC), through the Life Sciences Interface Doctoral Training Centre (LSI DTC).

Personally, I would like to thank Amy Zavatsky and Julie Stebbins, for giving me the opportunity to travel this path and for their support along it. They afforded me an academic and personal freedom which has had a profound effect on my life, having emigrated to the USA in early 2014 to be with my wife Samone, and frequently travelled to the USA beforehand.

I thank Jessica Leitch, for data on female distance runners, collected as part of her D.Phil. thesis, and for discussions and feedback related to the associated work (Chapter 4).

I wish to thank all the participants in this study, including those who were involved in the preliminary data collection, and the staff at the Oxford Gait Laboratory who assisted with the data collection and afforded me use of the gait laboratory.

In the summer of 2015, I returned to Oxford to continue this work. For this, I am indebted to Amy and Julie for the faith they had in me to continue when I returned to teaching. I thank Saint Christopher's School in Richmond, Virginia, for absolving me of my professional responsibilities for the summer after my first year teaching, and Sean Ledger and Oliver Langford for their support whilst in Oxford. The close friendship of Sean and Ollie throughout my D.Phil studies has been invaluable.

Also, a chance discussion with Oliver late at night after a Tuesday evening track session was the catalyst for much of the statistical analyses in this thesis, and my rekindled interest in statistics.

At Saint Christopher's School I am particularly grateful to Ron Smith and Jim Boyd. Discussions about Oxford in the staff room with Ron made me sufficiently nostalgic to return, and sitting in Jim's office was the closest thing to a meeting with my supervisors. These daily interactions kept me connected to Oxford and to the idea of continuing this thesis.

To Sean, Oliver, Glen Wright-Colopy, Giovanni Cotugno, Joshua Entwistle, Andrew Lanham, Thomas Quirk, James Taylor and all members of the Espresso-Bar Cowley, for our time at Iffley Road, South Park, University Park, Pembroke College playing fields, Green route, 26 Marston Street, and The Library, I consider them highlights during so many difficult days, weeks and months.

To my parents Dorette and Lauro, and sister Christina, I cannot express my gratitude. In a parallel universe, there is another 'me', for whom there is no 'you', and they did not even get close to finishing their thesis. Look Chrissy, I wrote it! It exists, it is real, and I have *powered through*.

Finally, I thank Samone. Her patience, unwavering support, understanding and love has seen me through this and so much more. For my thesis, if not for her, I would always have wondered 'what if?'

Contents

Acknowledgements **i**

List of Figures **xi**

List of Tables **xiv**

1 Introduction **1**

1.1 Primary aim 2

1.2 Secondary aims 7

1.2.1 Barefoot running as a biomechanical ‘stress test’ 8

1.2.2 Coordination and coordinative variability: a dynamical systems theory perspective 9

1.3 Thesis Overview 10

2 Background **13**

2.1 Scientific background 13

2.1.1 The running gait cycle and the motor control system 14

2.1.2 The kinematics of running 16

2.1.2.1 The ankle joint and surrounding articulations 17

2.1.2.2 Sagittal plane kinematics 18

2.1.2.3 Frontal plane kinematics 22

2.1.2.4 Transverse plane kinematics . . . 24
2.1.3 Lower-limb skeletal and muscular anatomy . . . 25
2.1.3.1 Hip . . . 25
2.1.3.2 Knee . . . 28
2.1.3.3 Ankle . . . 31
2.2 Methodological background . . . 34
2.2.1 Human motion analysis . . . 34
2.2.1.1 Techniques . . . 34
2.2.1.2 Running gait analysis . . . 35
2.2.2 Electromyography . . . 36
2.2.2.1 Motor unit action potential . . . 36
2.2.2.2 Techniques . . . 37
2.2.2.3 Limitations . . . 38
2.3 Summary . . . 38

3 Data collection methods and kinematic models 39

3.1 Subjects . . . 39
3.1.1 Study design . . . 39
3.1.2 Recruitment . . . 40
3.1.3 Inclusion/exclusion criteria . . . 40
3.2 Apparatus . . . 42
3.2.1 Motion Capture . . . 42
3.2.2 Surface Electromyography . . . 42
3.2.3 Treadmill . . . 42
3.3 Kinematic models . . . 43

3.3.1 Definition of the global and local coordinate frames 43
3.3.2 Model overview 44
3.3.3 Segment coordinate systems 46
3.3.4 Joint angles 51
3.4 Experimental protocol 52
3.4.1 Laboratory preparation 52
3.4.2 Subject background 54
3.4.3 Anthropometric assessment 55
3.4.4 Strength testing 56
3.4.5 Subject preparation 56
3.4.6 Data capture 57
3.4.6.1 Subject calibration 57
3.4.6.2 Treadmill data collection 60
3.5 Data post-processing 61
3.5.1 Subject model calibration 61
3.5.2 Kinematics 63
3.5.3 Surface Electromyography (EMG) 65
3.6 Summary 65

4 Barefoot running kinematics for highly trained habitually shod runners 66

4.1 Introduction 67
4.2 Methods 68
4.2.1 Subjects 68
4.2.2 Experimental data collection and data processing 69
4.2.3 Data analysis 69

4.2.4 Foot-strike strategy . . . 71
4.2.5 Anatomical parameters . . . 72
4.2.6 Statistical analysis . . . 72
4.2.6.1 Exploratory analysis . . . 72
4.2.6.2 Statistical testing for kinematics . . . 73
4.2.6.3 Logistic regression on injury rate data . . . 74
4.3 Results . . . 75
4.3.1 Subjects . . . 75
4.3.2 Foot-strike strategy . . . 76
4.3.3 Kinematic variability . . . 76
4.3.4 Comparison of the FSA and FSS . . . 81
4.4 Discussion . . . 83
4.4.1 Kinematic variability . . . 84
4.4.2 Comparison with previous literature . . . 87
4.4.3 Comparison of the FSA and FSS . . . 91
4.4.4 Gender . . . 93
4.4.5 Injury rate data . . . 94
4.4.6 Limitations . . . 95
4.5 Conclusion . . . 97

5 Velocity and condition effects on foot-strike kinematics 99

5.1 Introduction . . . 100
5.2 Methods . . . 101
5.2.1 Subjects . . . 101
5.2.2 Experimental data collection and data processing . . . 101

5.2.3 Data analysis . . . 102
5.2.4 In-shoe foot inclination . . . 102
5.2.5 Centre of mass . . . 103
5.2.6 Stride length . . . 103
5.2.7 Statistical analysis . . . 103
5.2.7.1 Exploratory analysis . . . 105
5.2.7.2 Model selection and fitting . . . 105
5.3 Results . . . 107
5.3.1 Final models . . . 107
5.3.1.1 Condition and velocity . . . 107
5.3.1.2 Stride length . . . 110
5.3.1.3 Centre of mass to heel progression . . . 111
5.3.2 Condition . . . 111
5.3.3 Velocity . . . 112
5.3.4 Within-subject and between-subject variation . . . 113
5.4 Discussion . . . 113
5.4.1 Condition . . . 116
5.4.2 Velocity . . . 117
5.4.3 Within-subject and between-subject variation . . . 119
5.4.4 Limitations . . . 122
5.5 Conclusion . . . 123

6 Lower-leg electromyography for running **124**

6.1 Introduction . . . 125
6.2 Methods . . . 127

6.2.1 Subjects . . . 127
6.2.2 Experimental data collection and data processing . . . 127
6.2.3 Data analysis . . . 127
6.2.4 In-shoe foot inclination . . . 128
6.2.5 Statistical analysis . . . 128
6.3 Results . . . 131
6.3.1 Final models . . . 131
6.3.2 Condition . . . 140
6.3.3 Velocity . . . 141
6.3.4 Foot-strike angle . . . 141
6.4 Discussion . . . 145
6.5 Limitations . . . 149
6.6 Conclusion . . . 151

7 Lower extremity coordination for running: a dynamical systems perspective 152

7.1 Introduction . . . 153
7.1.1 Background . . . 153
7.1.2 Literature review . . . 157
7.2 Methods . . . 160
7.2.1 Subjects . . . 160
7.2.2 Experimental data collection and data processing . . . 160
7.2.3 Continuous Relative Phase . . . 162
7.2.4 Directional statistics . . . 165
7.2.5 Data analysis . . . 167
7.2.6 Statistical analysis . . . 168

7.3 Results . . . 169
7.3.1 Hilbert transform versus (x, v) construction . . . 172
7.3.2 Running related injuries . . . 172
7.3.3 Final models . . . 172
7.3.4 Condition . . . 175
7.3.5 Velocity . . . 175
7.3.6 Foot-strike angle . . . 182
7.3.7 Within-subject and between subject variation . . . 183
7.4 Discussion . . . 183
7.4.1 Running-related injuries . . . 184
7.4.2 Comparison with previous literature . . . 185
7.4.3 Condition . . . 187
7.4.4 Velocity . . . 189
7.4.5 Foot-strike angle . . . 191
7.4.6 Within-subject and between-subject variation . . . 193
7.5 Limitations . . . 194
7.6 Conclusion . . . 196

8 Conclusion and future work **197**

8.1 Conclusion . . . 197
8.2 Future work . . . 201

References **205**

A Calculating joint kinematics **229**

B Anatomical frame misalignment affects joint kinematics **234**

C Subject information **237**

C.1 A summary of injury developments 237

C.2 Anthropometric data and running history 237

List of Figures

2.1.1 The gait cycle 14

2.1.2 The kinematics of locomotion 15

2.1.3 The anatomical planes and directions 17

2.1.4 Bones and joints of the foot 17

2.1.5 Definition of joint motion 19

2.1.6 Muscular anatomy for the hip: gluteal and iliopsoas groups 20

2.1.7 Muscular anatomy of the thigh 20

2.1.8 Muscular anatomy of the lower leg: posterior and anterior groups 22

2.1.9 Muscular anatomy of the hip: adductor group 23

2.1.10 Skeletal anatomy of the pelvis and femur 25

2.1.11 Muscular anatomy of the hip: external rotator group 26

2.1.12 Skeletal anatomy of the anterior tibia and fibula 29

2.1.13 Muscular anatomy of the lower leg: lateral group 32

2.2.1 The anatomy of a motor unit 37

3.3.1 Kinematic model abstractions 45

3.3.2 Oxford Foot Model with tibia segment 45

3.3.3 Pelvis segment axes and anatomical markers 46

3.3.4 Femur segment axes and anatomical markers, and knee joint centre calculation 48

3.3.5 Tibia segment axes and anatomical markers 49

3.3.6 Hindfoot segment axes and anatomical markers 50

3.3.7 Forefoot segment axes and anatomical markers 51

3.4.1 Subject preparation and data collection process 53

3.4.2 Foot Thong™ 57

3.4.3 EMG electrode placement 58

3.4.4 Lower limb markers 59

3.5.1 Subject calibration procedure in Vicon Nexus 63

4.3.1 Repeatability of FSA 79

4.3.2 Within-subject kinematic variability 80

4.3.3 Between-subject kinematic variability 82

4.4.1 Body alignment at FS compared to Williams *et al.* [208] 88

4.4.2 Foot-strike angle and FSA variability predict injury 95

5.2.1 Boxplots showing variation of FSA with velocity and condition 106

5.2.2 Residual analyses which justifies the application of a hierarchical model 107

5.3.1 QQ-plots of random coefficients for velocity and condition effects on FSA . . . 109

5.3.2 Raw data versus final fitted models condition and velocity effects on FSA . . . 114

5.3.3 Between-subject variation for final models 115

6.2.1 Gamma distribution fit to RMS EMG data 130

6.2.2 Model residuals versus fitted values exhibit heteroscedasticity 132

6.3.1 QQ-plots of random coefficients for *tibialis anterior* during pre-activation phase 134

6.3.2 Raw data versus final models per subject for the *tibialis anterior* pre-activation 142

6.3.3 Raw data versus final models for subject MG 143

6.3.4 Fixed effects models 144

7.1.1 Global body segment orientation versus joint angle 154

7.3.1 crp(τ) and vcrp(τ) for sagittal plane coupling 170

7.3.2 crp(τ) and vcrp(τ) for EVTIR plane coupling 171

7.3.3 Phase planes using traditionl and Hilbert transform methods 173

7.3.4 Phase plane dynamics for segments in the sagittal plane 174

7.3.5 crp(t) data calculated using a traditional phase space construction 174

7.4.1 crp(t) data for EVTIR as a function of velocity 191

7.4.2 Phase plane dynamics as a function of velocity for EVTIR 192

A.0.1 The global and local frames 230

List of Tables

1.3.1 Summary of model predictors and responses variables 12

3.3.1 Anatomical locations of pelvis segment markers 46

3.3.2 Anatomical locations of femur segment markers 48

3.3.3 Anatomical locations of tibia segment markers 49

3.3.4 Anatomical locations of hindfoot segment markers 50

3.3.5 Anatomical locations of forefoot segment markers 50

3.3.6 Anatomical locations of shoe segment markers 51

4.2.1 Temporal parameters and discrete kinematic variables 71

4.3.1 Subject demographics 76

4.3.2 Kinematic variable results for joint angle trajectories 77

4.3.3 Kinematics variable results for joint angular velocities 78

4.4.1 Temporal parameter results 93

4.4.2 Running-related injury model 95

5.3.1 Model coefficients for velocity and condition effects on FSA 109

5.3.2 Velocity and condition effects on FSA 110

5.3.3 Velocity and condition effects on centre-of-mass distance from heel 112

6.2.1 Time periods for EMG parameters 128

6.3.2 Model coefficients for the *tibialis anterior* 135

6.3.3 Model coefficients for the *gastrocnemius medialis* 136

6.3.4 Model coefficients for the *gastrocnemius lateralis* 137

7.2.1 Summary of data size 167

7.2.2 Segment couplings for analysis 167

7.2.3 Time periods for parameter calculation 168

7.3.1 Impact phase crp(τ) 176

7.3.2 Impact phase vcrp(τ) 177

7.3.3 Stance phase crp(τ) 178

7.3.4 Stance phase vcrp(τ) 179

7.3.5 Swing phase crp(τ) 180

7.3.6 Swing phase vcrp(τ) 181

7.3.7 crp(τ) and vcrp(τ) summary 182

C.1.1 Summary a injury development 237

C.2.1 Anthropometric data 238

Nomenclature

AF Anatomical frame

AIC Akaike information criterion

AL Anatomical landmark

ANOVA Analysis of variance

BF Barefoot

COM Centre of mass

crp*(t)* Continuous relative phase

DST Dynamical systems theory

EMG (surface) electromyography

EVTIR Rearfoot coronal plane to tibial transerse plane (coupling)

FFS Forefoot-strike

FS Foot strike

FSA Foot-strike angle

FSS Foot-strike strategy

GLMM Generalized linear mixed model

h:f Ratio of the hip width to the femur length

ITBS Iliotibial band syndrome

LMM Linear mixed model

MCS Motor control system

MP Midpoint of the heel and toe markers

MTF Marker technical frame

MUAP Motor unit action potential

NRFS Non rearfoot-strike running

OFM Oxford Foot Model

PFPS Patellofemoral pain syndrome

PiG Plug-in gait

RFS Rearfoot-strike

ROM Range of motion

SD Shod

SMaRT Selection method for a representative trial

TF Technical frame

TFL *Tensor fascia latae*

TO Toe off

UCM Uncontrolled manifold (hypothesis)

VC Vector coding

vcrp*(t)* Continuous relative phase variability

vGRF Vertical ground reaction force

Chapter 1

Introduction

The first section of this chapter presents the motivation and objectives of this thesis and places them within the context of current knowledge. This is followed an outline of each chapter.

Distance running is an accessible and popular sport [127, 151], and a recent resurgence of interest in barefoot (BF) running has occured in the past decade [94]. This is thanks to the dissemination of a large body of biomechanics research into mainstream culture. Individuals have attempted BF running to improve efficiency, get past injury, and because of media interest [94]. With this, there has been a drive to create 'minimalist' shoes which mimic BF running and 'maximalist' running shoes which provide large amounts of cushioning in the style of traditional running shoes. From an engineering perspective, traditional running shoes and BF running, by being the limits of cushioning, mark relevant mechanical boundary conditions for affecting running biomechanics.

Barefoot running has been purported by some as the 'natural' way to run and kinematic adaptations in foot-strike associated with BF running have been hypothesized to reduce injury risk even for shod (SD) running [122]. Foot-strike strategy (FSS) is related to initial orientation of the foot when it strikes the ground. Runners are typically categorized into discrete groups according to one of three landing strategies: rearfoot-strike (RFS) running landing with the heel

first, midfoot-strike running (MFS) landing with the foot flat on the ground, and FFS running landing on the ball of the foot. Manipulating FSS, which is also affected by foot condition (*i.e.* SD versus BF) [43], has been encouraged [176] on the basis that it reduces overall injury rate [39]. Compared to habitually SD RFS runners, the external loading rate during the impact phase of gait is reduced for habitually BF FFS runners [125], and it is possible to reduce impact peaks in habitually SD injured runners by manipulating FSS under instruction whilst SD [176]. However, in habitually SD runners, BF FFS running is associated with higher Achilles tendon strain than BF RFS running [4] and loading rates are higher for BF versus SD running in the absence of instruction [43].

Running gait is repeatable, but varies from stride-to-stride, and appreciating the sources and magnitudes of variability in running biomechanics will facilitate more nuanced insights. There are a set of statistical analysis methods which may do this, but they are not yet widely or effectively applied in running biomechanics research.

1.1 Primary aim

In 2000, De Wit *et al.* [43] studied the biomechanics of SD overground running in a standardized neutral shoe and for BF running. They analysed stance phase kinetics and kinematics for nine moderately trained and habitually SD RFS runners (30 to 40 km week^{-1}) with two high speed video cameras in the sagittal (500 and 250 Hz) and frontal (200 Hz) planes. Subjects ran both BF and SD, and using ten independent trials, they found BF running had a significantly larger external loading rate than SD running. It was suggested that runners attempt to limit local pressure at the heel for BF running by plantarflexing the foot immediately before FS. Large variations were observed between runners for frontal plane kinematics, leading the authors to suggest there is no uniform BF running adaptation strategy for all runners concerning rearfoot

kinematics outside of the sagittal plane. It is possible to quantify, using appropriate hierarchical statistical models, the magnitude of within-subject and between-subject variability but, such information was not reported by De Wit *et al.* Such an approach may facilitate more accurate study of frontal plane kinematics.

Stacoff *et al.* [190] went a step further than skin-mounted retro-reflective markers and used markers mounted on bone pins to study the tibiocalcaneal kinematics of overground BF and SD running in five individuals who ran BF and SD. It is unclear whether these subject had any previous running experience and their habitual FSS was not reported. Subjects ran using a standardized test shoe, and in the same test shoe with five modifications. They concluded that differences between tibial and calcaneal movement patterns were small and unsystematic (the difference between mean total calcaneal eversion and internal tibial rotation between conditions was 1°). This study suggests that caution should be applied when analysing non-sagittal plane angles at the rearfoot. It also suggests that discrete kinematic parameters from rearfoot motion may not be precise enough to distinguish BF and SD running gait. Rather, continuous time behaviour and joint or segment coupling may provide further insights into the similarities and differences between BF and SD running. This study collected overground running along a 9.35 metre runway, which may limit its extension to continuous running and the sample size was small.

Lieberman *et al.* [125] extended research in BF and SD running by studying habitual BF and habitual SD runners. They found different loading rates for each condition and a different characteristic transient (forces during the first 50 ms of stance) vertical ground reaction force (vGRF) between two groups of six recreational runners when they ran BF. Habitual BF runners exhibited lower loading rates than habitual SD runners, suggesting that the habitual use of footwear alters kinematics. By modelling the lower leg as an L-shaped pendulum subjected to an inelastic collision with the ground, they concluded that a forefoot or midfoot-strike pattern

would lower the effective mass of the foot hitting the ground compared with a RFS pattern. This is because kinetic energy at impact is stored as rotational kinetic energy for the FFS runner. Leiberman *et al.* associated habituated foot conditions with a particular FSS. Specifically, habitual BF runners opted for a FFS strategy, whereas habitually SD runners chose a RFS strategy. Hatala *et al*. [87] published work which did not corroborate this finding, and more recent research demonstrates that the running style which emerges for habitually BF runners is gender specific and dependent on running experience [166]. There are also different distributions of FS strategies across the three typical running styles for habitually BF runners, minimalist shoe users, and habitually conventional running shoe users [114, 123]. Lieberman *et al.* [125] studied the Kalenjin tribe in Kenya, whilst Hatala *et al.* studied 38 members of the Daansanach tribe, also in Kenya. Hatala *et al.* found that the habitually BF runners preferred to run with RFS, even though they corroborate the finding that FFS running reduces the magnitude of impact loading. They noted that training level, substrate mechanical properties, running distance, and running frequency all influenced the selection of FSS and that higher percentages of midfoot and forefoot strikes occured as speed increased. Whilst both tribes are habitually BF, it should also be noted that the Kalenjin tribe are the Kenyan tribe responsible for nearly all Kenya's national records and typically more often take part in competitive running.

In the SD condition, although it is purported that shoes make specific subject-level alterations to kinematics which minimize injury risk, it has long since been shown that subjects' kinematics do not consistently behave as a shoe may be designed. Specifically, in a study of five runners performing in five different shoes, statistically-significant subject-shoe interactions occured for all studied ground reaction force parameters. Thus, knowledge of shoe characteristics in the absence of subject characteristics provides little information regarding the effects of different types of shoe on foot mechanics [12]. It is plausible, therefore, that using a standardized shoe in research versus subjects' own shoes many not reduce variability in a group

of runners' foot mechanics as is often desired. However, muscle activity in each shoe may be different and so give clues about the underlying adaptation. This is a particular avenue of study in orthotic intervention. Footwear can also affect knee and ankle joint variability, possibly by altering sensory inputs [112]. These observations provide motivation for using statistical anaylsis methods which allow the effect of condition to have random variation at the subject level when studying muscle activity.

More recently, studies have identified that within habitually SD runners broadly, there are three groups of individuals. One group has a RFS when both BF and SD, a second group FFS when both BF and SD and a third group RFS when SD and midfoot-strike or FFS when BF [2, 85]. It is not yet clear why this is the case and little is known about this in the context of highly trained distance runners. A study of BF and minimally SD runners in a recreational road race found both groups demonstrated RFS, midfoot-strike and FFS strategies. In this case, without knowledge of the runners' training background it is not possible to relate these finding to habituation. The effect of habituation to a particular foot condition remains an area of discussion [87, 123, 125], despite mechanical hypotheses to motivate particular adaptations, particularly with respect to FSS. Therefore, to avoid confounding variables associated with habituation, it is best to study a homogenous group of runners habituated to one foot condition. Simultaneously studying kinematics and muscle activity may faciliate a better understanding of the interaction between movement (kinematics) and physiology (muscle activity) in, for example, the development of injury [4]. To rigorously quantify kinematics, it is only appropriate to use 3D kinematic analysis. Furthermore joint and segment coupling behaviour, whilst difficult to interpret, is a promising area of study. This is particularly relevant in light of recent methodological developments applied to biomechanics [113, 175].

Individuals run at a variety of velocities even on a single aerobic run. Whilst the population of trained runners typically run at prescribed velocities, it is sensible to characterize a set of

physiologically relevant running velocities for this group. As velocity increases, TO occurs relatively earlier in the gait cycle and runners typically transition from a RFS pattern to a FFS pattern (Section 2.1.1). With increases in velocity come increases in the range of motion of the hip, knee (particularly during swing phase) and ankle joints. At FS the hip is more flexed and at TO it is more extended. There are also changes in lower leg muscle activity as velocity changes. When sampling a range of steady-state aerobic running velocities in trained runners, are there significant changes in lower-leg muscle activity?

Competitive runners typically train at a variety of sub-maximal velocities to optimize their physiological response. Training may also have an appreciable effect on running gait (Section 1.2.2, [148]). Therefore, understanding the response of running gait at a variety of velocities is pertinent for competitive runners. Subtle interactions between condition and velocity which may occur at sub-maximal velocities may be missed without the application of appropriate statistical modeling techniques.

Evidently, there is an extensive body of literature studying the biomechanical differences between BF and SD running. However, variability in running biomechanics in general, and for highly trained distance runners specifically, has rarely been rigorously quantified or accounted for. Foot-strike strategy is affected by foot condition [43] and velocity [22, 65]. However, variations in FSS between and within individuals exist for reasons which as are yet not well understood. We know how interventions may relate to changes in FSS in general, but it is difficult to identify which biomechanical behaviours are associated with particular, subject-specific (or group-specific) FSS. One question which remains open is: what makes a group of individuals exhibit a variety of FSS at the same speed or even for their preferred speed? Importantly, given the inherent variability which exists with FSS for a given individual, how do we characterize FSS? For example, how do we reconcile FSS grouping with the fact that any given individual may exhibit a range of particular FSs across a number of strides? Furthermore, is this variation

biomechanically significant? Whilst studies attempt to simplify their analysis with grouping by FSS, these questions require the collection and detailed analysis of a large number of gait cycles for a given individual. As of yet, outside of a recent study by Mann et al. [131], it is not customary to use statistical models which account for the random variation between and within individuals, nor has variation of FSS at the subject level been extensively studied for running gait. This thesis uses statistical analysis techniques from population modeling [163] to study the population of highly trained distance runners. In light of this, the primary aim of this thesis is to:

- Study between- and within-subject variability and, whilst accounting for variability, also provide a description of BF and SD running at aerobic training velocities for uninjured trained male distance runners.

The experimental conditions of running BF or SD, and of running at three sub-maximal velocities, serve as a set of meaningful and informative situations for the study population. This objective is carried out for spatio-temporal and partial lower-limb kinematics (Chapter 5), for muscular response of the prime agonists cross the ankle joint (Chapter 6), and for coordination and coordinative variability for the lower limbs (Chapter 7). Condition, velocity, and FSS are hypothesized to affect (and change with) kinematics, muscle activity, inter-segment coordination, and inter-segment coordinative variability.

1.2 Secondary aims

Motor control adaptations are often quantified by way of assessing within-subject variability. Within an individual, variability may be described as the normal variations that occur in motor performance across multiple repetitions of a task [193]. Such variability in movement may be functional: allowing for adaptations to the environment, a reduction in injury risk, and help

in optimizing movement coordination [11]. Pertinent questions posed by Stergiou *et al.* [192] include asking what the sources of variability are and how do they interact in the production of the observed variation of movement. Furthermore, is variability associated with disease or health?

1.2.1 Barefoot running as a biomechanical 'stress test'

Over time, running affects the composition of mechanical structures in the body by, for example, increasing bone mineral density, increasing the cross-sectional area of muscle fibres, and for distance running by increasing the proportional of type I ('slow twitch') muscle fibres [139]. Through repetitive (over)loading it may lead to successful adaptation or injury. Thus the population of trained runners, from which this study is a sample, will have a body composition which is adapted to SD running. Additionally, training affects the motor control system and therefore individuals with an extensive history of running training will be adapted to the motor control task of running as compared with untrained individuals [148]. It is also reasonable to expect that an individual is adapted to their habitual condition in terms of typical behaviour and variability [124], which for the present study population is SD. From an engineering perspective, perturbing a system by stressing and straining it mechanically may elicit a response which informs on the mechanical properties of the system. Therefore, one secondary aim of this thesis is to:

- Present the idea of using BF running to identify atypical running gait as part of a biomechanical 'stress test' for running-injury risk diagnostics.

Running BF marks a mechanical boundary condition by having no external cushioning and the act of BF running for habitually SD runners is also typically an acute change. This thesis considers the typical value of FSA, the variability of FSA within a subject, and the interaction

of the two as predictor variables. This idea, whilst not without limitation, is supported by the collection of running-related injury data in the sample of subjects.

1.2.2 Coordination and coordinative variability: a dynamical systems theory perspective

Dynamical Sytems Theory (DST) [34,77,102,104,196,197] provides a framework within which coordination and coordinative variability may be interpreted. The theory suggests that biological systems try to find the most stable solution for a given movement task by self-organizing according to biomechanical, environmental and morphological constraints. Generally, decreased variability represents stable behaviours. Dynamical systems theory also suggests that in certain systems when variability increases to a critical level, the system becomes unstable and transitions to a new movement pattern, with lower variability. A detailed discussion of coordination and coordinative variability in the context of DST is left to Section 7.1, but briefly, coordination is defined as the coupling of body segments, where the orientation of these body segments are defined in a global reference frame. A coordinative structure is an abstract representation of this coupling, and coordinative variability is the variability of these coordinative structures.

In a study of competitive race walkers using methods from DST [32], higher competition standards were associated with decreased coordinative variability in skill- and performance-related kinematic variables. This emphasizes, in a first step, the study of homogenuous competitive athletes as a distinct population. There is an hypothesis that a decrease in coordinative variability is associated with running-related injury [77]. However, methodological advancements in how coordination and coordinative variability are quantified [113, 175] require that coordination and coordinative variability in the population of injured trained distance runners be revisited. Thus, a sub-aim of this thesis, which is conditional upon the primary aim, is

introduced:

- Quantify coordination and coordinative variability from a dynamical systems perspective, whilst accounting for between-subject variability, for the population of uninjured, trained, and male distance runners.

Coordination and coordinative variability are studied as a function foot condition and velocity whilst accounting between-subject variability. Applying the statistical methodology from the primary aim facilitates a better characterization of the population from which the present study sample was drawn.

1.3 Thesis Overview

Table 1.3.1 summmarizes the predictor and response variables studied in this thesis as function of each chapter.

Chapter 2 presents details pertaining to running gait, including a discussion of muscle function, anatomy, and measurement techniques in running gait analysis.

Chapter 3 outlines the data collection procedure and kinematic models in this thesis.

Chapter 4 studies BF running kinematics at a fixed velocity. Stride-to-stride variation in kinematics is quantified within the framework of a typical gait analysis study. A discrete FSS and continuous FSA parametrization are compared in regard to their associations with kinematic variables. The secondary aim to present the novel idea of using BF running as a diagnostic tool is part of this chapter, but limited to a discussion point only.

Chapter 5 explains and formally introduces a linear mixed-effects model, and the technique is applied to study FSA. The primary aim of this thesis is investigated for three kinematic variables.

Chapter 6 presents lower-leg electromyography (EMG) data for the *tibialis anterior*, *gastrocnemius medialis,* and *gastrocnemius lateralis* muscles as a function of condition, velocity, and FSA. The primary aim of this thesis is investigated for muscle function.

Chapter 7 investigates the secondary aim to quantify coordination and coordinative variability from a dynamical systems perspective. This is therefore necessarily related to the primary aim. Tools from DST are used to study inter-segment couplings. This chapter also clarifies the appropriate application of DST in the context of running biomechanics and reviews relevant literature in detail.

Chapter 8 summarizes the conclusions and provides recommendations for future work.

	Predictor variables				
Chapter 4 response variables	$FSA \mid FSS$	σ_{FSA}	Gender | h:f	Condition[a]	Vel[b]
Duration of stance phase	✓		✓		
Duration of one stride	✓		✓		
Stance duration	✓		✓		
Cadence	✓		✓		
Joint angle at FS[c] & TO[c]	✓		✓		
Maximum joint angle[c]	✓		✓		
Time of maximum joint angle[c]	✓		✓		
Joint ROM between FS and peak[c]	✓		✓		
Joint angle velocity at FS[c] & TO[c]	✓		✓		
Maximum joint angle velocity[c]	✓		✓		
Time of maximum joint angle velocity[c]	✓		✓		
Probability of injury[d]	✓	✓			

	Predictor variables				
Chapter 5 response variables	$FSA \mid FSS$	σ_{FSA}	Gender[d]	Condition	Vel
Stride length				✓	✓
COM-heel progression				✓	✓
FSA	n/a			✓	✓

	Predictor variables				
Chapter 6 response variables	$FSA \mid FSS$	σ^{e}_{FSA}	Gender[d]	Condition	Vel
tibialis anterior EMG	✓			✓	✓
gastrocnemius medialis EMG	✓			✓	✓
gastrocnemius lateralis EMG	✓			✓	✓

	Predictor variables				
Chapter 7 response variables	$FSA \mid FSS$	σ^{e}_{FSA}	Gender[d]	Condition	Vel
PelThi crp(τ) and vcrp(τ)	✓			✓	✓
ThiTib crp(τ) and vcrp(τ)	✓			✓	✓
TibRft[a] crp(τ) and vcrp(τ)	✓				✓
RftFft[a] crp(τ) and vcrp(τ)	✓				✓
EVTIR[a] crp(τ) and vcrp(τ)	✓				✓

Table 1.3.1: Summary of model predictors and responses, according to each chapter number. Abbreviations: FSA - Foot-strike angle; FSS - Foot-strike strategy; σ_{FSA} - standard deviation of FSA for a subject; h:f - ratio of inter-asis distance to femur length; Vel - velocity; FS - foot-strike; TO - toe-off; ROM - range of motion; COM - centre of mass; EMG - electromyography signal; PelThi - pelvis-thigh; crp(τ) - continuous relative phase; vcrp(τ) - variability of continuous relative phase; ThiTib - thigh-tibia; TibRft - tibia-rearfoot; RftFft - rearfoot-forefoot; EVTIR - rearfoot eversion-tibia internal rotation.
[a]Barefoot running only
[b]Running at 3.58 ms^{-1} only
[c]measured for all three anatomical planes of the hip, rearfoot and forefoot, and for the sagittal and coronal planes of the knee
[d]Males only
[e]Not applicable when FSA is a covariate in a mixed-effect model.

Chapter 2

Background

The first part of this chapter defines the gait cycle of running as compared to walking (Section 2.1.1) and describes the kinematics of running (Section 2.1.2). This chapter then presents overviews of how movement is measured (Section 2.2.1) and how muscle activity is quantified (Section 2.2.2), and discusses basic considerations and limitations within the context of the analysis of running. Human anatomical structure and function is described with particular attention paid to structures and actions which affect bipedal running gait (Section 2.1.3).

2.1 Scientific background

In this section, gait analysis is briefly introduced and the running gait cycle is described and contrasted with walking. This is followed by a description of running gait with respect to lower-limb kinematics and muscle group activity and function. A detailed description of skeletal and muscular anatomy and mechanical function is presented in Section 2.1.3.

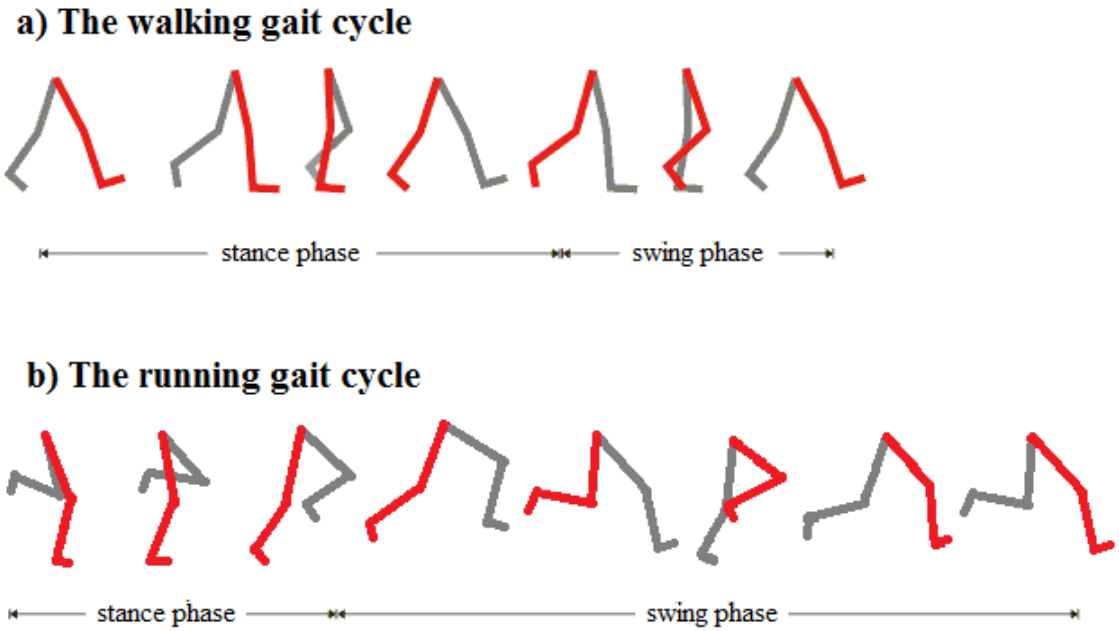


Figure 2.1.1: The gait cycle for a) walking and b) running. The gait cycle begins when one foot (red) contacts the ground and ends when the same foot next contacts the ground.

2.1.1 The running gait cycle and the motor control system

Gait analysis is concerned with the movement of the limbs during locomotion and the basic unit for measurement in gait analysis is termed the gait cycle (Figure 2.1.1). The gait cycle begins when one foot contacts the ground and ends when the same foot next contacts the ground. For each leg, the gait cycle is split into stance phase (foot in contact with the ground) and swing phase (foot not in contact with the ground). Stance phase begins when the foot contacts the ground at FS, and ends when the foot leaves the ground at toe-off (TO). Swing phase begins at TO and ends at FS. As speed increases, TO occurs earlier in the gait cycle, the duration of stance phase decreases and the proportion of time spent in swing phase increases as a percentage of the gait cycle [133]. Walking is defined by the existence of double support phases (*i.e.* when both feet contact the ground), hence successive stance phases for each leg overlap, whereas running is defined by the presence of double swing phase (*i.e.* time period when neither foot contacts the ground) and therefore successive swing phases overlap.

Measured ratios of stance to swing phase are 62:38 for walking, 38:62 for running and as

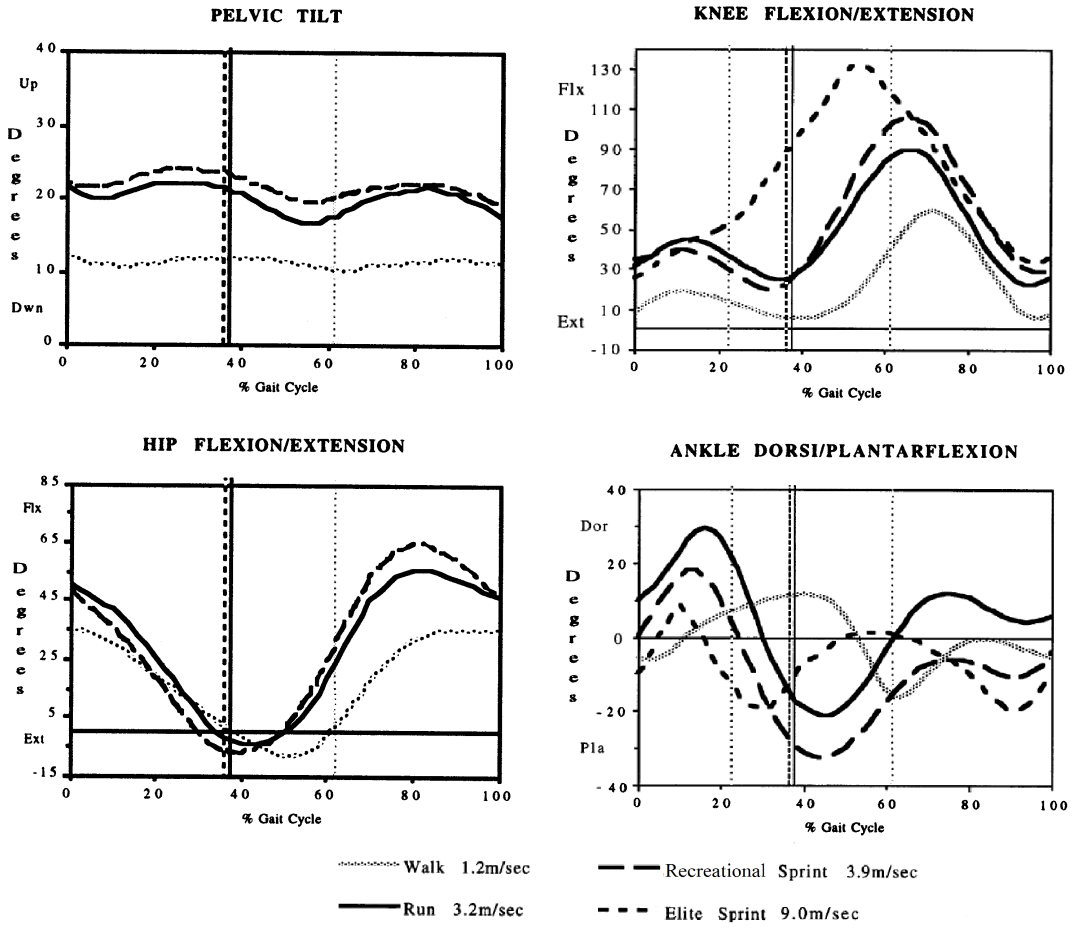


Figure 2.1.2: The kinematics of locomotion. For a complete gait cycle, beginning at FS and with a vertical line marking TO, the characteristic sagittal plane (side view) pelvis segment motion and joint motion for hip, knee and ankle. Data for knee and ankle joint motion are presented for walking (dotted), running (solid), recreational sprinting (long dashed) and elite sprinting (short dashed). Data for pelvis segment motion and hip joint motion are presented only for walking (dotted), running (solid) and recreational sprinting (long dashed). TO is at approximately 62% for walking, 38% for running, 36% for recreational sprinting and 22% for elite sprinting. Modified from [151].

much as 22:78 for elite sprinting [132]. Joint range of motion in the sagittal plane (as if viewing from the side) is much larger in running than in walking at the hip, knee and ankle (Figure 2.1.2). Generally, as running speed increases one changes from a heel (rearfoot) landing to a forefoot landing. This change in foot landing typically marks the difference between running and sprinting. For elite sprinting the heel may in fact never contact the ground at all [151]. Sprinting may be considered as a different gait mode to running because of the difference in the goal to be achieved. Distance running is performed over longer distances than sprinting and

primarily with aerobic metabolism. Sprinting is performed at high velocities without regard for maintaining aerobic metabolism. Efficient sprinting is a learned skill, whereas the development of economical distance running technique is a natural process [25].

Gait is regulated by the motor control system (MCS), which comprises networks of neurons from the central nervous system and the intraspinal nervous system, and hence undergoes conscious and automated regulation [27, 156]. Central pattern generators are neural networks producing rhythmic pattern outputs and their existence is postulated in mammals [186], including humans [26,49,55]. Animal studies have demonstrated that different locomotor patterns are influenced by muscle performance or sensory feedback [158] and/or by reconfiguring a neural network [71]. In cats, the entire range of speeds of forward progression and gaits are observed by increasing only the strength of mesencephalic locomotor region stimulation [143, 184, 185]. The mesencephalic locomotor region is a locomotor control centre in the brainstem, which first discovered in cats, has been found in all vertebrate species to date [118]. The mesencephalic locomotor region controls motor activity and filters sensory feedback. Gait analysis includes the study of human movements and may be used to direct and assess treatments in a clinical setting, investigate injury mechanisms and understand properties of the MCS.

2.1.2 The kinematics of running

Running is a bouncing gait: the body's centre of mass (COM) slows and lowers during the first half of stance phase and accelerates forwards and upwards into flight during the second half [80]. The remainder of this section describes the motions of the hip, knee and ankle together with the activity and function of the muscles which control these motions. This is discussed in terms of the three anatomical planes of the body: sagittal (as viewed from the side), frontal (coronal - as viewed from in front) and transverse (as viewed from above) - see Figure 2.1.3. This material is based mainly on the review by Novacheck [151] and the recent paper by Hamner

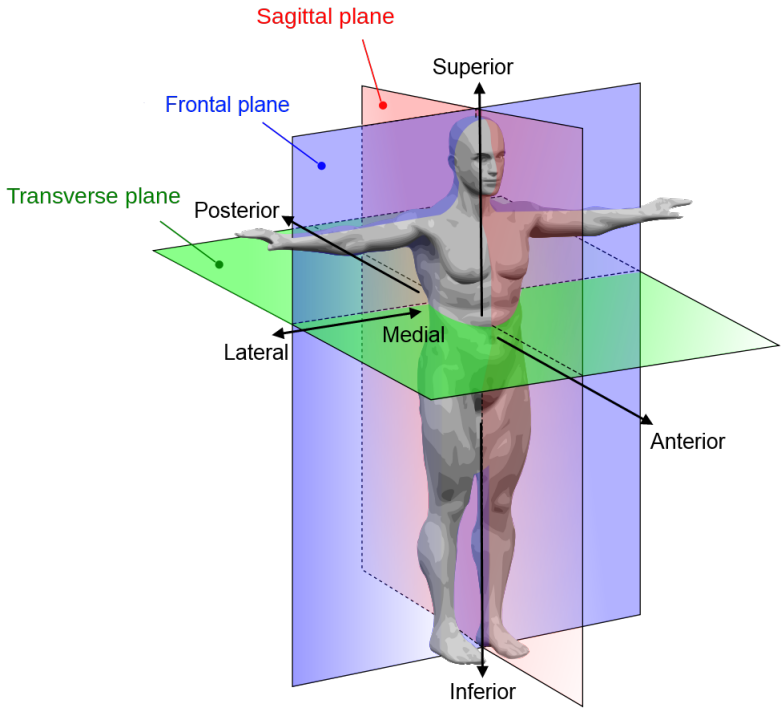


Figure 2.1.3: The anatomical planes and directions. Modified from [177].

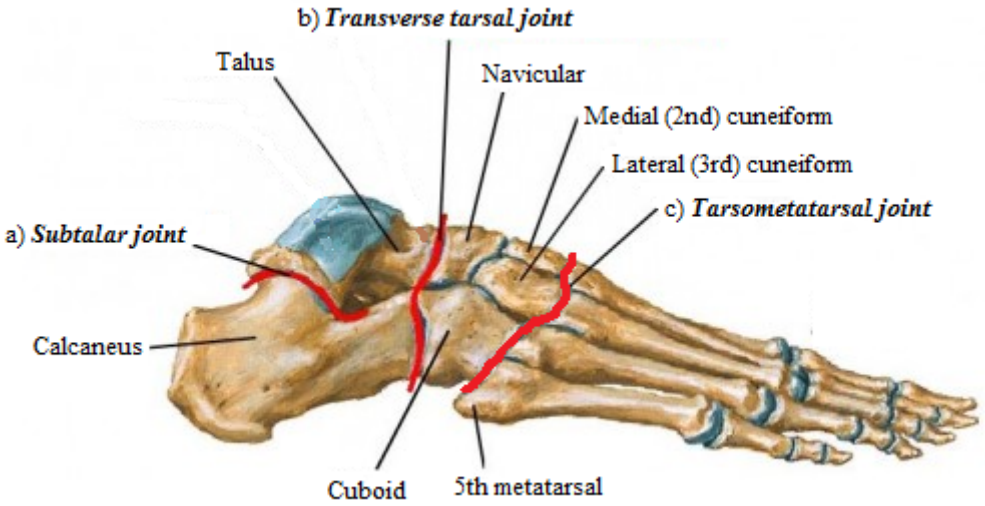


Figure 2.1.4: Bones and joints of the foot. The red lines mark the a) subtalar b) transverse tarsal (Chopart) and c) tarsometatarsal (Lisfranc) joint. Modified from [149].

and Delp [80].

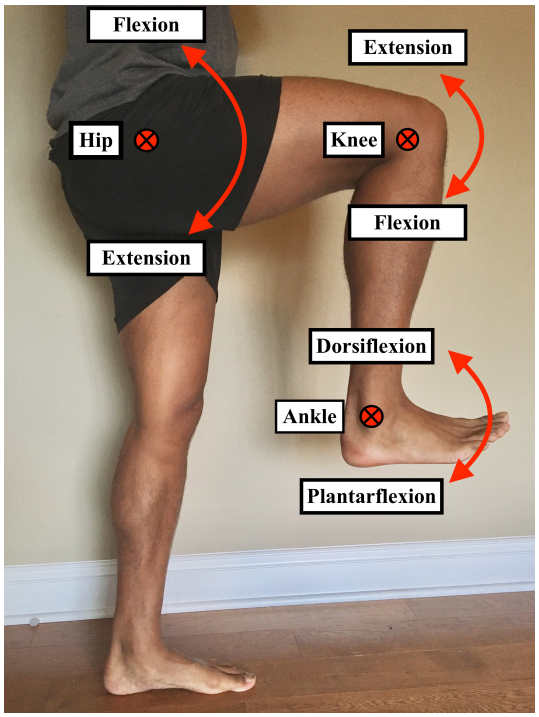
2.1.2.1 The ankle joint and surrounding articulations

The ankle region comprises many joints (Figure 2.1.4), whose functionality is crucial during locomotion. Movement of the ankle joint occurs mainly through the talocrural, subtalar and

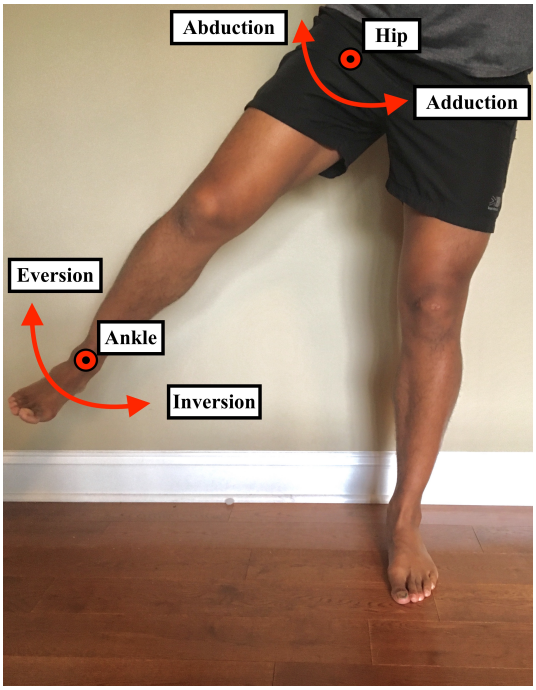
inferior tibiofibular joints. There is a lack of consistency in the literature regarding the use of the terms eversion and inversion versus pronation and supination when referring to the rearfoot motion relative to the tibia. The subtalar joint, formed by the articulation of the talus and calcaneus, has an oblique axis which extends forwards in the anterior, superior and medial directions [35, 91, 97, 99, 134, 174]. Therefore, rotations about this axis may be described as exhibiting motion in all three anatomical planes. Motion about this subtalar joint axis is known as pronation and supination [99, 134, 210]. The multi-segment foot model used in this thesis defines the rearfoot as the calcaneus. The model assumes that movement of the talocrural and subtalar joints contribute jointly to the motion of the rearfoot relative to the tibia. Therefore, use of the terms pronation and supination to describe these motion of the rearfoot relative to the tibia is inappropriate. For terminological consistency with this model, the terms eversion and inversion of the rearfoot are used. Eversion and inversion are defined as rotations about an anterior-posterior axis in the calcaneus which occurs in the frontal plane.

2.1.2.2 Sagittal plane kinematics

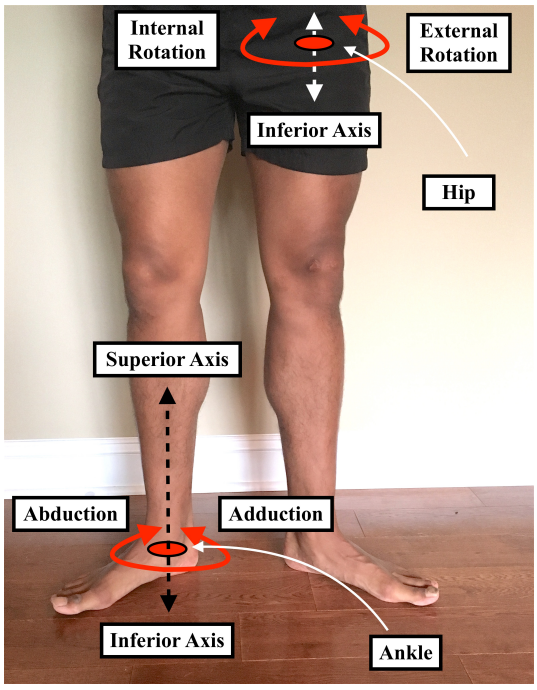
In general, the transitions from walking to running and running to sprinting involve increasing levels of flexion and decreasing pelvic motion. In the sagittal plane (side view), the hip is flexed (Figure 2.1.5) at FS, extending during stance phase with maximum extension shortly after TO. The hip flexes again during mid-swing phase to a maximum at contralateral FS, before extending more as the foot reaches the ground for FS. Immediately after FS, the hip extends as the COM moves over the supporting leg because of the concentric contraction of the posterior hip (gluteal) muscles (Figure 2.1.6). Later in stance phase the hip continues extending, controlled by eccentric contraction of the anterior hip (iliopsoas) muscles (Figure 2.1.6). During swing phase, the anterior hip muscles concentrically contract to flex the hip before the posterior hip and thigh (hamstring) muscles (Figure 2.1.7) decelerate the thigh and initiate an extending mo-



(a) Sagittal view and the medio-lateral axes: hip and knee joint flexion and extention, and ankle joint dorsi- and plantarflexion.



(b) Frontal view and the antero-posterior axes: hip and knee joint abduction and adduction, and ankle joint inversion and eversion.



(c) Frontal view and the inferior-superior axes: hip and knee joint rotatation, and ankle joint abduction and adduction.

Figure 2.1.5: Motion of the hip, knee, and ankle joints.

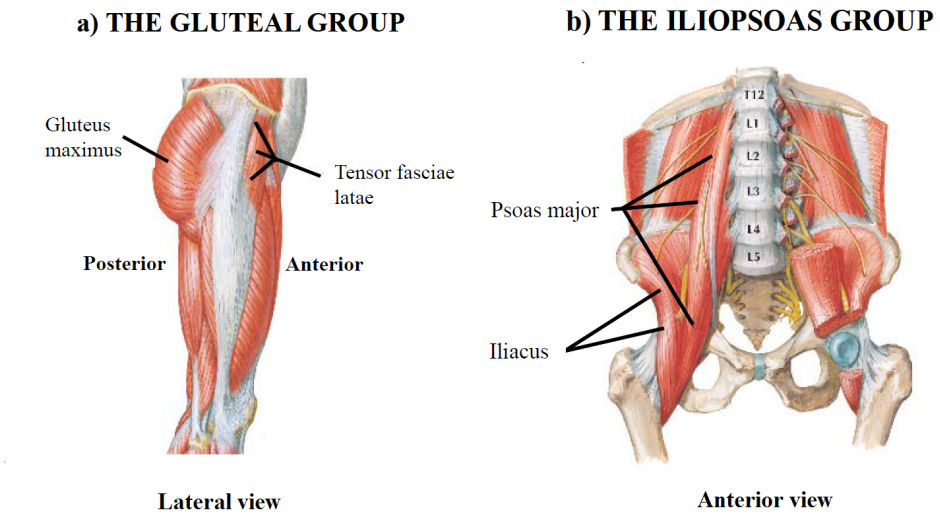


Figure 2.1.6: Muscular anatomy for the hip. The gluteal group (a) comprises the *gluteus maximus*, *gluteus medius* (not shown), and *gluteus minimus* (not shown). The *tensor fascia latae*, whilst not strictly part of the gluteal group, is innervated by the superior gluteal nerve. The iliopsoas group (b) comprises the *psoas major* and *iliacus*. Modified from [120, 149].

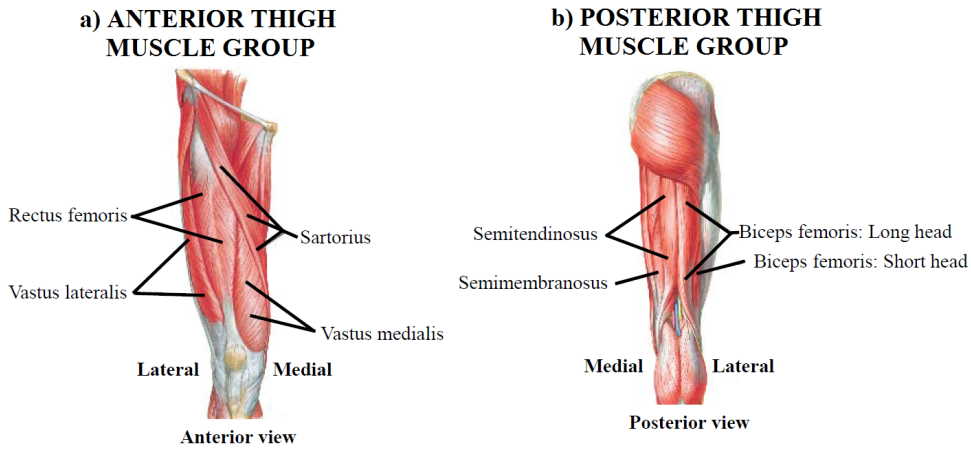


Figure 2.1.7: Muscular anatomy of the thigh. The anterior thigh muscle group comprises the *rectus femoris*, *vastus lateralis*, *vastus intermedius* (not shown) and *vastus medialis*. Collectively, they are known as the quadriceps muscles. The *sartorius* muscle is also shown. The posterior thigh muscles comprise the hamstring muscles *biceps femoris* (long and short head), *semitendinosus*, *semimembranosus*) and *popliteus* (not shown). Modified from [120, 149].

tion in preparation for FS. Whilst not observed during walking, a hip which is extending as the foot strikes the ground during running avoids excessive decelerations of the COM which would otherwise occur [151].

The knee is in a slightly flexed state at FS and remains flexed throughout the gait cycle. Contraction of the anterior thigh (quadriceps) muscles (Figure 2.1.7), which begins in late swing

phase, allows for muscle force production and therefore shock absorption at FS. The knee flexes more during the first half of stance phase as the progression of the body COM slows. A stance phase peak knee flexion of approximately 45° is reached before the knee extends towards TO. At TO, the knee typically exhibits approximately 25° degrees of flexion. Biomechanical models suggest that throughout stance phase the hamstring muscles act to accelerate the body's COM downward, under concentric and then eccentric contraction during the first and second half of stance phase respectively. During swing phase, there is a similar pattern of a flexing motion followed by an extending motion, with peak flexion angles being larger (> 90°) than during stance phase and larger for running versus walking. The posterior thigh muscles, which eccentrically decelerate the thigh, also help to decelerate the tibia and assist to induce knee flexing immediately prior to FS.

The global position of the foot with respect to the floor varies between individuals, with observations of rearfoot, midfoot and FFS all common. In walking and rearfoot-strike (RFS) running, the ankle plantarflexes immediately after FS. In RFS running, the ankle joint then dorsiflexes towards midstance, whereas for FFS running, the ankle joint only dorsiflexes, which occurs immediately after FS and towards midstance. After peak dorsiflexion at around midstance, the ankle plantarflexes towards TO, finishing stance phase in plantarflexion and reaching peak plantarflexion soon after TO. The *gastrocnemius* and *soleus* muscles (Figure 2.1.8) undergo eccentric and concentric contractions to decelerate and accelerate the body's COM vertically and dorsi- and plantarflex the ankle in each half of stance phase. Contraction of the *tibialis anterior* also assists with tibial advancement over the ankle. During swing phase, concentric contraction of the *tibialis anterior* induces ankle dorsiflexion.

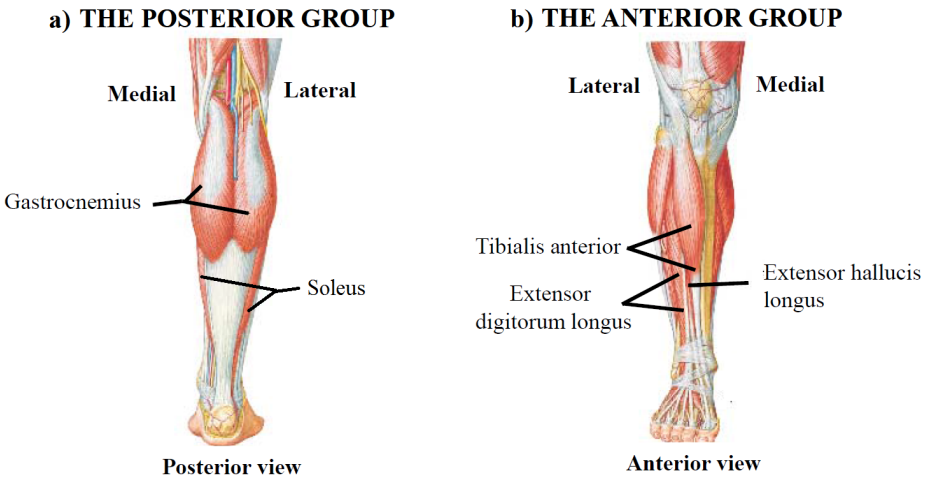


Figure 2.1.8: Muscular anatomy of the lower leg. The posterior (a) and anterior (b) muscles of the lower leg. The *gastrocnemius*, *soleus*, *tibialis posterior* (not shown), *flexor hallucis longus* (not shown) and *flexor digitorum longus* (not shown) constitute the posterior group. The anterior group comprises the *tibialis anterior*, *extensor hallucis longus*, *extensor digitorum longus* and *peroneus tertius* (not shown). Modified from [120, 149].

2.1.2.3 Frontal plane kinematics

Motion in the frontal plane is smaller than in the sagittal plane. Whilst motion at the knee and ankle joints is limited by medial and lateral collateral ligaments, motion at the hip is significant. Frontal plane kinematics are important in mimizing upper body motion. At FS, as the supporting limb is loaded, the pelvis, which is initially raised on the contralateral side, remains relatively stationary. The hip joint (the relative orientation of the femur with respect to the pelvis), which is initially adducted, adducts further to absorb shock. This shock-absorbing mechanism is similar to that seen in the sagittal plane at the knee joint. At the hip joint, muscles in the gluteal group produce force (mainly through the *gluteus medius* and *tensor fascia latae*) whilst eccentrically contracting. The pelvis then lowers (the contralateral side drops) throughout the rest of stance phase until double swing, where the contralateral side of the pelvis is at its lowest (most oblique). At the same time, the hip abducts, thus nearly mirroring pelvic motion, finishing slightly abducted at TO. The adductor group (Figure 2.1.9) (specifically, the *adductor longus* [27]) is active during late stance phase, possibly helping to stabilize the pelvis during

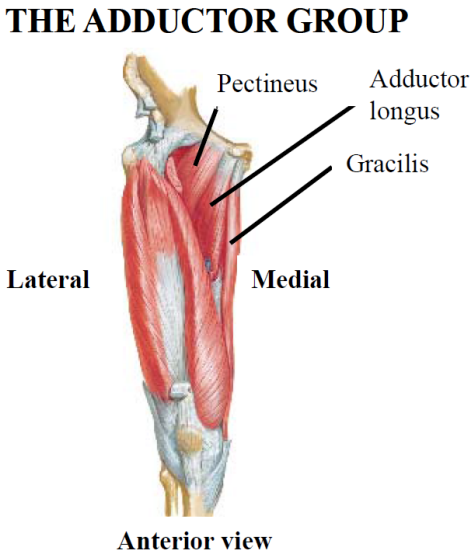


Figure 2.1.9: Muscular anatomy of the hip. The adductor muscle group comprises the *pectineus*, *adductor minimus* (not shown) (sometimes considered part of the *adductor magnus*), *adductor brevis* (not shown), *adductor longus*, *adductor magnus* (not shown) and *gracilis*. Modified from [120, 149].

propulsion phase as the hip joint abducts. The pelvis segment and hip joint motion reverses during double swing, allowing the pelvis to elevate and aid in foot clearance.

For RFS running, at FS the rearfoot is inverted and proceeds to evert towards midstance under loading. This motion is controlled by eccentric contraction of the *tibialis posterior* [170] and coupled with internal rotation of the tibia with respect to the rearfoot [90, 128]. As the rearfoot everts the forefoot also everts, 'unlocking' the transverse tarsal (Chopart) joint thus increasing the flexibility of the foot. This allows the foot to act as a shock absorber. Around midstance and roughly synchronous with the initiation of ankle plantarflexion, the rearfoot inverts and the tibia externally rotates with respect to the rearfoot [90, 128], and the forefoot inverts resulting in a locked transverse tarsal joint towards TO.

In FFS running the rearfoot is plantarflexed and slightly inverted at FS and there is less eversion towards foot-flat compared to RFS running. The rearfoot continually dorsiflexes towards foot-flat (for RFS running there is plantarflexion followed by dorsiflexion) under the control of the *gastrocnemius*. The Chopart joint initially remains locked [120, 164] and the arch of

the foot, which is initially loaded, begins to stretch. As the forefoot everts the rearfoot everts, 'unlocking' the Chopart joint thus increasing the flexibility of the foot. This allows the foot to continue to act as a shock absorber as the arch continues to stretch. From midstance to TO foot motion for FFS and RFS is similar.

2.1.2.4 Transverse plane kinematics

Transverse plane movements are small and difficult to measure. Muscle activity contributions are also difficult to measure and therefore mentioned sparingly in this section. In midswing, the side of the pelvis associated with the swinging leg is in front to maximize stride length. For example, with respect to the direction of travel, if the right leg is swinging, then at midswing the right side of the pelvis is in front of the left side (internally rotated). This contrasts with walking, where maximum pelvis internal rotation occurs at FS. In walking, this still acts to maximize stride length, but it also decelerates the body. At initial contact in running, the pelvis is very slightly externally rotated with respect to the stance leg, thus maximizing horizontal propulsion and avoiding unwanted decelerations. The pelvis also functions as a pivot for counter-rotating the shoulders and legs. Angular momentum caused by the movement of legs about the vertical axis is counterbalanced by that due to the rotation of the arms [80]. For example, with the right leg maximally forwards during swing phase, the left shoulder is maximally forward and the pelvis is neutral.

Running involves the coordinated movement of several body segments and, although there is variation between individuals, with an understanding of healthy runners' movement patterns it is possible, with the aid of quantitative motion analysis, to identify significant differences due to interventions and pathology.

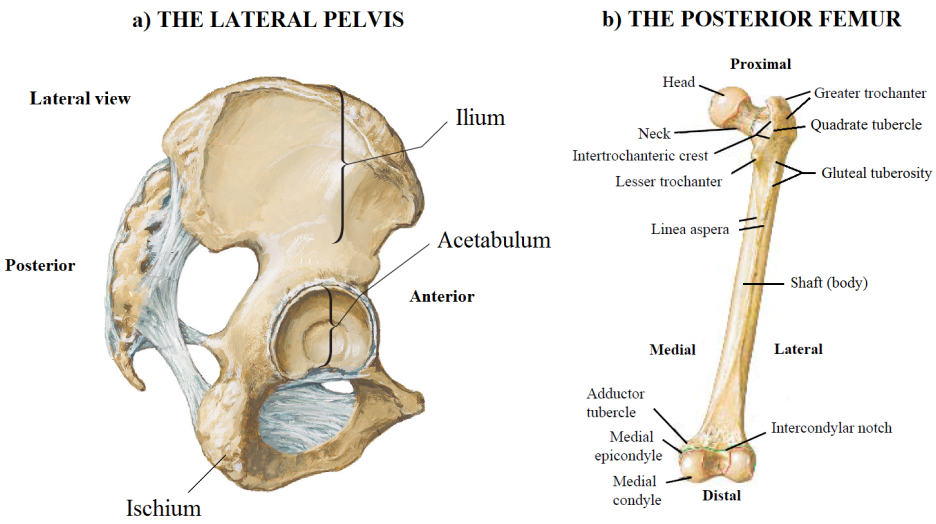


Figure 2.1.10: Skeletal anatomy of the pelvis and femur. In the pelvis (a) three bones, the ischium, ilium and pubis (not shown), fuse to form the acetabulum. The femur (b) articulates with the acetabulum to form the hip joint. Modified from [120, 149].

2.1.3 Lower-limb skeletal and muscular anatomy

This section presents the detailed skeletal and muscular anatomy of the lower limb, paying particular attention to structures and functions relevant for running.

2.1.3.1 Hip

The pelvic bone articulates with the femur to form the hip joint. The pelvic bone is formed by the fusion, during puberty, of the ischium, ilium and pubis (Figure 2.1.10). These three bones come together to form a concave surface known as the acetabulum (the socket), which articulates with the rounded proximal femoral head (the ball) to form the hip joint, making it an example of a ball-and-socket-joint. The femoral head connects to the femoral shaft via the femoral neck. The greater trochanter is the most lateral part of the femur and serves as an insertion for the gluteal muscles. The lesser trochanter, located inferior and posterior to the femoral neck, serves as the attachment of the tendon for the *psoas major* and *iliacus* muscles. Between the two trochanters and posterior is a bony ridge known as the intertrochanteric crest. The quadrate tubercle is near the middle of the intertrochanteric crest and acts as one insertion

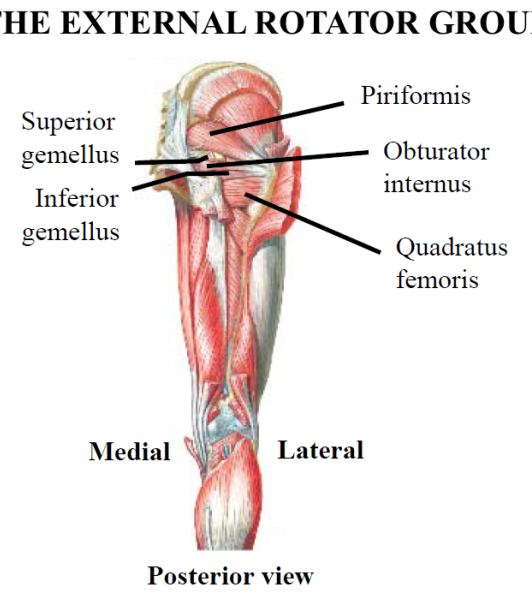


Figure 2.1.11: Muscular anatomy of the hip: the external rotator group comprises the quadratus femoris, piriformis, superior and inferior gemelli, obturator internus and obturator externus (not shown). Modified from [120, 149].

point of the *quadratus femoris*. This is a strong external rotator and adductor of the thigh which stabilizes the hip joint.

The femoral shaft is almost cylindrical in form and narrowest at the middle. The linea aspera is a rough, posterior and longitudinal ridge along the femur. Proximally and laterally a rough, almost vertical, ridge, known as the gluteal tuberosity, acts as the insertion of the *gluteus maximus*. Distally, the margins diverge as the femur forms as two roughly spherical projections, known as the medial and lateral condyles. Distally at the summit of the medial condyle, fibres of the *adductor magnus* insert on the adductor tubercle. The *adductor magnus*, which originates from the pubis and ischium, inserts also along the linea aspera laterally and proximally (proximally, it is occasionally known as the *adductor minimus*). The *adductor magnus* is medial to the *gluteus maximus*, inserting with a broad aponeurosis (a sheet of tendinous tissue).

The muscles at the hip may be split into the gluteal (posterior) group , iliopsoas (anterior) group (Figure 2.1.6), external rotator group (Figure 2.1.11) and adductor (medial) group (Figure 2.1.9). The gluteal group comprises the *glutei maximus*, *medius* and *minimus*. The *tensor fascia*

latae (TFL), which is anterior and lateral to the hip, is innervated by the superior gluteal nerve. The *gluteus maximus* is the largest, strongest and most superficial of the muscles in this group. It acts to extend and externally rotate the hip and attaches to the hip along the *iliacus*, to the femur at the gluteal tuberosity and to the iliotibial tract. During running, the *gluteus maximus* muscle is thought to function only concentrically during hip extension, particularly from late swing phase to the first half of stance phase. The *gluteus medius* and *gluteus minimus* function to abduct and rotate the hip. During running the *gluteus medius* acts continuously to provide a moment. It eccentrially controls hip adduction in the first half of stance phase in running, thus acting as a stabilizer. During propulsion in the second half of stance phase, the *gluteus medius* contracts concentrially, thereby abducting the hip and generating power. *Gluteus medius* insufficiency has been associated with patellofemoral pain syndrome (PFPS) [48, 98], a common running related injury [120]. The main function of the TFL is to sustain tension in the iliotibial tract. The neck of the femur gives the hip joint reaction force a moment arm long enough to cause a non-trivial bending moment in the femoral shaft [56, 58]. This is counteracted by tension in the TFL and hip abductors. Also, activation of the TFL leads to abduction, flexion and internal rotation of the hip joint. Because both the TFL and *gluteus maximus* share an insertion along the iliotibial tract, dysfunction of one may have effects on the other.

The iliopsoas group comprises two large muscles, the *psoas major* and *iliacus*, which function to flex the hip. Unilateral contraction of the *psoas major* induces lateral bending of the trunk, whilst bilateral contraction flexes the trunk. Both muscles insert at the lesser trochanter of the femur. The *psoas major* originates from the vertebral body and intervertebral discs of the T12 and L1 to L5 vertebrae and the *iliacus* originates along a large, smooth, concave surface on the internal sides of the ilium (iliac fossa). Fibre type composition as a function of the level of origin for the *psoas major* muscle suggests that caudal (lower) fibres act as the main flexor of the hip joint whilst cranial (upper) fibres act posturally as a stabilizer of the lumbar

spine, sacroiliac and hip joints. From the cranial to caudal regions of the *psoas major* the percentage of type I ('slow twitch') decreases and the percentage of type IIA ('fast twitch') fibres increases [7]. Therefore, the type I fibres are associated with stability and the type IIA fibres are associated with inducing flexion. Together with the hip extensors, the hip flexors are responsible for increased power generation in running and sprinting, by pulling the thigh forward during swing phase.

Each muscle in the external rotator originates from the hip bone and inserts on or near the greater trochanter of the femur, all working to externally rotate the hip. Muscles whose primary role is external rotation are the *quadratus femoris*, the *piriformis* (which inserts into the greater trochanter), the *superior* and *inferior gemelli* (which insert into the upper and lower edges of the *piriformis* tendon respectively) and the *obturator internus* and *externus*. The *obturator externus* also acts to adduct the thigh. Other muscles which contribute to external hip rotation, although it is not their primary function, include lower fibres of the *gluteus maximus*, the *gluteus medius* and *gluteus minimus* (when the hip is extended), the *sartorius* muscle (longest muscle in the body) and the *psoas major*.

The adductor group muscles originate on the pubis and ischium and insert along the medial ridge of the linea aspera. In order of their insertion points and moving distally, the muscles are the *pectineus*, *adductors minimus* (sometimes considered part of the *adductor magnus*), *brevis*, *longus* and *magnus* and the *gracilis*. The *gracilis* is a thin flat muscle which, as it crosses the hip and the knee, also functions to flex and internally rotate the knee. The external rotator and adductor muscle groups function primarily as stabilizers.

2.1.3.2 Knee

The femoral condyles articulate with the medial and lateral condyles of the tibia (Figure 2.1.12). The patellar groove, through which the patella slides, is anterior to the distal aspect of the femur.

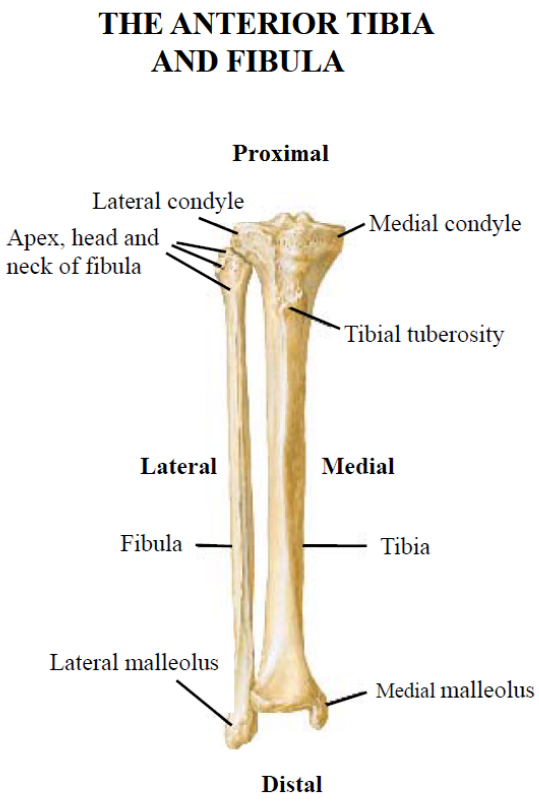


Figure 2.1.12: Skeletal anatomy of the anterior tibia and fibula. Modified from [120, 149].

These three articulating surfaces form the knee joint. The tibiofemoral articulation performs the weight-bearing function of the joint, whilst the patellofemoral articulation allows the muscles crossing the knee joint to exert larger extensor moments by increasing their leverage. In the cavity between the two condyles, the cruciate ligaments connect the femur and tibia. The patella covers and protects the anterior surface of the knee joint. The large articular surfaces of the knee, femoral head, sacroiliac joint and lumbar centra are thought to have played a significant role in human evolution because they allow for dissipation of the large and repetitive ground reaction forces associated with running [21].

The muscles crossing the knee joint may be separated into anterior and posterior groups (Figure 2.1.7). The anterior group, known also as the quadriceps muscles, comprises four muscles: the *vasti lateralis*, *intermedius* and *medialis* and, most superficial, the *rectus femoris*. Only the *rectus femoris* originates from the hip, from a groove on the iliac portion of the acetabulum,

and from the anterior superior iliac spine. The *vasti* originate on the femur. Indirectly, all four muscles insert into the tibia, which occurs over the patella and through the patellofemoral ligament. Whilst all four muscles function to extend the knee, only the *rectus femoris* acts to flex the hip. The magnitude of the peak knee extensor moments tend to be higher during running than sprinting because of the greater degree of knee flexion during loading in running gait [151].

Three muscles, the *biceps femoris* (comprising a long and short head), *semitendinosus* and *semimembranosus*, are commonly known as the hamstring muscle group. Together with the *popliteus*, they constitute the posterior thigh muscle group. These muscles assist in flexing the knee and, to a lesser extent, extending the hip. The *biceps femoris* originate from the ischial tuberosity (long head) and the lateral aspect of the linea aspera (short head). Distally, an aponeurosis, posterior to the long head, receives fibres from the short head before ultimately inserting as a tendon laterally onto the head of the fibula, which itself articulates with the lateral tibial condyle. The *semitendinosus*, a muscle medial and posterior to the femur, is so named because of a long insertion tendon to the medial surface of the tibia. The *semitendinosus* originates on the ischial tuberosity from the same tendon as the long head of the *biceps femoris*. Proximally and close to their origin, an aponeurosis also joins the *semitendinosus* and long head of the *biceps femoris*. The *semimembranosus*, the most medial hamstring, also originates from the ischial tuberosity. The muscle inserts mainly along a horizontal groove on the posterior, medial aspect of the medial condyle of the tibia. If the knee is flexed, the *semitendinosus* and *semimembranosus* internally rotate the thigh whilst the *biceps femoris* may externally rotate the thigh. The *popliteus* originates from the lateral femoral condyle and inserts on the posterior surface of the tibia. When the knee is fully extended, it assists in initiating knee flexion by internally rotating the tibia to 'unlock' the knee.

The hamstring muscles exemplify a recurring anatomical motif, exhibited throughout the lower limb, where the musculature is concentrated proximally and long tendons connect them

to distal lever arms. By concentrating mass proximally, the inertia of rapidly moving distal segments is minimized. Thus, when the hamstring muscles act to control rapid knee extension in late swing phase during running, their anatomical structure clearly assists this function.

2.1.3.3 Ankle

The tibia and fibula form the lower leg (Figure 2.1.12). The tibia is larger and stronger than the fibula and acts as the predominant weight-bearing structure in the lower leg. The fibula is lateral to the tibia and serves to stabilize the ankle joint by providing leverage for the muscles crossing the ankle. The distal aspects of the fibula and tibia articulate with the talus to form part of the ankle joint, referred to as the talocrural joint. The medial and lateral prominences formed by the distal ends of the tibia and fibula are known as the medial and lateral malleoli, respectively.

The foot (Figure 2.1.4) is a complex structure of twenty-six bones which include the talus. The foot can be subdivided into the rearfoot, midfoot and forefoot. The rearfoot is composed of the talus and calcaneus with the articulation of the talus and calcaneus known as the subtalar joint. The midfoot comprises five bones: the cuboid (proximal and lateral), navicular (proximal and medial) and three cuneiform bones (distal and medial). The midfoot and rearfoot articulate at the transverse tarsal joint (Chopart joint), which comprises two articulating surfaces: the calcaneus and cuboid (calcaneocuboid joint) and the talus and navicular (talonavicular joint). Finally, the forefoot is composed of the metatarsal bones and, more distally, the phalanges. The first ray comprises one metatarsal and two phalanges, whereas the remaining four rays have one metatarsal and three phalanges. The tarsometatarsal joint (Lisfranc joint) comprises the articulation of the distal aspect of the three cuneiform bones, with the proximal aspect of the first, second and third metatarsal and the distal aspect of the cuboid bone with the two proximal surfaces of the fourth and fifth metatarsals.

The ankle muscles may be separated into the posterior, anterior (Figure 2.1.8) and lateral

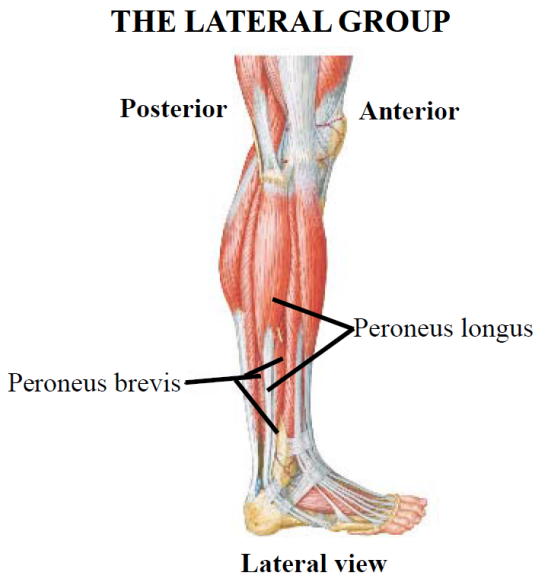


Figure 2.1.13: Muscular anatomy of the lower leg: the lateral group comprises the peroneus longus and peroneus brevis which both act to evert and plantarflex the ankle. Modified from [120, 149].

(Figure 2.1.13) groups. The posterior muscle group comprises the *gastrocnemius*, which itself splits into the lateral and medial compartments, the *soleus*, the *tibialis posterior* and the *flexors hallucis* and *digitorum longus*. The *gastrocnemius* is the largest and most superficial muscle, originating on the posterior surface of the femoral condyles and inserting at the calcaneus. Thus, contraction induces ankle plantarflexion and knee flexion, although action at the ankle is most significant. The *soleus* is deeper than the *gastrocnemius* muscle and, because it originates on the tibia and inserts on the calcaneus, acts only to plantarflex the ankle. When the knee is flexed and the *gastrocnemius* slackens, the *gastrocnemius*' capacity to plantarflex the ankle or knee is reduced. Whilst both muscles (*gastronemius* and *soleus*) also contribute to forward acceleration, muscle driven simulations have identified the *soleus* as the main contributor of upwards and forward COM acceleration [80]. The *tibialis posterior* is a deep muscle, originating from the posterior surface of the tibia, fibula and interosseus membrane (a broad, thin plane of fibrous tissue between the tibia and fibula). Distally the muscle splits, passing beneath the medial malleolus before the main portion inserts into the tuberosity of the navicular and to the plantar

surface of the first cuneiform. The *tibialis posterior* plays a significant role in lower leg stability, particularly for running, and contraction of the *tibialis posterior* induces inversion and assists plantarflexion. The *flexor hallucis longus* originates posteriorly from the middle third of the fibula, passes behind the medial malleolus and inserts at the base of the distal phalange of the hallux. The insertion tendon extends along the plantar side of the foot. The *flexor hallucis longus*, like the *tibialis posterior*, helps invert the foot. Furthermore, the muscle flexes the great toe, supinates the ankle and weakly assists ankle plantarflexion. The *flexor digitorum longus* originates posteriorly from the tibia, also passes behind the medial malleolus and inserts at the base of the distal phalanges of the second to fifth metatarsals. The muscle inverts the foot, flexes the toes and very weakly assists ankle plantarflexion.

The anterior group includes the *tibialis anterior*, *extensor hallucis longus*, *extensor digitorum longus* and *peroneus tertius*. The *tibialis anterior* originates laterally from the proximal end of the tibia and the lateral condyle. It passes over the ankle to insert on the medial cuneiform and first metatarsal of the foot. Contraction induces dorsiflexion and inversion for the foot. Wavelet analysis of the *tibialis anterior* muscle activity during stance has shown that SD running induces delays in post heel strike activity as compared to BF running [205]. The *extensor digitorum longus* is lateral to the *tibialis anterior* and between these lies the *extensor hallucis longus*. The *extensor digitorum longus* originates from the lateral condyle of the tibia and anterior surface of the fibula and inserts dorsally into the distal phalanges of the four lateral digits. It extends the lateral four toes and assists ankle dorsiflexion. The *extensor hallucis longus* originates from the fibula and inserts on the dorsal side of the distal phalanges of the great toe. It acts to extend the great toe and also assists ankle dorsiflexion. The *peroneus tertius* originates from the distal, anterior aspect of the fibula and inserts on the dorsal surface of the fifth metatarsal, aiding eversion and (weakly) dorsiflexion of the foot.

The lateral group, comprising the *peroneus longus* and *peroneus brevis*, acts to evert and

plantarflex the ankle. Both originate from the fibula and pass behind the lateral malleolus. The *peroneus longus* inserts into the lateral side of the first cuneiform and first metatarsal, whilst the *peroneus brevis* inserts into the fifth metatarsal.

2.2 Methodological background

This section summarizes the relevant methdological background.

2.2.1 Human motion analysis

Human motion analysis aims to quantify the mechanics of the musculo-skeletal system for specific, functional tasks such as running. Gait analysis is a clinical tool routinely used to identify and treat pathology and assess the efficacy of interventions. This section gives a brief description of the applied techniques, followed by an overview of some of the challenges associated with running gait analysis.

2.2.1.1 Techniques

Video analysis has been used extensively in running gait analysis, even in recent studies [43, 125, 150], and remains an accessible technique. It often allows for immediate feedback and gives opportunities to make qualitative analyses. Two-dimensional analysis is typically used only to quantify sagittal plane motion. Whilst video analysis may be reliable for walking gait in this plane [201], studies looking at running gait only partially support the use of 2D analysis. It is thought that, with respect to pathology, many clinically relevant kinematic differences occur outside the sagittal plane. Using 2D video analysis, Maykut *et al.* [136] studied peak contralateral pelvic drop, peak hip adduction angle and peak knee adduction angle, demonstrating high intra-tester reliability. Using the intra-class correlation coefficients as a metric [107], intra-tester

reliability was high (0.951 to 0.976). The intra-class correlation describes how strongly units in the same group (*i.e.* testers) resemble each other. When Maykut compared their results to the 3D motion analysis, they found only moderate correlations (0.539 to 0.623), and the only bilateral correlations were found for hip adduction. 2D motion analysis may be reliable for a given tester, but further work is needed on inter-tester reliability. It is clear that to date, whilst 2D motion analysis show promising signs of utility for those with limited resources, 3D motion analysis remains superior. The gold standard in running gait analysis lies with three-dimensional motion analysis (stereophotogrammetry), the method used in this thesis.

Stereophotogrammetry involves tracking markers, placed on anatomical landmarks, with several cameras. This allows for a virtual three-dimensional reconstruction of marker coordinates from the two-dimensional images from each camera. Using subject-specific biomechanical models, these markers can be used to define rigid-body segments, which enable one to calculate the three-dimensional angles between adjacent segments and quantitatively compare individuals. Using principles from classical mechanics it is then possible to quantify musculoskeletal mechanics.

2.2.1.2 Running gait analysis

Compared with walking, in running gait analysis ranges of motion are higher, movements are faster and on occasion, particularly with demanding data collection protocols, excess perspiration interferes with adhesion of markers to the skin. These issues necessitate higher capture rates, larger capture volumes (gait laboratories are typically designed to cater for walking gait analysis) and well controlled ambient environments. The use of a treadmill (or instrumented treadmill) is common because it addresses the issue of capture volume size and even allows for continuous data collection. In a study comparing overground and treadmill running kinematics, two-dimensional video analysis, captured at 100 Hz, was used and identified both systematic

and subject-dependent components [150]. Subjects ran at four speeds, in two types of shoe and in both scenarios. Although subjects systematically planted their feet in a flatter position on the treadmill than overground, the effect of overground versus treadmill running on most kinematic variables was subject-dependent and inconsistent. Typically, the majority of comparisons show no significant differences between overground and treadmill running and those which are significant exist mainly at speeds in excess of 5 ms^{-1} [207]. More recent work using an instrumented treadmill [172] suggested that, while significant differences between treadmill running exist for gait events associated with knee kinematics, peak vGRF, joint moments and joint power trajectories, running mechanics are still comparable to overground running, provided the surface is sufficiently stiff and the belt speed is well regulated. Others have observed that familiarity with a treadmill can affect biomechanics [117]. Despite minor differences between overground and treadmill running, the treadmill still provides a well controlled environment which allows for reproducible results.

2.2.2 Electromyography

Electromyography (EMG) is a technique used to study the electrical activity of the skeletal muscles. However, the most basic function of EMG is to identify whether a muscle is active or inactive. It may also identify muscular fatigue [82, 83] and potentially the type of muscle fibre which is active [205].

2.2.2.1 Motor unit action potential

A motor unit is defined as one motor neuron, together with the skeletal muscle fibres innervated by its axonal terminal (Figure 2.2.1) [23]. A short lived electrical impulse created within a neuron, known as an action potential, is mediated by ionic currents along the neuron to the neuromuscular junction. The action potential is transmitted across the junction into the muscle

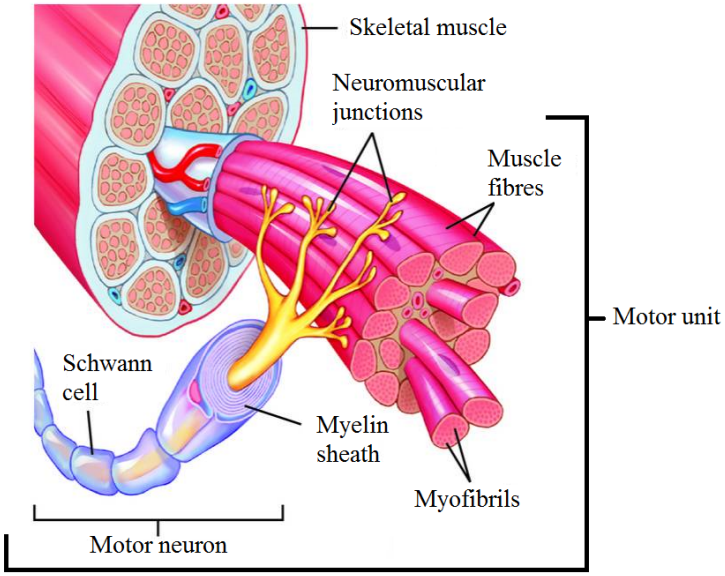


Figure 2.2.1: The anatomy of a motor unit. A single motor unit comprises a single motor neuron and the muscle fibres that it innervates. Modified from [144].

and innervates the muscle fibres. The sum of this electrical activity across the muscle fibres is known as a motor unit action potential (MUAP) and, typically, an EMG signal is the measurement of many of these MUAPs. The composition of the motor unit (the number of muscle fibres and the type of muscle fibres) and many other factors affect the precise signal from a motor unit [109].

2.2.2.2 Techniques

There are two EMG techniques in clinical use. Intramuscular EMG inserts two needle electrodes through the skin and into the muscle of interest to measure the activity of a small number of muscle fibres. Whilst this technique may target specific, deep muscles, it is often considered invasive and is often unnecessary in clinical practice. Surface EMG uses two surface mounted electrodes to measure muscle activity. With this method the skin is cleaned and shaved to reduce electrical resistance. Surface EMG gives a more general picture of muscle activity than intramuscular EMG and is suitable for studying large, superficial muscle groups.

2.2.2.3 Limitations

Signal quality for surface EMG suffers in the presence of adipose tissue below the surface of the skin but for the group studied in this thesis, the presence of adipose tissue is very limited. Also, whilst the innervation of a motor unit causes muscle fibres to contract and generate a force, the mathematical relationship between the MUAP and muscle force production is complicated and highly nonlinear.

2.3 Summary

This chapter provided scientific and methodological background by describing the kinematics of running and providing an overview of how movement and muscle activity are measured in the context of running. A description of human anatomy relevant to the study of running biomechanics was also presented. The following chapter presents the data collection methods and the kinematic models applied in this thesis.

Chapter 3

Data collection methods and kinematic models

The primary aim of this thesis is so study between- and within-subject variability and, whilst accounting for variability, also provide a description of BF and SD running at aerobic training velocities for uninjured trained male distance runners. In the interests of enabling the reproducibility of this work, this chapter describes the subject recruitment procedure, experimental apparatus, three-dimensional kinematic models, data collection protocol and post-processing procedure used in this thesis. Briefly, an anthropometric assessment was followed by motion capture and muscle activity data recordings. Recordings of kinematics and lower-leg muscle activity data for running in nineteen male subjects were used for analysis.

3.1 Subjects

3.1.1 Study design

The study was an analytic, observational, cross-sectional study within a group of male distance runners. Two interventions were applied: changes in velocity and a change in foot condition.

Velocity was randomized but foot condition was not randomized because foot markers could not be attached to the skin after the removal of shoes and socks due to excessive perspiration (Section 3.4.6.2). This may have led to bias associated with elevated sensory feedback induced by extended periods of BF running. It is possible, for example, that subjects were systematically de-sensitized to heel-striking for the SD condition.

3.1.2 Recruitment

Ethical approval for this study was granted by the Central Oxford University Reseach Ethics Committee (MSD/IDREC/C1/2011/41). Nineteen male subjects (mean age 22.7 years, min 19, max 31) were recruited from the Oxford University Cross Country Club. Potential volunteers were contacted via email to the club mailing list with an invitation letter and the inclusion/exclusion criteria attached. Eligibile volunteers who expressed an interest in participating in the study were given detailed information via email and invited to ask questions before confirming a time for data collection. Volunteers were informed that travel expenses would be reimbursed upon completion of the data collection exercise and that the results of the gait analysis would be reported to them on completion of the study. Subjects provided informed consent to take part in the study. Data for eight subjects from a previous study [120] was pooled with this study.

3.1.3 Inclusion/exclusion criteria

The inclusion criteria were:

- Over eighteen years of age at time of data collection.
- Male.
- Undertook a weekly running volume greater than 25 miles week^{-1}.

- Uninjured in the preceding six months. An injury was defined as a running-induced ailment which reduced the weekly running volume to below ten miles per week for at least three consecutive weeks. Non running-induced injury ailments which reduced running volume were not considered injuries.

- No history of lower limb surgery.

- Able to run at six minutes per mile (16.0 kph or 4.44 ms^{-1}) continuously for more than ten minutes.

Potential participants were excluded from the study if they failed to meet any of the above selection criteria. The study was designed to include only trained adult distance runners who would not fatigue significantly during the data collection. All participants were competitive distance runners who undertook structured training programs. Therefore, the data collection procedure was designed to minimize significant disruption to their daily training regime.

There are known differences in running kinematics between gender [60] and therefore a single gender was chosen to increase the power of the study. It was required that the subjects' weekly training volume (greater than 25 miles $week^{-1}$) was approximately an order of magnitude larger than the distance covered during the data collection and that they could run for longer than twice the time of the longest trial at the fastest speed (more than ten minutes at 16.0 kph). The study was limited to the healthy population of distance runners. Therefore participants were uninjured at the time of data collection. This criteria was used to lower the incidence of short term and/or long term pathological biomechanics.

In practice, all subjects had been competitive athletes for at least two years, could run for at least 60 minutes at 16.0 kph and ran in excess of 25 miles $week^{-1}$ (mean 54, standard deviation 15). Subjects consented to being contacted six and twelve months after data collection to note any injuries sustained during the period after the study.

3.2 Apparatus

All apparatus was situated in the Oxford Gait Laboratory (Nuffield Orthopaedic Centre, Oxford University Hosptials NHS Trust, Tebbit Centre, Windmill Rd, Headington, Oxford, OX3 7HE). The analogue EMG signals were synchronized, through an analog-to-digital card, to the Vicon motion capture system.

3.2.1 Motion Capture

The motion capture system consisted of twelve F-series MX cameras (Vicon, Oxford, UK) with a capture rate of 200 Hz. Each camera emitted an infra-red signal, which upon reflection from spherical retro-reflective markers, built a 2D image of reflective surfaces. The markers were 9 mm in diameter and attached to the skin using double-sided wig tape. The cameras were positioned such that every marker was visible to at least two cameras at any time, thus allowing information from two or more 2D images to be used to reconstruct the marker positions in 3D space. The mean residual error following calibration was less than 0.3 mm. Three-dimensional analysis was chosen because it reflects the gold standard for gait analysis (Section 2.2.1.2).

3.2.2 Surface Electromyography

Surface EMG is a non-invasive technique for measuring skeletal muscle activity. A wireless surface EMG system (Cometa Wave Wireless EMG, Milan, Italy) with Ag/AgCl electrodes recorded raw EMG signal at 1 kHz as the potential difference across the electrodes.

3.2.3 Treadmill

A treadmill (Ultim8 Active8 Deluxe Treadmill, Ultim8 Fitness Ltd, UK) was used for running data because it offers a well controlled and reproducible environment for data collection. The

available walkway was seven metres long, and therefore considered too small to study running gait at the prescribed velocities. The sub-maximal velocities studied in this thesis are also below the typical velocity at which overground and treadmill running kinematics diverge (Section 2.2.1.2, [207]), and are therefore assumed to be representative of overground running. The treadmill was placed in the capture volume, with two mechanical fans nearby to cool the subject during data collection. The maximum speed of the treadmill was 16.0 kph, with increments of 0.1 kph and the incline range was from 0% to 10% with increments of 0.5%. The incline was fixed at 0% for all trials. The running area was 1290 mm x 450 mm.

3.3 Kinematic models

This section introduces the framework upon which joint kinematics are calculated, followed by a detailed description of the kinematic models used in the thesis. Finally, there is a brief discussion of how anatomical frame misalignment affects joint kinematics.

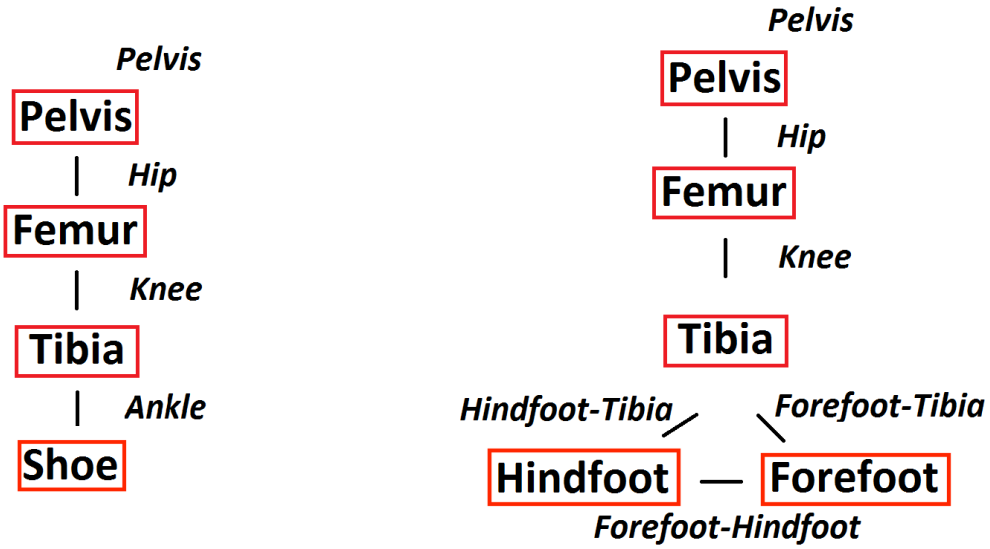
3.3.1 Definition of the global and local coordinate frames

To calculate joint kinematics, it is first necessary to define the global and local coordinate frames. The global (stereophotogrammetric) frame is a static frame [29] arbitrarily defined using a calibration object in the capture volume. The set of axes is used to give marker position coordinates. A local frame is embedded in a body segment and generally referred to as a technical frame (TF). These frames are reconstructed at each time step using the position of (at least) three non-collinear skin mounted markers (technical markers) and tracked by the stereophotogrammetry system. Thus, this marker technical frame (MTF) describes the position in space of the body segment under analysis. The MTF is arbitrary and therefore these technical markers do not necessarily coincide with anatomical landmarks (ALs), allowing clusters

of markers to also be used. An anatomical frame (AF) is defined to meet the requirements for intra- and inter-subject repeatability but more importantly, to represent the underlying position of the bony anatomy. A TF is constructed from surface mounted markers which are typically placed on ALs. The AF is defined using a transformation from the MTF during an anatomical calibration (static trial). Through the proper selection of anatomical frames, it is possible for the given rotations to correspond to functional anatomy. For a general mathematical description of how joint angles are calculated in gait analysis, refer to Appendix A.

3.3.2 Model overview

Models of the pelvis, both legs and both shoes were implemented for the SD condition (Figure 3.3.1a). The pelvis and femur segments were based on the Vicon Plug-in Gait (PiG) model [41, 100], whilst the tibia (strictly, composed of the tibia and fibula), hindfoot and forefoot segments were based on the Oxford Foot Model (OFM) (Figure 3.3.2) [191]. For the BF condition (Figure 3.3.1b) the pelvis, femur and tibia segments were identical to the SD model. Therefore, it is possible to make direct comparisons between condition of the pelvis, hip and knee kinematics. In the interest of consistency with Stebbins *et al.*, the term 'hindfoot', which described the posterior foot segment, is used in this chapter. However, in the rest of the thesis 'hindfoot' is used interchangeably with the term 'rearfoot'. The OFM is a lower-leg model which defines the tibia and a three segment foot comprising the hindfoot, forefoot and hallux segments. The model allows for six possible degrees of freedom between each segment (three rotational and three translational) because relative motion between each segment is decribed without inter-segment constraints. The segment axes correspond approximately to the anatomical axes of each segment. Subjects wore their own shoes and therefore it was not practical to permanently alter the shoe, for example, by cutting the material to attach markers to the foot. Therefore, the palpation and viewing of anatomical landmarks was restricted. The calculation of the ankle joint



(a) SD model.

(b) BF model.

Figure 3.3.1: Kinematic model abstractions. Segments (with borders) and joints (without borders).

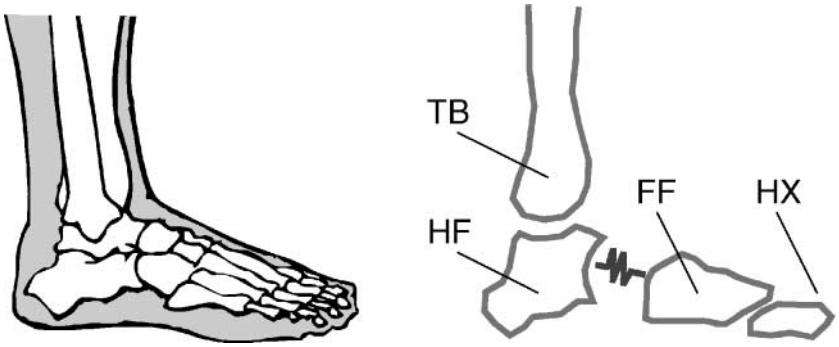


Figure 3.3.2: Oxford Foot Model with tibia segment [30]. The model simplifies the 28 bones of the foot to three segments. TB-Tibial segment (tibia and fibula), HF-Hindfoot segment (calcaneus and talus), FF-Forefoot segment (five metatarsals) and HX-Hallux segment (Hallux proximal phalanx). The HX segment was not modelled in this study.

angle is omitted because PiG ankle joint kinematics are not presented in this thesis. However, the shoe markers provide the foundation for the foot segment and thus, the calculation of FSS and FSA (Section 5.2.1). What follows is a brief description of the BF and SD kinematic models. Attention is paid to the anatomical definitions. A more detailed description of the OFM is given in [191].

Marker	Anatomical location
SACR	Midway between posterior superior iliac spines
R/LASI	Right and left anterior superior iliac spine

Table 3.3.1: Anatomical locations of pelvis segment markers.

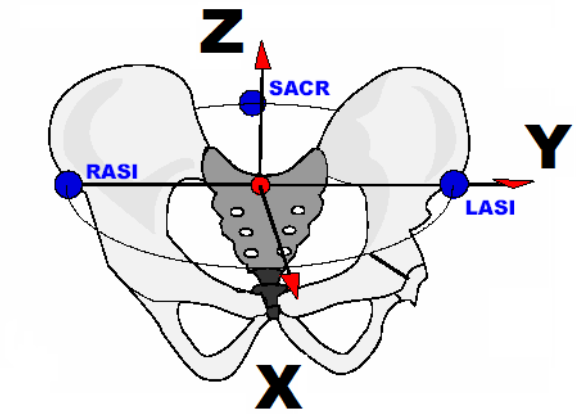


Figure 3.3.3: Pelvis segment axes and anatomical markers. Sacral marker (SACR) and the left (LASI) and right (RASI) anterior superior iliac spines.

3.3.3 Segment coordinate systems

The segments' coordinate systems were defined by retro-reflective markers placed on anatomical landmarks and other easily accessible points of the body. Therefore the segment coordinate systems were AFs.

The pelvis segment was defined in the global coordinate system and had six degrees of freedom. For the BF and SD models, all segments besides the pelvis had three relative rotational degrees of freedom.

The pelvis segment (Table 3.3.1, Figure 3.3.3) coordinate system origin was at the midpoint of the two anterior superior iliac spine (ASIS) markers. The ray from the right to left ASIS defined the Y axis. This ray, together with another ray from the sacrum (SACR) through the origin defined a plane. The Z axis was upward and perpendicular to the plane, and the X (forward) axis was defined so as to form a right-handed coordinate system. The Newington-

Gage model [41] was used to find the hip joint centres (HJC). In the pelvis coordinate system

$$x = C\cos\theta\sin\beta - (t+m)\cos\beta$$

$$y = \mp(C\sin\theta - a)$$

$$z = -C\cos\theta\cos\beta - (t+m)\sin\beta$$

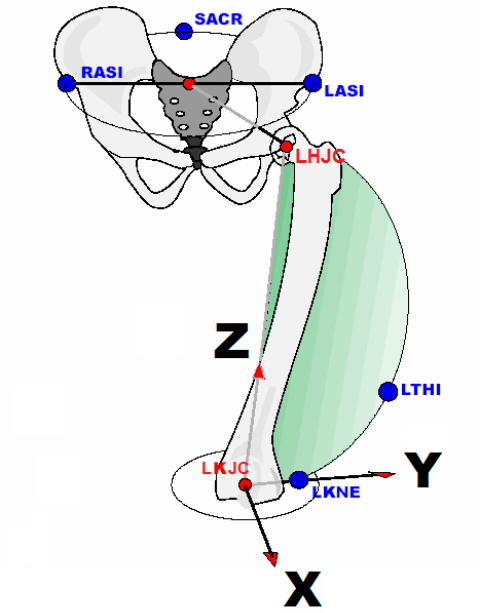
where $C = 0.115\,(\text{mean leg length}) - 15.3$, $\theta = 0.5^{\text{rad}}$, $\beta = 0.314^{\text{rad}}$, $t = 0.1288\,(\text{leg length}) - 48.56$, $m =$ marker radius, $a = 0.5\,(\text{inter-ASIS distance})$. The left hip was taken as the positive y direction and the right hip was taken as the negative y direction. These equations are derived from radiographic measurements and a linear regression model.

The femur segment (Table 3.3.2, Figure 3.3.4a) coordinate system origin was at the knee joint centre (KJC), which was a virtual marker. A virtual marker, which is typically more reliable than a physical marker [187], is a position in space calculated using the position of real markers and anatomical measurements. For calculation of the KJC (Figure 3.3.4b), a plane was defined by the thigh wand marker (THI), lateral femoral condyle marker (KNE) and HJC positions. The KJC was the vertex of the right triangle within the plane such that the other vertices were the KNE and HJC, and the KJC-KNE line segment had a measure of half the sum of the knee width and marker diameter. In the plane defined by KNE-KJC-HJC, the ray pointing from KJC to KNE defined the Y axis and the ray from KJC to HJC defined the Z axis. Given the construction of the KJC, the Y and Z axes were necessarily perpendicular. The X axis was defined so as to form a right-handed coordinate system.

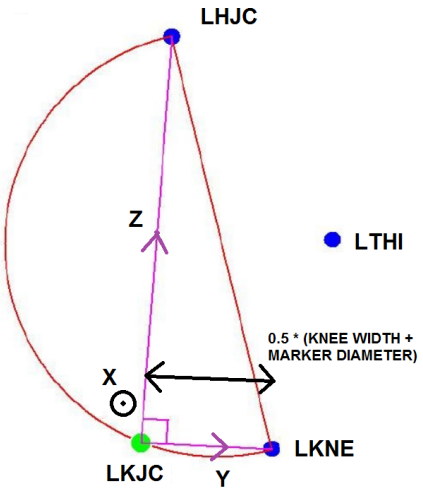
The tibia coordinate system origin is at the ankle joint centre (AJC) (Table 3.3.3, Figure 3.3.5). Analogous to the KJC calculation, the AJC is defined within the plane of the KJC, tibial wand marker (TIB), and lateral malleolus marker (ANK). The AJC is the right angled vertex of a right angle triangle defined by the points ANK, AJC and KJC. The distance between the AJC

Marker	Anatomical location
HJC	*Hip joint centre*
THI	Thigh wand marker between KNE and greater trochanter
KNE	Lateral femoral condyle
KJC	*Knee joint centre*

Table 3.3.2: Anatomical locations of real and virtual (in italic) femur segment markers.



(a) Femur segment axes and anatomical markers.



(b) Knee joint centre (LKJC) calculation. Markers for hip joint centre (LHJC), thigh wand marker (LTHI) and lateral femoral condyle (LKNE) are in the same plane.

Figure 3.3.4: Femur segment axes and left (L) knee joint centre (KJC) calculation.

and ANK is half the sum of the ankle width and the marker diameter. The Z axis points from AJC to KJC and the Y axis, through AJC and ANK, points left. The X axis was defined so as to form a right-handed coordinate system.

The calcaneus defines the hindfoot, and it is assumed (Section 2.1.2.1) that motion of the talocrural and subtalar joints contribute jointly to motion of the hindfoot (*i.e.* rearfoot) relative to the tibia [191]. The hindfoot segment coordinate system had its origin at the heel marker (HEE) (Table 3.3.4, Figure 3.3.6). The Y axis was normal (left) to the plane defined by the HEE, the proximal calcaneus marker (PCA) and static midpoint of the sustentaculum tali (STL)

Marker	Anatomical location
KJC	*Knee joint centre*
MML*	Medial malleolus
ANK	Lateral malleolus
TIB	Tibial wand marker, not collinear with ANK and KNE
AJC	*Ankle joint centre*
HFB†	Head of the fibula
TUB†	Tibial tuberosity
SHN†	Anterior aspect of shin

Table 3.3.3: Anatomical locations of real and virtual (in italic) tibia segment markers. * denotes removal after static trial. † denotes markers used for redundancy.

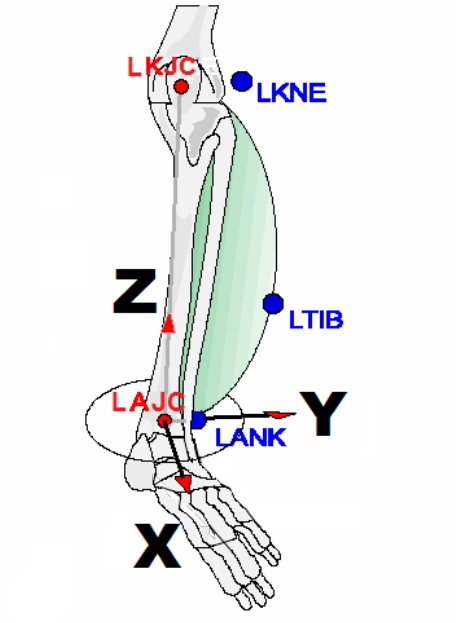


Figure 3.3.5: The tibia segment axes and anatomical markers. The ankle joint centre (LAJC) is calculated using the same method as for LKJC in 3.3.4b but, using LKJC, the tibial wand marker (LTIB), the lateral malleolus marker (LANK), and ankle width measurement.

and lateral calcaneus (LCA) markers. The Z axis is taken as parallel to the floor (from the static calibration), through the origin at the HEE, and in the plane previously described. The X axis is mutally perpendicular to form a right-handed coordinate system.

For the forefoot segment (Table 3.3.5, Figure 3.3.7), the X axis is normal (downward) to the (transverse) plane defined by the distal 1st metatarsal head (D1M) and 5^{th} metatarsal markers (P5M, D5M). The forefoot segment coordinate system has its origin between the 2^{nd} and the 3^{rd} metatarsal heads (TOE), projected into the transverse plane. The proximal end of the 1^{st}

Marker	Anatomical location
HEE	Posterior distal apsect of calcaneus
PCA*	Posterior proximal aspect of the calcaneus
LCA	Lateral calcaneus
STL	Sustentaculum tali

Table 3.3.4: Anatomical locations of hindfoot segment markers. * denotes removal after static trial. A calcaneal wand marker (CPEG), often used for redundancy, was omitted from this segment model because of practical constraints associated with running.

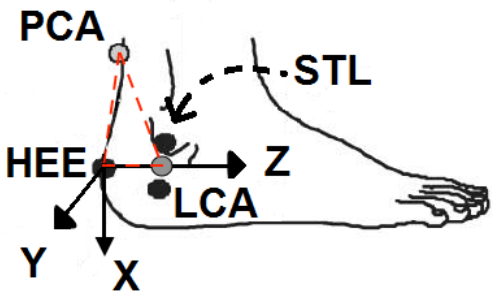


Figure 3.3.6: Markers and axes defining the hindfoot segment for the Oxford Foot Model. The Y axis is normal to the plane (red) defined by the heel marker (HEE), the proximal calcaneus marker (PCA), and the midpoint of the sustentaculum tali (STL), lateral calcaneus (LCA) markers. The Z axis is in the aforementioned plane and parallel to the floor (in the static calibration). Modified from [30].

Marker	Anatomical location
P1M	Posterior and dorsal 1^{st} metatarsal
D1M*	Distal and medial 1^{st} metatarsal
P5M	Proximal and lateral 5^{th} metatarsal
D5M	Distal and lateral 5^{th} metatarsal
TOE	Between the 2^{nd} and 3^{rd} distal metatarsal

Table 3.3.5: Anatomical locations of forefoot segment markers. * denotes removal after static trial.

metatarsal (P1M) is projected into the transverse plane and the Z axis is then defined, using three points all in the transverse plane, as forwards along a line half the distance between P1M and P5M and through the TOE. For the left and right leg, the Y axis is defined so to form a right-handed coordinate system.

The shoe segment (Table 3.3.6) heel marker (SHEE) was on the rear aspect of the shoe and the front shoe marker (STOE) was between the 2^{nd} and 3^{rd} distal metatarsal heads, when

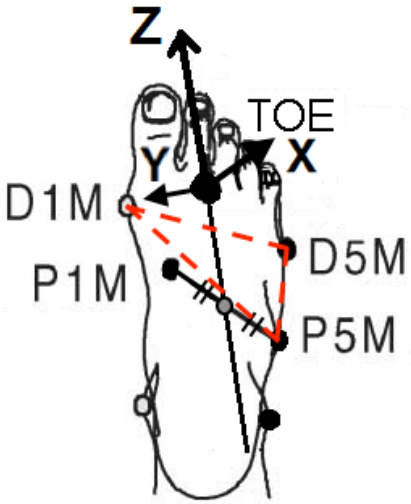


Figure 3.3.7: Forefoot segment for the Oxford Foot Model. The transverse plane (red) is defined by markers for the proximal (P5M) and distal (D5M) heads of of the 5^{th} metatarsal, and the distal head (D1M) of the 1^{st} metatarsal. A marker (TOE) is placed between the 2^{nd} and 3^{rd} metatarsals. The TOE marker is projected into the aforementioned plane and then serves as the origin. The Z axis is along the line from the midpoint of P5M and the proximal head of the 1^{th} metatarsal, also projected into the transverse plane, to the TOE. Modified from [30].

Marker	Anatomical location
SHEE	Rear aspect of the shoe
STOE	Between the 2^{nd} and 3^{rd} distal metatarsals
SPCA	*Rear of the shoe, proximal and vertical to the SHEE during standing*
SLCA	*Lateral side of the heel counter, level with the SHEE*
SSTL	*Medial side of the heel counter, level with the SHEE*

Table 3.3.6: Anatomical locations of shoe segment markers. Redundant markers are in italic.

palpated through the shoe. PiG ankle joint kinematics for SD running are not presented in this thesis and therefore, in the interests of brevity, the definition of the shoe segment axes are not discussed.

3.3.4 Joint angles

Joint angles were calculated following a YXZ Euler rotation of the relative orientations of two segments. The Y, X and Z axes correspond to flexion/extension, ab-/adduction, and internal/external rotation or inversion/eversion (at the ankle and rearfoot) or supination/pronation

(at the forefoot) respectively. The hip joint angles give the femur segment orientation relative to the pelvis segment, the knee joint angles give the tibia segment orientation relative to the femur segment and the ankle angles give the foot segment orientation relative to the tibia segment. The ankle flexion angle is offset by 90°. The hindfoot-tibia, forefoot-tibia and forefoot-hindfoot motion is, in each case, the motion of former segment relative to the motion of the latter segment. For example, the hindfoot-tibia angle is the hindfoot angle relative to the tibia.

3.4 Experimental protocol

An anthropometric assessment and basic strength test were carried out, followed by questions regarding the subjects' running background (Section C.2.1). One of three testers experienced in routine clinical gait analysis, marker placement, and EMG, placed the markers and electrodes following the same standardized procedure. Two testers were physiotherapists and one was a clinical scientist. The total experimental procedure lasted two hours. The subject preparation, anthropometric assessment and running background check lasted approximately 30 minutes whilst data collection lasted approximately 90 minutes. Figure 3.4.1 summarizes the subject preparation and data collection procedure.

3.4.1 Laboratory preparation

Before data collection, the laboratory was cooled to between 16°C and 19°C. The cooler temperature reduced sweating which could cause markers to become detached during trials. Once cooled, doors and windows were closed to block infra-red sunlight which may have been detected by the cameras, and the kinematic capture volume was calibrated. A calibration object with five retro-reflective markers at known separations was waved within the capture volume for calibration. The same calibration object was then located at a specific point in the laboratory to

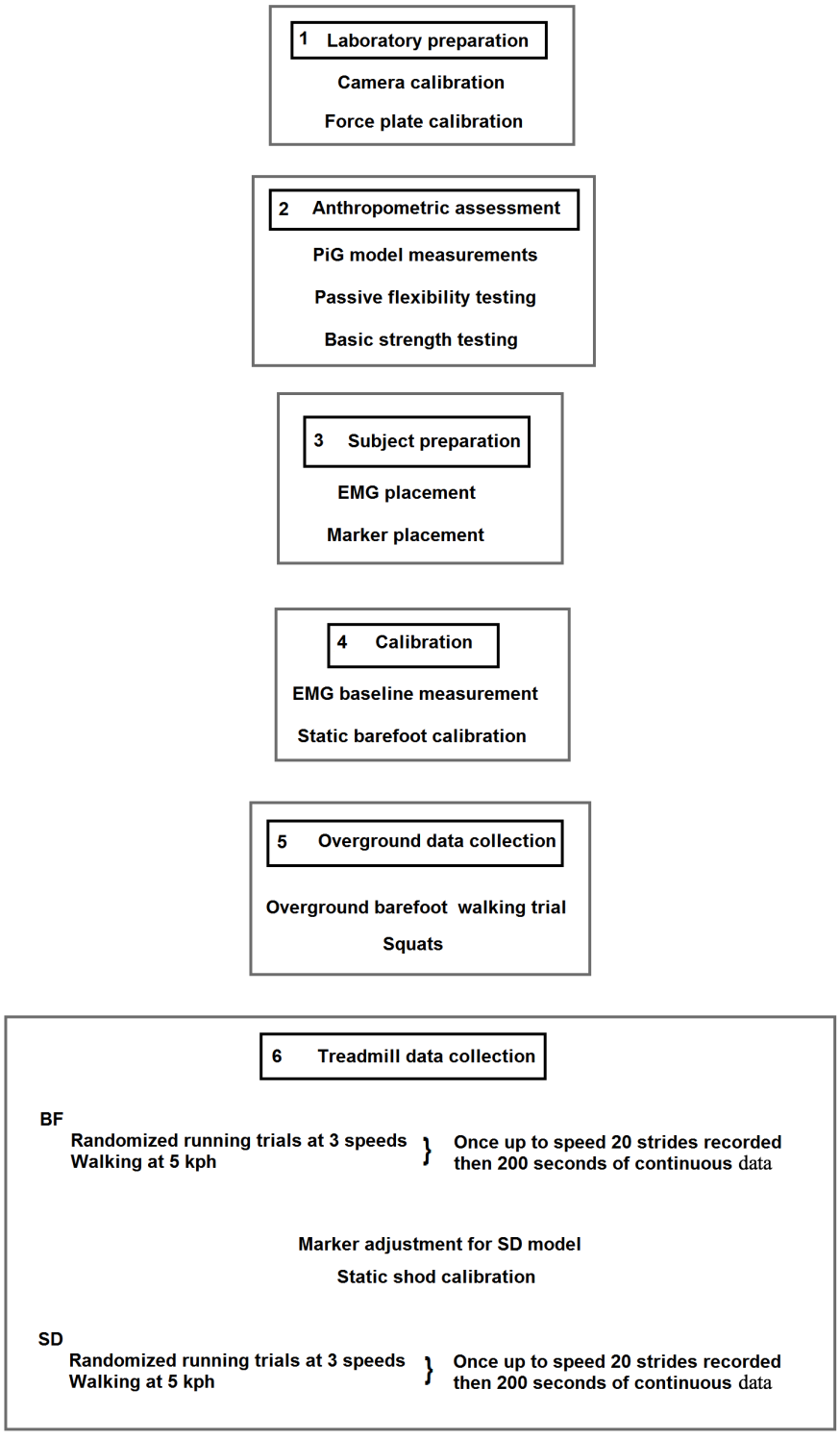


Figure 3.4.1: Subject preparation and data collection process summary

define the origin of the capture volume. The calibration object was then moved to a known distance from the origin to check the calibration was valid. Finally, following standard protocol in the gait laboratory, the three force plates (Advanced Mechanical Technology, Inc., Watertown, MA, USA) were zeroed and the vertical ground reaction force for a known mass was measured. Where any measurements were beyond an acceptable range, the whole calibration procedure was repeated. If data were collected for two or more subjects on one day, the calibration was performed once, before the first subject arrived.

3.4.2 Subject background

Upon arrival, the procedure for the experimental protocol was explained and subjects were invited to ask questions. The participant's recent (previous three to six months) average weekly running frequency, volume and approximate proportion of volume of running on grass, road, track or other surfaces were recorded. The dominant leg was identified by asking with which foot the subject would preferentially kick a football. For all subjects, the dominant leg was identified as the right leg.

The subjects used their own shoes for the SD condition. Subjects were specifically instructed to bring the training shoes in which they completed most of their weekly volume of running. The assumption was that subjects would have adapted their biomechanics most to these shoes and that BF running would provide a large yet physiologically relevent deviation from this state. The shoe model and UK size were recorded. The study did not use a standardized shoe type because specific shoes have been shown to interact differently and unpredictably with a population of runners [12] and therefore add further unknowns to the experiment. Furthermore, it was assumed that if subjects become injured whilst running, it is likely that they would do so in the shoes they used for the study as it was in those shoes that they completed most running. The use of orthotics was permitted only if it was customary for the subject to use them whilst run-

ning. The date of issue and frequency of use of the orthotic were recorded as *"always/walking only/running only/never*".

3.4.3 Anthropometric assessment

Measurements were taken by one of the testers. The subject's height and inter-ASIS distance, measured using a wall mounted and digital caliper respectively, were necessary for the PiG model. The inter-ASIS distance was used for approximating the lateral position the HJC. The leg length, measured using a tape measure from ASIS, via the medial femoral condyle, to the medial malleolus was also used in the calculation of the HJC. The knee and ankle widths were measured using a digital caliper and used for calculating the KJC and AJC respectively. Measurements of foot length, truncated foot length, arch height, calf circumference and Achilles tendon moment arm were also taken. Measurements of the foot length and truncated foot length were made using a digital caliper. The whole foot length was measured from the heel to the distal end of the longest toe. The truncated foot length was measured from the heel to the 1^{st} metatarsal head, parallel to the long axis of the foot. The arch height was measured using a ruler at half the length of the foot. The truncated foot length and arch height measurements were used to calculate the arch height index. The calf circumference was measured parallel with the floor at the largest part of the *gastrocnemius*. The Achilles tendon moment arm was estimated from the lateral malleolus to the posterior surface of the Achilles tendon using a tape measure, parallel with the floor with the subject standing.

Approximate angles for the passive range of motion at the hip, knee and ankle were estimated visually. This was to check for asymmetries in the passive flexibility at the joints and if the range was within that of healthy adult males. The specific measurements were: hip flexion, extension, adduction, abduction, internal and external rotation, knee flexion and extension, ankle dorsi-flexion with knee flexed at 90° and ankle dorsi-flexion with knee extended.

3.4.4 Strength testing

As a basic strength test, subjects were asked to complete ten one-legged calf raises and a one-legged squat to at least 90° with their unsupported leg kept straight in front of them. This test was performed to highlight any significant muscle weaknesses which may have affected the subjects' injury risk. Subjects were permitted to balance themselves for the calf raises, but not for the squat. If the subject could not complete the task, the number of calf raises completed and/or approximate maximum angle of the squat were recorded.

3.4.5 Subject preparation

Subjects were offered the use of a Foot Thong™ (Bloch UK Ltd, London, UK) (Figure 3.4.2) to protect their feet from the rough surface of the treadmill when running in the BF condition. The Foot Thong™, when used, was fitted immediately before EMG electrodes and retro-reflective markers were attached. Surface electrodes were placed according to Surface Electromyography for Non-Invasive Assessment of Muscles (SENIAM) guidelines [95]. To assist with the aquisition of a clear signal, the skin was shaved, abraded and cleaned using alcohol wipes. Electrode pads were placed on the *gastrocnemius medialis*, *gastrocnemius lateralis,* and the *tibialis anterior* muscles for both legs. Wireless transmitters were connected and secured using double-sided wig tape and all apparatus was secured using 3M™ Coban™ Brand Self-Adherent Wraps. The electrode to measure *gastrocnemius lateralis* activity was placed on the lateral muscle belly on a line a third of the way from the head of the fibula to the heel. The *gastrocnemius medialis* electrode was placed on the medial muscle belly on a line one third of the way from the medial femoral condyle to the heel. Finally, the *tibialis anterior* electrode was placed one third of the way from the head of the fibula to the medial malleolus, just lateral to the tibial crest (Figure 3.4.3). Markers were attached to anatomical landmarks defining the BF kinematic



(a) Dorsal surface

(b) Plantar surface

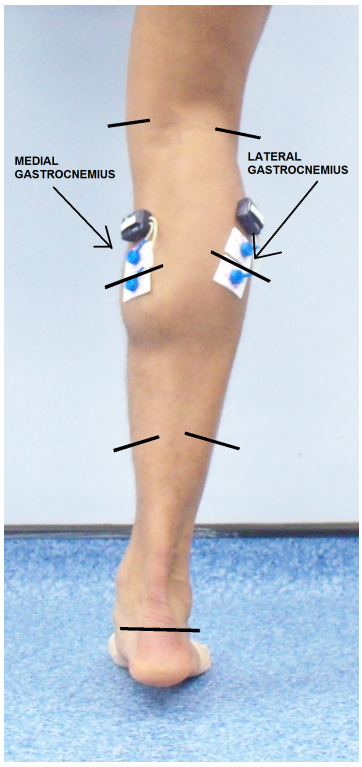
Figure 3.4.2: Foot Thong™

models (Figure 3.4.4). A permanent pen was used to show the marker positions to ensure if any markers detached, they could be accurately replaced.

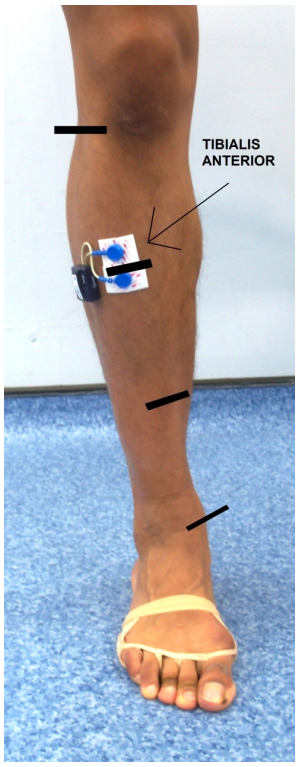
3.4.6 Data capture

3.4.6.1 Subject calibration

The subjects were asked to hop on both legs and stand on their heels to check for a clear signal from the EMG electrodes. Hopping activated the *gastrocnemius* muscle whilst standing on the heels activated the *tibialis anterior*. For this study, the EMG gain was adjusted from the Oxford Gait Laboratory protocol for walking and reduced from 2.5 V to 1.25 V. This ensured that the



(a) *Gastrocnemius medialis* and *gastrocnemius lateralis*



(b) *Tibialis anterior*

Figure 3.4.3: Placement of *gastrocnemius lateralis*, *gastrocnemius medialis*, and *tibialis anterior* electrodes, with the Foot Thong™. The black lines illustrate how the lower leg is split into thirds.

signal did not saturate during running.

A static trial was recorded in the capture volume and reconstructed immediately to ensure no markers were obscured. Any reflective clothing causing phantom markers was covered with masking tape. The calibration markers (MMA, PCA and D1M) were removed and the subject sat on a chair and was instructed to relax whilst a thirty second trial was recorded to measure baseline EMG activity levels. As part of standard as associated proctocol, five continuous two-legged squats to 90° were captured. A demonstration was given and subjects were specifically instructed to keep their heels on the ground and bend their knees to approximately 90°. At least three overground BF walking trials were performed by the subjects at a self-selected walking speed along a seven metre walkway. These trials were used for the dynamic calibration of the PiG model thigh offset parameter. As the thigh wand marker was not placed on anatomical land-

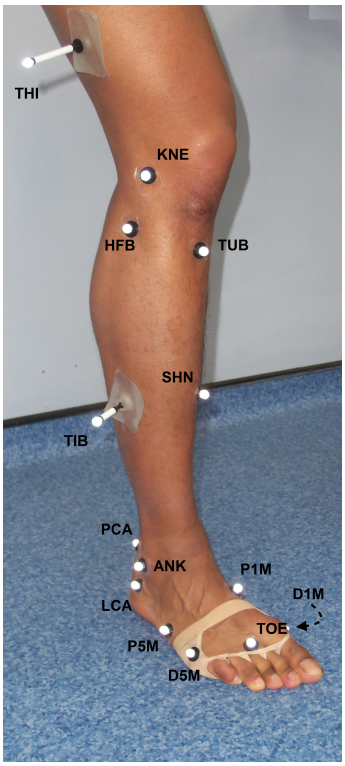


Figure 3.4.4: Lower limb markers with Foot Thong™. Markers for the heel (HEE) and sustentaculum tali (STL) and medial malleolus (MML) are not shown. The shin (SHN), tibial tuberosity (TUB) and fibula head (HFB) are used to define TFs. More detail may be found in [191].

marks an optimization procedure was used under the assumption that the knee angle variation is minimized during overground walking [9].

The walking trial was also used to identify any clear walking gait abnormalities. Where abnormalities were apparent, the data was not to be used. However, for all subjects, kinematics for walking fell within normal ranges for adult men compared to the Oxford Gait Laboratory database. Beginning with overground BF walking trials on a hard surface may have de-sensitized subjects to heel striking whilst running. Whilst this is a limitation of the current protocol, it is reasonable to expect than any BF running would be preceded by a non-negligible period of BF walking, both as part of any experimental protocal which includes a period of acclimitization period, and for any BF running outside of an scientific experiment.

3.4.6.2 Treadmill data collection

The order of running speeds was randomly selected separately for BF and SD trials. Trials were performed at 16.0 kph (4.44 ms^{-1}), 14.3 kph (3.97 ms^{-1}) and 12.9 kph (3.58 ms^{-1}). These speeds correspond approximately to the spectrum of aerobic running speeds on flat ground for competitive distance runners. The subjects were asked to build up to each speed in their own time and data capture was initiated once the treadmill had reached the required speed. For the first part of the trial, twenty consecutive strides were recorded. Without the subject stopping, a further 200 seconds of data were recorded. After the last running trial, the subject walked at 5 kph (1.38 ms^{-1}) for twenty strides plus a further 200 seconds. To avoid fatigue, the subjects were given ample recovery time between trials and confirmed their recovery vocally before beginning the next trial.

If during the first part of a trial of 20 strides, one or more markers became unattached, the markers were replaced and the trial was repeated. If markers became unattached less than 90 seconds into the second part of the trial, the second part of the trial was repeated. Between each trial, markers were replaced if necessary and any excess sweat was removed with paper towels. Another static trial was performed when markers were detached during the trial.

BF trials were performed first, followed by SD trials. This constraint was imposed after preliminary data collections. Owing to excessive perspiration, foot markers could not be attached to the skin after the removal of shoes and socks. It follows, therefore, that subjects were assumed not to suffer from fatigue associated with first running BF during the data collection. It also follows that there is an assumption of no hysteresis as function of footwear. It is therefore possible that this protocol led to bias in the results. For SD running trials all OFM markers were removed. Once the shoe was fitted the MMA marker was reattached. The modified HEE (SHEE), TOE (STOE) markers, along with three redundant markers (SPCA, SLCA, and SSTL), were also attached to the shoe. Markers were placed by Mr Richard Franzese. A static trial was

recorded and reconstructed for the SD condition and phantom markers caused by the reflective surfaces of the shoe were removed by covering the appropriate parts of the shoe with masking tape. Another static trial was recorded if necessary and the calibration markers were removed. Subjects ran again at 16.0 kph, 14.3 kph and 12.9 kph in a randomized order and walked at 5 kph before all apparatus was removed. Twenty strides plus 200 seconds of data were captured for each trial. Finally, the subjects were invited to ask questions before leaving.

Although FSS was often clear, during the running trials a video of the foot in the sagittal plane was recorded using a handheld camera at 15 Hz (T328w, High Tech Computer Corporation) for up to five seconds. The purpose of this video was to confirm the FSS for the trial.

3.5 Data post-processing

Data were processed using Vicon Nexus (Vicon Nexus Version 1.7.1, Vicon Motion Systems, Oxford, UK) and MATLAB (MATLAB version 2011b, MathWorks Inc., Natick, MA, USA).

3.5.1 Subject model calibration

Using Vicon Nexus, marker trajectories were reconstructed in 3D using a set of parameters modified from walking and optimized through trial and error for running. In particular, the minimum number of cameras necessary to start a marker trajectory was two and only one was needed to continue a trajectory. As running involves faster movements than walking, the estimated marker movement speed upon reconstruction was set to a maximum of 800 mm s^{-1}.

Once the markers were automatically labelled, subject-specific parameters necessary for kinematic modeling were added for the static trial. The markers were automatically labelled for all dynamic trials. Following the Oxford Gait Laboratory protocol, marker trajectories for overground walking and short treadmill trials were filtered using a Woltring filtering routine

with predicted Mean Square Error (MSE) value set at 20. The filtering routine used a quintic spline routine and the MSE algorithm filtered the entire data range with a constant value, treating all parts of the data the same.

In the overground walking trials, the PiG angle trajectories were generated. The flexion-extension axis of the knee depends on THI position because the marker is used to determine the location of the KJC (see Section 3.3.3). Precision error associated with identifying the knee flexion-extension axis propagates into error in the knee joint angles. To minimize error in the knee joint angles, Baker *et al.* [9] proposed the application of a correction factor to compensate for misplacement of THI. Therefore, a program to minimize the knee abduction/adduction over the trial and optimize the position of the thigh marker [178] was applied to the PiG angle trajectories. The program functioned by creating virtual thigh markers from rotating the true THI through a known angle, about the axis between the HJC and KNE. The knee abduction/adduction trace was calculated as if the virtual thigh marker was used. The model used the virtual marker position which gave the minimum root-mean-squared deviation (RMSD) from the mean of the knee abduction/adduction angle trace across a stride. The given offset was then used as the optimized thigh offset parameter in the model. The range of offsets were typically between $\pm 18^{\circ}$ ($\mu \pm \sigma = -4.7 \pm 8.7$). Quality checks were incorporated into the model to identify excessively large angle trace variances, ensure sensible behaviour of the data and highlight where the thigh rotation angle for minimum variance lay outside of the range tested. Once the thigh offset was optimized, it was added to the gait model parameters and the static model was updated to give a new KJC. Using the offset (tibial torsion: $\mu \pm \sigma = -14 \pm 7$) between the new knee flexion axis and the ankle flexion axis defined through the ANK and MML, an updated AJC was calculated when the static gait model was run for a second time.

For the OFM the HEE marker and STL-LCA mid-point were set to have the same vertical position as the TOE marker because during standing, the foot was assumed to be parallel to the

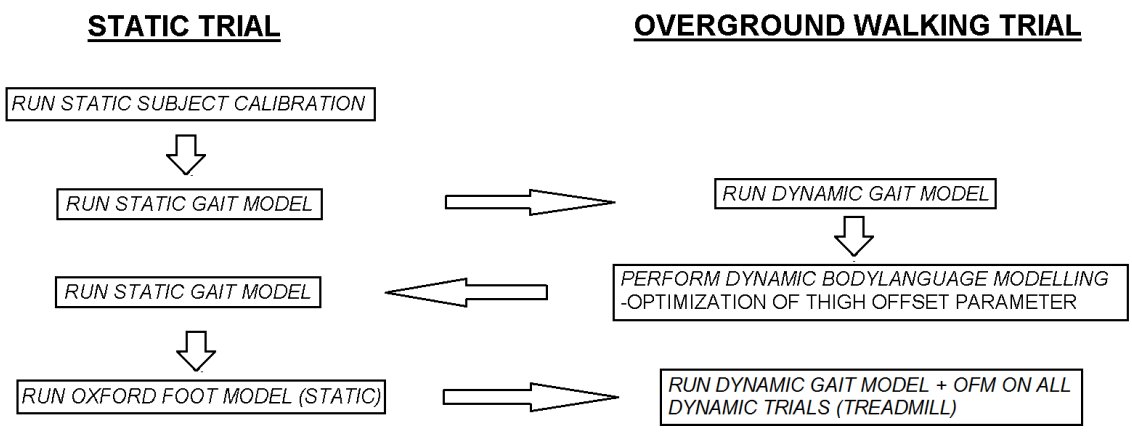


Figure 3.5.1: A summary of the subject calibration procedure in Vicon Nexus.

floor. The calibration process is summarized in Figure 3.5.1.

In the SD static trial, the mandatory parameters together with the BF optimized thigh offset parameter were set before the PiG static gait model parameters were calculated. Both models used the same tibia segment which in turn depended on the new femur orientation so, once the static offsets were calculated, the PiG and OFM parameters were (re-)calculated for the SD trials. The abduction/adduction angle traces were compared qualitatively for the optimized and zero thigh offset models to assess whether a smaller variance was clearly observed using the optimized thigh offset angle.

The optimization procedure which generated the offset parameters was performed for over-ground walking trials. The same parameters were then used for the SD model as the femur and tibia segment definitions (and the KJC and AJC) were the same.

3.5.2 Kinematics

The short treadmill running and walking trials were autolabeled in Vicon Nexus and checked throughout the trial to identify and eliminate errors. Gaps in the marker trajectories were automatically cubic spline filled if less than five frames and smoothed or filled using a marker on the same segment as a template if the predicted cubic spline filling was spurious. Data were

excluded where gap sizes were greater than 40 frames, if there was excessive flickering, or if moderate size (30-40 frames) gaps were repeated for each gait cycle. Other gaps were individually filled. A negligible amount of data was excluded. Where artefacts were observed, the source of the error was identified. Specifically, the trace of the distance between markers was checked for artefacts and compared with the motion of the markers in the virtual capture volume. Once the error was identified, the appropriate marker was either spline or template filled across the necessary frames or, where possible, reconstructed with custom written BodyBuilder code using other markers in the segment.

Angle data for the kinematic models were exported as text files. The marker trajectories from the 200 second trials were exported both filtered (using the Woltring filter) and unfiltered. Kinematic data was time normalized in MATLAB using an anti-aliasing (lowpass) finite impulse response filter to 101 points from 0% to 100% in 1% increments.

The O'Connor method [153] was used to identify the FS time using only filtered marker trajectory data. For this method, the velocity of the midpoint of the HEE and TOE markers (MP) is calculated using the finite difference method. The vertical MP velocity had a characteristic shape, with a local minimum corresponding to FS and a local maximum corresponding to TO. The algorithm searched for the maxima within a window size of the order the gait cycle time and then searched for minima within a window an order of magnitude smaller. To identify the correct minima, the vertical height of MP was constrained within 35% of the heel heights encountered during the trial. This successfully eliminated any local MP velocity minima during swing phase.

A modified version the Maiwald method [130] identified TO time using foot marker data. The algorithm identified the peak positive acceleration of the TOE marker (the original method uses a Hallux marker) which was also associated with a positive vertical HEE marker velocity.

3.5.3 Surface Electromyography (EMG)

The EMG signal was exported from Vicon Nexus unfiltered and in MATLAB, the raw EMG signal was band pass filtered (30 Hz to 400 Hz) to reduce noise and movement artefacts.

3.6 Summary

This chapter has presented the data collection methods and kinematic models used in this thesis. The kinematic models and post-processing techniques in this study were, as far as possible, based on clinically relevant models and procedures. Therefore, it is expected that clinicians and researchers alike find the replication of the methods, reproducibility, and interpretation of the results equally intuitive and accessible. The remainder of this thesis comprises studies to addresses the aims outlined in Chapter 1.

Chapter 4

Barefoot running kinematics for highly trained habitually shod runners

The aim of this chapter is to present and discuss the kinematics of BF running for uninjured, trained male and female runners. There is evidence in the literature to suggest particular FSS are associated with particular running kinematic characteristics [19,164,183]. These differences may be related to the elevated overall injury risk seen for RFS running [39]. We hypothesize, therefore, that in this observational, cross-sectional study there are a variety of FSS and that they are associated with statistically significant differences in running kinematics.

A sub-aim of this chapter is to compare the implications of classification based on a discrete, compared to continuous, parametrization of FSS, known as FSA. An accepted discrete FSS grouping [6] and a continuous parametrization, based on the global foot segment orientation, are used.

Male and female runners' kinematics are analysed in this chapter and known gender effects on SD running kinematics [60] are investigated here as a function of anatomical parameters. In particular, the hypothesis that a larger hip width to femur length ratio (h:f) found in females [209] is associated with larger amounts of hip adduction, is tested.

4.1 Introduction

Studies which have investigated FSS and the effects of different FSS have tended to categorize runners into discrete groups according to one of three landing strategies: RFS running landing with the heel first, midfoot-strike running landing with the foot flat on the ground and FFS or toe [152] running landing on the ball of the foot. In some studies [4], the definition of FSS has been based on kinetics and the presence or absence of an impact peak, which is a fundamentally flawed approach given vertical ground reaction force impact peaks have been observed for both habitual FFS and habitual RFS runners [202]. Foot-strike strategy exists as a continuous function and it has recently been suggested that classifying runners into discrete groups might be too simplistic [6, 31, 195]. Altman and Davis [6] recently defined a measure referred to as FSA, which presents a continuous quantification of FSS and provides the ability to assess gradations of strike patterns. The FSA is the angle of the sole of the foot with respect to the ground. Exploring the relationship between running kinematics and the FSA as opposed to FSS might allow for a better understanding of the implications of FSS on running injury biomechanics. Recent work looking at SD running has suggested that RFS running is associated with an elevated overall injury risk [39] but also that changing FSS may predispose runners to different types of injuries [19].

In the present work, kinematic parameters which summarize running gait kinematics and are comparable to previous literature are measured in a sample of highly trained distance runners. Furthermore, the inferences and implications for continuous (FSA) and discrete (FSS) parametrizations of FSA are discussed and compared here. It was hypothesized that a continuous parametrization has higher statistical power because of better accuracy in quantifying FSS, and that rearfoot plantarflexion at FS, rearfoot angular velocity at FS and peak rearfoot dorsiflexion velocity would be strongly correlated with the FSA and FSS, where FSS is split as

RFS and non-rearfoot strike (NRFS) running. Based on the assumption that the FSA does not influence kinematics in this highly trained population, no other significant differences related to the FSA were anticipated. To increase statistical power, speed matched data from highly trained female runners [120] was included in this study. Therefore, because the subject group in this study included both male and female runners, known gender differences between lower-limb joint angles during running [60, 209] were investigated. It was hypothesized that peak hip adduction angle would differ significantly between genders because of differences in h:f between males and females [209]. The effect of gender was tested for in all statistical tests pertaining to the main questions posed in this chapter. Therefore, in cases where gender was not a significant effect, adding data for female subjects necessarily increased the statistical power.

4.2 Methods

4.2.1 Subjects

The subject inclusion and exclusion criteria for the male subjects have been previously described (Section 3.1). Female subjects were also included for analysis. The female data formed part of a previous study in the same laboratory [120] and the inclusion and exclusion criteria were similar. The differences were that female subjects had run a minimum of 32 kilometres week^{-1} for at least six weeks prior to testing (males ran at least 40 kilometres week^{-1}) and could sustain a pace of 3.58 ms^{-1} for at least ten minutes (males had to be able to run at 4.44 ms^{-1} for ten minutes). The minimum running distance and speed criteria were specified to ensure that only athletes of a competitive standard were included in the study and that all participants were injury-free at the time of testing. The exclusion criteria were the same as previously described (Section 3.1).

4.2.2 Experimental data collection and data processing

Kinematic data for the female subjects running BF were collected as follows: subjects were asked to familiarize themselves with the treadmill, before the treadmill velocity was gradually increased to 2.96 ms^{-1}, at which point thirty strides were recorded. The treadmill velocity was then increased gradually to 3.33 ms^{-1} and another thirty strides were recorded. The process was repeated again at 3.58 ms^{-1}. The data used in the following analysis came from the recording of thirty strides at 3.58 ms^{-1}. The fitness levels of both female and male athletes were considered to be high. Therefore the difference in data collection protocol was assumed to not effect kinematics because the procedure did not induce fatigue in either gender, and all subjects were given time to familiarize themselves with the treadmill. The data processing procedure for the male and female subjects up to the point of extracting the joint angles from Vicon Nexus software, including calculation of FS and TO time was identical, and has been described elsewhere (Section 3.5.2).

One velocity of 3.58 ms^{-1} was used for analysis because it was the single common velocity recorded in both studies. The addition of the female gait data facilitated an increase in sample size to improve statistical power and the inclusion of females allowed for a gender comparison.

4.2.3 Data analysis

For all subjects the leg on which one stands when kicking a football was used for analysis to reduce heterogeneity in kinematics [10]. All discrete parameters presented were calculated in the time domain, prior to any temporal normalization. For visualization, stance phase angle trajectory data were time normalized using an anti-aliasing zero lag low-pass finite impulse response filter to 51 points that represented 0 to 100% of the stance phase. To remain consistent with the literature, event timings are presented as a percentage of stance phase, but they were

also calculated in the non-normalized time domain. The development of chronic injuries is believed to occur because of the repetitive loading of the musculo-skeletal system during weight bearing. Therefore, kinematic analysis is limited to stance phase, in accordance with previous literature [18, 125, 164, 183, 188, 190, 208].

It is customary in clinical gait analysis to use a representative gait cycle for analysis. With this method it is important to first assess observed within-subject variability to exclude data exhibiting artefacts imposed by the signal processing routines when it smoothed the marker trajecory data. For each subject, between fifteen and thirty-one consecutive (and sequential) and time-normalized stance phases were visually checked for consistency and any data with sharp discontinuities, which were physically implausible, were rejected from further analysis. Data were qualitatively checked, based broadly on knowledge of reported results in literature, for consistency in peak values, range of motion (ROM) and time to peak value. For the comparison of FSS classification methods, a representative trial for each subject was selected and all subsequent statistical analyses were performed on the representative trial, including calculation of the between-subject kinematic variability. The representative trial was selected with the Selection Method for a Representative Trial (SMaRT) method [181], using eleven angles from the hip (three), knee (two; the knee rotation angle was omitted), rearfoot relative to tibia (three) and forefoot relative to rearfoot (three). The Oxford Foot Model (OFM) knee rotation angle was omitted because the measurement is considered unreliable and furthermore, the thigh offset optimization (Section 3.4.6.1) was applied to the frontal plane angular trajectory, which further altered the knee transverse plane angular trajectories. Briefly, for a given subject with n time normalized gait cycles, the SMaRT method applies a principal component analysis for the j^{th} angle for each gait cycle separately, outputting $n-1$ principal components for each of the n trials. Then, for the j^{th} angle, the median of each of the $n-1$ principal components is calculated across all n trials. Finally, for each of the n gait cycles, the Euclidean distance to the median

Temporal parameters	
Stance time	Duration of stance phase (s).
Stride time	Duration of one stride (s).
Stance period	Stance duration as a percentage of the gait cycle (% gait cycle).
Cadence	Number of strides s^{-1}.
Discrete kinematics variables	
FSA	Foot segment angle (relative to treadmill) at FS.
θ_{FS}	Joint angle at FS (deg).
θ_{TO}	Joint angle at TO (deg).
θ_{peak}	Maximum joint angle (deg).
$t_{\theta-peak}$	Time of maximum joint angle (% stance).
θ_{exc}	Joint ROM between FS and peak (deg).
ω_{FS}	Joint angle velocity at FS (deg s^{-1}).
ω_{TO}	Joint angle velocity at TO (deg s^{-1}).
ω_{peak}	Maximum joint angle velocity (deg s^{-1}).
$t_{\omega-peak}$	Time of maximum joint angle velocity (% stance).

Table 4.2.1: Temporal parameters and discrete kinematic variables used to quantify lower limb joint kinematics during running.

principle component score is calculated for the j^{th} angle and summed across all the angles. The representative trial chosen was the trial with the smallest summed distance. Using this method, the data used in the following analysis pertains to a real, measured gait cycle, rather than a virtual one.

For each trial, the parameters given in Table 4.2.1 were calculated and the discrete kinematic variables were calculated for each joint angle.

4.2.4 Foot-strike strategy

The heel and toe markers defined the foot segment and the FSA was defined relative to the treadmill surface. In the global coordinate system the treadmill inclination was defined by two markers placed adjacent to the moving belt. To allow for the calculation of FSA, the inclination of the moving belt was assumed to be the same as the inclination defined by the two stationary markers.

Participants' FSS was classified according to the FSA [6] relative to the treadmill and a RFS was defined as a FSA greater than 8° of dorsiflexion relative to the treadmill surface. This cut off was derived from the correlation between strike index and FSA observed by Altman and Davis, such that greater than 8° of dorsiflexion related to striking with the posterior third of the foot. Strike index is a measure of which part of the foot contacts the ground and is quantified with pressure sensors. A strike index between 0% and 33% corresponds to initial contact with the posterior third of the foot (RFS), 33% to 66% corresponds to the middle third (midfoot strike running) and 67 to 100% corresponds to the anterior third (FFS) of the foot. For a FSA less than or equal to 8° of dorsiflexion, the FSS was defined as a NRFS. Thus, the NRFS category contained both mid- and FFS runners. The FSA for the representative trial was used for the formal classification of FSS.

4.2.5 Anatomical parameters

To account for known anatomical differences between genders [93], the subject specific inter-asis distance and femur length, calculated from real and virtual markers, were used to derive the hip-width-to-femur-length ratio (h:f) as the hip width divided by the femur length.

4.2.6 Statistical analysis

Statistical analysis was performed using MATLAB (MATLAB version 2013b, MathWorks Inc., Natick, MA, USA).

4.2.6.1 Exploratory analysis

Box plots, the median values and the inter-quartile ranges were used for exploratory analysis. Two sample t-tests with unequal variance were used to compare between genders for the temporal parameters and for FSA. To test for normality of distributions, the Shapiro-Wilk test

was applied. To retain statistical power ($\pi > 0.80$) given the small sample size ($n = 27$), the significance level, α, was set conservatively at 0.1.

4.2.6.2 Statistical testing for kinematics

To test for statistical effects of FSA and gender on kinematic variables of interest, for each dependent variable, θ, a multiple linear regression model was used to investigate the effect of the FSA and gender (Equation 4.2.1).

$$\theta_i = \beta_0 + \beta_{FSA} FSA_i + \beta_G G_i + \beta_{FSA:G} (FSA : G)_i + \varepsilon_i \tag{4.2.1}$$

where β_0 is the intercept and thus population mean, FSA_i and G_i are the FSA and gender respectively (male is 0, female is 1) for the i^{th} subject and β_{FSA} and β_G are the corresponding regression coefficients. The parameter $\beta_{FSA:G}$ is the regression coefficent for the interaction term between FSA and gender and $(FSA : G)_i$ is the corresponding interaction term for the i^{th} subject. Finally ε_i is the measurement error for the i^{th} subject. From this saturated model, at each step of the analysis a single term (deemed non-significant if $p \geq 0.1$) was removed (taking the hierarchy of interactions into account). The model was re-fitted (with this term removed) to the data and the process repeated. This continued until the most parsimonious model was reached. Studentized residuals, calculated by dividing a residual by an estimate of its standard deviation, were used for model diagnostics. Diagnostics were performed with the final model to identify potential non-observations, defined loosely as influential outliers. Influential points were defined as those with a Cook's distance [36] greater than $4n^{-1}$, where n is the number of observations in the sample. The Cook's distance is an estimate of the influence of a data point when performing a least squares regression, which measures the effect of deleting an observation. It may be interpreted as the distance one moves in the confidence ellipsoid that represents the region of plausible values of parameters. The significance for identifying

a potential outlier was set as $\alpha = 0.05$ and a Bonferroni correction was applied to account for repeated measures [54]. Where non-observations were identified, the model was re-fitted (with the observation removed) and the process was repeated until no points were considered non-observations. The Shapiro-Wilk test for normality was performed to check for normality of the residuals. Where the normality condition was not satisfied, the results were flagged but not rejected. This is because we are not interested in accuracy of the regression coefficients *per se*, but mainly their statistical significance (or lack thereof). The same process was repeated for the discrete parametrization, FSS. For this β_{FSA} and FSA were replaced by β_{FSS} and FSS, where RFS is 1 and NRFS is 0 respectively. To account for kinematic parameters being drawn from the same part of the gait curve, Bonferroni corrections were applied. Specifically, for θ_{FS}, θ_{peak} and θ_{exc}, the significance level for each parameter was set to 0.033. For ω_{FS} and ω_{peak}, the significance level was adjusted to $p = 0.05$. The significance level for θ_{TO}, ω_{TO}, $t_{\theta-peak}$, and $t_{\omega-peak}$ remained at $p = 0.10$. Finally, the adjusted Pearson's correlation coefficient, R^2_{adj}, provided a metric to compare the model goodness of fit for each classification method.

4.2.6.3 Logistic regression on injury rate data

A logistic regression was used to assess the correlation between the predictors FSA and FSA variability, and a response of probability of sustaining a running-related injury. A logistic regression was used because the outcome (injured or uninjured) was binary. The definition of injury was the same as the exclusion criteria (Section 3.1) and a subject became injured if they sustained an injury at any point within twelve months of the data collection. A summary of the subsequent injuries is given in Appendix C.1. To remain consistent with all statistical analyses in this chapter, the representative FSA was used for each subject, and the standard deviation σ of the measured FSA was used to quantify variability. The logistic regression model for the

probability of injury for the i^{th} subject was

$$\Pr(\text{Injury}_i) = \frac{1}{1+e^{-[\beta_0+\beta_1 \mathbf{X_i}]}}$$

$$\beta_1 = \begin{bmatrix} \beta_{FSA} \\ \beta_\sigma \\ \beta_{FSA:\sigma} \end{bmatrix} \text{ and } X_i = \begin{bmatrix} FSA_i \\ \sigma_i \\ (FSA:\sigma)_i \end{bmatrix}$$

where β_σ was regression coefficient for FSA variability, $\beta_{FSA:\sigma}$ was the regression coefficient for the interaction term, and $(FSA:\sigma_i)$ was the interaction term for the i^{th} subject. To calculate the odds ratio for a particular variable, coefficients in the model must be exponentiated.

The C-statistic [86], equal to the area under a receiver operator curve, was used as a measure of goodness of fit for the logistic regression. The range of the statistic is $[0.5, 1.0]$, where 0.5 indicates a poor model and 1.0 indicates a perfect prediction model.

4.3 Results

Following visualization of the data, trials were removed for three male subjects: MD (2 of 17 trials), MG (5 of 27 trials) and MM (2 of 20 trials) owing to the presence of artefacts in the angular trajectories.

4.3.1 Subjects

Twenty-seven habitually SD competitive distance runners took part in this study (Table 4.3.1). One male subject described himself as ambidextrous but a test identified his preference to kick a football whilst standing on his left leg.

Subject demographics	**Male**	**Female [120]**
Number of participants	19	8
Age (year)	23 ± 3	24 ± 8
Height (m)	1.78 ± 0.06	1.69 ± 0.10
Weight (kg)	64.8 ± 6.6	55.6 ± 7.8
Running volume (km week^{-1})	86.2 ± 23.9	54.4 ± 16.1

Table 4.3.1: The mean and standard deviation of male and female demographics

4.3.2 Foot-strike strategy

A variety of FSS were employed by the study group and on an individual level some subjects exhibited high variability in their FSS. The orientation of the treadmill with respect to the global x-y plane was 0.85°. From the representative trial the discrete FSS grouping identified eleven RFS runners (eight male, three female) and sixteen NRFS runners (eleven male, five female) and in the sample of representative trials the FSA was normally distributed (p = 0.99) with mean 6.90° and standard deviation 7.81°. When analysing all gait cycles 33% of subjects (eight males, one female) exhibited both RFS and NRFS foot strikes. For 93% of subjects, the FSS for the representative trial was in agreement with the most common FSS across all measured gait cycles. Only two subjects, MM and MS, showed disagreement. Analysis of the subject-specific FSA variability suggested that FSA was, on the whole, repeatable, and the inter-quartile range was independent of FSA. However, exploratory analysis identified three subjects: MC, MF, and MG as outliers (Figure 4.3.1). There was no difference in FSA between genders (p = 0.77).

4.3.3 Kinematic variability

The joint angle and angular velocity trajectories for the measured stance phases were used to confirm that qualitatively, subject gait was repeatable across the gait cycle (Figure 4.3.2). Between-subject variability was higher than within-subject variability (Tables 4.3.2 and 4.3.3). Generally, within-subject mean joint angle variability was low (< 2°) (Table 4.3.2). Within-

	θ_{FS} (deg)	θ_{TO} (deg)	θ_{peak} (deg)	$t_{\theta-peak}$ (s)	θ_{exc} (deg)
Hip flexion	40.0† (5.5) [1.3]	-7.4*† (6.3) [1.1]	40.0 (5.5) [1.3]	1.1 (6.0) [0.4]	-47.5*† (5.7) [1.3]
Hip adduction	3.6† (3.5) [1.1]	-5.8†‡ (2.8) [0.7]	7.3*† (4.3) [1.1]	33.7 (12.8) [4.7]	3.9* (2.5) [0.8]
Hip internal rotation	-11.0 (6.7) [2.1]	-3.7 (5.4) [1.2]	2.5 (5.4) [1.3]	48.7 (29.5) [10.8]	13.6 (6.2) [2.3]
Knee flexion	15.7 (3.0) [1.4]	9.8†‡ (5.1) [1.3]	39.0 (3.8) [1.3]	40.9*† (3.4) [1.3]	23.3 (3.7) [1.5]
Knee abduction	1.3 (3.1) [0.6]	3.6 (3.1) [0.3]	-1.2 (4.0) [0.7]	39.5 (23.3) [5.7]	-3.9 (2.7) [0.7]
Rearfoot dorsiflexion	-4.0* (10.9) [1.4]	-17.6* (7.5) [1.4]	13.8* (7.0) [0.8]	54.1†‡ (3.4) [1.4]	18.9* (4.8) [1.2]
Rearfoot adduction	1.6 (7.7) [0.9]	0.4 (6.2) [0.7]	-10.2 (6.7) [0.7]	40.7‡ (6.6) [5.1]	-12.0 (4.1) [1.1]
Rearfoot inversion	11.9 (7.3) [1.1]	12.8 (6.5) [1.1]	-4.2 (6.5) [1.0]	46.7† (7.7) [3.4]	-16.3 (5.1) [1.4]
Forefoot dorsiflexion	-5.1 (6.6) [0.7]	-8.1*† (7.7) [0.8]	10.2 (6.7) [0.5]	59.9† (8.3) [2.8]	15.5*† (4.5) [0.8]
Forefoot abduction	0.0*† (7.5) [0.7]	3.6† (7.5) [0.8]	-6.2 (6.5) [0.6]	54.4 (16.9) [7.6]	-6.6*† (3.0) [0.9]
Forefoot inversion	6.0* (5.8) [0.8]	5.1 (5.7) [0.7]	2.0 (5.2) [0.7]	35.4 (27.6) [9.5]	-4.2* (2.8) [0.9]

Table 4.3.2: Kinematic results: the group mean (n = 27), group standard deviation (curved brackets) and group mean within-subject variation [square brackets] for kinematic variables are presented. The group standard deviation was calculated as the standard deviation of the representative trials (one per subject) whilst the group mean within-subject variation was calculated as the mean of the standard deviation per subject. *, † and ‡ denote significant main effects of FSA and gender and an interaction effect respectively at $p < 0.10$, following Bonferroni correction (Section 4.2.6.2).

	ω_{FS} (deg s^{-1})	ω_{TO} (deg s^{-1})	ω_{peak} (deg s^{-1})	$t_{\omega-peak}$ (s)
Hip flexion	-147† (52) [17]	-161* (63) [22]	-40*† (60) [18]	33.3 (24.6) [9.5]
Hip adduction	15* (42) [13]	-45† (44) [12]	70*† (42) [15]	21.0 (8.5) [4.5]
Hip internal rotation	215 (196) [73]	-161 (79) [37]	354 (162) [56]	12.6 (13.1) [7.6]
Knee flexion	170 (73) [27]	-99† (115) [35]	390*† (92) [24]	20.8† (3.3) [1.7]
Knee abduction	14 (57) [22]	-33 (35) [10]	-119 (61) [25]	36.5 (22.4) [9.7]
Rearfoot dorsiflexion	-1* (107) [28]	-414*† (105) [32]	282* (77) [20]	24.8*‡ (6.1) [2.0]
Rearfoot adduction	-91* (83) [25]	-15 (82) [22]	-232 (82) [24]	20.4* (17.0) [5.0]
Rearfoot inversion	-73†‡ (103) [37]	115† (119) [32]	-309† (109) [35]	21.5 (6.2) [1.9]
Forefoot dorsiflexion	40* (46) [20]	-254† (84) [24]	224*† (71) [15]	24.8* (8.2) [3.4]
Forefoot abduction	-33 (69) [24]	85* (63) [24]	-128* (65) [18]	28.0 (22.0) [7.5]
Forefoot inversion	-58 (84) [27]	-19 (48) [20]	-126 (62) [20]	30.5 (36.9) [12.6]

Table 4.3.3: Kinematic results: the group mean (n = 27), group standard deviation (curved brackets) and group mean within-subject variation [square brackets] for kinematic variables are presented. The group standard deviation was calculated as the standard deviation of the representative trials (one per subject) whilst the group mean within-subject variation was calculated as the mean of the standard deviation per subject. *, † and ‡ denote significant main effects of FSA and gender and an interaction effect respectively at $p < 0.10$, following Bonferroni correction (Section 4.2.6.2).

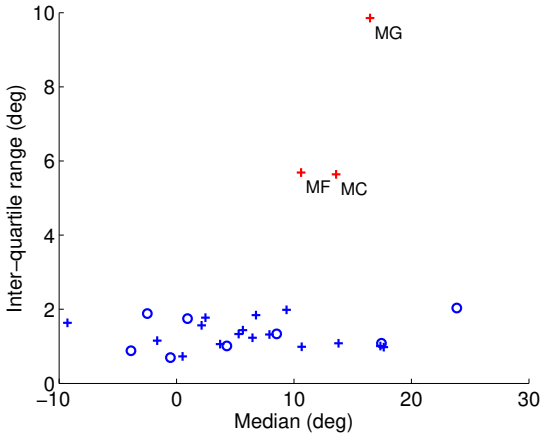
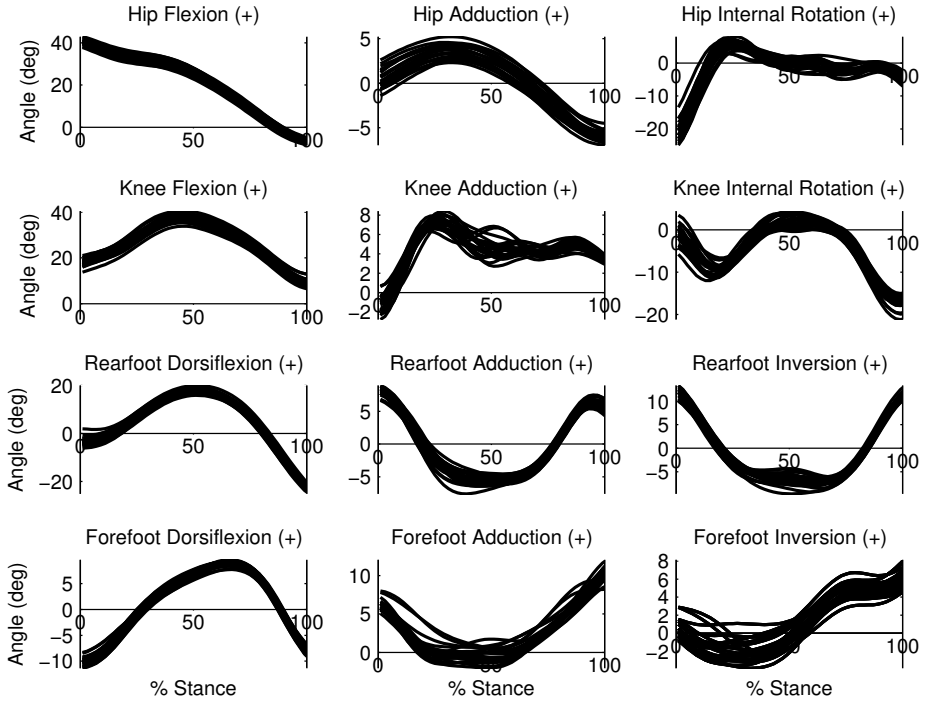


Figure 4.3.1: In general the FSA was repeatable for male (pluses) and female (circles) subjects but, three subjects (red) showed high stride-to-stride variability compared to the rest of the group (blue).

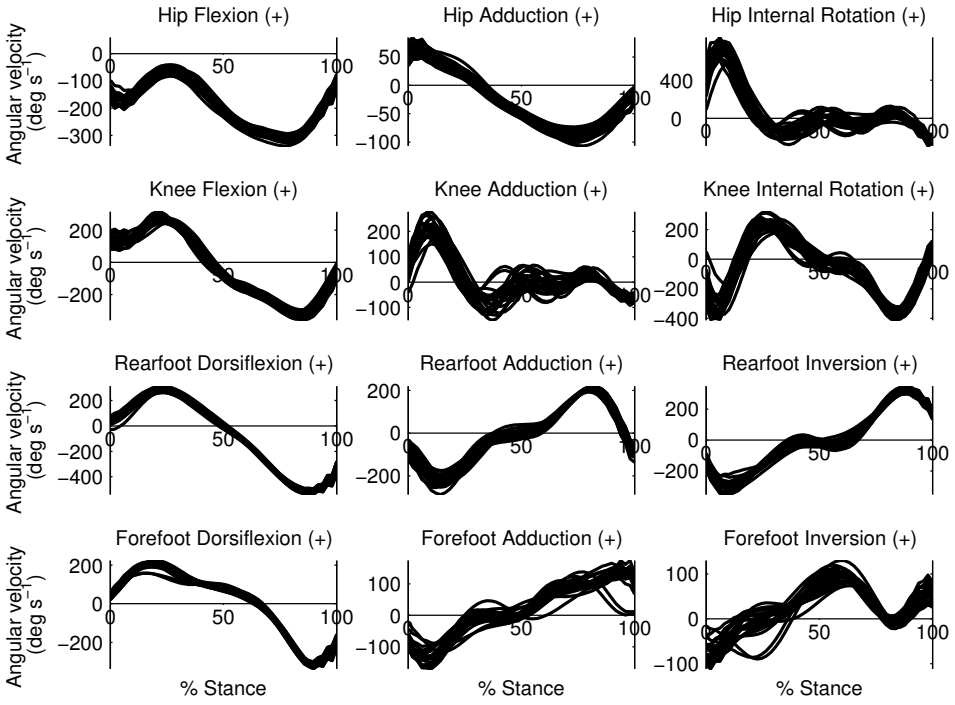
subject variability was high (> 50 deg s^{-1} or 10% stance) for the hip rotation (ω_{FS}, ω_{peak} and $t_{\theta-peak}$) (Table 4.3.3) and forefoot inversion ($t_{\theta-peak}$ and $t_{\omega-peak}$). This variability may be explained for some subjects by the presence of multiple maxima in the data.

Between-subject variability was high for hip rotation (ω_{FS} and ω_{peak}), rearfoot dorsiflexion (θ_{FS} and ω_{FS}) and rearfoot inversion (ω_{FS} and ω_{peak}). The hip joint variability follows from the high within-subject variability. Between-subject variability of rearfoot motion demonstrates the variation in FSS and subsequent motion during early stance phase in this sample. Variability between subjects in $t_{\theta-peak}$ and $t_{\omega-peak}$ was high (> 15 % stance) for hip flexion ($t_{\omega-peak}$), hip internal rotation ($t_{\theta-peak}$), knee abduction ($t_{\theta-peak}$ and $t_{\omega-peak}$), rearfoot adduction ($t_{\omega-peak}$), forefoot abduction ($t_{\theta-peak}$ and $t_{\omega-peak}$) and forefoot inversion ($t_{\theta-peak}$ and $t_{\omega-peak}$). Knee abduction was highly variable between subjects, possibly because of the thigh wand marker optimization procedure and the OFM was used, and was therefore excluded from further statistical analysis. Two subjects, MF and MG, showed high stride-to-stride variability for time to peak forefoot abduction and inversion. Forefoot motion data for these subjects were excluded from further statistical analyses owing to their lack of repeatability.

Time series data from representative trial angular trajectory (Figure 4.3.3a) and angular



(a) Joint angle trajectories for subject MO



(b) Joint angle velocity trajectories for subject MO

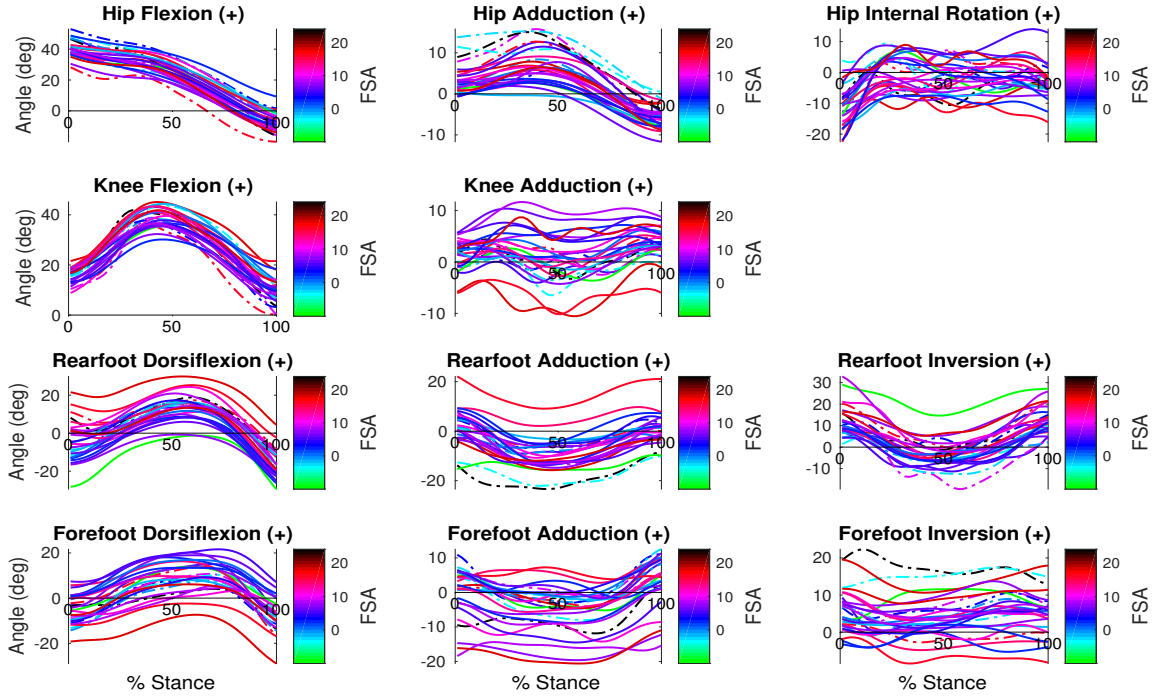
Figure 4.3.2: Within-subject variability shows stride-to-stride repeatability

velocity (Figure 4.3.3b) qualitatively demonstrate some of the kinematic changes with FSA.

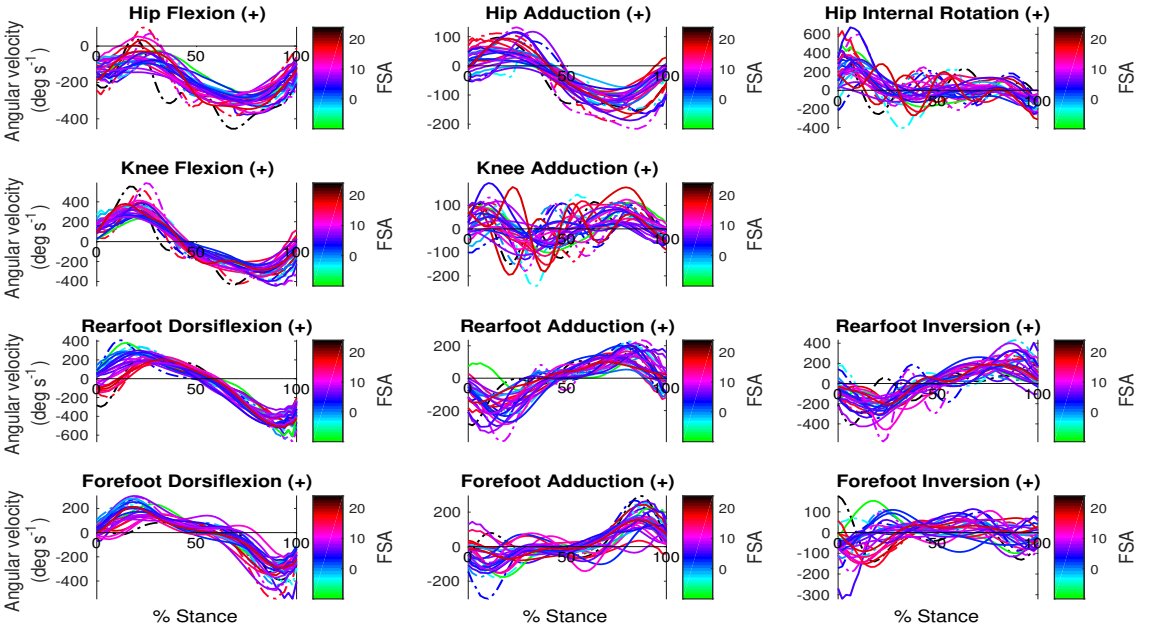
4.3.4 Comparison of the FSA and FSS

Both FSA and FSS were significant main effects for temporal differences and kinematic differences at the hip, knee, rearfoot and forefoot. Stance phase as a proportion of the gait cycle increased with more dorsiflexed foot contact (FSS: $p = 0.041$; FSA: $p < 0.001$). The continuous parameterization found that stance phase duration increased with more dorsiflexed FSA ($p = 0.005$). Associations for kinematics were most evident for sagittal plane angle and angular velocity parameters for motion at knee, rearfoot and forefoot, with changes also for hip frontal plane motion. These kinematics are associated with movement typically related to the loading response. As hypothesized, both parameterizations showed significant effects for rearfoot dorsiflexion at FS (FSS: $p < 0.001$; FSA: $p < 0.001$), rearfoot peak dorsiflexion (FSS: $p = 0.006$; FSA: $p = 0.002$) and rearfoot dorsiflexion velocity at FS (FSS: $p < 0.001$; FSA $p < 0.001$). A more dorsiflexed FSA was associated with more rearfoot dorsiflexion at FS and TO, increased peak rearfoot dorsiflexion, less rearfoot dorsiflexion ROM and slower and later peak rearfoot dorsiflexion velocity. Initial forefoot dorsiflexion did not vary with FSS or FSA. In general elsewhere in the sagittal plane, changes in forefoot motion mirrored those of rearfoot motion.

The continuous parametrization FSA was statistically more powerful than the discrete parameterization. Analyses identified main effects of FSA on transverse plane rearfoot motion, with an interaction between FSA and gender for frontal plane motion. The presence of interaction effects implies that the effect of FSA is dependent on gender. More dorsiflexed FSA was associated with faster rearfoot eversion ($p < 0.004$) (females only) and faster rearfoot abduction ($p = 0.009$) velocities at FS. At the forefoot more dorsiflexed FSA was associated with more forefoot inversion at FS ($p = 0.013$), more forefoot eversion ROM ($p < 0.001$), less forefoot abduction ROM ($p = 0.014$) and slower peak forefoot abduction velocity ($p < 0.001$). More dor-



(a) Angular Trajectory



(b) Angular Velocity

Figure 4.3.3: Representative trial kinematics for both male (solid line) and female (dash-dot line) subjects and for each joint angle. Data is colour coded with respect to FSA.

siflexed FSA was also a main effect for faster hip peak adduction velocity ($p = 0.018$) and more hip adduction ROM ($p = 0.005$) but FSS was not. Overall, FSA was a significant main effect for 33 kinematic and two temporal parameters, whereas FSS was a significant main effect for 25 kinematic and one temporal parameter. For FSA and FSS, six and nine kinematics parameters respectively had a significant interaction effect. Significant interactions (Equation 4.2.1) were identified with both parameterizations for five parameters: hip adduction at TO (FSS: $p = 0.069$; FSA: $p = 0.076$), knee flexion at TO (FSS: $p = 0.012$; FSA: $p = 0.033$), time to peak rearfoot dorsiflexion (FSS: $p = 0.041$; FSA: $p = 0.047$), time to peak rearfoot abduction (FSS: $p = 0.011$; FSA: $p = 0.081$) and rearfoot inversion velocity at FS (FSS: $p < 0.001$; FSA: $p = 0.005$).

Where both were significant main effects, FSA was more significant 65% of the time (13 out of 20). FSS was more significant generally for angular velocity parameters, where the fine detail of FSA may be too precise and suffer from overfitting. Where FSA or FSS was significant, using the measure R^2_{adj}, on average FSA (40%) and FSS (38%) account for similar amounts of variation.

4.4 Discussion

Temporal and kinematic parameters were assessed in a group of uninjured male and female runners in order to quantify normal BF running gait in habitually SD runners. Between and within subject variation was observed for the kinematic variables FSA and FSS, and significant effects of FSA and gender on kinematics were observed for kinematics of the hip, knee, rearfoot and forefoot. The objective continuous parametrization was statistically superior. Whilst the continuous parametrization provided a better model fit in most cases, as quantified by R^2_{adj}, it was not significant. Nevertheless, this confirms the hypothesis that changes in FSA are associated with kinematics changes and motivates its inclusion as an independent variable when comparing BF

and SD running.

4.4.1 Kinematic variability

Typically, individuals are classified according to FSS, but this may not be appropriate for all subjects. Most classifications are done in shoes by virtue of the fact that most runners run in shoes and overground. However, when classifying in the BF condition individuals may be categorized differently. We generally see RFS running in shoes but not necessarily in the BF condition [114].

Leiberman *et al.* [125] studied a group of habitually SD runners who were all SD RFS runners and 88% of the runners were classified as RFS runners for BF running. This is a higher proportion than the observation here where 41% of runners were RFS BF runners. This difference may arise because of the differences in competitive standard, surface (treadmill versus overground), and running velocity.

Assigning a specific FSS to a given subject implicitly assumes that a repeatable strike pattern exists, and extrapolates the given classification to all analyzed gait cycles. The results here suggest that for some subjects such an extrapolation is inappropriate. Following discrete classification 33% of subjects exhibited both RFS and NRFS running patterns across the strides in the data set and even with the continuous classification, the variation in FSA was uncharacteristically large for 11% of subjects when compared to the entire study group. Even under tightly controlled conditions in a homogeneous group, a subset of the population may be classified as either RFS or NRFS runners depending on which gait cycle(s) are used for analysis. Studies which classify FSS attempt to address this issue by classifying a subject according to the most repeatable FSS [39, 69] or by including kinetic parameters within the definition of RFS or NRFS [4, 69]. Such parameters include the presence or otherwise of an impact peak for RFS runners or the location of the centre of pressure (on the heel for RFS). The inclusion of the

presence or absence of an impact peak is inappropriate when studying habitually SD runners because the absence of an impact peak has only been observed for habitually BF FFS runners whilst in the BF condition [122]. Because kinetic data during treadmill running was not measured here, the behaviour of kinetic parameters could not be studied to support or contradict the assumptions made in other work.

Many other studies limit their sample to only RFS runners [60, 189, 190, 208]. Whilst this may appear biased, these studies generally look at only SD running. It may be that the present study group are mostly RFS runners when SD and therefore may not have been omitted from other studies. Regardless, it is still unsatisfactory to omit healthy runners from studies if one seeks to characterize a sample representative of the trained runners, given the higher prevalance of NRFS in the trained population. It is not reasonable to assume habitually SD NRFS runners are outliers, as is implicit when only RFS runners are studied. By including more subjects and using methods from population modeling, a more accurate description of the population is obtained. The difficulty of defining one FSS is partially addressed by using the objective measure FSA and considering the distribution of FSA and hence an appreciation of the variability. Some individuals exhibit large variations in FSA - an observation which may be biomechanically relevant. In the present study two groups may be tentatively identified: one with high variability and one with low variability in FSA. Variability for habitually SD runners [124] is similar in magnitude to the 'low variability' group here. De Wit *et al.* [43] suggested that a runner orients their foot to limit local heel pressure. Whilst subject-specific tolerance of local heel pressure and different amounts of proprioceptive feedback may explain why different individuals choose different FSAs, significant changes in variability of FSA are less intuitive to explain. Subjects with high variability may fail to consistently control for plantar surface pressure, hence explaining why some individuals find BF treadmill running uncomfortable. One subject who showed high variability in FSA (MC) expressed without prompting that BF treadmill running was par-

ticularly stressful and uncomfortable. Further work measuring subjective comfort levels and plantar pressure would be of value in developing this idea further. If comfort was a relevant factor, one may anticipate that in the habitually SD condition, FSA variability would be consistently low across the entire study group for SD running especially. An alternative explanation to the higher FSA variability is that artefacts exist in the trajectory of either the TOE or HEE marker at FS, but this is unlikely.

Foot-strike angle did not correlate with injury rate (Table 4.4.2), but it is already clear that FSA variability is an important factor in any discussion of FSA or FSS. Furthermore, a decrease in the complexity[1] of FSA time series for SD running has recently been associated with injury [131]. Variability and complexity are different concepts: variability is typically quantified by some linear measure of variation which does not depend of the sequence of a time series, whereas as complexity [131] measures do depend on the times series sequence. Individuals with low FSA variability and high complexity are less susceptible to injury than high variability runners. Although this may appear counter-intuitive, it is important to acknowledge that complexity and variability are not the same concepts. The observed high variability in this study may reflect the motor control system (MCS) failing to adapt to BF running effectively. An adaptation in the motor control system may become observable because of the perturbation from switching to BF running, and these adaptations may reflect a propensity for running-related injury.

Subject gait was repeatable. Using a representative trial has merit if we wish to look at typical gait behaviour and use real data. However, it is imperative to visually check multiple strides for consistency before identifying a representative trial as not all individuals show repeatability everywhere. To avoid taking a summary statistic per subject, statistical analyses which account for repeated measures would be an improved method (Chapter 5). This would also avoid the over simplification of FSS behaviour in particular.

[1]Complexity, as quantified by detrended fluctuation analysis, is a measure of the self-similarity of a time series and therefore necessarily depends of the sequence of the time series.

4.4.2 Comparison with previous literature

There are temporal and kinematic differences between the current study and previous work on BF running [18,43,125,164,183,188,190,208], many of which may be readily explained given hypotheses presented in the literature. In the context of the previous work, results presented here appear valid. The differences in temporal parameters between studies may be explained by the different velocities, surfaces and subject running background in each study. Shih *et al.* [183] captured data at significantly slower velocities (2.5 ms^{-1}) for untrained runners instructed to run with a particular FSS, whilst Bonacci *et al.* [18] studied significantly faster overground velocities (approximately 4.6 ms^{-1} on average) for trained runners. With the work here included, across the studies as velocity increases, cadence and stride length increase. Squadrone [188] studied experienced BF runners who appear to have a significantly higher cadence and shorter stride length at comparable velocities. This may be a long term adaptation of habitually BF runners to the BF condition which reduces loads and may therefore protect the runner from injury [5,43,57,79,89,92]. Recent work by Boyer *et al.* [19] in the SD condition, which controlled for stride length and FSS in trained runners, associated decreases in stride length with a change in biomechanical parameters which indicated a reduction in injury risk. They suggest that changes due to FSS predispose runners to different types of injury and changes due to stride length are responsible for the changes in overall injury risk.

The Lieberman study [125] may show differences in FSA, ankle dorsiflexion and knee flexion angle at FS because statistical analyses were performed on very specific groups running overground: habitually BF FFS runners at 3.9 ms^{-1}; habitually SD RFS runners at 4.0 ms^{-1}; and habitually SD Kenyan adults running at 5.9 ms^{-1}. Significant differences between overground and treadmill running are found at velocities above 5.0 ms^{-1} [207] so caution is necessary when directly comparing the kinematics of the Kenyan runners to the other group running at slower speeds. Nevertheless, the increased velocity may explain the increasingly anterior foot

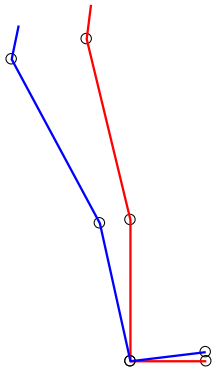


Figure 4.4.1: Stick figure representing body alignment from the present study at FS (blue) compared to Williams *et al.* [208] (red). There is a significant difference in hip flexion between studies.

landing observed for Kenyan compared runners to others. For the other two conditions, whilst comparable with respect to velocity, the statistical analyses are applied only to the habitually SD RFS runners and habitually BF FFS runners. The present study did not select one type of FSS for BF running so, by definition, one would anticipate the differences observed between the present study and the results from Lieberman. Lieberman argues that habituation to BF running affects FSA and therefore the external loading. Once again familiarity with BF running may be relevant for discerning differences between the current study and the studies by Lieberman *et al*. The De Wit [43] study considered a group of runner more comparable to the current study (trained, running at 3.5 ms^{-1}), finding a similar range of FSA for BF running.

Williams *et al.* [208] studied overground BF running at a similar velocity (3.35 $ms^{-1} \pm 5\%$) and did not instruct on FSS. They observed an average strike index of 45.7 % (midfoot strike) (range 17-83%). The subjects were not as experienced as the present study group. The study found smaller hip flexion angles at FS (20.8 (mean) $\pm$ 11.3 (s.d) versus 40.0 $\pm$ 5.5). This is coupled with potentially small increases in ankle dorsiflexion at FS (0.0 $\pm$ 7.3 versus -5.6 $\pm$ 10.8) and no significant differences in knee flexion angle at FS (13.6 $\pm$ 5.1 versus 15.7 $\pm$ 3.0). Together, this implies that in the horizontal direction, the COM distance from the point of ground contact may be smaller than in the present study, as the body may be more vertically

aligned (Figure 4.4.1). This has implications for the posterior ground reaction forces which may be related to the level of training; inclusion for the Williams study was running at least 6 miles week^{-1} and at least three days week^{-1}, and the mass and height were 79.99 $\pm$ 9.53 kg and 1.81 $\pm$ 0.07 m. Boyer *et al.* [20] found that for trained runners, habitual FFS runners typically have larger posterior ground reaction forces than habitual RFS runners at FS. This may be influenced by body geometry at FS. The higher proportion of NRFS in the trained population in this study may exhibit higher posterior ground reaction forces than those in the Williams study. To minimize braking forces, subject with large masses may alter their COM position compared to low mass subjects. Alternatively, running on a less compliant surface (*i.e.* overground instead of on a treadmill) may necessitate a more anterior COM mass position at FS to lower posterior ground reaction forces.

Knee angles and angular velocities are similar to other studies but once again, velocity effects may contribute to the observed differences. Increases in velocity, and therefore ground reaction force, may lead to increases in peak knee flexion as an adaptation of the loading mechanics. Slower knee flexion velocity at FS and later relative timing of peak knee flexion, as compared with overground running at the same velocity [43] may reflect an adaptation to the softer treadmill surface. Using shoes, Ferris *et al.* [62] found that for high speed (5 ms^{-1}) running, humans increase leg stiffness as the surface becomes more compliant to allow the effective vertical stiffness to remain constant over a variety of surfaces, where the effective vertical stiffness is the ratio of the peak ground reaction force to the COM vertical displacement from the position at FS to the moment the COM reaches its lowest point. De Wit suggests there is no equivalent compensation in the BF condition and that for BF running, adaptations in stride kinematics are largely due to changes in geometry at FS at the ankle and knee. However, as the FSA and knee angle at FS do not differ from the work of De Wit, the differences observed between the studies may be from an increase in surface compliance for the treadmill with respect

to overground. The differences between running on a force-plate integrated treadmill versus a floor mounted force plate would provide greater insight into this.

Rearfoot frontal plane motion is variable between subjects [43]. By using inter-cortical bone pins, Stacoff *et al.* [190] looked more directly at bone movement for overground running. Studies using skin mounted markers may overestimate the amount of rearfoot motion, hence explaining the larger rearfoot eversion and abduction excursion angles in the present study.

Elite runners have higher incidences of NRFS running. A higher level of training may lead to the higher incidence of NRFS running in the present study group and explain why rearfoot kinematics are most similar to FFS recreational runners [164]. Another consideration is that the increases in rearfoot inversion at FS, rearfoot eversion excursion, peak rearfoot eversion velocity, peak rearfoot abduction, rearfoot abduction excursion and peak rearfoot abduction velocity for the present study may reflect an adaptation of the loading response with higher velocity. Stacoff's subjects ran between 2.5 ms^{-1} and 3.0 ms^{-1} whilst subjects in a study by Pohl and Buckley [164] ran at self-selected jogging speeds and the subjects in the present study ran at 3.58 ms^{-1}. Changes in frontal plane rearfoot orientation (inversion/eversion) at FS may allow for more pronounced movements during the loading response, allowing the rearfoot to become more compliant in the frontal and transverse planes and adapt sufficiently to the demands of running at higher velocities (Chapter 7).

Forefoot kinematics for this study group are different to those of recreational RFS runners [164] owing again to the distribution of FSS present naturally in the highly trained population. With the forefoot not contacting the ground at FS, it is not loaded during early stance phase in the same manner as for toe-heel-toe running and forefoot dorsiflexion and abduction excursion may differ accordingly. Peak forefoot dorsiflexion occurs earlier in the gait cycle than for toe running in untrained runners [164]. If the heel does not touch the ground, as for toe running, the work of the intrinsic foot muscles will be different to when the heel does touch

the ground. The implications for this are unknown but may result in more physiological work for toe running versus toe-heel-toe or heel-toe running [4]. Yet, for minimalist SD running, which is associated with more toe-heel-toe running compared to traditional SD running, intrinsic foot muscles increase in cross-sectional area and volume compared to traditionally SD runners [139].

4.4.3 Comparison of the FSA and FSS

In addition to the anticipated rearfoot kinematic differences observed, the general kinematic loading strategy changes with FSA. Runners who land on their forefoot exhibit faster joint rotation velocities at the foot but slower and smaller movements in the sagittal plane for the knee and in the frontal plane for the hip. Only the continuous parametrization FSA was associated with hip frontal plane kinematics, emphasizing its utility.

For habitually SD competitive runners in the SD condition and overground, medial and posterior impact peaks are present in the ground reaction force when FFS running and the associated shear loading rates are also greater. This is the case both for habitual FFS runners running with a FFS, and for habitual RFS running with a converted FFS [20]. Frontal and transverse plane kinematic changes seen for foot motion here may reflect FS specific loading strategies. This conclusion has its limitations; whilst tibio-calcaneal bone movements do not change significantly for BF versus SD running in recreational runners running overground [190], it is not clear the same may be said for highly trained runners at moderate to high velocities on a treadmill.

In this study, in general the running kinematics of subject-selected FSS are similar to the kinematics of actively induced FSS running. Sagittal plane ROM changes are in agreement with Valenzuela *et al.* [202]. Whilst inducing changes in FS pattern significantly affects rearfoot kinematics [164], for subject-selected FS strategies, foot segment kinematic differences are

more difficult to ascertain. Subjects naturally running with a more dorsiflexed FSA exhibited less forefoot dorsiflexion and forefoot abduction excursion whilst changes in times to peak rearfoot abduction, rearfoot eversion, forefoot dorsiflexion and forefoot abduction were not affected by FSA, all in agreement with Pohl and Buckley [164]. Changes in rearfoot eversion and abduction peak angles and excursion angles were not corroborated but, rearfoot and forefoot joint angle velocities in the frontal and transverse planes were affected, suggesting underlying similarities may exist. During impact, the higher joint velocities may reflect the higher posterior and medial ground reaction forces observed previously for FFS running [20].

Across the trained population and without intervention, RFS runners are reported by Daoud *et al.* [39] to have a higher risk of injury than FFS runners, motivating a detailed cross-sectional study without altering the natural FSA. However, when subjects who were not consistently in one FSS group were omitted from the Daoud study, associations between FSS and injury became less significant.

Boyer *et al.* [20] showed that FS index partially explains differences between habitual and converted FFS runners' kinetics in shoes, suggesting that FFS strategy may actually increase impact-related injury risk in the long term, given that habitual FFS runners had higher shear impact forces than habitual RFS. Also, average contact forces at the ankle are 41.7% higher for FFS running [173] which has implications for injury. For BF running, whilst initial rearfoot and forefoot orientation changes with FSA generally, forefoot-rearfoot and/or rearfoot-tibia motions are tightly coupled [164] for different, induced FSS. It would be valuable to understand with more accuracy how joint coupling varies with FSA, and what role muscle physiology plays in FSA.

Temporal parameters	Male	Female
Stance time (s)	0.23 ± 0.01	0.23 ± 0.01
Stride time (s)	0.69 ± 0.02	0.70 ± 0.03
Stance as % gait (%)	33.0 ± 1.5	33.2 ± 1.9
Cadence (strides s^{-1})	2.90 ± 0.10	2.87 ± 0.15

Table 4.4.1: The mean and standard deviation of temporal parameters for males and females

4.4.4 Gender

There were no statistically significant differences in temporal parameters between genders (Table 4.4.1), but gender was a significant predictor for hip, knee, rearfoot and forefoot motion. In general, females had more and faster hip motion and faster knee motion than males across stance phase (Figure 4.3.3b).

Main effects of gender on foot motion were identified but many may be extraneous; when starting with a saturated linear regression model only 33% (4 out of 12) of foot kinematic parameters identified gender as a significant main effect given both a discrete and continuous parameterization. This may result from the small sample of females studied, compounded with the typically small movements at the foot. This may also be relevant for interaction effects. Interaction effects identified for foot motion may be extraneous. Nevertheless, for females time to peak knee flexion ($p < 0.001$) and peak rearfoot dorsiflexion (FSS: $p = 0.026$; FSA: $p = 0.040$) was earlier whilst time to peak forefoot dorsiflexion ($p = 0.048$) and peak rearfoot inversion ($p = 0.036$) was later.

Anatomical characteristics are important factors for hip motion, both between and within sexes. Boxplots identified one subject (FI) as an outlier for the parameter h:f. With their data omitted h:f followed a normal distribution ($p = 0.633$). Females had a larger h:f than males ($p = 0.096$) and h:f was a significant predictor for hip peak adduction angle (pooled: $p < 0.001$; male: $p < 0.001$; female: $p = 0.023$), hip adduction ROM (pooled: $p < 0.001$; male: $p = 0.002$; female: $p = 0.005$) and peak hip adduction velocity (pooled: $p < 0.001$; male: $p < 0.001$; female:

$p < 0.001$). As the pelvis becomes wider compared to the femur length, the peak hip adduction, hip adduction ROM and hip peak adduction velocity increase. When gender was replaced with h:f, statistical tests did not identify FSA as a significant predictor for hip peak adduction, hip adduction ROM or hip peak adduction velocity both between and within sexes. For the datasets studied here, variations in motion at the hip due to gender are explained by subject anatomy.

The results here corroborate previous findings [60, 209] which identify differences between genders for hip frontal plane motion. Greater demand on the gluteus maximus for females and thus earlier muscle fatigue is related to the increased peak hip adduction in females and the etiology of patello-femoral pain syndrome [209]. The present work, undertaken in the absence of fatigue, does not refute that hip and femur anatomy explains functional differences in hip movement regardless of gender. Furthermore, these differences may also be compounded by individual FS kinematics such that individuals who strike the ground with their heel and also have a wide pelvis compared to their femur length may load the gluteal muscles far more than those who strike on the ball of their foot and have a narrow pelvis compared to their femur length.

4.4.5 Injury rate data

Foot-strike angle variability, quantified as the standard deviation of FSA for each subject, correlated with the probability of injury (Table 4.4.2). Higher variability correlated with a higher probability of injury, and the interaction between FSA and FSA variability was also correlated with injury rate. For subjects with low FSA variability, injury rate was generally independent of FSA. However, for high FSA variability subjects, FFS runners were more likely to be injured than RFS runners (Figure 4.4.2). The odds ratio from the interaction term was 0.85, calculated as $\exp[-\beta_{FSA:\sigma}]$. This may explain the decrease in Pr(Injury) with increase in FSA at both levels of variability. This results contradicts the observation that RFS running is associated with

Coefficient	Estimate	Standard error	p-value
β_0	-4.001	2.227	0.072*
β_{FSA}	0.133	0.174	0.444
β_σ	2.523	1.368	0.065*
$\beta_{FSA:\sigma}$	-0.163	0.104	0.117

Coefficient	Estimate	Lower CI	Upper CI
C-statistic	0.83	0.68	0.98

Table 4.4.2: Model coefficients for the logistic regression model. The C-statistic suggests a strong prediction model.

higher rates of injury [39] and points to a more intricate relationship between FSS and injury rate, whereby variability FSA is relevant.

4.4.6 Limitations

Analysis was limited to kinematic and spatiotemporal variables. Kinetic data was not recorded and muscle activity data is not presented. Therefore it is not possible to comment directly on

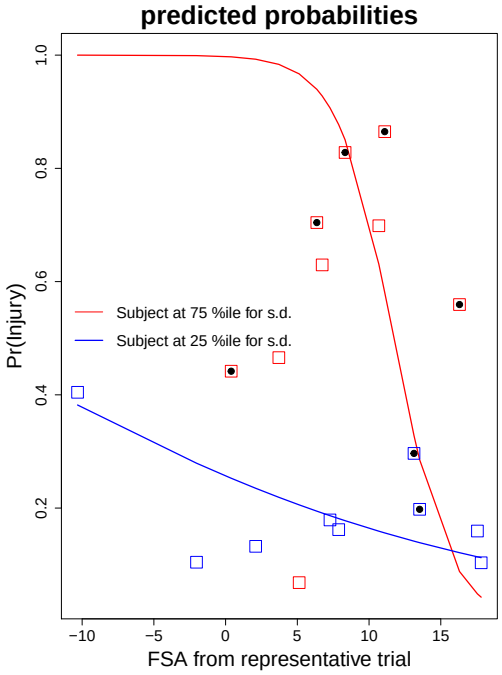


Figure 4.4.2: Results for the logistic regression (Section 4.2.6.3). Predicted probabilities for each subject, where a filled square represents a subject who suffered an injury. Blue and red squares are subjects with variability below and above the median respectively. Finally, the red curve is the model fit given a standard deviation at the 75^{th} percentile, whilst the blue curve is the model fit given a standard deviation at the 25^{th} percentile.

the mechanical loading of joints or action of the muscles. However, Chapter 6 presents a study of the effects of FSA on lower-leg muscle activity.

Treadmill and overground running kinematics differ, particularly above 5.0 ms^{-1}. In comparing the present results to previous literature both scenarios are considered for discussion but the velocities studied here were below 5.0 ms^{-1}. Extending the conclusions here to overground running still has its limitations. The work of Lieberman for Kenyan runners at 5.9 ms^{-1} and the subsequent aforementioned differences demonstrate this. Furthermore, extending the conclusions here to high velocity (> 5.0 ms^{-1}) overground running which, for this study group is very pertinent as they compete at high velocities, is actively discouraged. Runners typically run at such high velocities in spiked shoes and experience heavy fatigue. Such studies are of interest but their emphases - running biomechanics under the influence of fatigue and the use of spiked shoes - are beyond the scope of this chapter. The majority of individuals running are also not highly trained, unlike the present study group. As no control group of recreational runners was studied here, direct comparisons between highly trained and recreational runners are also made with caution.

Foot-strike angle was a predictor in statistical analyses, but it is not strictly controlled for because individuals were not instructed to alter their FSA or FSS. It is therefore not possible to talk directly about causality even though many of the inferences are in agreement with previous work where FSA was controlled for. Rather, the results in this chapter serve to quantify variation in kinematics as a function of a subjects' typical FSA. Comparisons were made between genders and the results corroborated previous work. The significance level for this study was kept at 10% and Bonferroni corrections were applied to particular parameters to retain statistical power at the expense of identifying only large effects. An increase in sample size, particularly for the female population, would necessarily improve the statistical power of this study.

With respect to injury rate the standard deviation is a linear measure of variation but, because

the MCS responds to sensory feedback, nonlinear time series analysis techniques may be more appropriate [131, 148]. Also, data for eighteen subjects were used for the analysis, with seven subjects sustaining an injury. The number of subjects and thus injuries were small. With three predictors this may be an issue, in light of the heuristic of using ten outcomes per predictor [1] and the natural interest in predicting injury. Specifically, with fewer than ten strides, maximum likelihood estimates are biased, estimates of standard errors may be poor, and the model may suffer from overfitting. More data are needed for further, direct discussion of injury rate as a function of FSA or FSA variability. In addition, no follow-up gait analyses were performed and subjects did not typically run BF. Foot-strike angle variability should be measured for the SD condition in order to make a more robust assessment of the association between the probability of injury and variability. This information will inform on the assertion that BF running is a necessary or sufficient (or both) perturbation for a biomechanical 'stress test'.

4.5 Conclusion

In the absence of fatigue a variety of FSS exist in the population of uninjured, highly trained athletes and a continuous parametrization of the FSS, referred to here as FSA, is statistically superior to a discrete classification for identifying how foot orientation at FS relates to kinematics. FSA is associated with different loading kinematics during stance phase at all joints. To better understand the relationship between FSA and gait, the accurate analysis of multiple gait cycles may be beneficial because the parameter FSA is subject specific, varies from stride-to-stride, and for some individuals shows high variability. Individuals with high variability in FSA for BF running may also be susceptible to running-related injury, particularly if they exhibit anterior FS patterns. For the remaining chapters, we consider FSA as a continuous parameter of interest and include multiple gait cycles per subject for analysis to account for stride-to-stride

variations.

In trained populations, gender differences in hip kinematics associated with injury exist and have been explained as an anatomical predisposition. Conditioning programs which account for this may be of value for minimizing any risks for both recreational and trained runners. Future work should use the more accurate and objective measure FSA to ascertain its relative importance in injury development, focussing upon how individuals' kinematics, kinetics, and muscle physiology alter during the onset of fatigue. For example, does one control for comfort over muscle (dys-)function and if so, how? Also, what do highly trained populations do and does this have implications for the recreational runner?

Chapter 5

Velocity and condition effects on foot-strike kinematics

This study looked at the effects of velocity and barefoot or shod running on FSA strategy within a set of relevant aerobic training velocities in the present study group of highly trained male distance runners. Velocity and condition effects on stride length and the COM distance from the heel at FS were also studied. Given that FSA varies between and within subjects (Chapter 4), statistical techniques which quantify the magnitude of between-subject variation were used. In the SD condition the in-shoe foot inclination and therefore global foot incline was calculated.

This chapter demonstrates that subjects employ running strategies which are dependent on foot condition. This may be related to the comfort associated with deformation of the heel pad during running, or novelty associated with BF running. Foot-strike angle was independent of velocity for BF running, but more foot dorsiflexion occured higher velocity in the SD condition. The strategies may have implications for running-related injury.

5.1 Introduction

In general, faster running leads to more plantarflexion of the foot at FS [151]. Other factors affecting FS strategy include footwear [125, 188], performance level [84, 115] and terrain [70]. To accurately measure the influence of these parameters it is advised that one measure multiple strides and account for inter-subject variability [14].

Nigg [150] identified kinematic changes between treadmill and overground running which could be described as systematic (*i.e.* fixed) and subject dependent (*i.e.* random). His study used a repeated-measures ANOVA but the number of repeated measures was not reported directly, with the lower limit set at three strides. Given that repeated-measures ANOVA tests may introduce sampling bias with missing data, hierarchical mixed-effect models are preferable as data need not be excluded to satisfy model assumptions [110, 145]. Furthermore, with hierarchical mixed-effect models it is possible to quantify the magnitude of the random variation in the context of the magnitude of the fixed effects. Such an approach therefore allows for a robust analysis of the between-subject variation which is recommended but rarely performed in biomechanics research. Whilst data collection is often limited by practical constraints, the same is not true for statistical analyses.

The previous chapter identified correlations between FSA and kinematics and the correlations observed for subject-selected FSA generally agreed with studies in which it is controlled [164]. It is valuable, therefore, to consider how FSA varies within and between subjects for controlled interventions of condition and velocity which reflect realistic behaviours. This affords context to the results of the previous chapter. Barefoot running triggers a decrease in stride length which could reduce ground reaction forces and sagittal plane joint moments [199]. Furthermore Boyer *et al.* [19], using one velocity of 3.35 ms^{-1}, identified interactions between the effects of FSA, stride length, and foot placement on running kinematics.

It is hypothesized that there are significant fixed main effects of condition and velocity on FSA. In particular, compared to BF running, shoes cause more dorsiflexion for the FSA, and increases in velocity cause more plantarflexion in FSA [22]. Stride length, and the distance between an approximation to the COM and the heel were calculated. Longer strides were hypothesized for SD running [188], and longer strides and a shorter distance between the COM and heel were hypothesized for higher velocity.

A mixed-effect model is hypothesized to be a significant improvement on any fixed-effect model. This is because a mixed-effect model accounts for both fixed effects and the random variation of the fixed effects at the subject level.

5.2 Methods

5.2.1 Subjects

The subject inclusion and exclusion criteria have been previously described (Section 3.1). Nineteen male highly trained distance runners were studied.

5.2.2 Experimental data collection and data processing

The data collection and processing procedures have been described elsewhere (Sections 3.4 and 3.5). Briefly, subjects ran for approximately 200 seconds at each of three velocities (3.58, 3.97 and 4.44 ms^{-1}) in a randomized order BF and then SD. Barefoot running was studied first, allowing markers to be placed on the bare foot before excessive perspiration disrupted skin marker adhesion.

5.2.3 Data analysis

Discrete kinematics parameters were calculated as previously described (Section 4.2.4) for all gait cycles. Briefly, between 15 and 31 consecutive gait cycles (10 to 20 seconds) were analysed for the leg on which the subject usually stands to kick a football. This leg corresponds to the definition of the non-dominant leg (Section 3.4.2). This number was determined by the maximum number of gait cycles available for each trial.

5.2.4 In-shoe foot inclination

Running shoes have a raised heel and therefore, the foot inside the shoe is more plantarflexed than the sole of the shoe. Accounting for this offset allows for a comparison of the global foot inclination between the BF and SD condition. As subjects wore their own shoes, the in-shoe foot inclination varied across the study group. Therefore, for each shoe model (one per subject) the manufacturer, model and size were recorded. The shoe length and heel drop measurements (in mm), found from the manufacturer websites, were used to calculate a shoe-specific, and therefore subject-specific, in-shoe foot inclination, ϕ_i , for the i^{th} subject as

$$\phi_i = -\tan^{-1}\left(\frac{\text{heel drop}_i}{\text{shoe length}_i}\right) \tag{5.2.1}$$

where ϕ_i is negative and is therefore the amount of plantarflexion of the foot, relative to the sole of the shoe. This offset was then added to the measure of the shoe sole angle which was calculated from the STOE and SHEE markers in a method similar to that for the BF condition (Section 4.2.4).

5.2.5 Centre of mass

The COM was taken as the position of the sacrum marker (SACR). The COM displacement from the heel along the direction of motion was calculated as follows: a vector from the COM to the heel marker (HEE) in the transverse plane was calculated after setting the vertical position of the SACR to match the HEE. A vector which joined the position of the HEE marker at FS to the position of the HEE mark twenty-five frames after FS defined the direction of progression, because heel was likely to be on the treadmill during this period. Using the cosine rule, the angle between these vectors was calculated. With the angle, the length of the vector from COM to HEE along the direction of progression was calculated.

5.2.6 Stride length

Stride length was calculated using the velocity of the treadmill multiplied by the time between successive foot strikes of the same foot.

5.2.7 Statistical analysis

Specific trials have a different number of samples for FSA. In repeated-measures ANOVA tests, missing data can introduce sampling bias and inflated rates of Type I error (a "false positive"). To avoid this, and to also quantify variability, a more general hierarchical linear mixed-effects model (LMM) was used for statistical analysis. Mixed-effects model are typically seen when a primary interest of the modeler is to make inferences about the population from which a sample was taken, which necessarily requires one to quantify between-subject variability. Gait analysis studies typically employ repeated-measures ANOVA tests and to knowledge of the author, there are few instances in gait analysis where mixed-effects models were applied [131] and developed based on a set of sound statistical principles [163]. A hierarchical LMM is mixed

because it contains both fixed effects and random effects, and hierarchical because it can model variation at more than one level. As an example, a fixed effect might be the effect of wearing running shoes on the FSA for a typical subject. A random effect on this parameter would exist for each individual subject, and describe the shift of this fixed effect away from the typical value for the subject of interest. For the purpose of fitting the model, the estimated parameter is the variance of the set of random effects across all subjects in the sample, and assumed to characterize a Gaussian distribution with a mean of zero. It is conceivable that two populations might have the same fixed effect, but the variance of the random effects may be different because the variability for the two populations is different. The sample of subjects in this thesis is drawn from the population of highly trained, habitually SD male distance runners. Therefore, the between-subject variability is characterized for this population only. At the population level, data are correlated within each subject, but at the subject level, observations are uncorrelated and independent. This hierarchical structure avoids bias towards data from particular subjects. The model is linear because the predictor function is a linear combination of coefficients. For the purposes of this chapter, we wish to consider random variation of the fixed effects, which vary at the subject level. In general, for j^{th} group which contains n_j observations, the response y_j is

$$y_j = X_j\beta + Z_j b_j + \varepsilon_j \tag{5.2.2}$$

where X_j is a n_j by p design matrix for p predictor variables (for the specific predictor variable order, see Equation 5.3.2) and n_j observations for the j^{th} group; β is a p by 1 vector of the fixed effects regression coefficients; Z is a n_j by q design matrix for the q random effects; b is a q by 1 vector of random effects coefficients and $b \sim \mathcal{N}_q\left(0, \Sigma^2\right)$, where Σ^2 is the variance-covariance matrix of the random effects; and ε_j is a n_j by 1 vector of random errors where $\varepsilon_j \sim \mathcal{N}\left(0, \sigma_\varepsilon^2\right)$ where σ_ε^2 is the variance of the random errors.

5.2.7.1 Exploratory analysis

With two conditions and three fixed velocities, condition and velocity were treated as categorical and ordinal variables respectively. Boxplots (Figure 5.2.1) were used to visualize their effects on FSA. The effects of condition appeared to be fixed, with variation between subjects. The effect of velocity appeared to be small, if significant at all.

Analysis of the residuals from fixed effects models suggested hierarchical models were more appropriate (Figure 5.2.2a). Specifically, the 99% confidence bands of the model residuals per subject from the fixed effects models did not all cross zero. This implied there was significant variation between subjects for which the fixed effects models did not account. Analysis of the residuals from final hiercarchical models suggested this variation was appropriately accounted for (Figure 5.2.2b).

5.2.7.2 Model selection and fitting

Given an initial hierarchical LMM with a random intercept per subject, chi-square likelihood ratio tests were used to compare the significance of adding an extra random effect at the subject level into the model. Subsequently, Q-Q plots of the more complicated model residuals were tested for normality. If the residuals were not normal, their respective models were disregarded.

As is customary in hierarchical mixed-model fitting, final models were fitted using the restricted maximum likelihood approach. This method can produce unbiased estimates of the variance and covariance parameters. Final models were fitted with a variance-covariance matrix which reflected the zero or non-zero correlations between random variables. For example, if initial fitting did not identify significant covariance between random coefficients, the model was re-fitted with the covariance parameter assumed to be zero.

The distributions of the random coefficients were checked for normality with Q-Q plots. If outliers were observed, they were removed and the model was re-fitted to check whether they

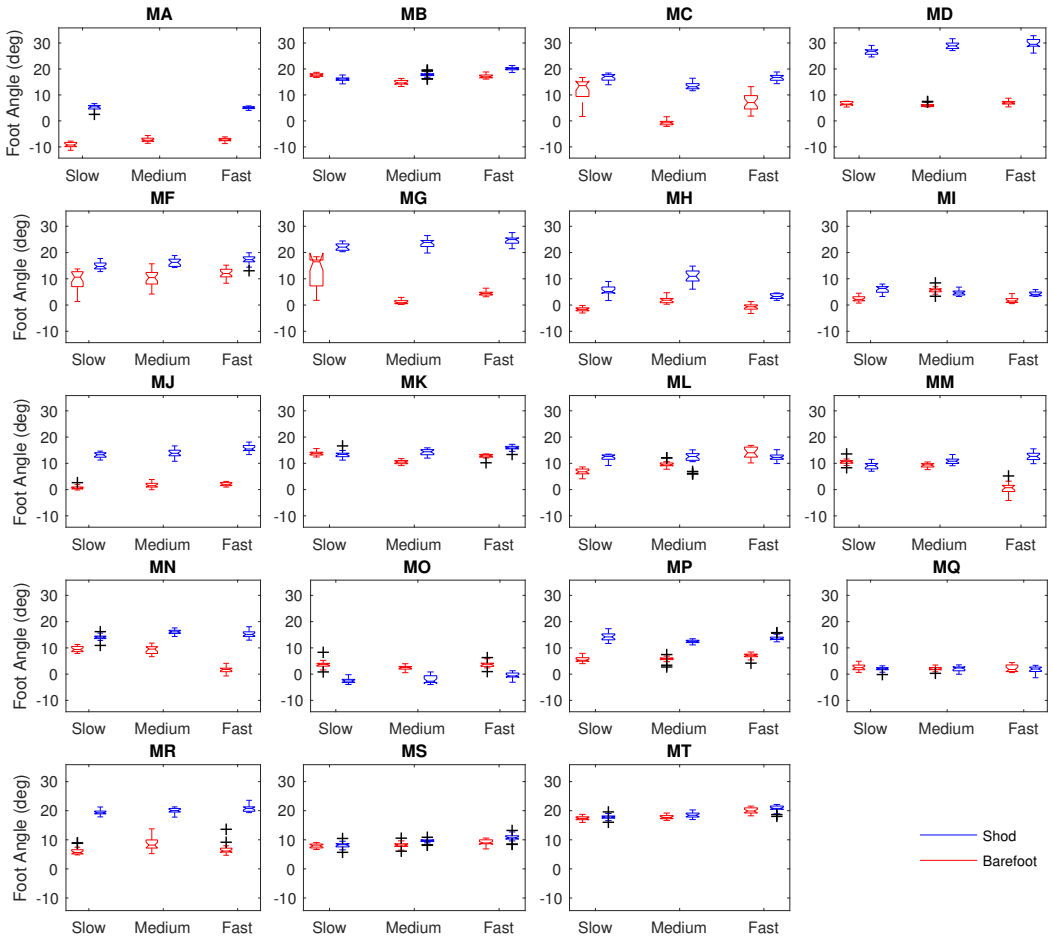
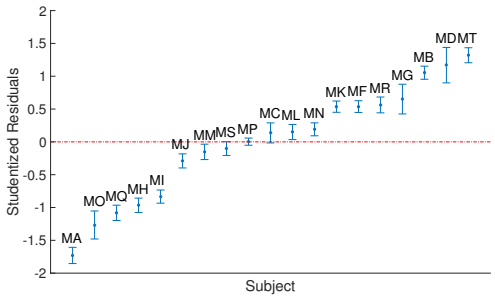
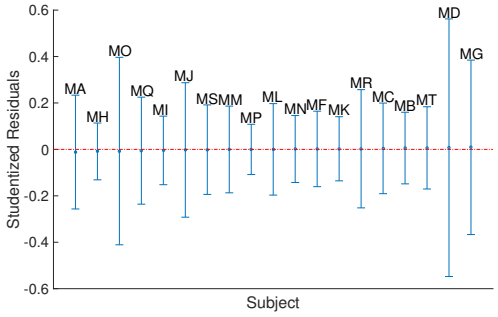


Figure 5.2.1: Boxplots per subject illustrate the effect of condition (red: BF; blue: SD) and velocity on foot angle with respect to the treadmill surface (FSA) at FS. The magnitude of the effects of condition and velocity vary between subject. A positive foot angle corresponds to dorsiflexion with respect to the ground. '+' denotes an outlier. Note that no data were collected for subject MA at the medium velocity in the SD condition.

influenced the inferences about parameter significance. Where they did, they were considered as influential outliers, and removed. Final model residuals and random coefficients were checked for normality and only the results from statistical models which satisfied these assumptions are presented and discussed. The significance level was set to $\alpha = 0.05$.



(a) Confidence intervals for the fixed effects model with an interaction term do not all cross zero. Significant variation which exists at the subject level is not accounted for.



(b) Confidence intervals for the final hierarchical LMM (Equation 5.3.1) all cross zero. The model accounts for significant subject level variation.

Figure 5.2.2: Plots of model residuals, grouped by subject, justify the application of a hierarchical model. Error bars denote 99% confidence intervals about the mean (circle). The example is drawn from Section 5.3.1.1.

5.3 Results

5.3.1 Final models

This section presents the final models applied for statistical analyses. In total 2219 observations were analysed with an average of 20 per trial and 116 per subject. In all cases, likelihood ratio tests showed mixed-effect models to be a significant improvement on fixed-effect models.

5.3.1.1 Condition and velocity

The final statistical model (Equation 5.3.1) was a hierarchical LMM. It is interpreted as each subject having a similar underlying FSA. Variation between subjects was accounted for to give a more accurate estimate of FSA for the underlying population. The final model, where subscript ij denotes the i^{th} observation for the j^{th} subject, was

$$\text{Level 1:} \quad FSA_{ij} = \beta_{0j} + X_j\beta_{1j} + \varepsilon_{ij} \tag{5.3.1a}$$

$$\text{Level 2:} \quad \begin{aligned} \beta_{0j} &= \beta_0 + b_{0j} \\ \beta_{1j} &= \beta_1 + b_{1j} \end{aligned} \tag{5.3.1b}$$

where $\varepsilon_{ij} \sim \mathcal{N}\left(0, \sigma_{\varepsilon}^2\right)$ are the residuals of the i^{th} stride for the j^{th} subject, and X_j is a design matrix for the j^{th} subject. The coefficient β_{0j} is the subject-specific intercept for the reference condition of BF running at 3.58 ms^{-1}, comprising a fixed term β_0, the population mean for FSA, and a random term b_{0j}. The choice of reference condition is arbitrary and does not affect validity of the model. Fixed effect parameter estimates are interpreted as changes from the reference condition. The coefficient β_{1j} is a vector of fixed and random effects given as

$$\beta_{1j} = \begin{bmatrix} \beta_C \\ \beta_{V_m} + b_{V_m j} \\ \beta_{V_f} + b_{V_f j} \\ \beta_{C:V_m} \\ \beta_{C:V_f} \end{bmatrix} \tag{5.3.2}$$

where β_C, β_{V_m} and β_{V_f} are the fixed effects coefficients for condition, medium velocity and fast velocity respectively. The terms $b_{V_m j}$ and $b_{V_f j}$ are random effects of medium and fast velocity which vary between subjects. The random coefficients $b_{ij} \sim \mathcal{N}_3\left(0, \Sigma^2\right)$ where the variance-covariance matrix, Σ^2, was calculated as

$$\Sigma^2 = \begin{bmatrix} \sigma_0^2 & 0 & 0 \\ 0 & \sigma_{V_m}^2 & 0 \\ 0 & 0 & \sigma_{V_f}^2 \end{bmatrix} \tag{5.3.3}$$

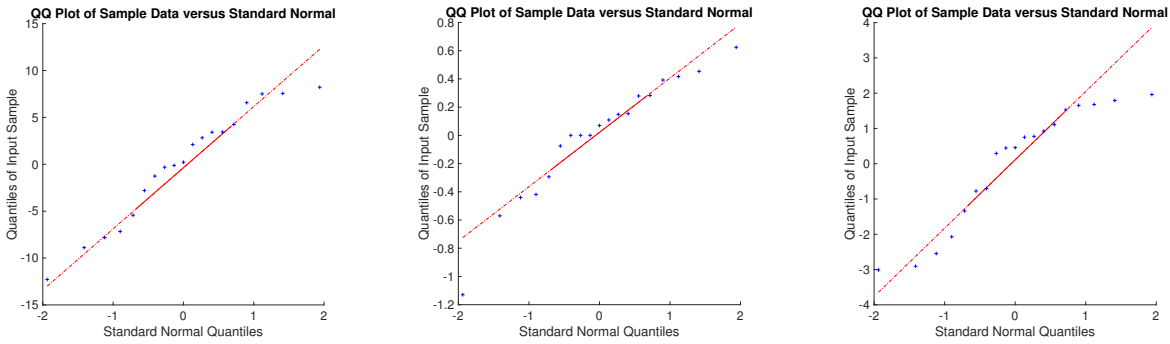
where σ_0^2, $\sigma_{V_m}^2$ and $\sigma_{V_f}^2$ are the standard deviations of the random intercept, random effect of medium velocity and random effect of fast velocity respectively. This matrix implies that the random effects were independent of each other, because the off-diagonal covariance terms are equal to zero. The final model coefficients are given in Table 5.3.1, and the model accounted for 77% of the variation ($R_{adj}^2 = 0.77$). Three subjects, MC, MG and MH, were identfied as influen-

Coefficient	Estimate	Standard error	p-value
β_0	7.179	1.405	< 0.001*
β_C	5.057	0.260	< 0.001*
β_{V_m}	0.208	0.328	0.526
β_{V_f}	-0.771	0.487	0.113
$\beta_{C:V_m}$	-0.102	0.392	0.795
$\beta_{C:V_f}$	2.132	0.365	< 0.001*

Coefficient	Estimate	Lower bound	Upper bound
σ_0	6.072	4.370	8.437
σ_{V_m}	0.701	0.291	1.684
σ_{V_f}	1.802	1.229	2.643
σ_ε	3.630	3.524	3.740

Coefficient	Estimate
R^2_{adj}	0.77

Table 5.3.1: Fixed and random effects coefficients for the effects of condition (β_C), velocity (medium: β_{V_m}; fast: β_{V_f}), and their interaction (medium: $\beta_{C:V_m}$; fast: $\beta_{C:V_f}$) on FSA. Fixed coefficients are with respect to the reference condition, which is BF running at 3.58 ms^{-1}. The sample mean in the reference condition is given by β_0. Random effects coefficients for the intercept (σ_0) and velocity (σ_{V_m} and σ_{V_f}), and the residuals (σ_ε), are given as standard deviations with 95% confidence intervals. * denotes significance at the 5% significance level. The adjusted coefficient of determination R^2_{adj} quantifies the final model goodness of fit.



(a) Intercepts, b_{0j} (b) Medium velocity, $b_{V_m j}$ (c) Fast velocity, $b_{V_f j}$

Figure 5.3.1: Quantile-quantile plots of random coefficients from Equation 5.3.1, with details from Equations 5.3.2 and 5.3.3. The coeffcients were normally distributed.

tal outliers from their medium velocity random coefficients and their medium velocity data was not included when fitting the final model. QQ-plots (Figure 5.3.1) qualitatively demonstrate that the random coefficients were normally distributed for the final model.

Coefficient	Estimate	Standard error	p-value
β_0	2.467	0.018	< 0.001*
β_C	0.100	0.010	< 0.001*
β_{V_m}	0.197	0.003	< 0.001*
β_{V_f}	0.447	0.003	< 0.001*
$\beta_{C:V_m}$	0.023	0.004	< 0.001*
$\beta_{C:V_f}$	0.016	0.004	< 0.001*

Coefficient	Estimate	Lower bound	Upper bound
σ_0	0.080	0.058	0.111
σ_C	0.040	0.028	0.056
σ_ε	0.043	0.041	0.044

Coefficient	Estimate
R^2_{adj}	0.96

Table 5.3.2: Fixed and random effects coefficients for the effects of condition (β_C), velocity (medium: β_{V_m}; fast: β_{V_f}), and their interaction (medium: $\beta_{C:V_m}$; fast: $\beta_{C:V_f}$) on stride length. Fixed coefficients are with respect to the reference condition, which is BF running at 3.58 ms^{-1}. The sample mean in the reference condition is given by β_0. Random effects coefficients for the intercept (σ_0) and condition (σ_C), and the residuals (σ_ε), are given as standard deviations with 95% confidence intervals. * denotes significance at the 5% significance level. The adjusted coefficient of determination R^2_{adj} quantifies the final model goodness of fit.

5.3.1.2 Stride length

A hierarchical LMM for the effect of condition and velocity on stride length fit to data, with a random intercept and random effect of condition (Table 5.3.2, Equation 5.3.4) was

$$\text{Level 1:} \quad S_{ij} = \beta_{0j} + X_j\beta_{1j} + \varepsilon_{ij} \tag{5.3.4a}$$

$$\text{Level 2:} \quad \begin{aligned} \beta_{0j} &= \beta_0 + b_{0j} \\ \beta_{1j} &= \beta_1 + b_{1j} \end{aligned} \tag{5.3.4b}$$

where S_{ij} is stride length, β_{1j} is a vector of fixed and random effects, given as

$$\beta_{1j} = \begin{bmatrix} \beta_C + b_{Cj} \\ \beta_{V_m} \\ \beta_{V_f} \\ \beta_{C:V_m} \\ \beta_{C:V_f} \end{bmatrix} \tag{5.3.5}$$

where all parameters are as described earlier, with additionally that b_{Cj} is the random effect of condition at the subject level. The random coefficients $b_{ij} \sim \mathcal{N}_2\left(0, \Sigma^2\right)$, where

$$\Sigma^2 = \begin{bmatrix} \sigma_0^2 & 0 \\ 0 & \sigma_C^2 \end{bmatrix} \tag{5.3.6}$$

where σ_C^2 is the standard deviation of the random effects of condition.

5.3.1.3 Centre of mass to heel progression

A hierarchical LMM as previously described (Equation 5.3.4), quantified the effects of velocity and condition on the distance between COM and the heel along the direction of progression, S_{ij} (Table 5.3.3).

5.3.2 Condition

Condition was a significant main fixed effect on FSA, such that the foot became more dorsiflexed for SD running. Inclusion of condition as a random effect invalidated the model for the effect on FSA (Section 5.3.1.1).

As hypothesized, stride length was significantly longer for SD running. The distance along the direction of progression between the COM and the heel marker shortened for SD running,

Coefficient	Estimate	Standard error	p-value
β_0	284.0	5.9	< 0.001*
β_C	-17.7	2.9	< 0.001*
β_{V_m}	13.5	0.8	< 0.001*
β_{V_f}	30.3	0.8	< 0.001*
$\beta_{C:V_m}$	3.3	1.1	< 0.004*
$\beta_{C:V_f}$	4.7	1.1	< 0.001*

Coefficient	Estimate	Lower bound	Upper bound
σ_0	25.6	18.5	35.6
σ_C	12.1	8.7	17.0
σ_ε	10.9	10.6	11.3

Coefficient	Estimate
R^2_{adj}	0.88

Table 5.3.3: Fixed and random effects coefficients for the effects of condition (β_C), velocity (medium: β_{V_m}; fast: β_{V_f}), and their interaction (medium: $\beta_{C:V_m}$; fast: $\beta_{C:V_f}$) on COM distance from the heel along the direction of progression. Fixed coefficients are with respect to the reference condition, which is BF running at 3.58 ms^{-1}. The sample mean in the reference condition is given by β_0. Random effects coefficients for the intercept (σ_0) and condition (σ_C), and the residuals (σ_ε), are given as standard deviations with 95% confidence intervals. * denotes significance at the 5% significance level. The adjusted coefficient of determination R^2_{adj} quantifies the final model goodness of fit.

but this may be attributed to measuring the heel counter of the shoe versus the heel of the foot, which for the SD running is more posterior to the ankle joint centre. The reduction in distance of approximately 17 mm is comparable to the anterior-posterior thickness of the heel counter of the shoe.

5.3.3 Velocity

The effect of velocity was significant as an interaction with condition at the fastest velocity. The difference in FSA between BF and SD running was significantly larger for fast running. Put another way, FSA changed more between condition at the highest velocity. The main effect of fast velocity narrowly missed significance, with the coefficient suggesting more plantarflexion occured at FS in the BF condition as velocity increased. With the interaction term considered,

more dorsiflexion occurred for SD running as velocity increased.

Stride length increased with velocity and an interaction term suggested the increase in stride length from BF to SD running was larger for higher velocities. The distance along the direction of progression between the COM and the heel at FS increased with velocity and the magnitude of this increase was significantly larger for SD running.

5.3.4 Within-subject and between-subject variation

In general the model fit well to data (Example: Figure 5.3.2). With respect to the FSA model (Section 5.3.1.1), for the three subjects who were outliers (MC, MG and MH), two (MC and MG) also showed high stride-to-stride variability at 3.58 ms^{-1} previously (Chapter 4). Subject MO showed the opposite condition effect to all other subjects, such that more dorsiflexion was observed for the BF condition. Finally, subject MD adapted his FSA far more than predicted by the model.

The variance for the random variation of velocity effect per subject was large (Table 5.3.1) compared to the magnitude of the fixed effects. Furthermore, the random variation of the intercept between subjects was the same order of magnitude as the fixed effect of condition with respect to the reference condition (Figure 5.3.3).

If we frame the unexplained variance ε_{ij} as the (upper limit of) within-subject variability, the within-subject variation in FSA may have implications for FSS mis-classification, particular for BF running.

5.4 Discussion

This study looked at the effects of velocity and foot condition on FS strategy within a set of relevant aerobic training velocities in the present study group of highly trained male distance

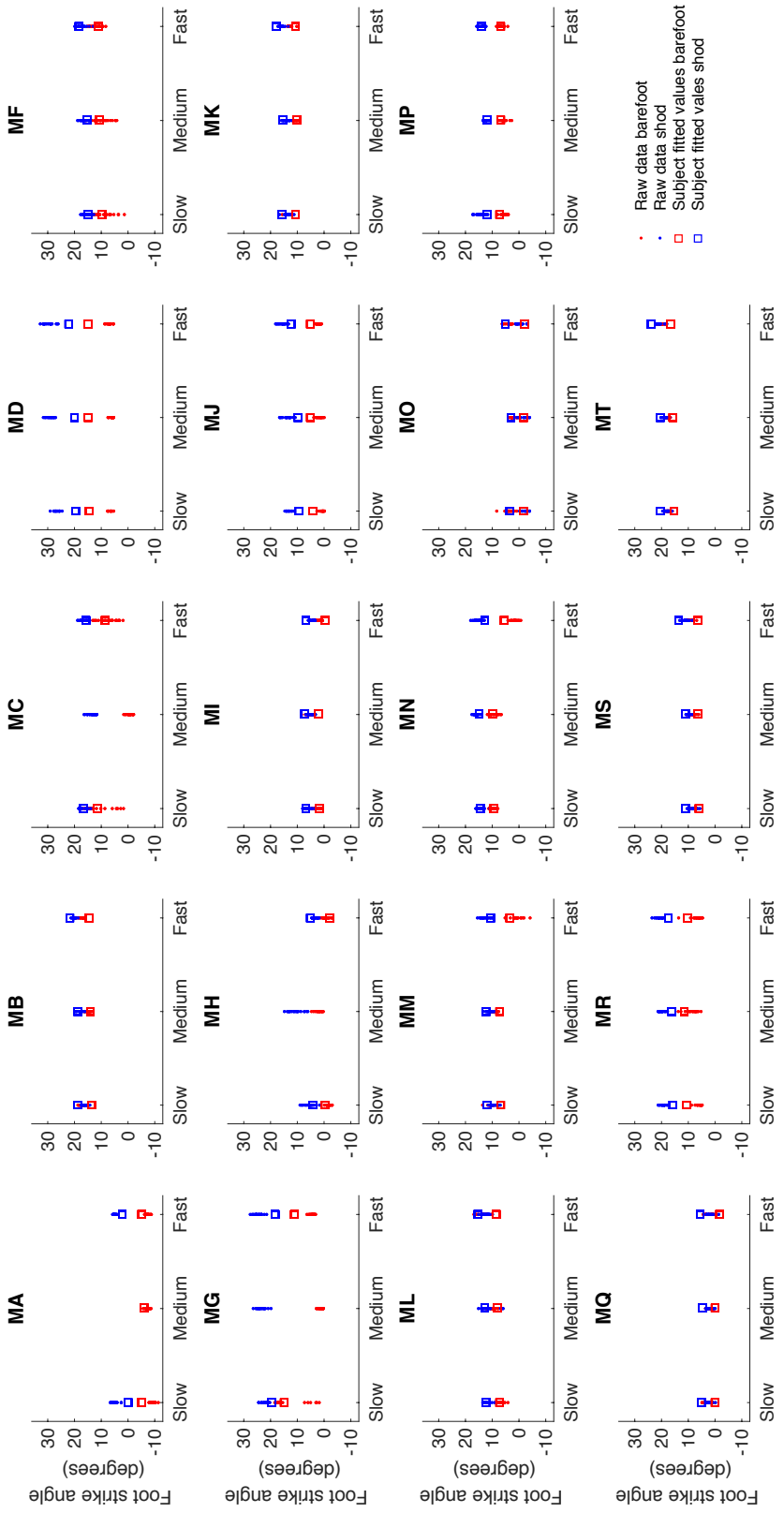


Figure 5.3.2: From Equation 5.3.1, plots per subject of the raw data (dots) and final fitted model (open squares) for BF (red) and SD (blue) running show good agreement ($R^2_{adj} = 0.77$).

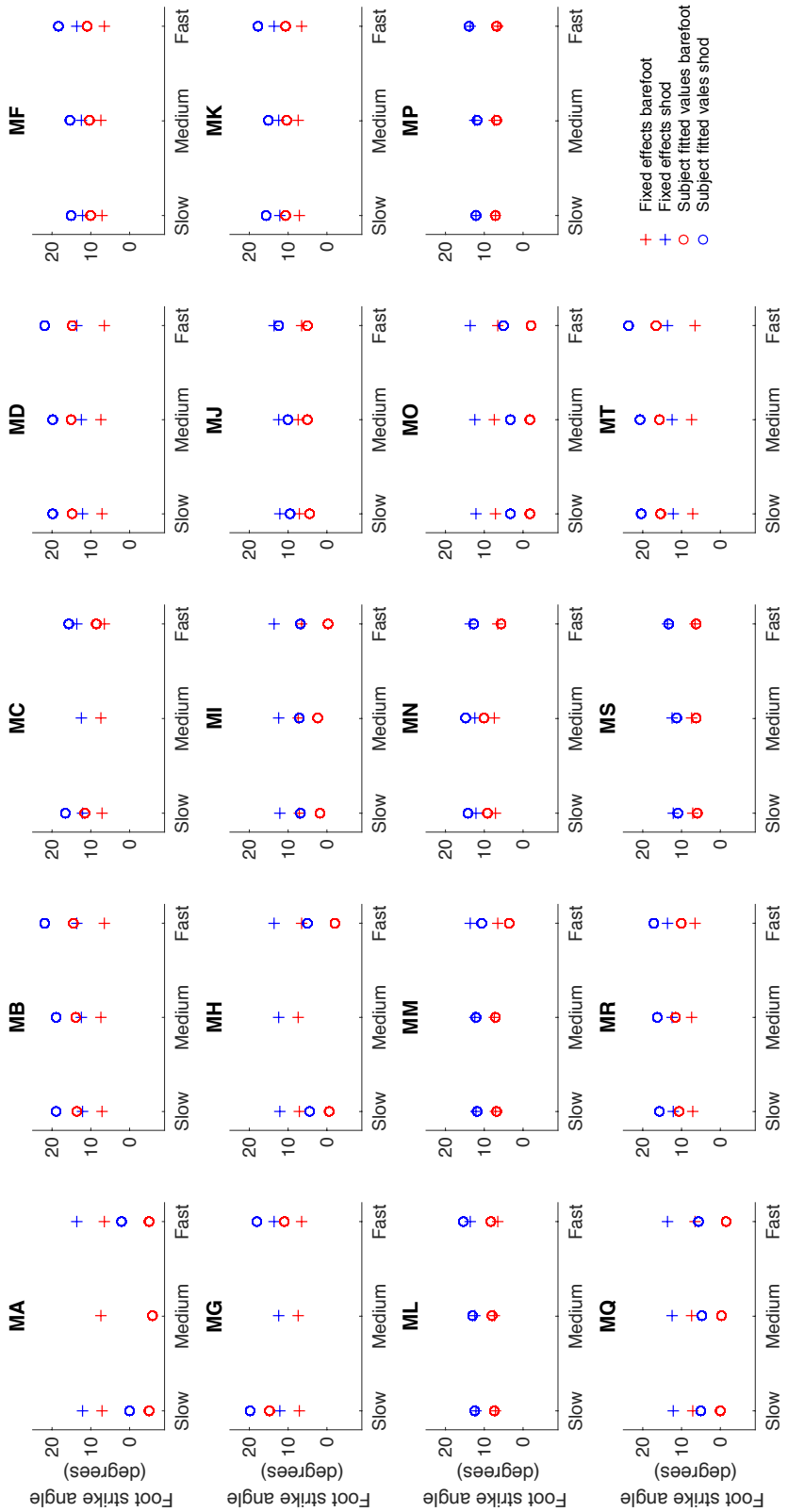


Figure 5.3.3: Plots per subject of the fixed effects (pluses) and the final fitted model (open circles) including the random effects for BF (red) and SD (blue) running. Random variation between subjects was of the same order of magnitude as the fixed effect of condition.

runners. Valid hierarchical LMMs, which accounted for between-subject variation, were superior to standard fixed-effect models (Section 5.3.1). An in-shoe foot inclination offset allowed for the comparison of the global foot incline across conditions. The hypothesized significant main effect of condition was corroborated, but the effect of velocity was non-trivial, demonstrating an interaction with condition. Individuals increase their stride length and the distance between their COM and foot to accommodate speed increases but, maintain a fixed FSA for BF running. The behaviour of a small subset of individuals was anomalous in the BF condition, potentially because of particular discomfort in the condition. As subjects in this study are habitually SD, the novelty of BF running may be responsible for many of the observed differences between condition.

5.4.1 Condition

Condition was significant as a main effect on FSA and interacted with velocity (Table 5.3.1). This compounds the issues faced when 'characterizing' individuals as particular foot strikers. The FSA, and therefore FSS, is subject-specific (Figure 5.2.2), stride-specific, condition-specific and potentially shoe-specific. The FSA for a runner in the BF condition may be similar to another individual running SD, even though the shoe has a fixed effect across the sample. The magnitude of the variation in FSA between individuals is the same order of magnitude as the effect of foot condition. Statistical methods which account for variation between individuals, for example a random intercept model, are therefore highly desirable in hypothesis testing. As comfort is perceived by a subject, variation in the sensitivity of pressure receptors and pain receptors may explain this variation. Alternatively, improvements in running economy may drive the change in FSA with foot condition. However, in a recent study of habitually barefoot or minimally SD runners [159], whilst minimalist-shoe running with a FFS was more economical than traditional-shoe RFS running, for a given foot condition RFS and FFS running did not dif-

fer in running economy. It is possible that any metabolic benefit of an increase in elastic energy utilization is negated by the forces required by the *gastrocnemius* during FFS running compared with RFS running [75].

Stride length, which varies with condition, may be a valuable predictor for running kinematics and may be included as a stride-dependent parameter.

5.4.2 Velocity

Foot-strike strategy is velocity dependent. The nature of the changes in FSA with velocity depend on the condition under study, possibly because of the different levels of comfort associated with maximal and sub-maximal deformation of the heel pad [43] for BF and SD running respectively. For BF running there is no change (or a negligible change) in FSA as velocity increases but, in the SD condition the subjects increase foot dorsiflexion at FS as velocity increases. Increases in velocity are achieved by increasing stride length and possibly, increasing the distance along the direction of progression between the COM and heel and FS. An increasingly extended leg position with higher velocity may contribute to more RFS running for SD running at high velocity. This may also lead to larger braking forces at the foot. In the SD condition, this may not be painful and hence increasing dorsiflexion at FS is not actively avoided. Furthermore, at sub-maximal velocities, RFS running may be more economical than FFS running [154], explaining why for the SD condition, runners exhibit more dorsiflexed FSA. In the BF condition, where heel pad deformation is maximal, higher braking forces may be more painful such that increased dorsiflexion is avoided.

In the BF condition we do not see increases in plantarflexion as velocity increases. For high plantarflexion FSA, posterior impact force peaks occur whereas for high dorsiflexion FSA running they do not [20]. Therefore, increasing plantarflexion may also cause pain, but through increases in friction with the treadmill surface rather than through heel pad deformation.

The increase in foot dorsiflexion at FS with higher velocity for SD running is generally contradictory to previous work [22, 151] but a recent study, which also applied LMM in a study of recreational runners, corroborates this finding [131]. The set of speeds studied in this chapter, whilst relevant for aerobic training, is narrow, but the absence of a statistically significant difference between slow and medium velocity SD running are consistent with a recent study by Briene *et al.* [22]. In the study, which considered a wider velocity range of SD running, (3.2 ms^{-1} to 6.1 ms^{-1}) the difference between 3.2 ms^{-1} and 4.1 ms^{-1} was not statistically significant. Regardless, the observed adaptations of FSA may not extend to those which occur over a wider velocity scale. For the velocities studied, changes in proprioceptive feedback which are realized as pain from changes in FSA, may not be sufficient to limit such changes in the SD condition. Studying more velocities, and enough such that the variable may reasonably be modeled as continuous, would be an improvement on this work. Nevertheless, by accounting for individual variation, the results here are an accurate portrayal of the true fixed effects in this velocity range.

There may be a relatively stable, speed independent but subject-specific FSA for BF running at the first attempt, possibly motivated by a reduction in pain. For SD running in highly trained runners, pain may not be a consideration, as there is a speed dependence such that individuals readily and systematically alter their FSA by exhibiting more foot dorsiflexion at FS. At the first attempt running BF, the propensity for individuals to run with a FS strategy which does not adapt to changes in velocity may have implications for repetitive strain injury. Increased Achilles tendon loading rates [4] and calf pain [69] have been observed for FFS running and transitions to FFS running respectively. Coupled with a less adaptable FS pattern, leading to repetitive strain, this may be an injury concern for newly-transitioned BF runners.

5.4.3 Within-subject and between-subject variation

This statistical analysis allows for variation between subjects to be quantified and accounted for to give a more accurate estimate of the underlying behaviour. With that, a small subset of subjects have been identified as exhibiting outlying random variation. With this distribution of random variables estimated, it is possible to quantify the probability of a particular parameter value being observed. When studying different groups, this ability may be of value for identifying potentially anomalous behaviour.

The results suggest that individual subjects may exhibit increases in dorsiflexion for FSA at FS as velocity increases, whilst others demonstrate the opposite. By quantitatively accounting for this it is possible to make inferences about subject-specific versus systematic effects with more confidence than in previous studies [150].

For individuals who find running uncomfortable, there may be a state where they are highly variable, even within a given condition. This may explain the observations of, in particular, subjects MC and MG. Both subjects exhibited high levels of variability in the BF condition at 3.58 ms^{-1} (Chapter 4, Figure 4.3.1) and were outliers with respect to their medium velocity random variables. These differences may arise because BF running was particularly novel for these subjects. Recent work by Mann *et al.* [131] found that running-related injury was associated with less stride-to-stride randomness in FSA for recreational runners, as quantified using detrended fluctuation analysis [88]. Whilst the methodology was different, quantifying the randomness of the FSA time series may be of interest. Incidentally, the Mann study used LMMs in its statistical analyses but unfortunately, results pertaining to between-subject variation are not reported explicitly. The study, which considered only SD running, found that subjects tended to strike with more dorsiflexion in FSA as velocity increased around their preferred speed. This is corroborated by the results here, even though the Mann study used a preferred speed. The sample was drawn from the population of recreational runners and pressure insole devices rather than

motion analysis was used to measure FSS. In another study [22] using hierarchical models, the initial foot contact pattern, defined as strike index and measured using a plantar pressure plate, became more anterior with higher velocity for particular subjects, but stayed constant for others. This again emphasizes the value of using hierarchical models to quantify subject-specific behaviours. The study also identified typical and atypical RFS runners, based on the centre of pressure trajectory.

Independent of the outliers, within-subject (*i.e.* unexplained) variance ε_{ij} has implications for FSS classification. For SD running, the coefficients (Table 5.3.1) suggest most subjects are RFS runners ($\beta_0 + \beta_C = 12.24$), and when accounting for ε_{ij}, most of their foot strikes would be RFS. However for BF running the observed population mean for FSA is 7.18°, which is close to the RFS-NRFS boundary of 8°. Therefore, when classifying an individual according to the most likely strike type if, for example, their mean FSA is 7.18°, a large proportion of their observed foot strikes will by classified in a different category to their mean FSA. Quantitatively, with mean of 7.18°and ε_{ij} of 3.63°, the probability of observing a RFS from a set of foot strikes is calculated from the normal cumulative density function as

$$P(\text{BF RFS}) = 1 - F(x) = 1 - \frac{1}{2}\left[1 + \text{erf}\left(\frac{x-\mu}{\sigma\sqrt{2}}\right)\right]$$
$$P(\text{BF RFS}) = 1 - F(8.0) = \frac{1}{2}\left[1 + \text{erf}\left(\frac{8.00 - 7.18}{3.63\sqrt{2}}\right)\right]$$
$$P(\text{BF RFS}) = 1 - F(8.0) \approx 0.41$$

For the NRFS classification, approximately 41% of foot strikes will be RFS, and attempting to classify FSS for BF running [2, 85, 114] may be misleading. For SD running, this will not

typically be an issue. For an individual with a FSA of 12.24° the calculation for SD running is

$$P(\text{SD RFS}) = 1 - F(8.0) = 1 - \frac{1}{2}\left[1 + \text{erf}\left(\frac{8.00 - 12.24}{3.63\sqrt{2}}\right)\right]$$

$$P(\text{SD RFS}) = 1 - F(8.0) \approx 0.88$$

Therefore, approximately 12% of strides would not reflect the RFS classification. A recent study justified classifying a subject as a RFS runner if 90% of their foot strikes were RFS [69]. Therefore, even a conservative cut off is comparable to the realistic rate of strides which do not reflect the classification. Thus, by classifying subjects according to SD FSS, subjects may be unnecessarily excluded from studies, which will then lead to a unnecessarily low statistical power and a higher proportion of false negative results (Type II error). Furthermore, the true variability in the population will not be captured when, for example, studies seek to classify the proportions of subjects who switch FSS when running BF versus SD.

A recent study [124] using 2D video analysis found that, in their habitual condition, habitually BF runners have more variability in FSA than habitually SD runners. Within-subject variability is comparable with this study, but slightly lower than the variability observed in [124]. The authors argue that variability in FSA is beneficial for runners. The study did not experimentally control for velocity, and the results in this chapter show a clear interaction between condition and velocity in an habitually SD population. In the study, whilst collinearity between the nine predictors was investigated, the authors only reported that a mimimum for two strides were collected for each of the minimum of 16 different conditions. This is a methodological issue because typically, when trying to fit a regression model, ten to fifteen data points per predictor are necessary and the total number of data points are not directly reported.

5.4.4 Limitations

The novelty of running BF for the sample of habitually SD runners is likely to influence the results. Differences in the mechanics of the shoe versus the bare foot may be diminished in comparison to the novelty of BF running. The Foot Thong™, by potentially reducing discomfort caused shear forces on the fore foot, may have allowed subjects to strike the treadmill with more plantarflexion. However, the Foot Thong™ was very rarely used (three subjects). Nevertheless, extending results beyond a comparison between SD running and first-attempt BF running, is discouraged. However, given that most runners who undertake BF running, do so for only a small portion of their total running volume [94], there is value in studying novice BF running because it is typical for any 'BF runner' to have only a limited experience of the condition relative to SD running.

This analysis was focused on the global orientation of the foot, and measures of ankle joint kinematics were not included in this analysis; in the absense of directly comparable kinematic models of the rearfoot, analysis of the ankle joint kinematic was not performed. However, ankle joint kinematics are of clinical interest because they inform on functional adaptations. Therefore it is highly recommended that an analysis which appropriately accounts for between-subject variability be performed.

Velocity is a continuous variable but too few velocities were sampled to allow verification of the particular shape of the continuous function. Whilst models run with velocity as a continuous predictor (units ms^{-1}) provided similar inferences to those presented here, more work is needed to verify this.

If runners were recorded at faster and slower velocities than those sampled here, the speed dependent behaviour may change. The near significance for fast velocity may reflect this. Also, the observations here may be dependent on the physiological demands of the velocity under study. For example, if individuals were running to achieve physiologically demanding perfor-

mance targets, they may not control for foot discomfort.

Subjects move with respect to the treadmill surface during each stride. Therefore, stride length calculations could be improved by accounting for translation of the foot with respect to the treadmill surface.

5.5 Conclusion

The random variation between individuals within a given condition (*e.g.* running BF) is the same order of magnitude as the change from a fixed effect of condition. By appropriately accounting for this large variation, changes in FSA with velocity for the range studied appear to contradict consensus (for BF running) that runners exhibit more foot plantarflexion at FS with respect to the ground as velocity increases. Rather, for SD running, subjects increase foot dorsiflexion as velocity increases. This may arise from the influence of discomfort or novelty associated with BF running, but not SD running, at aerobic training velocities. The absence of any speed dependency for FSA in the BF condition may elevate the risk of injury at the acute stage by increasing the repetitive loading.

With the appropriate application of hierarchical LMM, it is possible to draw inferences which have not previously been readily accessible in the biomechanics community.

Chapter 6

Lower-leg electromyography for running

This chapter presents and discusses electromyography (EMG) data for running during different parts of the gait cycle as a function of condition and velocity. Foot-strike angle (FSA), which has been implicated in running injury risk, and shown to vary in a non-trivial manner (Chapter 5), is treated as a covariate per gait cycle. In hypothesis tests, first and second order interactions are included, given results from Chapter 5, where the interaction between condition and velocity was a significant effect on FSA. Muscle activity for the *tibialis anterior, gastrocnemius medialis* and *gastrocnemius lateralis* are measured, and generalized linear mixed models (GLMM) are applied to account for the random variation within and between subjects, the non-normal distribution of the EMG response variable, and heteroscedasticity.

The *gastrocnemius medialis* pre-activation is more sensitive to changes in condition and footwear than the *gastrocnemius lateralis*. This may reflect a subtle difference between the function of the *gastrocnemius medialis* and *gastrocnemius lateralis* muscles during running gait, and have implications for muscle fatigue.

6.1 Introduction

Previous work presented in this thesis found that velocity and condition influence FSA, possibly due to comfort because of maximal versus sub-maxinal deformation of the heel pad for BF versus SD running, such that FSA changed as a function of velocity for SD, but not BF running (Section 5.4). Study of individuals' physiology may inform on the implications of controlling movement patterns. Using EMG analysis, it is possible to establish links between movement patterns and physiology. We may use EMG analysis to understand why movement occurs and suggest alterations to training programs and movement patterns if necessary. This chapter aims to understand the effects of velocity and condition, whilst accounting for FSA, on lower-leg EMG signals at particular parts of the gait cycle. Specifically what is the muscle function around FS and how does this explain movement? Conversely, how does movement explain the muscle function?

It has been suggested that increased plantarflexion during BF running is caused by higher pre-activation of the *triceps surae* muscles [50] and lower pre-activation of the *tibialis anterior* [205]. This is characteristic of an 'impact-reduction' style [69] which lowers or even completely removes the vertical ground reaction force impact peak and reduces the loading rate [46]. By reducing loading rate, it is hypothesized that the risk of tibial stress fractures decreases. In the present work, FSA is considered a covariate because it is not an intervention in this study. Changes in FSA are hypothesized to correlate with changes in the EMG signal. Subjects with more plantarflexion at FS are hypothesized to demonstrate higher levels of *gastrocnemius lateralis* and *gastrocnemius medialis* muscle activity and lower *tibialis anterior* muscle activity, as observed in previous studies.

In the previous chapter there was no significant effect of velocity on FSA for the BF condition. Given that FSA is hypothesized to affect EMG pre-activation, and velocity does not affect

FSA in the BF condition, no changes in pre-activation with velocity are anticipated for BF running. Results from the previous chapter demonstrated that changes in velocity caused changes in FSA for the SD condition. In this chapter we may test the hypothesis that velocity affects pre-activation for SD running, whilst accounting for variation due to changes in FSA. We hypothesize that by accounting for variation due to FSA, there is no significant effect of velocity for SD running, to support the hypothesis that changes in pre-activation arise from changes in foot-fall strategy.

For heel-toe running, it has been suggested that changes in EMG for lower extremity muscles are more velocity than condition dependent [108]. However, with FSA as a covariate, we may quantify the relative significance of velocity and condition for both heel-toe running and non-heel-toe running to more accurately understand the relative magnitudes of the effects of velocity and condition. We hypothesize that, for RFS (*i.e.* heel-toe) running, the magnitude of the effect of condition is larger than the effect of velocity in the range studied. This is driven by the assumption that, for the present sample of runners, the physiological demands of removing running shoes are higher than the demands induced by running at 16.0 kph versus 12.9 kph. Further, it is hypothesized that *gastrocnemius* muscle activity lowers whilst *tibialis anterior* muscle activity increases for SD versus BF running, reflecting the anticipated response of anterior and posterior muscle to mechanical moments for heel-toe running.

Few studies account for between-subject variation. The previous chapter used an LMM but, because the root-mean-square (RMS) of a signal takes only positive values, an LMM is invalid here. Specifically, the distribution of RMS EMG measurements over the timescales in this study follow a non-Gaussian distribution. Therefore, GLMM are necessary. These models, which may be applied to distributions of response variables which are non-Gaussian, are applied to data in this study.

6.2 Methods

6.2.1 Subjects

The subject inclusion and exclusion criteria have been previously described (Section 3.1). Data for seventeen subjects were used for analysis. Of the nineteen subjects recruited for the overall study, one subject (MF) was excluded because during data collection the EMG gains were incorrectly set and another subject (ML) did not have EMG data.

6.2.2 Experimental data collection and data processing

The data collection and processing procedure has been described elsewhere (Sections 3.4 and 3.5). Briefly, subjects ran for approximately 200 seconds at each of three velocities (3.58, 3.97 and 4.44 ms^{-1}) in a randomized order first BF, and then SD. Barefoot running was studied first, allowing markers to be placed on the foot before excessive perspiration disrupted skin marker adhesion. Raw surface EMG signals were measured for the *gastrocnemius medialis*, *gastrocnemius lateralis* and *tibialis anterior* muscles.

6.2.3 Data analysis

Although as few as 6-10 gait cycles are sufficient to produce a representative EMG pattern [182], typically 20-40 cycles are used [96,101,147] and here, based on the maximum number of strides available, between 15 and 27 consecutive gait cycles were analysed for each subject.

The root mean squared (RMS) value of the EMG signal was calculated for five time periods (Table 6.2.1), to most directly measure muscle signal power. Parameters were chosen so as to compare with literature [69] and focus on parts of the gait cycle typically associated with injury, proprioception and likely influences by FSA.

Time periods	
Pre-activation	The 50 ms before FS
Impact phase activation	The first 30 ms following FS
Braking phase	From 30 ms to 50% stance phase
Stance phase	During foot contact, from FS to TO
Stride cycle	Between successive foot strikes

Table 6.2.1: Time periods: The root-mean-squared value of the EMG signal was calculated for the given time periods.

6.2.4 In-shoe foot inclination

The in-shoe foot inclination was calculated as described elsewhere (Section 4.2.4). Comparisons of FSA between BF and SD running are made between the orientation of the foot as measured directly from skin mounted markers, and from the calculated orientation of the foot inside the shoe.

6.2.5 Statistical analysis

Exploratory analysis and the domain of the EMG response data motivated the application of a GLMM [137] to data. A GLMM is an extension of an LMM, which was applied in Chapter 5. In a GLMM, response variables may be drawn from distributions which are non-Gaussian [51, 119, 213] and rather than modeling the responses directly, a link function is applied to relate the response to a linear predictor. A GLMM is capable of modeling heteroscedastic data, avoiding transformation bias which arises from transforming response data. Heteroscedasticity is where the variance of the data is not independent of the data value, as is the case for the current dataset when fitted with an LMM. Transformation bias refers to the alteration of the variance structure because of manipulating the response data. Assumptions must be made about the distribution of the random effects, the distribution of the response variable given the nature of

the random effects, and a link function must be determined. The linear predictor η has the form

$$\eta = X\beta + Zb$$

where in general X is an N by p design matrix for p predictor variables and N observations; β is a p by 1 vector of the fixed-effects regression coefficients; Z is an N by q design matrix for the q random effects; b is a q by 1 vector of the random-effects coefficients and $b \sim \mathcal{N}\left(0, \Sigma^2\right)$, where Σ^2 is the variance-covariance matrix of the random effects. The link function, g, applied to data in this chapter, known as the log link function, was used to relate the conditional expectation $\mathbb{E}[y \mid \beta, b]$ of the outcome y to the linear predictor η and was given as

$$g\left(\mathbb{E}[y \mid \beta, b]\right) = \ln\left[\mathbb{E}[y \mid \beta, b]\right] = \eta$$

The choice of the log link function was motivated by the EMG response data taking only real positive values. This also required a distribution of the response data which would allow for a positive mean value, which here was a gamma distribution. A gamma distribution with a log link function fit well to response data (Figure 6.2.1). The inverse link function h was therefore

$$h(\eta) = g^{-1}(\eta) = \exp[\eta]$$

which gave the response y as

$$y = h(\eta) + \varepsilon$$

where y and ε were a N by 1 vectors of the response variable and the residual errors respectively and $y \sim \Gamma(k, \theta)$, with k as the shape parameter and θ as the scale parameter. It is important to note that the distribution of the residual errors may be non-Gaussian and for a gamma distributed

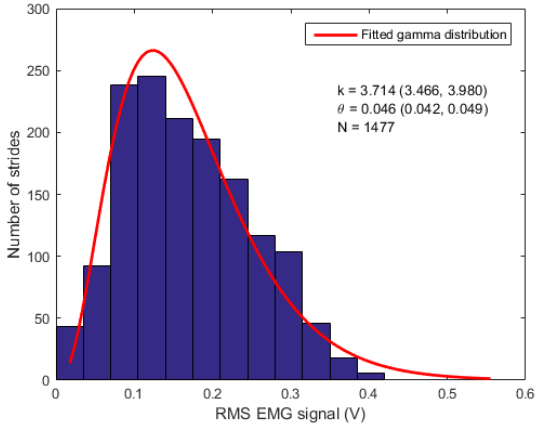


Figure 6.2.1: Visual inspection showed the distribution of EMG response variables fit well to a gamma distribution. Data were taken from the RMS EMG responses for the *tibialis anterior* muscle pre-activation for all subjects and both conditions. The shape and scale parameters k and θ with their 95% confidence intervals are reported, together with the total number or observations, N.

GLMM with a log link function the distribution of random effects is assumed to be Gaussian.

A saturated model included the three main effects of condition, velocity and FSA, together with first and second order interactions. The interactions which included FSA were present to account for variance, such that hypothesis tests on condition and velocity were more powerful. Hypothesis testing was performed on the saturated models, thus avoiding the inflation of Type I errors (false positives) associated with stepwise regression using multiple predictors [146]. Inspecting the residuals grouped by subject from fitting a GLM suggested that, for all models, a random intercept at the subject level was required. Velocity and condition were considered independently as random effects in each model. Visual inspection of the residuals, grouped by subject and effect, were used to ascertain where an additional random effect was required to explain variation. Likelihood ratio tests were used to test for any significant improvement on the random intercept model. The normality assumptions of the random effects coefficients were checked visually using quantile-quantile plots, and random effects were rejected if they did not satisfy the assumption of normality. Either a diagonal or fully parameterized covariance matrix Σ^2 was fitted to the final model. Unless a likelihood ratio test identified the model with a fully

parametrized Σ^2 as significantly better than the model with a diagonal Σ^2, the more parsimonious case of the diagonal Σ^2 (*i.e.* uncorrelated random effects) was chosen. In cases where models with a random effect of velocity and a random effect of condition were both valid, a final model with both velocity and condition as random effects was fitted. If either effect no longer satisfied the normality assumption in this final model, the previous model with the lowest Akaike Information Criterion (AIC) [3] score was chosen as the final model. Assuming the number of observations is far larger than the number of fixed-effect coefficients, the AIC is an unbiased estimator of the relative amount of information lost between an approximating model and the true generating mechanism for the data. The AIC penalizes unnecessarily complicated models and is appropriate when comparing two (or more) potential models, where smaller magnitudes for the AIC indicate less lost information.

The dispersion δ calculated for the GLMM here as k^{-1}, is the analogue of the variance of the residuals for LMM. Five statistical test were performed on a single gait cycle. Therefore, a Bonferroni correction [54] was applied with $n = 5$, giving a significance level of $\alpha = 0.01$ for each parameter, thus maintaining a family-wise error rate of $\alpha_f = 0.05$. Standardized residuals versus the model fitted values for final models were checked using scatter plots and demonstrated that data were heteroscedastic (Figure 6.2.2).

6.3 Results

6.3.1 Final models

A summary of the nature of the significant fixed effects is given in Table 6.3.1. To account for variation at the subject level, the applied GLMM was also a hierarchical model. Equation 6.3.1 is the general form of the models for the EMG response data and contains a random intercept for the EMG data at the subject level. The model is interpreted as each subject having a similar

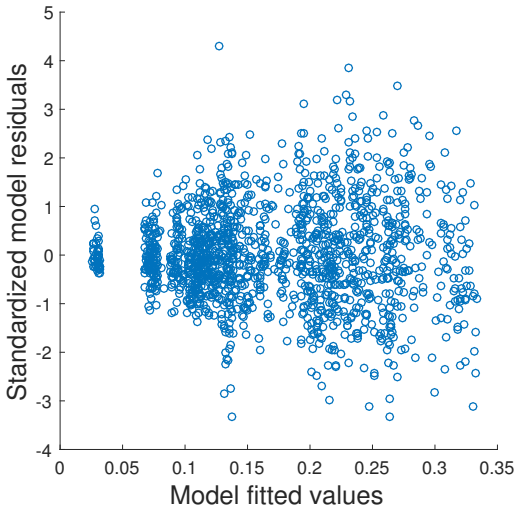


Figure 6.2.2: A plot of the standardized model residuals versus the model fitted values demonstrate heteroscedasticity. The variance of the residuals increases as the fitted values increase in magnitude. A GLMM can effectively model heteroscedastic data.

	TA					**GM**					**GL**				
Coeff.	P	Im	Br	Sta	Str	P	Im	Br	Sta	Str	P	Im	Br	Sta	Str
β_C		↓	↓	↓		↓	↓	↓		↓	↓	↓	↓	↓	↓
β_{V_m}			↓					↓			↓	↓	↓	↓	↓
β_{V_f}	↑		↑	↑	↑		↑	↑	↑	↑		↑	↑	↑	↑
β_{FSA}	↑				↑	↓	↓				↓		↓		↓
$\beta_{C:V_m}$			↑			↑	↑	↑	↑	↑	↑	↑	↑	↑	↑
$\beta_{C:V_f}$						↑		↑		↑					
$\beta_{C:FSA}$	↑			↑	↓										
$\beta_{V_m:FSA}$			↑	↑		↑	↑	↑	↑	↑	↑	↑	↑	↑	↑
$\beta_{V_f:FSA}$	↓				↓					↓	↑				
$\beta_{C:V_m:FSA}$			↓	↓		↓	↓	↓		↓	↓	↓	↓	↓	↓
$\beta_{C:V_f:FSA}$							↑				↓	↑		↑	

Table 6.3.1: Summary of the significant fixed effects in all models for all five time periods (P: pre-activation; Im: impact; Br: braking; Sta: stance; Str: stride) at $\alpha_f = 0.05$, following a Bonferroni correction. ↑ and ↓ suggest an increase and decrease respectively in EMG for the given effect, compared to the reference condition of slow velocity BF running with FSA = 0. ↑ for the β_{FSA} suggest an increase in EMG with more foot dorsiflexion at FS. The muscles are TA: *tibialis anterior*, GM: *gastrocnemius medialis*, and GL: *gastrocnemius lateralis*.

underlying EMG signal. Between-subject variation is accounted for to get a more accurate estimate of the signal for the underlying population. The models are of the form

$$\textbf{Level 1: } Response_{ij} = \exp\left[\beta_{0j} + X_j\beta_{1j}\right] + \varepsilon_{ij} \tag{6.3.1a}$$

$$\textbf{Level 2:} \quad \begin{aligned} \beta_{0j} &= \beta_0 + b_{0j} \\ \beta_{1j} &= \beta_1 + b_{1j} \end{aligned} \tag{6.3.1b}$$

where ε_{ij} are the residuals of the i^{th} stride for the j^{th} subject and X_j is a design matrix for the j^{th} subject. The coefficient β_{0j} is the intercept for the j^{th} subject, where β_0 is the fixed component representing the population mean for the reference condition and b_{0j} is the random component representing random variation at the subject level, j. The vector of ceofficients β_{1j} comprises β_1, which are the fixed-effect coefficients and b_{1j}, which are the random effects for the j^{th} subject. For the j^{th} subject this is given, in general and for the saturated case, as

$$\beta_{1j} = \begin{bmatrix} \beta_C + b_{Cj} \\ \beta_{V_m} + b_{V_m j} \\ \beta_{V_f} + b_{V_f j} \\ \beta_{FSA} \\ \beta_{C:V_m} \\ \beta_{C:V_f} \\ \beta_{C:FSA} \\ \beta_{V_m:FSA} \\ \beta_{V_f:FSA} \\ \beta_{C:V_m:FSA} \\ \beta_{C:V_f:FSA} \end{bmatrix} \tag{6.3.2}$$

with coefficients β_C for condition, β_{V_m} and β_{V_f} for medium and fast velocity respectively, β_{FSA} for FSA, first order interactions as $\beta_{C:V_m}$, $\beta_{C:V_f}$, $\beta_{C:FSA}$, $\beta_{V_m:FSA}$, $\beta_{V_f:FSA}$, and second order interactions $\beta_{C:V_m:FSA}$ and $\beta_{C:V_f:FSA}$. Condition and velocity potentially had random effects components. Therefore, the coefficients $b_{ij} \sim \mathcal{N}_4\left(0, \Sigma^2\right)$, where the variance-covariance matrix

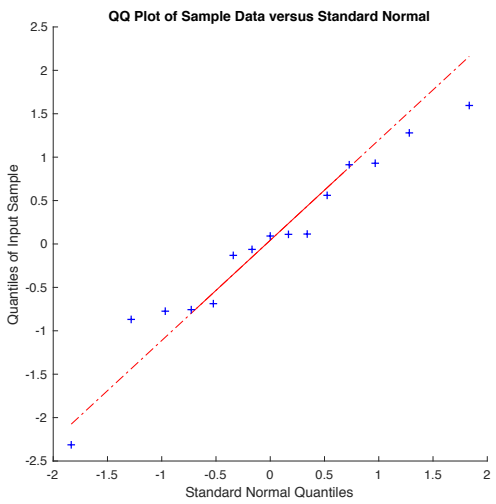


Figure 6.3.1: QQ-plots of the random coefficients (intercepts) from Equation 6.3.1b for the *tibialis anterior* during pre-activation phase. Coefficients were normally distributed.

Σ^2 was given, for the case of saturated random effects, as

$$\Sigma^2 = \begin{bmatrix} \sigma_0^2 & \rho_{0:C}\sigma_0\sigma_C & \rho_{0:V_m}\sigma_0\sigma_{V_m} & \rho_{0:V_f}\sigma_0\sigma_{V_f} \\ \rho_{C:0}\sigma_C\sigma_0 & \sigma_C^2 & \rho_{C:V_m}\sigma_C\sigma_{V_m} & \rho_{C:V_f}\sigma_C\sigma_{V_f} \\ \rho_{V_m:0}\sigma_{V_m}\sigma_0 & \rho_{V_m:C}\sigma_{V_m}\sigma_C & \sigma_{V_m}^2 & \rho_{V_m:V_f}\sigma_{V_m}\sigma_{V_f} \\ \rho_{V_f:0}\sigma_{V_f}\sigma_0 & \rho_{V_f:C}\sigma_{V_f}\sigma_C & \rho_{V_f:V_m}\sigma_{V_f}\sigma_{V_m} & \sigma_{V_f}^2 \end{bmatrix} \tag{6.3.3}$$

where σ_0, σ_C, σ_{V_m}, and σ_{V_f} are the standard deviations of the random intercepts, effects of condition, medium velocity, and fast velocity respectively. The parameters ρ are the correlation coefficients between random effects, given by subscripts. A total of 1610 gait cycles were studied for 15 of 16 subjects. There was a mean of 17 gait cycles for each trial and 103 gait cycles per subject. All final models satisfied the assumption of normality for the distribution of random effects. The random effects for the *tibialis anterior* pre-activation phase are given as an example (Figure 6.3.1). A random intercept was included in the final model.

To illustrate the interpretation of the fixed-effects model coefficients, the following is a worked example using the *tibialis anterior* muscle during the pre-activation phase. Note that random effects exist at the subject level. The reference condition is running at the slowest

	Pre-activation			**Impact**			**Braking**			**Stance**			**Stride**		
Coeff.	Est.	S.E.	p-value	Est.	S.E.	p-value	Est.	S.E.	p-value	Est.	S.E.	p-value	Est.	S.E.	p-value
β_0	-2.352	0.144	< 0.001*	-2.651	0.137	< 0.001*	-3.054	0.123	< 0.001*	-3.037	0.108	< 0.001*	-2.837	0.096	< 0.001*
β_C	-0.120	0.053	0.024	-0.378	0.093	< 0.001*	-0.210	0.044	< 0.001*	-0.322	0.048	< 0.001*	0.074	0.075	0.329
β_{V_m}	0.042	0.039	0.275	-0.079	0.067	0.243	-0.108	0.032	0.001*	-0.080	0.035	0.023	0.086	0.038	0.025
β_{V_f}	0.154	0.039	< 0.001*	0.069	0.069	0.314	0.144	0.033	< 0.001*	0.132	0.036	< 0.001*	0.226	0.044	< 0.001*
β_{FSA}	0.029	0.003	< 0.001*	0.009	0.005	0.073	-0.001	0.002	0.707	0.004	0.003	0.173	0.021	0.002	< 0.001*
$\beta_{C:V_m}$	-0.092	0.076	0.226	0.069	0.133	0.603	0.195	0.063	0.002*	0.157	0.069	0.024	-0.016	0.036	0.667
$\beta_{C:V_f}$	-0.057	0.069	0.403	0.297	0.120	0.013	-0.019	0.057	0.740	0.118	0.062	0.059	0.023	0.033	0.482
$\beta_{C:FSA}$	0.016	0.004	< 0.001*	0.017	0.007	0.012	0.002	0.003	0.478	0.010	0.004	0.005*	-0.010	0.003	0.003*
$\beta_{V_m:FSA}$	-0.002	0.004	0.607	0.010	0.007	0.118	0.020	0.003	< 0.001*	0.016	0.003	< 0.001*	|·|	0.002	0.944
$\beta_{V_f:FSA}$	-0.013	0.004	< 0.001*	-0.002	0.006	0.778	0.001	0.003	0.785	|·|	0.003	0.931	-0.012	0.002	< 0.001*
$\beta_{C:V_m:FSA}$	0.002	0.006	0.744	-0.011	0.010	0.250	-0.015	0.005	0.002*	-0.016	0.005	0.002*	|·|	0.003	0.916
$\beta_{C:V_f:FSA}$	0.005	0.005	0.342	-0.019	0.009	0.040	0.005	0.004	0.257	-0.006	0.005	0.196	0.006	0.002	0.013
Coeff.	Est.	Lower	Upper	Est.	Lower	Upper	Est.	Lower	Upper	Est.	Lower	Upper	Est.	Lower	Upper
σ_0	0.545	0.376	0.790	0.484	0.332	0.707	0.467	0.321	0.678	0.404	0.278	0.588	0.363	0.247	0.534
σ_C													0.214	0.137	0.336
σ_{V_m}													0.116	0.076	0.178
σ_{V_f}													0.136	0.090	0.206
$\sqrt{\delta}$	0.257	0.248	0.267	0.461	0.445	0.478	0.217	0.210	0.225	0.240	0.232	0.249	0.102	0.098	0.106
Coeff.		Est.			Est.			Est.			Est.			Est.	
R^2_{adj}		0.84			0.49			0.77			0.65			0.93	

Table 6.3.2: Model coefficient (Coeff.) estimates for the *tibialis anterior* muscle, where $|\cdot|$ denotes the absolute value is less than 0.001. For each time period, fixed-effects coefficient estimates (Est.) are presented, calculated as described in Section 6.3.1, with standard error (S.E.) and the p-value. * denotes significance at $\alpha_f = 0.05$, following a Bonferroni correction. The standard deviation of the random coefficients, σ, and estimates of the correlation coefficients, ρ, are presented with 95% confidence intervals (where significantly different from zero). The estimate $\sqrt{\delta}$, which quantifies the spread of the residuals in a manner analogous to the standard deviation of the residuals in a LMM, is reported with 95% confidence intervals. The adjusted coefficient of determination R^2_{adj} quantifies the final model goodness of fit.

	Pre-activation			**Impact**			**Braking**			**Stance**			**Stride**		
Coeff.	Est.	S.E.	p-value	Est.	S.E.	p-value	Est.	S.E.	p-value	Est.	S.E.	p-value	Est.	S.E.	p-value
β_0	-1.920	0.154	< 0.001*	-1.724	0.112	< 0.001*	-1.465	0.069	< 0.001*	-1.681	0.077	< 0.001*	-2.184	0.081	< 0.001*
β_C	-0.641	0.144	< 0.001*	-0.506	0.073	< 0.001*	-0.149	0.026	< 0.001*	-0.125	0.058	0.032	-0.177	0.024	< 0.001*
β_{V_m}	-0.144	0.088	0.103	-0.143	0.059	0.016	-0.075	0.021	< 0.001*	-0.031	0.033	0.359	-0.018	0.040	0.656
β_{V_f}	0.258	0.108	0.017	0.173	0.060	0.004*	0.058	0.022	0.007*	0.130	0.040	0.001*	0.149	0.043	0.001*
β_{FSA}	-0.044	0.006	< 0.001*	-0.032	0.005	< 0.001*	-0.004	0.002	0.011	-0.001	0.002	0.580	-0.000	0.002	0.875
$\beta_{C:V_m}$	0.424	0.109	< 0.001*	0.460	0.111	< 0.001*	0.301	0.040	< 0.001*	0.103	0.039	0.008*	0.350	0.038	< 0.001*
$\beta_{C:V_f}$	0.233	0.090	0.010*	-0.042	0.097	0.664	0.134	0.035	< 0.001*	0.081	0.032	0.011	0.093	0.033	0.005*
$\beta_{C:FSA}$	0.015	0.009	0.082	0.001	0.006	0.887	0.005	0.002	0.011	-0.003	0.003	0.327	0.003	0.002	0.124
$\beta_{V_m:FSA}$	0.037	0.007	< 0.001*	0.037	0.006	< 0.001*	0.016	0.002	< 0.001*	0.011	0.003	< 0.001*	0.010	0.003	< 0.001*
$\beta_{V_f:FSA}$	-0.002	0.007	0.789	0.013	0.006	0.028	0.003	0.002	0.147	-0.004	0.003	0.148	-0.008	0.003	0.004*
$\beta_{C:V_m:FSA}$	-0.039	0.008	< 0.001*	-0.036	0.009	< 0.001*	-0.023	0.003	< 0.001*	-0.008	0.003	0.010	-0.027	0.003	< 0.001*
$\beta_{C:V_f:FSA}$	0.007	0.007	0.315	0.027	0.008	0.001*	-0.002	0.003	0.458	0.003	0.003	0.180	0.003	0.003	0.269
Coeff.	Est.	Lower	Upper	Est.	Lower	Upper	Est.	Lower	Upper	Est.	Lower	Upper	Est.	Lower	Upper
σ_0	0.571	0.393	0.829	0.404	0.281	0.581	0.266	0.186	0.381	0.297	0.207	0.426	0.316	0.221	0.453
σ_C	0.386	0.258	0.575							0.163	0.110	0.241			
σ_{V_m}	0.242	0.156	0.376							0.097	0.065	0.145	0.131	0.088	0.194
σ_{V_f}	0.340	0.225	0.516							0.127	0.086	0.189	0.140	0.094	0.207
$\rho_{0:C}$	0.068	-0.464	0.564							-0.030	-0.554	0.511			
$\rho_{0:V_m}$	-0.787	-0.929	-0.439							-0.775	-0.921	-0.437	-0.730	-0.898	-0.376
$\rho_{0:V_f}$	-0.844	-0.948	-0.579							-0.181	-0.611	0.330	-0.351	-0.711	0.156
$\rho_{C:V_m}$	0.197	-0.382	0.665							-0.140	-0.642	0.445			
$\rho_{C:V_f}$	-0.171	-0.634	0.383							0.270	-0.269	0.680			
$\rho_{V_m:V_f}$	0.912	0.670	0.979							0.539	0.037	0.824	0.727	0.342	0.903
$\sqrt{\delta}$	0.350	0.338	0.362	0.434	0.420	0.449	0.155	0.150	0.161	0.124	0.120	0.128	0.128	0.124	0.132
Coeff.		Est.			Est.			Est.			Est.			Est.	
R^2_{adj}		0.82			0.54			0.73			0.85			0.84	

Table 6.3.3: Model coefficient (Coeff.) estimates for the *gastrocnemius medialis* muscle. For time period, fixed-effects coefficient estimates (Est.) are presented, calculated as described in Section 6.3.1, with standard error (S.E.) and the p-value. * denotes significance at $\alpha_f = 0.05$, following a Bonferroni correction. The standard deviation of the random coefficients, σ, and estimates of the correlation coefficients, ρ, are presented with 95% confidence intervals (where significantly different from zero). The estimate $\sqrt{\delta}$, which quantifies the spread of the residuals in a manner analogous to the standard deviation of the residuals in a LMM, is reported with 95% confidence intervals. The adjusted coefficient of determination R^2_{adj} quantifies the final model goodness of fit.

	Pre-activation			**Impact**			**Braking**			**Stance**			**Stride**		
Coeff.	Est.	S.E.	p-value	Est.	S.E.	p-value	Est.	S.E.	p-value	Est.	S.E.	p-value	Est.	S.E.	p-value
β_0	-2.433	0.126	< 0.001*	-2.219	0.145	< 0.001*	-1.755	0.078	< 0.001*	-1.925	0.085	< 0.001*	-2.420	0.083	< 0.001*
β_C	-0.398	0.074	< 0.001*	-0.480	0.082	< 0.001*	-0.118	0.032	< 0.001*	-0.164	0.029	< 0.001*	-0.167	0.028	< 0.001*
β_{V_m}	-0.335	0.060	< 0.001*	-0.348	0.066	< 0.001*	-0.120	0.026	< 0.001*	-0.156	0.024	< 0.001*	-0.139	0.023	< 0.001*
β_{V_f}	0.140	0.063	0.028	0.366	0.070	< 0.001*	0.138	0.027	< 0.001*	0.182	0.025	< 0.001*	0.166	0.024	< 0.001*
β_{FSA}	-0.047	0.005	< 0.001*	-0.017	0.005	0.001*	0.001	0.002	0.535	-0.003	0.002	0.066	-0.006	0.002	0.002*
$\beta_{C:V_m}$	0.739	0.120	< 0.001*	0.543	0.132	< 0.001*	0.298	0.051	< 0.001*	0.327	0.047	< 0.001*	0.315	0.046	< 0.001*
$\beta_{C:V_f}$	0.208	0.103	0.044	-0.185	0.114	0.103	0.031	0.044	0.480	-0.020	0.041	0.630	0.020	0.039	0.607
$\beta_{C:FSA}$	0.012	0.006	0.042	-0.002	0.007	0.805	0.002	0.003	0.536	0.005	0.002	0.039	0.005	0.002	0.038
$\beta_{V_m:FSA}$	0.067	0.006	0.000	0.059	0.007	0.000	0.018	0.003	0.000	0.022	0.002	0.000	0.020	0.002	0.000
$\beta_{V_f:FSA}$	0.032	0.006	< 0.001*	-0.001	0.007	0.847	-0.001	0.003	0.668	-0.003	0.002	0.162	-0.004	0.002	0.122
$\beta_{C:V_m:FSA}$	-0.078	0.009	< 0.001*	-0.054	0.010	< 0.001*	-0.022	0.004	< 0.001*	-0.026	0.004	< 0.001*	-0.025	0.004	< 0.001*
$\beta_{C:V_f:FSA}$	-0.022	0.008	0.007*	0.033	0.009	< 0.001*	0.005	0.004	0.194	0.009	0.003	0.007*	0.006	0.003	0.045

Coeff.	Est.	Lower	Upper	Est.	Lower	Upper	Est.	Lower	Upper	Est.	Lower	Upper	Est.	Lower	Upper
σ_0	0.463	0.321	0.669	0.540	0.374	0.778	0.300	0.210	0.431	0.330	0.231	0.473	0.324	0.227	0.465
$\sqrt{\delta}$	0.407	0.392	0.422	0.460	0.444	0.476	0.179	0.173	0.185	0.164	0.159	0.170	0.155	0.149	0.161

Coeff.	Est.	Est.	Est.	Est.	Est.
R^2_{adj}	0.61	0.57	0.72	0.78	0.80

Table 6.3.4: Model coefficient (Coeff.) estimates for the *gastrocnemius lateralis* muscle. For each time period, fixed-effect coefficient estimates (Est.) are presented, calculated as described in Section 6.3.1, with standard error (S.E.) and the p-value. * denotes significance at $\alpha_f = 0.05$, following a Bonferroni correction. The standard deviation of the random coefficients, σ, and estimates of the correlation coefficients, ρ, are presented with 95% confidence intervals (where significantly different from zero). The estimate $\sqrt{\delta}$, which quantifies the spread of the residuals in a manner analogous to the standard deviation of the residuals in a LMM, is reported with 95% confidence intervals. The adjusted coefficient of determination R^2_{adj} quantifies the final model goodness of fit.

velocity and in the BF condition for a FSA of 0°, which is generally considered a NRFS [6]. For this reference condition the underlying population EMG signal is calculated by evaluating $\exp[\beta_0]$. By using data from Table 6.3.2 we find

$$EMG = \exp[-2.352] = 0.095\,V$$

where V is volts. Next, to calculate the EMG signal for running at 3.58 ms^{-1} and in the SD condition for an individual with a FSA of 0°, we evaluate

$$EMG = \exp[\beta_0 + \beta_C]$$

which, using the laws of exponents becomes

$$EMG = \exp[\beta_0] \cdot \exp[\beta_C]$$

and by substitution of data from Table 6.3.2, we find

$$EMG = 0.095 \cdot \exp[-0.120]\,V$$

$$EMG = 0.095 \cdot 0.887\,V \tag{6.3.4a}$$

which simplifies to

$$EMG = 0.084\,V$$

The result in Equation 6.3.4a may be interpreted as saying a change from BF to SD running induced a 11.3% reduction in *tibialis anterior* pre-activation. However, the $p-$value for the coefficient β_C is 0.024, meaning the coefficient is not statistically significantly different from zero and therefore there is no statistically significant change from BF to SD at FSA $= 0°$. Fast

running in the BF condition has an EMG signal calculated as

$$EMG = \exp\left[\beta_0 + \beta_{V_f}\right]$$

$$EMG = \exp\left[-2.352 + 0.154\right] V = 0.095 \cdot 1.167$$

$$EMG = 0.111V$$

This demonstrates an increase of 16.7% for EMG pre-activation compared with slow BF running. With a p-value of less than 0.001, this is statistically significantly different from zero at $\alpha = 0.01$, and therefore there is a change in EMG signal when changing from slow to fast BF running at FSA $= 0^\circ$. For more complicated comparisons to the reference condition, we may sum the exponents for the fixed effects to then calculate whether we increase or decrease with respect to the reference condition. For example, if we wish to compare BF running at the medium velocity for an FSA of 10° dorsiflexion to the reference condition, we calculate the voltage as

$$EMG = \exp\left[\beta_0 + \beta_{V_m} + 10 \cdot \beta_{FSA} + 10 \cdot \beta_{V_m:FSA}\right]$$

$$EMG = \exp\left[-2.352 + (0.042) + 10 \cdot (0.029) + 10 \cdot (-0.002)\right]$$

$$EMG = \exp\left[-2.352 + 0.312\right] = 0.095 \cdot 1.366$$

$$EMG = 0.130V$$

Note that β_{FSA} relates the change due to $+1^\circ$ change in FSA. There are interaction terms to consider and therefore the associated main effects, whether significant or not, must be included in the calculation of the EMG signal when higher order terms are present. With respect to statistical significance of the effects, analysis of the $p-$values show only β_{FSA} was statistically significant.

The final models fit well to data (Figure 6.3.2), as exemplified by data from the worked example for the *tibialis anterior* pre-activation and the generally high value of R^2_{adj}. Note that whilst some subjects do not have a full compliment of data (MA, MD, MN or MP), their results contributed to the accuracy of the model by increasing the number of subjects under study. Random variation of the fixed effects of condition or velocity, in addition to a random intercept, was significant in four out of fifteen cases and a full covariance matrix was fitted in three out of fifteen cases. Also presented are results from all fifteen models for one subject (MG) (Figure 6.3.3). As a graphical representation of data in Tables 6.3.2 to 6.3.4, Figure 6.3.4 presents the population level model fits for all models.

6.3.2 Condition

Shod running caused a reduction in EMG activity in 12 out of 15 models. Significant decreases in *tibialis anterior* EMG activity during impact phase likely contributed to the significant changes over stance phase (Table 6.3.2, β_C). Owing to a statistically significant interaction between condition and FSA, at large angles of dorsiflexed FSA, *tibialis anterior* activity is higher for SD running (Figure 6.3.4). However, this behaviour is reversed for plantarflexed FSA. Condition significantly affected *gastrocnemius medialis* signal for time periods around FS (Table 6.3.3). Pre-activation and impact phases account for 80 ms of the gait cycle ($\sim 10-15\%$) and changes in EMG during these time periods were large in magnitude, likely contributing to the observed significant differences in EMG signal over the entire gait cycle. Condition was a significant main effect across all time periods for the *gastrocnemius lateralis* (Table 6.3.4), where SD running caused a decrease in EMG signal.

6.3.3 Velocity

For the *tibialis anterior* muscle the main effects of fast velocity generally caused a significant increase in EMG activity (Table 6.3.2, β_{V_f}). Except for pre-activation (where fast velocity was not significant), fast velocity caused an increase in muscle activity for both *gastrocnemii* (Tables 6.3.3 and 6.3.4). There is, however, more noise and a higher probabiltiy of motion artefacts at higher velocity, which may influence the results. In regard to noise, one advantage of a GLMM is that it may appropriately account for heteroscedasticity, which is the manifestation of proportional error model.

As hypothesized, the main effect of velocity was not significant for *gastrocnemius medialis* activity around FS and interactions between condition and velocity were significant (Tables 6.3.3 and 6.3.1). This supports the hypothesis that in the BF condition, the velocities studied do not affect muscle pre-activation. However, in the SD condition, velocity had a significant effect on pre-activation, even though variance due to changes in FSA was accounted for.

For the *gastrocnemius lateralis* the main effect of velocity was significant for both medium and fast velocity. In the BF condition and for the mean BF FSA (7.9°), the medium velocity EMG response was similar in magnitude to slow velocity (Figure 6.3.4). Under increasingly dorsiflexed FSA, medium velocity running was more similar in magnitude to fast velocity running. For SD running, significant interactions and significant main effects of velocity meant the magnitude of the EMG response as a function of FSA was smaller.

6.3.4 Foot-strike angle

As hypothesized, FSA correlated with changes in pre-activation intensity for all muscles. For the *gastrocnemius* heads pre-activation decreased with increases in dorsiflexion whilst for the *tibialis anterior* at FS, individuals with more dorsiflexed FSA exhibited higher muscle activity

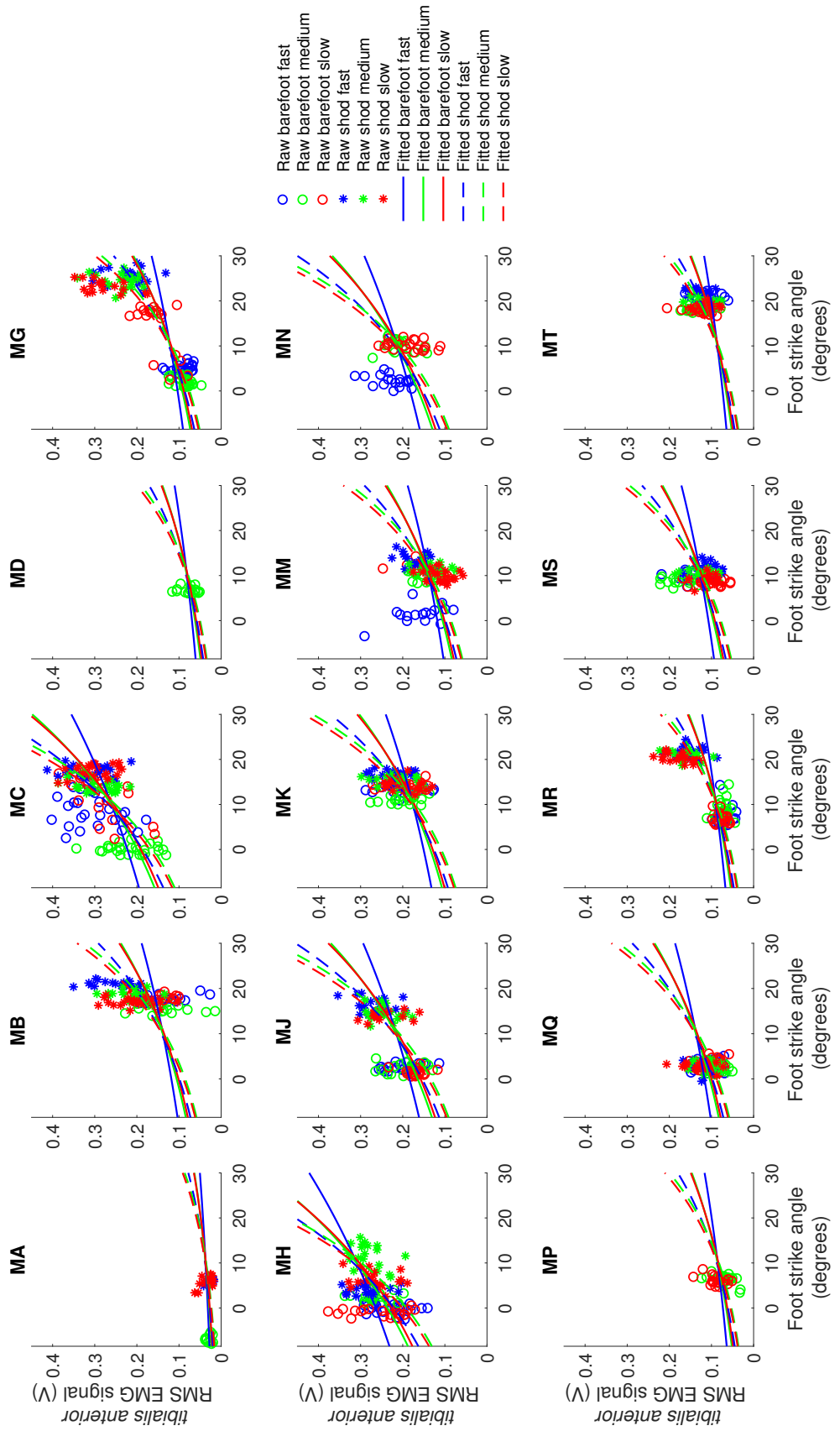


Figure 6.3.2: Plots per subject of the BF (circles) and SD (stars) data versus the fitted models (BF: solid; SD: dashed) show good agreement ($R^2_{adj} = 0.84$) for the *tibialis anterior* muscle pre-activation phase. Data are presented at all three speeds (red: slowest; green: medium; blue: fast). Four subjects (MA, MD, MN and MP) do not have a full compliment of data but nevertheless, their data contributes to the accuracy of the model. Differences between subjects in the shape of fitted models reflect variation in the intercept at the subject level.

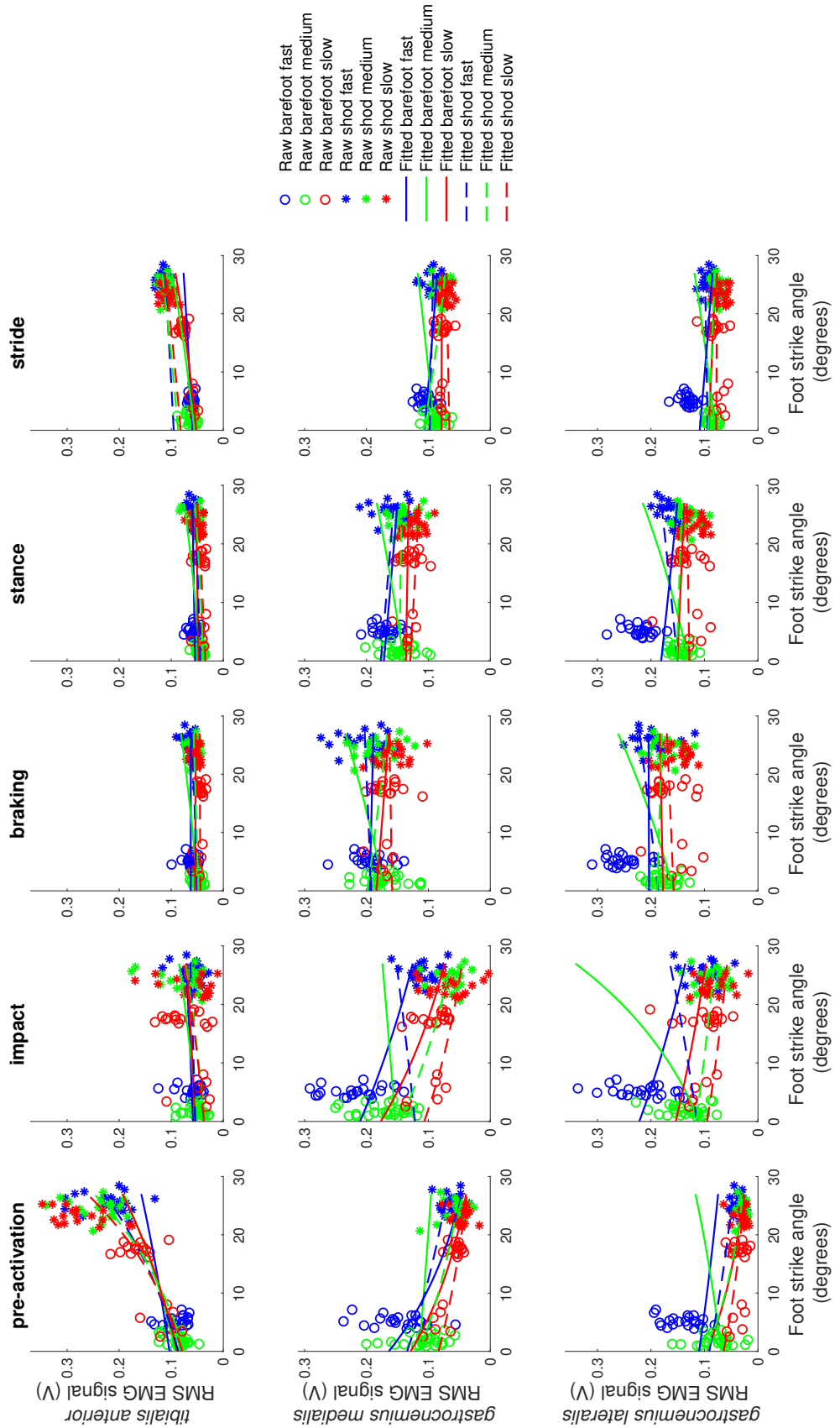


Figure 6.3.3: Data for each of the 15 fitted models for subject MG. Barefoot (circles) and SD (stars) data for each speed (red: slowest; green: medium; blue: fast) are presented, together with the subject-specific fitted models (BF: solid; SD: dashed).

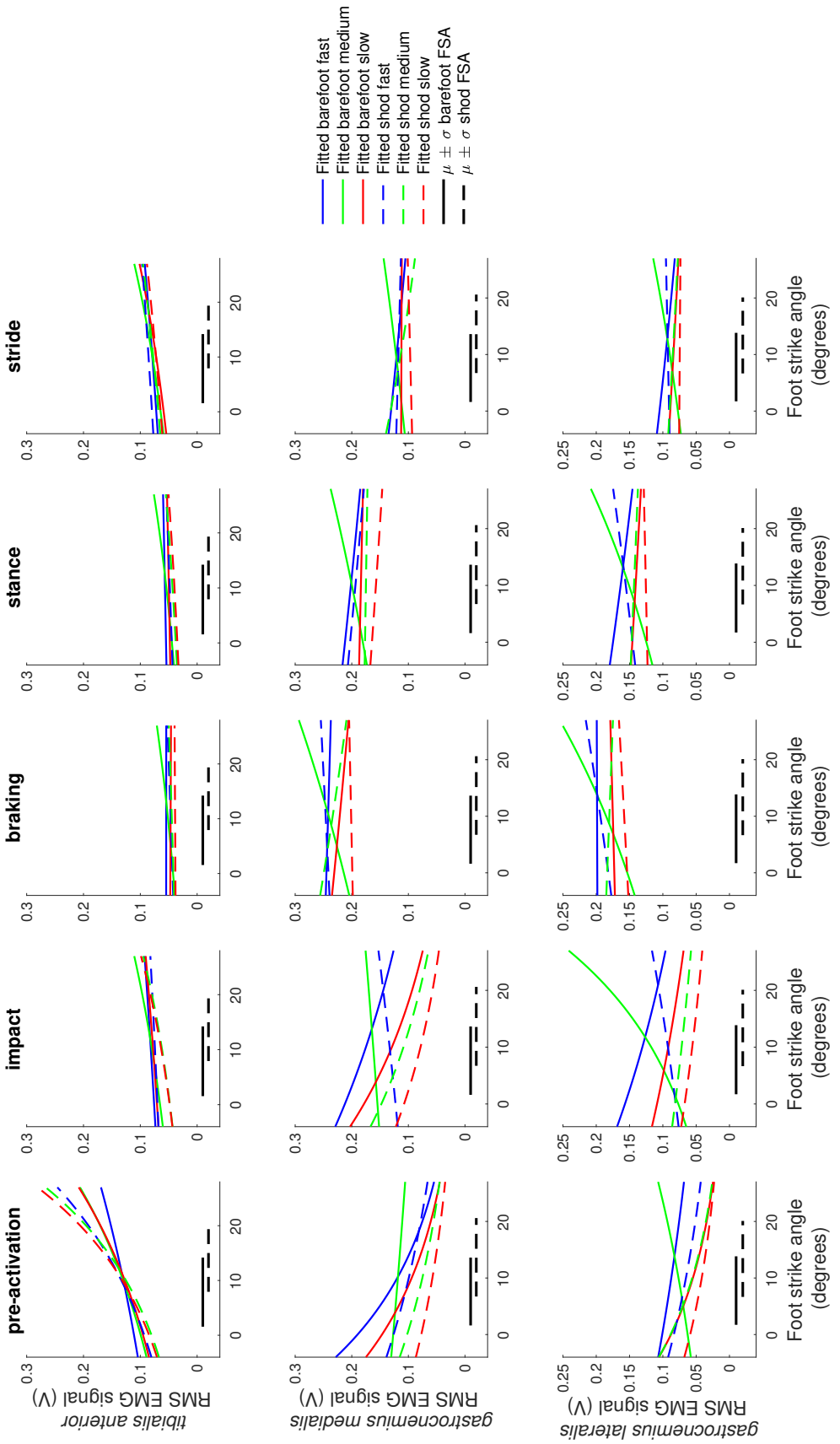


Figure 6.3.4: Fixed-effect models for all 15 fitted models. This is a graphical representation of data from Tables 6.3.2 to 6.3.4. Where interactions between the experimental effects and FSA, the most meaningful comparisons occur in the region where the solid and dashed black lines overlap. In this region we are likely to observe FSA which occur for both BF and SD running. Far from the region covered by the black lines extrapolation of results for either BF or SD running will occur.

(Figure 6.3.4). For BF running, the decrease as a function of FSA was more pronounced in magnitude for the *gastrocnemius medialis* than the *gastrocnemius lateralis.*

For the *tibialis anterior* and *gastronemius lateralis* muscles, correlations between FSA and EMG during pre-activation were likely responsible for the significant correlations between FSA and EMG observed over the gait cycle. FSA was a significant main effect for pre-activation and across the entire stride but generally not a significant main effect for braking and stance phase.

For the *gastrocnemius medialis*, FSA correlated with changes in EMG pre-activation and impact phase only. These changes were time localized and large in magnitude but typically not easy to observe without detailed statistical analysis. These observations may have implications for injury, insofar as *gastrocnemius medialis* fatigue, influenced by FSA, may occur because of changes in activity around FS. It is important to note that the correlations with FSA observed here are independent of foot condition and $\beta_{C:FSA}$is not statistically significant, which means that these correlations exist and have the same magnitude for both BF and SD running.

6.4 Discussion

The purpose of this chapter was to study the behaviour of EMG signals following changes velocity and condition, whilst also accounting for stride-specific FSA. A GLMM with random effects at the subject level accounted for between-subject variation and explained large amounts of variance in the data. Generally, the *tibialis anterior* muscle was not sensitive to changes in velocity or condition, and heads of the *gastrocnemius* responded differently around FS to changes in condition. With the statistical method applied, there is an observable level of independence in the function of the *gastrocnemius* heads during steady-state endurance running. Mechanisms of injury and fatigue which may be directly related to the activity of a particular *gastrocnemius* head may be investigated more accurately by applying GLMM.

Pre-activation of the *gastrocnemii* and *tibialis anterior* was significantly higher and lower respectively, for individuals with more foot plantarflexion at FS. Whilst the relationship between muscle force and EMG activity is nonlinear, there is approximately 50 ms between the onset of muscle activity and the onset of muscle force [109]. Thus, muscle activity in the pre-activation period suggests force production at and immediately after FS. Accordingly one would expect pre-activation in *gastrocnemius* muscles for FFS runners so the muscles may oppose the torque induced at FS. Pre-activation of the *tibialis anterior* for RFS runners is required to exert a force whilst the muscle is under eccentric contraction immediately after FS, controlling the landing of the forefoot after the heel has hit the ground [205]. The observed decrease is *tibialis anterior* muscle activity for subjects with more foot plantarflexion at FS may be reasoned through mechanical considerations. As there is more foot plantarflexion at FS, the point of contact of the foot moves anteriorly. However, the *tibialis anterior* exerts a moment across the ankle and resists foot plantarflexion. The requirement for this action of the *tibialis anterior* is reduced as point of contact moves anteriorly and ultimately, the foot actually plantarflexes after FS for FFS running.

The *tibialis anterior* activity deceased for SD running during impact, braking and stance phase. If we consider the case for RFS running (FSA = 0°), for which the parameters in Table 6.3.2 relate directly, this may arise because the mechanical properties of the shoe facilitate energy dissipation and thus reduce the need for the *tibialis anterior* to produce force to control the foot as it flattens. The increase in *tibialis anterior* activation observed for the fastest velocity may reflect that the rotational velocities of the limbs have increases sufficiently for the moment across the ankle to adjust accordingly. A study of the ankle joint kinematics are needed for a more rigorous assessment of this.

In the BF condition the *gastrocnemius medialis* may work to produce forces which assist control of the foot during impact phase. Owing to its anatomical location, the *gastrocnemius*

medialis may exert a force under eccentric contraction to control rearfoot eversion upon impact. Foot orientation at FS does not change significantly at these speeds and thus, *gastrocnemius medialis* pre-activation, which upon impact influences force production and kinematics, does not change either. An alternative explanation may be that the required muscular work may be high enough such that for novice BF running, it is physiologically difficult to increase activity as velocity increases. Whilst this latter argument may be valid for recreational populations and particularly those who do not engage in high intensity training, it is less plausible for the present population because the set of speeds studied are below those at which these individuals train and compete. The athletes in this study do not train or compete BF, but they regularly train and compete in spiked shoes and at speeds in excess of 5.5 ms^{-1}, which presumably requires far larger activation levels than the speeds considered here.

Movement strategies available for SD running may be unavailable for BF running because of constraints imposed by comfort. Shoes significantly decrease *gastrocnemius medialis* activity such that at all velocities in the SD condition, pre-activation is lower than for BF running. In the SD condition, shoes dissipate energy such that the *gastrocnemius medialis* may produce less force during impact phase and hence, lower levels of pre-activation are generally observed. Individuals may therefore voluntarily adapt their movement patterns whilst running SD, utilizing what appears to be available lower-limb muscle force production capacity in response to changes in velocity. In this study we statistically account for variation due to changes in FSA. Therefore, the changes in FSA observed between BF and SD running in the Chapter 5 are not responsible for the changes in EMG that we see for pre-activation in the SD condition here. In this cross-sectional study, a change in FSA was not induced. However, the results do not contradict the hypothesis that changes in FSA cause changes in EMG activation around FS.

When the foot is plantarflexed at FS, velocity effects are larger in magnitude and likely related to the stability role, during pronation, that the *gastrocemius medialis* performs in early

stance phase. The strong interactions reinforces the importance of accounting for FSA when analysing running gait. The Achilles tendon loading rate is higher for FFS runners [4], and this may be an important consideration even at low velocities due to *gastrocnemius medialis* function. Both the *gastrocnemius* and *soleus* contribute to forward acceleration although the *soleus'* main contribution is to upward COM acceleration [80]. The *gastrocnemius lateralis* may play a more important role than the *gastrocnemius medialis* in forward force production during mid to late stance, coinciding with the active peak in force production which typically exists. The *gastrocnemius lateralis* activity is likely related to the force production which causes an increase in velocity, whilst the *gastrocnemius medialis* is related to the stability role during early stance phase, particularly when in plantarflexion at FS.

Barefoot running exhibits higher muscle activity than SD running. Coupled with generally higher plantarflexion at FS, controlling for comfort in first-attempt BF running may increase the risk of particular injuries. This may explain the long term adaptations which occur [188] and motivate the voluntary adaptation of running biomechanics to actively avoid such injuries [176]. It is not clear how this would effect the overall injury rate in BF runners with different FSA.

The random variation of the condition response, σ_C, being present for *gastrocnemius medialis* pre-activation may reflect the variation in response for each subject as they prepare for FS when they use their personal running shoes. The magnitude of subjects' sensitivity to changes in foot condition varies randomly about the significant fixed effect. The absence of such variation for the *gastrocnemius lateralis* highlights another way in which the *gastrocnemius* heads behave differently, particularly arounds FS. The *gastrocnemius lateralis* does not exhibit random variation at the subject level for condition or velocity over any timescale, suggesting broadly systematic behaviour of the fixed effects exists at the population level.

The more systematic behaviour of the *gastrocnemius lateralis* may reflect the role of the muscle in assisting speed increases. One may expect that individuals increase their speeds in

a reasonably systematic way for both BF and SD running, by adapting behaviour during mid-stance, around the time of active peak force production. The more random variation in the *gastrocnemius medialis* may reflect the role the head plays in controlling foot-fall. The individual variation demonstrates how subjects have individualized adaptations to running BF versus SD. Additionally, simulations studies have identified higher *gastrocnemius medialis* force during impact and braking phase [4]. Therefore one subject who controls for comfort by adapting their FSA when BF running may be more or less susceptible to injury than another subject. To further study this, some kind of maximal voluntary contraction of the muscles may inform on subject-specific muscle capacities.

By accounting for random variation it is possible to revisit previous work with new analysis techniques. For example, Bates *et al.* [12] found significant subject-shoe interactions for ground reaction force data. It may be valuable to apply GLMM to revisit this data and other influential studies like it. One possible outcome would be that, by accounting for random variation at the subject level, there still exist underlying fixed behaviours for each shoe.

6.5 Limitations

The data fit well to a gamma distributed GLMM with a log link function. An alternative method would involve taking the natural logarithm of the response data and applying a linear mixed model to the transformed data. However, transforming the responses induces bias to the coefficients, meaning it is not always possible to transform the model coefficients back to the scale of the original data. Whilst the two approaches produce similar inferences, a GLMM was preferred and as such, the model parameters reported are transferable to the scale of the original data. Alternatively, sigmoid E_{max} may conceivably be more physiologically relevant model for an EMG signal and provide an upper bound for the EMG signal.

It is not valid to extrapolate model coefficients to data outside the measured FSA or velocity ranges. The mean plus one standard deviation of the observed BF and SD FSA for data in the models was $7.9^\circ \pm 6.3^\circ$ and $14.4^\circ \pm 6.5^\circ$ respectively.

The *tibialis posterior* is on the medial side of the lower leg and inferior to the *gastrocnemius* muscles. In running, this muscle is eccentrically loaded as the foot everts and therefore the increased activity may be related to cross talk from the *tibialis posterior* muscle in the *gastrocnemius medialis* signal. As amplitudes increases, crosstalk become more of a concern [37]. Therefore, high activity signals should be studied with more caution, particularly as no quantitative analysis of crosstalk was performed.

In the presence of significant interactions, it is often recommended to use effects coding for categorical variables. In this manner, whilst model coefficients are difficult to interpret, one avoids Type III errors (the right conclusion for the wrong reason). Using this method, hypothesis tests are performed with respect to the grand mean of the population. Typically, the hypotheses of interest in the present study are between groups rather than as compared to the grand mean and therefore, a reference condition is chosen in the present study. Neverthesless, it is acknowledged that using a weighted effects coding technique would allow for a larger variety of comparisons and avoid any Type III errors in the process.

This is a cross sectional study so we may not reject the hypothesis that individuals' FSA, a sagittal plane movement, has no effect on how their EMG changes with velocity. This leaves open the possibility that there are other aspects related to footwear which affect EMG including those related to frontal plane movement. Such considerations are beyond the scope of this thesis. However, as previously mentioned (Section 6.4), the present results do not contradict the hypothesis that individuals' FSA does affect how their EMG changes with velocity.

Owing to practical constraints, this data does not include force plate measurements and therefore, it is not possible to estimate muscle force using inverse dynamics. With force plate

data, software such as OpenSim, which has been used to study muscle force during running and jogging [33, 80, 81, 168], would allow for valuable insights in future work. It would also be more informative if kinematic data, particularly for the ankle joint, were included so that inferences may be made about the functional adaptations at the ankle and the corresponding muscular activity measured here.

As previously noted in Section 6.3.3, there may be artefacts in the EMG signal which affect the results. The influence of this was not quantified.

6.6 Conclusion

In this chapter muscle activity was studied as a function of foot condition and velocity. Between-subject variability, and non-normal, heteroscedastic EMG data was accounted for with GLMM. The two heads of the *gastrocnemius* responded differently to changes in velocity, condition, and FSA. For BF running, the *gastrocnemius medialis* may be more susceptible to fatigue due to increased activation compared to the *gastrocnemius lateralis*, possibly because the *gastrocnemius medialis* plays a role in stability for BF running.

Chapter 7

Lower extremity coordination for running: a dynamical systems perspective

This chapter investigates lower extremity coordination, defined as inter-segment coupling, of nineteen uninjured trained male distance runners for BF and SD running at three velocities, from a dynamical systems perspective. Four sagittal plane inter-segment couplings, and rear-foot coronal to tibial transverse plane (EVTIR) coupling are studied using continuous relative phase (crp(t)). Coordination and coordinative variability in the context of Dynamical System Theory (DST) is clarified, and an improved, recently developed, method for calculating crp(t) where a Hilbert transform is applied to centred angle trajectory data (Section 7.2.3). Therefore the results serve primarily to provide, for uninjured, highly trained male distance runners, well-defined bounds within which future studies can assess the importance of coordination and coordinative variability on injured populations.

Whilst coordination changed with velocity, condition and for different FSA, in general coordinative variability did not change. Also, differences in FSA between subjects may be biomechanically significant with respect to injury only in the context of training methodology.

Thigh-tibia (ThiTib) coordinative variability reduced at high velocity for all time periods

studied, and reduced during swing phase for increasing levels of foot plantarflexion at FS. This may reflect that high velocity FFS running is a more demanding coordinative task. Also in the sagittal plane, decreases in coordinative variability for progressively distal coupling relationships may reflect increases in the relative effort of the muscles crossing a joint whilst changes in rearfoot coronal plane dynamics during stance phase may reflect a healthy adaptation in the pronation mechanism to increased functional demands at higher velocities.

As with Chapter 5, LMM are applied to account for between-subject variation during statistical analysis, providing accurate and valid inferences.

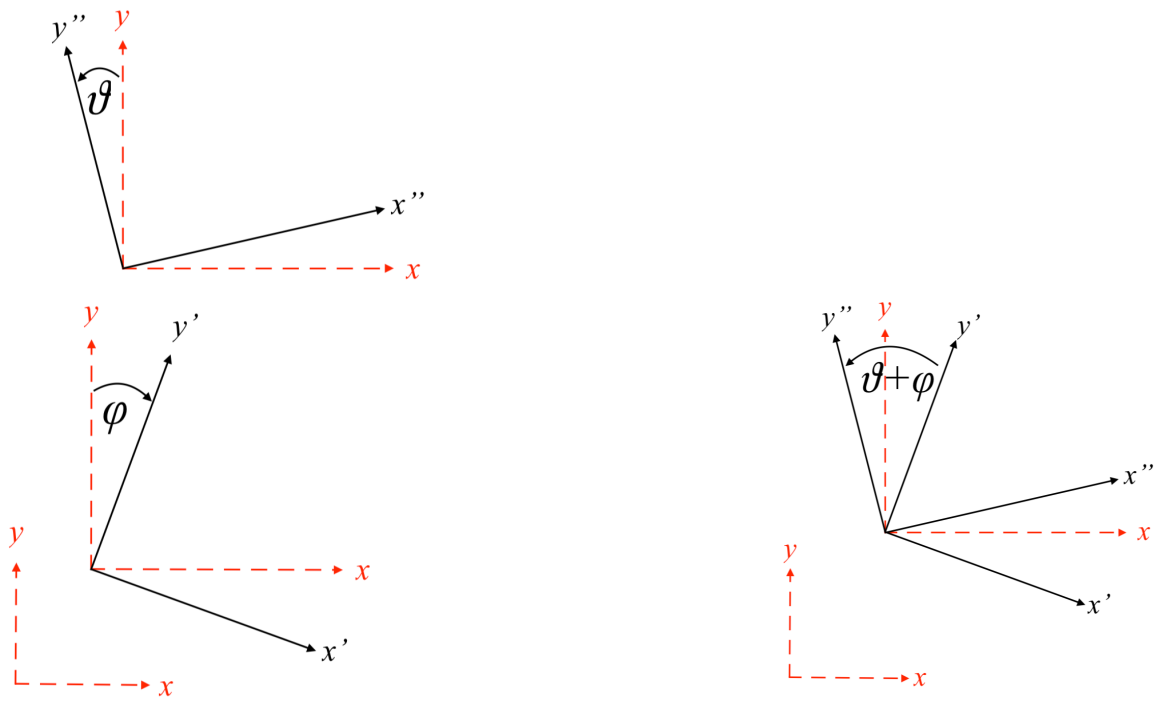
7.1 Introduction

Runners may adjust the kinematics of individual joints, but not change coordination patterns for the limbs involved [140, 142]. This demonstrates an important distinction between inter-segment coordination and joint kinematics. In this chapter, coordination is presented within the framework of DST, followed by a brief review of pertinent running biomechanics literature.

7.1.1 Background

The concept of a dynamical system has its origins in Newtonian Mechanics where, in the late nineteenth century, Henri Poincaré used the framework to study the three-body problem in celestial mechanics [165]. In biomechanics it follows that studying global body segment orientation (Figure 7.1.1), rather than joint angles, is more consistent with the original application of DST.

From a dynamical systems perspective, locomotion may be considered as an emergent behaviour, arising from the collective dynamics of contributing subsystems [200]. These subsystems include the central nervous system and musculoskeletal system. Other aspects, such as



(a) Global body segment orientation

(b) Joint angle

Figure 7.1.1: The distinction between global body segment orientation and joint angle for the two dimensional case. The angles θ and ϕ are angles relative to the some global coordinate system (red) and correspond to two global body segment orientations. The relative orientation of two coordinate systems is $\theta + \phi$ and correspond to one joint angle.

the environment (*e.g.* overground or treadmill locomotion) and the task of interest (*e.g.* fast running, slow running, walking, *etc.*) may contribute to the system behaviour [34].

DST allows a high dimensional system to be represented in a lower dimensional space such that behavioural predictions of the system, represented in this lower dimensional space, may be made. Dynamical systems theorists argue that the number of biomechanical degrees of freedom are greatly reduced through the development of coordinative structures. This reduced dimensionality encourages functionally preferred movement patterns to develop, known as attractor states [73]. Therefore in biomechanics, an attractor state is a stable pattern of behaviour for a reduced dimensional representation of a dynamical system (the body), which biomechanists argue is also a functionally preferred coordinative structure for a given task.

Attractors come in three forms: point (or equilibrium), periodic (or a limit cycle), and chaotic (or mixing) [34, 198]. Inter-segment coordination during running is naturally associ-

ated with a periodic attractor. For coupled limit cycle attractors (*i.e.* the phase plane of two separate body segments), the system could display phase locking, entrainment or structural stability [72, 105, 157]. Phase locking refers to coupled limit cycles having a fixed phase relationship. Such relationships would be attractive and stable. Entrainment is where one oscillator matches or displays a subharmonic ratio of another oscillator. Finally, structural stability is where an attractor remains in its preferred phasing relationship, regardless of any perturbations or changes in initial conditions.

In the language of control theory, DST theory predicts that scaling a control parameter (*e.g.* velocity or step frequency) will affect an order parameter (*e.g.* the continuous relative phase (crp(t)) between thigh and tibia segments in a global coordinate system). Biomechanists seek to identify control and order parameters, and their relationships, to understand the biomechanical system. Given an order parameter that describes a coordinative structure, which principles govern changes in coordination and what is the biomechanical (or otherwise) significance of such changes? Kelso [76, 104, 180] developed a dynamical systems approach which suggests that coordinative variability can be crucial when inducing a coordinative change. For example, the phase transition between walking and running is accompanied by increases in variability of the relative phase between joints of the lower extremity [47]. Also, decreases in attractor variability, measured as the mean standard deviation of the crp(t) between two body segments, have been associated with running injury [77, 142], on the basis that lower variability in 'absolute coordination' represents a repeatable action within a narrow range, causing forces to be distributed across a small surface area [78].

Studies of pistol shooting [8, 179] and finger tapping [52] demonstrate that expert individuals have lower 'end-point' or 'goal' variability than non-expert individuals. However, this is achieved through increases in 'coordinative variability'. Latash, in his Uncontrolled Manifold Hypothesis (UCM) [116], emphasizes that variability acquires significance only in the context

of a performance outcome. He argues that, given a multi-element system, an abstract 'controller' selects a subspace, from a larger state space, such that the variability of elements, as long as they are part of a UCM, are 'uncontrolled' and allowed to have high variability. Elements which are part of the UCM do not affect the desired performance outcome and are thus 'uncontrolled'. In gait dynamics, Hamill *et al.* [78] argue that the 'end-point' is, in fact, the maintenance of segmental relations (*i.e.* a coordination structure) over many cycles. In other words, the 'end-point' may be thought of as the maintenance of a stable attractor state.

Coordination is typically equated to coupling [78], but it is at this stage where misunderstandings arise. First, studies readily consider coupling between joints, segments or one segment and one joint as a coordinative structure [38, 59, 61, 90, 142]. The principles of DST are applied to the results regardless. This process belies the foundation of DST, which is based on the direct observation of physical objects. For this reason it is the coupling of body segments, specifically in a global reference frame, which is consistent with the foundations of DST. Within a DST framework, 'coordination' is specifically the coupling of body segments, which constitute a coordinative structure. Coordinative variability is the variability of these coupling relationships.

Given an appropriate measure, the loss of complexity hypothesis [126] relates a reduction in complexity to progressively unhealthy systems. A second misunderstanding is to equate complexity to variability. Complexity has its foundations in the self-similarity of a signal and is therefore fundamentally linked to the structure of a biological signal. Complexity is therefore nonlinear in nature because it is a measure which depends on the time series structure of a signal. In the case of $\mathrm{crp}(t)$, variability ($\mathrm{vcrp}(t)$) is a linear measure of system variation, and as such, does not depend on the inherent structure of a signal. Nevertheless, variability has a biomechanically relevant interpretation in the case of running injury research.

7.1.2 Literature review

The aspects of segment coupling of interest in this chapter are the phase relationships between adjacent body segments and their coordinative variability. Two continuous methods, vector coding (VC) and crp(t), have been applied to study coordinative variability. Advantages and disadvantages of each method are discussed in [40]. More recently, Miller [141] performed a systematic comparison of the two methods, ultimately cautioning against comparing studies where variability was quantified using VC versus crp(t). In theoretical cases, variability quantified by crp(t) agreed with DST on state space transitions more so than VC. Whilst the distinction was less clear for experimental data, recent improvements [113] with crp(t) methodology are encouraging and address known problems with crp(t) analysis [160]. Accordingly, for coordinative variability studies, those which used crp(t) are emphasized here and crp(t) is the chosen method for quantifying coordination and coordinative variability in this chapter. The method offers a more principled approach and is more consistent with theoretical examples.

Stergiou *et al.* [194] quantified intralimb coordination and coordinative variability for running over obstacles. In general, coordination changed as a function of time. As objects increased in height, more in-phase behaviours were observed during impact phase, even though variability did not change. The authors argued that these compensatory strategies worked to reduce higher impact forces and therefore injury risk. Changes in ThiTib and EVTIR segment coupling have implications for the distribution of forces during loading. The knee joint muscles attentuate up to 70% of the impact forces during running and subtalar pronation facilitates a reduction in these forces by extending the time for which they are attenuated [106, 194]. This study used sagittal and frontal plane video analysis and the traditional angle-velocity construction for crp(t) [77]. Furthermore, the absolute value of crp(t) was calculated, which may have implications for statistical analysis methods. In Chapter 6, calculating the root-mean-square (RMS) of electromyography (EMG) data, which was on the interval $[0,\infty)$, necessitated the use

of generalized linear mixed models to account for non-normally distributed data. Stergiou *et al.* [194] used a one-way repeated-measures ANOVA for statistical analysis, which assumes that response data is normally distributed. A discussion clarifying the nature of the absolute $\mathrm{crp}(t)$ data is lacking in the original paper.

Earlier work by Hamill *et al.* [77] hypothesized that lower variability in symptomatic individuals represented repeatable joint action within a narrow range. In their original paper, they related a decrease in $\mathrm{crp}(t)$ to symptomatic subjects with patellofemoral pain syndrome (PFPS). Tibial rotation was involved in all cases, demonstrating the importance of studying transverse plane motion, especially for PFPS studies. Unfortunately, there was no evidence of statistical anaylsis even at the most basic level of stating standard deviation or standard error.

Miller *et al.* [142] used $\mathrm{crp}(t)$, finding a significant reduction in coordinative variability for couplings associated with iliotibial band syndrome (ITBS) in individuals with a history of ITBS. They also recommended the study of segment coordination during swing phase. For ITBS, they suggested the lower $\mathrm{vcrp}(t)$ may be an artefact of their earlier injured states, which have remained observable during swing phase because of the lack of weight bearing or pain during swing phase. They also found no effect of fatigue on coordination. Increases in variability were observed only for couplings which involved a joint angle and a segment angle. As discussed in Section 7.1.1, to be consistent with the foundations of DST only inter-segment orientations are considered in the present study. By disregarding observations which included joint angles to consider only the $\mathrm{crp}(t)$ between body segments, reductions in variability for the injured population was observed. The authors suggested that by not accounting for between-subject variation, they failed to identify statistically significant effects. Linear mixed models applied in this chapter present a step forward in statistical methods, by accounting for between-subject variation.

Being a male and running more than 64 km week^{-1} are markers for injury risk [129,206] and

first-attempt BF running has been hypothesized to lead to an elevated risk of injury [155]. Injury rates in recent study of a similar demographic (highly competitive collegiate male distance runners) [39] were high compared to the recreational population. In this same study, FSA was retrospectively associated with injury [39]. In regard to coordination, Pohl and Buckley [164] found, using VC and joint angle trajectories, that rearfoot eversion to tibial internal rotation coupling was generally robust to deliberate changes in FS strategy (RFS, FFS, and toe-strike), although there was less transfer of rearfoot eversion to tibial rotation during impact for RFS running.

In the kinematic chain, the motion of one segment must influence the motions of adjacent segments. Studies to understand injury mechanisms have occasionally analysed couplings between non-adjacent segments [53, 140], but for simplicity only coordination between adjacent segments is measured in this chapter. This chapter presents the running biomechanics of highly trained runners, with a view to defining the range of 'healthy variability' in the context of changes in velocity, condition and FSA. The results may inform on the direction of future studies involving pathological populations.

Foot-strike angle is present as a covariate but no hypotheses related to specific injuries are considered. However, it is hypothesized that EVTIR coordination changes with FSA during impact phase, but not during stance or swing phase. Specifically, more out-of-phase behaviour is anticipated for RFS running. Furthermore, it is anticipated that coordinative variability changes with FSA during impact phase, reflecting an underlying elevated injury risk, manifested as lower variability, for individuals who strike the ground with more foot dorsiflexion.

Motivated by the observations of Stergiou *et al.* [194], more in-phase impact phase ThiTib and EVTIR coupling is hypothesized for higher velocities, to accommodate the typical force increases with running velocity.

BF running is hypothesized to have less coordinative variability than SD running. Given

the higher impact forces for BF versus SD running [125] in habitually SD runners, it is also hypothesized that there is more in-phase coupling for BF running as a response to higher impact forces [194].

Data on injury development were collected from a six and twelve month follow-up. In a qualitative comparison (Appendix C.1), injury rates are expected to be high compared to recreational populations.

7.2 Methods

7.2.1 Subjects

The subject inclusion and exclusion criteria have been previously described elsewhere (Sections 3.4 and 3.5). Nineteen trained healthy male distance runners were studied. Follow-up interviews were performed six and twelve months after data collection to record the development of any running related injuries.

7.2.2 Experimental data collection and data processing

The data collection procedure has been described previously (Section 3.4). The study of intra-limb coordination with crp(t) requires that global segment angles, rather than joint angles, be analysed [113]. A body segment is a dynamic system, represented in state space, and crp(t) quantifies the coordination between two such segments.

The Vicon software output joint angle data, as the distal segment relative to the proximal segment, and the orientation of the pelvis segment with respect to the global laboratory frame. When considering the joint orientation matrix (Appendix A), as is necessary for calculating the

orientation of progressively distal segments within the global frame, we have that

$$\mathbf{R}_{\mathrm{j}} = {}^{\mathbf{g}}\mathbf{R}_{\mathbf{p}}^{\mathrm{T}\,\mathbf{g}}\mathbf{R}_{\mathbf{d}} \tag{7.2.1}$$

Therefore, because for rotation matrices it is true that $\mathbf{R}\mathbf{R}^{\mathbf{T}} = \mathbf{I}$, it follows that

$${}^{\mathbf{g}}\mathbf{R}_{\mathbf{d}} = {}^{\mathbf{g}}\mathbf{R}_{\mathbf{p}}\mathbf{R}_{\mathrm{j}} \tag{7.2.2}$$

The orientation matrix $\mathbf{R_j}$ for the distal segment with respect to the proximal segment was calculated given a YXZ Euler rotation about $z_{\mathbf{p}}$, $x_{\mathbf{p}}$ and $y_{\mathbf{p}}$. Relative to the bony segment in the anatomical frames, the sequence of rotations corresponds to flexion-extension, followed by abduction-adduction and finally internal-external rotation. Therefore, given the joint angles as the distal relative proximal segment, all matrix multiplication operation are applied from the left. This gives $\mathbf{R_j}$ as

$$\mathbf{R_j} = \mathbf{R}_{\mathbf{j}\beta}\mathbf{R}_{\mathbf{j}\alpha}\mathbf{R}_{\mathbf{j}\gamma} \tag{7.2.3}$$

which, in general, may be written explicitly as

$$\begin{bmatrix} r_{11} & r_{12} & r_{13} \\ r_{21} & r_{22} & r_{23} \\ r_{31} & r_{32} & r_{33} \end{bmatrix} = \begin{bmatrix} \cos\beta\cos\gamma + \sin\alpha\sin\beta\sin\gamma & -\sin\gamma\cos\beta + \sin\alpha\sin\beta\cos\gamma & \sin\beta\cos\alpha \\ \cos\alpha\sin\gamma & \cos\alpha\cos\gamma & -\sin\alpha \\ -\sin\beta\cos\gamma + \sin\alpha\sin\gamma\cos\beta & \sin\beta\sin\gamma + \sin\alpha\cos\beta\cos\gamma & \cos\alpha\cos\beta \end{bmatrix} \tag{7.2.4}$$

For each case of ${}^{\mathbf{g}}\mathbf{R_d}$ in Equation 7.2.2, we obtain orientations of the distal segment in the global

laboratory frame of ${}^{\mathbf{g}}\alpha_{\mathbf{d}}$, ${}^{\mathbf{g}}\beta_{\mathbf{d}}$ and ${}^{\mathbf{g}}\gamma_{\mathbf{d}}$ as

$$
\begin{aligned}
{}^{\mathbf{g}}\alpha_{\mathbf{d}} &= \sin^{-1}(-r_{23}) \\
{}^{\mathbf{g}}\beta_{\mathbf{d}} &= \sin^{-1}\left(\frac{r_{13}}{\cos[{}^{\mathbf{g}}\alpha_{\mathbf{d}}]}\right) \\
{}^{\mathbf{g}}\gamma_{\mathbf{d}} &= \sin^{-1}\left(\frac{r_{21}}{\cos[{}^{\mathbf{g}}\alpha_{\mathbf{d}}]}\right)
\end{aligned}
$$

The pelvis orientation in the global frame is generated from a YXZ Euler rotation about $z_{\mathbf{p}}$, $x_{\mathbf{p}}$, and $y_{\mathbf{p}}$. This implies that ${}^{\mathbf{g}}\gamma_{\mathbf{d}}$, ${}^{\mathbf{g}}\alpha_{\mathbf{d}}$, and ${}^{\mathbf{g}}\beta_{\mathbf{d}}$ are the sagittal, frontal, and transverse plane angles (*i.e.* $z_{\mathbf{p}} \longrightarrow {}^{\mathbf{g}}\gamma_{\mathbf{d}}$, $x_{\mathbf{p}} \longrightarrow {}^{\mathbf{g}}\alpha_{\mathbf{d}}$, and $y_{\mathbf{p}} \longrightarrow {}^{\mathbf{g}}\beta_{\mathbf{d}}$). For each segment, orientations in the global frame were visually checked for consistency and to ensure angles were in the correct quadrant. It follows that the orientations of progressively distal segments in the global coordinate frame are calculated in a recursive manner.

7.2.3 Continuous Relative Phase

Intralimb coordination is quantified using $\mathrm{crp}(t)$. The analysis tool has been used in biomechanics as early as 1993 [24]. For lifting tasks, the phase angle relationships between joints were shown to be sufficiently sensitive to changes in object mass, lifting height, and load moment. The method of analysis is grounded in DST and requires a phase-space representation of segment dynamics. This method may be applied to both sinusoidal and non-sinsoidal (*i.e* a superposition of different sinusoidal waves) signals. Traditionally, segment motion in some global reference frame is represented in phase-space with the angular parameters θ (or x) and ω (or v). Following this, a phase portrait is centred and normalized such that comparisons between subjects and trials are possible. There are a variety of normalization procedures, each of which affects $\mathrm{crp}(t)$ results differently. Accordingly the output and interpretation of results change between studies [113, 160]. In particular, the normalization step introduces artefacts when the

original signal is non-sinuosidal. This is a pertinent issue in gait analysis because all gait data deviates slightly from sinusodial. Recently Lamb and Stöckl [113] introduced a method to calculate a phase space representation of segment motion based on an amplitude centred signal (*i.e.* a segment angle θ in the global coordinate frame) and its Hilbert transform [175]. This provides the correct phase angle, thus removing the need to normalize data onto a unit phase space. One begins by centring the segment angle data $\chi(t_i)$ as

$$x(t_i) = \chi(t_i) - min[\chi(t)] - \frac{max[\chi(t)] - min[\chi(t)]}{2} \tag{7.2.5}$$

Let $\mathscr{H}_t\{x\}$ be the output at time t of the Hilbert-transformed filter applied to the real signal $x(t)$, where specifically, the filter introduces a phase shift of $-\pi/2$ to each positive frequency and $+\pi/2$ to each negative frequency in $x(t)$. To appreciate the concept of a negative frequency, consider that any real signal may be split into equal contributions of positive (counter-clockwise) and negative (clockwise) frequencies by using Euler's identity, $2\cos(\theta) = \exp(j\theta) + \exp(-j\theta)$. The Hilbert transform allows for the transformation of any real signal into a complex, analytical signal $\zeta(t)$ [68] and is defined, in this case, as

$$\zeta(t) = x(t) + j\mathscr{H}_t\{x\} \tag{7.2.6}$$

where $j^2 = -1$ and an analytic signal is one with no negative frequency components. Based on the complex signal, the phase angle $\phi(t_i)$ at time t_i may be calculated as

$$\phi(t_i) = \tan^{-1}\left(\frac{\mathscr{H}_t\{x\}}{x(t_i)}\right) \tag{7.2.7}$$

The crp(t) between two signals $x_1(t)$ and $x_2(t)$ is calculated as their phase difference from

$$\text{crp}(t_i) = \phi_1(t_i) - \phi_2(t_i) \tag{7.2.8}$$

Using the identity

$$\tan^{-1}(a) - \tan^{-1}(b) = \tan^{-1}\left(\frac{a-b}{1+ab}\right) \tag{7.2.9}$$

and with substitutions of $a = \mathscr{H}_t\{x_1\}/x_1(t_i)$ and $b = \mathscr{H}_t\{x_2\}/x_2(t_i)$, it follows that by substitution from Equation 7.2.7 into Equation 7.2.8, and with algebraic manipulation

$$\text{crp}(t_i) = \tan^{-1}\left(\frac{\mathscr{H}_t\{x_1\}x_2(t_i) - \mathscr{H}_t\{x_2\}x_1(t_i)}{x_1(t_i)x_2(t_i) + \mathscr{H}_t\{x_1\}\mathscr{H}_t\{x_2\}}\right) \tag{7.2.10}$$

The method outlined in this section, and presented in [113] gives the most valid, robust, and intuitive results when compared to traditional techniques [24, 77, 121, 141, 142, 194], avoiding the following complications: 1) the numerical calculation of the angular velocity; and 2) an arbitrary normalization of the phase diagram.

The longest continuous times series of kinematic data for each trial, comprising multiple consecutive trials, was centred (Equation 7.2.5) before the crp(t) was calculated (Equation 7.2.10). Each stance phase and swing phase was normalized to 51 points from 0% to 100%. Swing phase, calculated from TO to FS, was attributed the FSA which occured at the end of swing phase. In a small number of cases, artefacts arose from the resampling process. The inbuilt polyphase filter occasionally failed to adequately resample jumps in the crp(t) time series. To guard against this, and frequency artefacts which would influence measures of variability [113, 194], all gait cycles were observed qualitatively for such artefacts and strides which exhibited artefacts were excluded from further analysis. A lower limit of five strides was used for each trial to ensure that the subsequent calculation of crp(t) was meaningful. If

there were fewer than five strides for a given trial, the trial was omitted.

7.2.4 Directional statistics

Depending on convention, crp(t) angles are on the interval $[-180°, 180°)$ or $[0°, 360°)$, or alternatively on the interval $[0°, 180°]$ if one is concerned only with the absolute value of the crp(t). For crp(t) data directional statistics must be used when calculating summary statistics such as the directional mean and circular standard deviation. For a normally distributed random variable X which lies on the interval $(-\infty, \infty)$, but is then wrapped onto the interval $[0°, 360°)$, we consider the data as a set of angular directions on the unit circle. This introduces periodicity, such that $\theta = \theta + 360k$ where $k \in \mathbb{Z}$.

For an illustration consider the directional mean and circular standard deviation of the set of angles 30° and 330°. Taking the arithmetic mean of the two numbers would give 180°, which is inappropriate because it does not reflect the mean orientation in two dimensions. Using directional statistics, angular variables are transformed into unit vectors in complex plane such that $z_i = Re^{j\theta_i}$. Following this transformation, for N complex numbers, we calculate the resultant vector using that

$$\mathfrak{Re}\{\bar{z}\} = \frac{1}{N}\sum_i \mathfrak{Re}\{z_i\} \tag{7.2.11}$$

$$\mathfrak{Im}\{\bar{z}\} = \frac{1}{N}\sum_i \mathfrak{Im}\{z_i\} \tag{7.2.12}$$

and therefore

$$\bar{z} = \bar{R}e^{j\bar{\theta}} = \mathfrak{Re}\{\bar{z}\} + j\mathfrak{Im}\{\bar{z}\} \tag{7.2.13}$$

By comparing Equation 7.2.13 with the first moment of the wrapped normal distribution [64], which is given as

$$\langle z \rangle = e^{j\mu - \frac{\sigma^2}{2}} \tag{7.2.14}$$

it is possible to estimate the directional mean μ and circular standard deviation σ by equating $\bar{z}$ to $\langle z \rangle$. Therefore, with $\bar{R}e^{j\bar{\theta}} = e^{-\frac{\sigma^2}{2}}e^{j\mu}$, by comparison, we have that

$$\mu = \text{Arg}\,(\bar{z}) \tag{7.2.15}$$

Given that $\bar{R} = e^{-\frac{\sigma^2}{2}}$, it follows that

$$\sigma = \sqrt{-2\ln \bar{R}} \tag{7.2.16}$$

This is the case if we have a normally distributed random variable, wrapped onto the interval $[0^\circ, 360^\circ)$. With this method, the directional mean of 30° and 330° is 0° and the circular standard deviation is $\sqrt{-2\ln\left(\frac{\sqrt{3}}{2}\right)} \approx 0.536$. We calculate $\bar{R}$ as the length of the mean resultant vector. Given that $z_1 = \frac{\sqrt{3}}{2} + j \cdot \frac{1}{2}$ and $z_2 = \frac{\sqrt{3}}{2} + j\left(-\frac{1}{2}\right)$ we have that $\bar{z} = \frac{1}{2}\left[\frac{\sqrt{3}}{2} + \frac{\sqrt{3}}{2}\right] + \frac{1}{2} \cdot j\left[\frac{1}{2} + \left(-\frac{1}{2}\right)\right]$, which simplies to $\bar{z} = \frac{\sqrt{3}}{2}$. Trivially as $\bar{z} \in \mathbb{R}$, it follows that $\bar{R} = \frac{\sqrt{3}}{2}$. As an extension, for a resultant vector of length $R = 1$, which implies that all vectors are along the same direction, we have a circular standard deviation of $\sigma = 0$. In the limiting case where for every vector, there is another vector in the opposite direction, the resultant vector length tends to 0, and the circular standard deviation tends to ∞.

In the analysis of this chapter, all calculations involving directional statistics were performed using the MATLAB toolbox CircStat [15], and $\text{crp}(t)$ was on the interval $[-180^\circ, 180^\circ)$. To align conventions with previous literature, a negative $\text{crp}(t)$ angle suggests the proximal segment leads the distal segment, whilst a positive angle suggests the distal segment leads the proximal segment. In-phase coupling was 0°, out-of-phase coupling was $\pm 90^\circ$, and anti-phase was -180°.

	Gait cycles	Trials	Gait cycles trial^{-1}
BF	698 ± 305	42 ± 14	16 ± 4
SD	801 ± 211	44 ± 11	18 ± 1

Table 7.2.1: A summary of the amount of data processed for statistical analysis. Data are summarized as mean $\pm$ st. dev.

Coupling relationship	Abbreviation
Pelvis sagittal - thigh sagittal	PelThi
Thigh sagittal - tibia sagittal	ThiTib
*Tibia sagittal - rearfoot sagittal	TibRft
*Rearfoot sagittal - forefoot sagittal	RftFft
*Tibia transverse - rearfoot coronal	EVTIR

Table 7.2.2: Segment couplings studied using $\text{crp}(t)$ and the abbreviations used in the text. '*' denotes BF-only data because of the inclusion of at least one OFM [191] foot segment.

7.2.5 Data analysis

Summary statistics for the amount of data used for the statistical analyses in the final models are given in Table 7.2.1. For two coupling relationships both BF and SD data were available, whilst for the other three only BF data were available. A summary of this and a list of abbreviations for the coupling relationships are given in Table 7.2.2. Using the Oxford Foot Model markers limited the study of TibRft, RftFft, and EVTIR to BF running only.

Given the time normalized data for a single gait cycle, the mean value for each of the $\text{crp}(\tau)$ was calculated over three time periods using directional statistics. The time periods (Table 7.2.3) were impact phase, stance phase, and swing phase.

Given all the time normalized gait cycles for a single trial, $\text{vcrp}(\tau)$ was calculated as the pointwise circular standard deviation (Equation 7.2.16) across all gait cycles in the trial. This generated a single time series of $\text{vcrp}(\tau)$ for a single trial. From this, the mean was calculated over the aforementioned time periods. The summary FSA was calculated as the median value across all strides for which $\text{crp}(\tau)$ data existed.

Time periods	
Impact phase	From 0%-16% stance phase
Stance phase	During foot contact, from FS to TO
Swing phase	From TO to FS

Table 7.2.3: crp(t) parameters for μ and σ. For the given time periods μ was calculated as the directional mean for each gait cycle and σ was calculated as the pointwise circular standard deviation for each trial.

7.2.6 Statistical analysis

Exploratory analysis was performed using the open source statistical software R (v3.3.1) [167] and initial models were fitted using the R package nlme [162]. Exploratory analysis identifed that the distribution of cleaned mean crp (τ) and vcrp(τ) was normal and localized away from the boundaries of the interval. This allowed for the application of LMM for statistical analysis of mean crp (τ) data. The model selection procedure in this chapter has been previously described (Section 5.2.7.2). Final models were fitted using MATLAB (V2016b, The Mathworks, Inc., Natick, MA, USA). For the case of EVTIR, crp(τ) data were distributed across the boundary of the domain. Therefore, all data were translated onto the interval $[0^\circ, 360^\circ)$ for statistical analysis. Data were centred around approximately 180°, which is anti-phase behaviour. The values 0° and 360° denote in-phase behaviour, and 270° and 90° correspond to out-of-phase coordination. For this case, a crp(τ) angle on the interval $(180^\circ, 360^\circ)$ suggests the proximal segment leads the distal segment and a crp(τ) angle on the interval $(0^\circ, 180^\circ]$ suggests the distal segment leads the proximal segment.

On a case by case basis a random intercept, random variation of the fixed effects, or no random effects were used in final models. A saturated fixed effects model was fitted to data and the necessity of a random intercept was assessed by considering the distribution of residuals, grouped by subject. A random intercept was added to the initial fixed effects model if and only if for the fixed effect model there was still variation at the subject level.

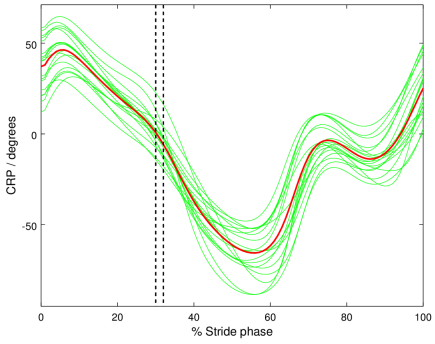
For the vcrp(τ) there were no repeated measures of any specific trial (*i.e.* the combination of a specific velocity and condition was measured only once per subject). Therefore, the most complex model was a random intercept model, fitted at the subject level.

Additional random effects were added to the random intercept model if model assumptions in the new model were satisfied. The assumptions were the normality of residuals and normality of random effects, as determined qualitatively from quantile-quantile plots. Additionally, an updated model was used only if the new model was a significant improvement on the old model. Likelihood ratio tests, with $p < 0.05$, defined an improvement upon any old model. For potential outliers, if their removal led to the loss of a significant association, they were removed, and no significance was reported. Covariance parameters were constrained to be zero if and only if they were not significantly different from zero, and such a model which did set them to zero, was a significant improvement on the unconstrained model. The evalutation of a better model was also performed using likelihood ratio tests.

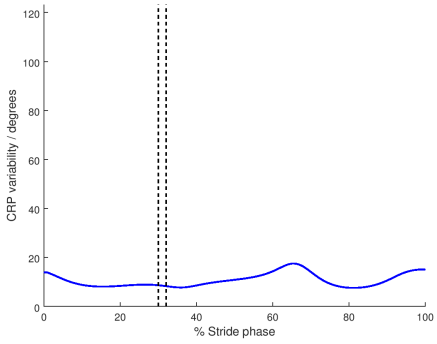
Three time periods were studied for each coupling relationship. Therefore a Bonferroni correction [54] was applied, which set the significance level as $\alpha = 0.0167$ for each fixed effect in any final model.

7.3 Results

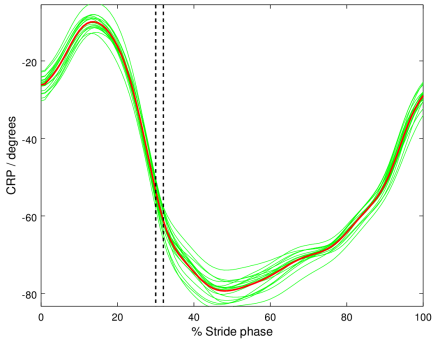
Sagittal plane (Figure 7.3.1) and EVTIR (Figure 7.3.2) crp(τ) and vcrp(τ) data for a representative subject (MN) are presented. In the sagittal plane, vcrp(τ) generally decreased in magnitude for progressively distal couplings. Subsets of data which were used in the final models for statistical analyses are presented.



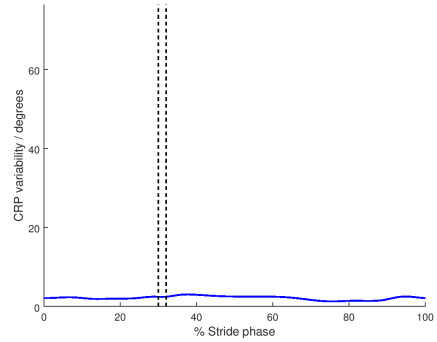
(a) PelThi crp(τ)



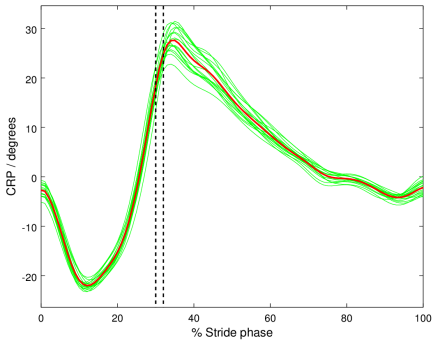
(b) PelThi vcrp(τ)



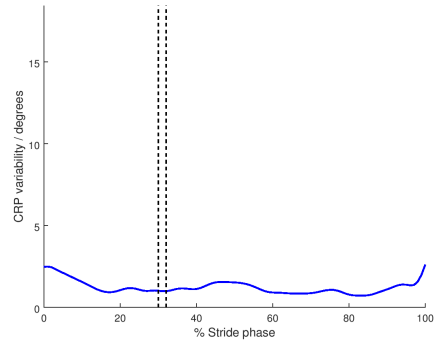
(c) ThiTib crp(τ)



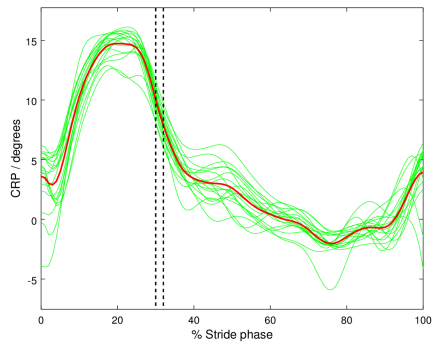
(d) ThiTib vcrp(τ)



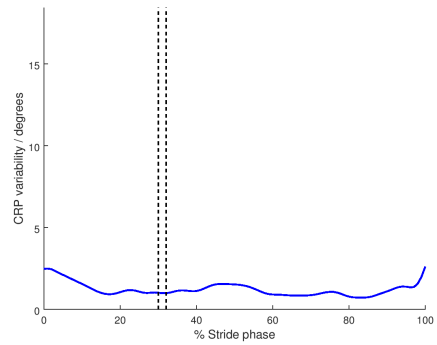
(e) TibRft crp(τ)



(f) TibRft vcrp(τ)

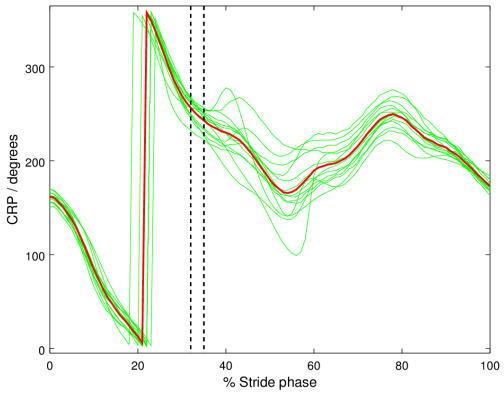


(g) RftFft crp(τ)

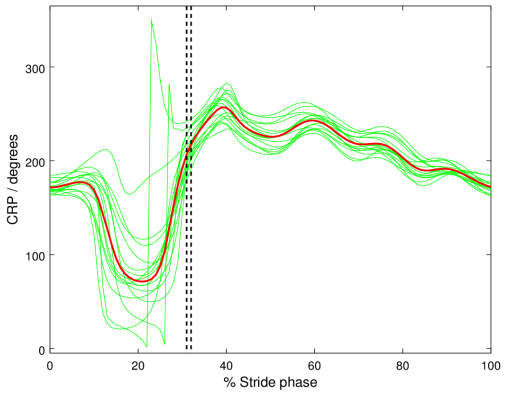


(h) RftFft vcrp(τ)

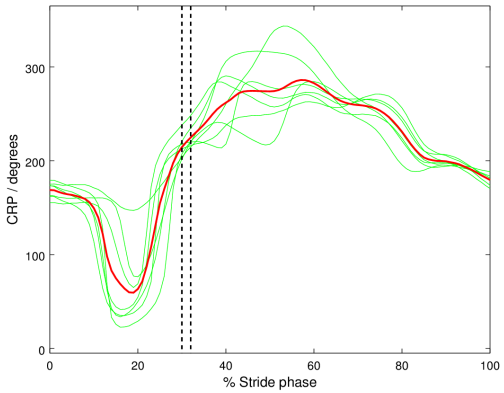
Figure 7.3.1: Sagittal plane crp(τ) (green and red) and vcrp(τ) (blue) for fast BF running. crp(τ) data for the individual gait cycles (green) and the trial mean (red) are presented. Toe-off occurs between the black dashed lines. Data are from subject MN running at the fastest velocity.



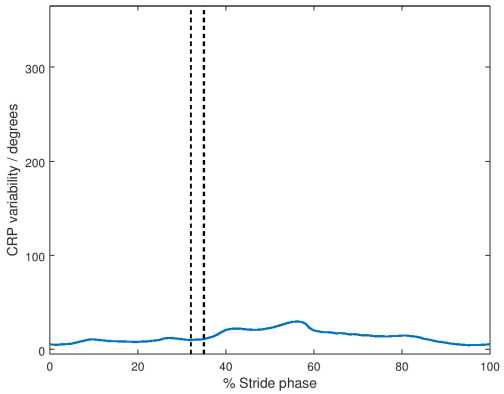
(a) Slow velocity crp(τ)



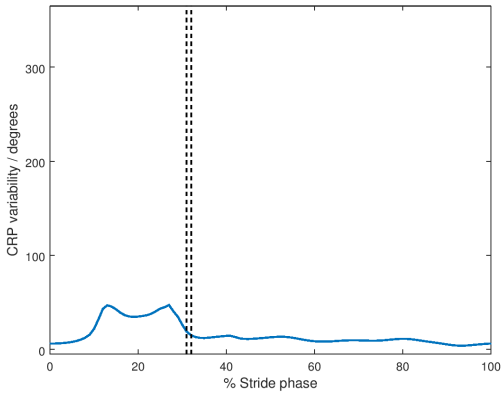
(b) Medium velocity crp(τ)



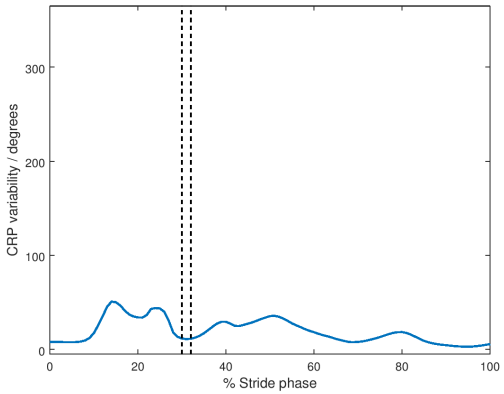
(c) Fast velocity crp(τ)



(d) Slow velocity vcrp(τ)



(e) Medium velocity vcrp(τ)



(f) Fast velocity vcrp(τ)

Figure 7.3.2: EVTIR coordination: The individual (green) and mean (red) crp(τ), and vcrp(τ) (blue) as a function of velocity for BF running. crp(τ) data for the individual gait cycles (green) and the trial mean (red) are presented. Toe-off occurs between the black dashed lines. Data are from subject MN running at the fastest velocity.

7.3.1 Hilbert transform versus (x, v) construction

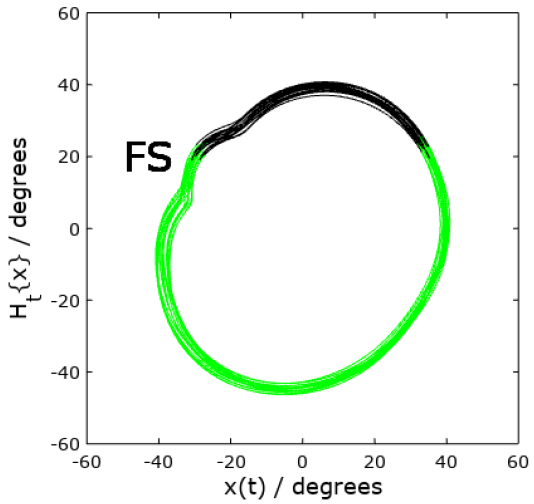
The Hilbert transform method is preferred because it can generate the instantaneous amplitude and phase of an arbitrary signal [175], whilst the (x, v) construction introduces oscillations which are artefacts of the calculation [67]. The phase plane of segments in the sagittal plane, constructed using the Hilbert transform method (Figure 7.3.3 and 7.3.4), are more circular than those generated using the traditional (x, v) method [77] (Figure 7.3.3). The Hilbert transform phase planes for segments here resemble those of harmonic oscillators and accordingly, adjacent segments resemble coupled harmonic oscillators. Data derived from the traditional (x, v) construction are comparable to results from previous literature (Figure 7.3.5). For example, similar to previous studies [77, 142], EVTIR data is bounded between approxmately $\pm 90^{\circ}$. However, owing to differences between the phase planes for the two methods, crp(τ) data from the Hilbert transform method was, in general, different to previous studies.

7.3.2 Running related injuries

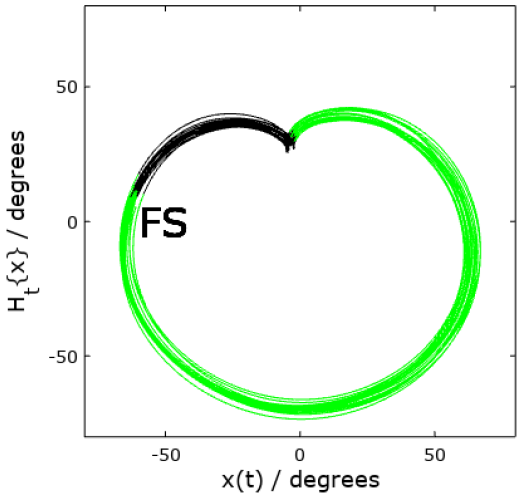
Follow-up interviews pertaining to running related injury development are summarized in Table C.1.1. No data were available for subject MQ. By six months 11% (two out of eighteen) of subjects had developed a running-related injury. At twelve months this rose to 39% (seven out of eighteen), with five new subjects developing an injury, and one subject (MC) suffering with the same injury.

7.3.3 Final models

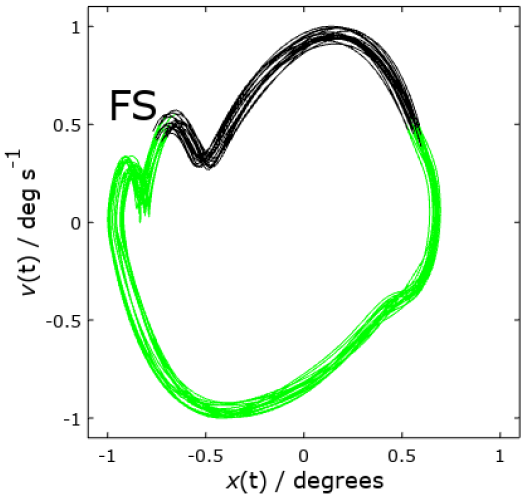
Final models were hierarchical LMM, as previously described by Equation 5.3.1, where fixed and random effects coefficients and variance-covariance parameters are given by Equations 6.3.2 and 6.3.3 respectively. Coefficients from the final models are presented in Tables 7.3.1



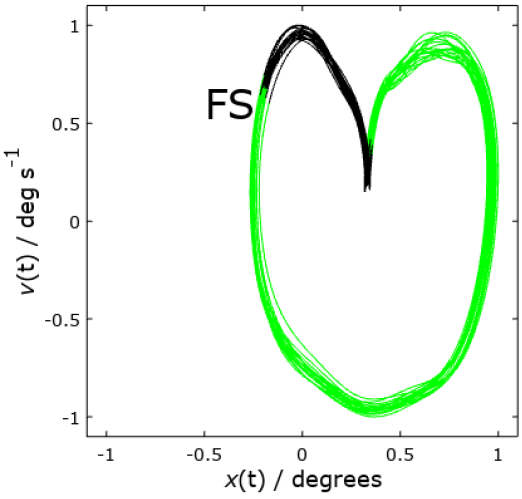
(a) Thigh phase plane with Hilbert transform



(b) Tibia phase plane with Hilbert transform

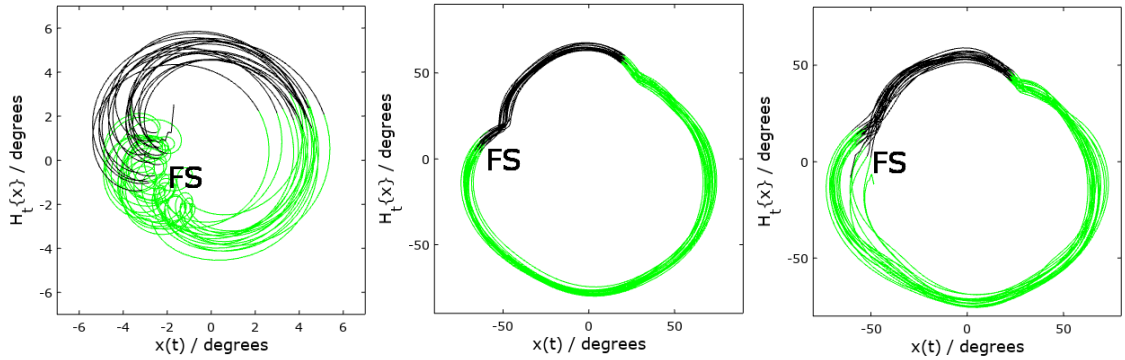


(c) Thigh phase plane with (x, v)



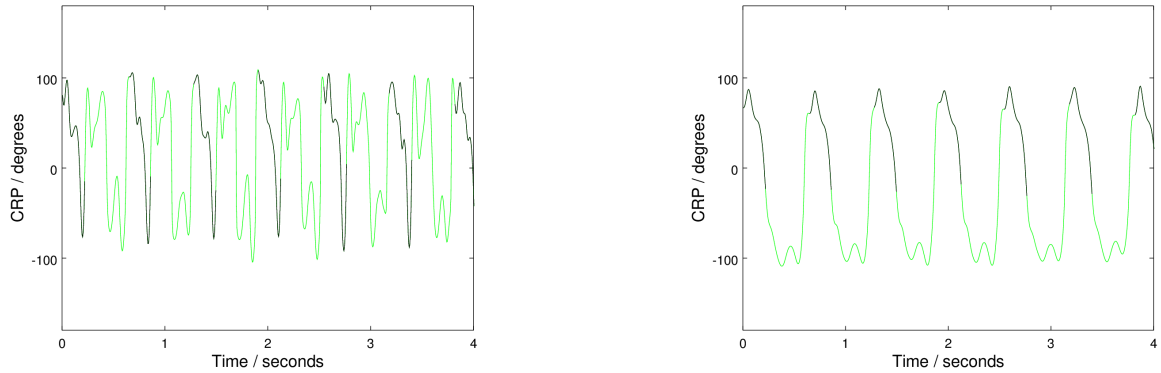
(d) Tibia phase plane with (x, v)

Figure 7.3.3: Phase planes constructed from the Hilbert transform (7.3.3a and 7.3.3b) and traditional (x, v) construction (7.3.3c and 7.3.3d). Data are presented for a representative subject (MN) at the fastest velocity. Stance phase is black, and swing phase is green. Phase planes generated using the Hilbert transform were naturally reflected about the x-axis. Therefore, for ease of comparison, all phase planes constructed using the Hilbert transform presented were reflected about the x-axis to align them with phase planes generated using traditional methods.



(a) Pelvis (b) Rearfoot (c) Forefoot

Figure 7.3.4: Phase plane dynamics for segments in the sagittal plane, constructed using the Hilbert transform. For the thigh and tibia phase planes see Figure 7.3.3a and 7.3.3b respectively. Data are from a representative subject (MN) running at the fastest velocity, with stance phase in black and swing phase in green.



(a) EVTIR crp(t) data for 4.47 ms^{-1} is comparable to results for the gait cycle reported by [142] between 3.05 ms^{-1} and 3.94 ms^{-1}, and to results for stance phase reported by [77] between 2.50 ms^{-1} and 3.50 ms^{-1}.

(b) ThiTib crp(t) data are comparable to the reported no-obstacle stance phase data in [194] and slow running in [121].

Figure 7.3.5: crp(t) data for a representative subject (MM) at the fastest velocity, constructed using the traditional (x,v) phase space representation [77,194], as a function of time. Successive stance phases (black) are superimposed upon the crp(t) time series (green). Data are comparable to previous studies for EVTIR [77, 142] and ThiTib [121, 194] coordination.

to 7.3.6. Intercepts for the Tables 7.3.2, 7.3.4, and 7.3.6 re-affirm that vcrp(t) decreased in magnitude for progressively distal couplings over all three time periods.

The adjusted coefficient of determination R^2_{adj} is reported for reference but, the purpose of the statistical models is for hypothesis testing only (and not prediction). Hence a low value of R^2_{adj} demonstrates only that the model does not explain much of the variance in the data. The

high explained variance for the mixed-effect model versus the one fixed effect model (Table 7.3.4) demonstrates that most variance in the data arises from between subject differences.

7.3.4 Condition

Condition effects were studied for PelThi and ThiTib coupling only. During impact phase and for ThiTib coupling, condition existed as a main effect and as a significant interaction with fast velocity and FSA respectively. Significant interactions existed for PelThi coupling, although an interaction between FSA and condition narrowly missed statistical significance. Therefore, the effects of velocity and FSA were dependent on whether the runner was BF or SD. In contradiction to hypotheses, SD running exhibited more in-phase coupling (Table 7.3.1; β_C for PelThi and ThiTib), seen as a crp(τ) value closer to 0°. Coupling magnitudes were also more robust to changes in velocity and differences in FSA for SD running.

The hypotheses included that BF running exhibited less coordinative variability than SD running. The results do not generally support this hypothesis. Coordinative variability was independent of condition for impact and stance phase, but it is possible that swing phase ThiTib coordinative variability is higher for SD running. The main effect of condition narrowly missed significance for swing phase.

7.3.5 Velocity

For increases in velocity, more in-phase coordination (*i.e.* closer to 0°) during impact was hypothesized for ThiTib and EVTIR coupling. Velocity was a significant main effect for crp(τ) and vcrp(τ), often when the thigh segment was involved in a coupling relationship. Of the 13 cases (out of 60) where medium or fast velocity was a significant main effect, 10 were with couplings involving the thigh segment, and 7 were for ThiTib coupling specifically. In general, high velocity was a significant main effect for coordination during impact but the nature of its

	PelThi			ThiTib			TibRft			RftFft			EVTIR		
Coeff.	Est.	S.E.	p-value	Est.	S.E.	p-value	Est.	S.E.	p-value	Est.	S.E.	p-value	Est.	S.E.	p-value
β_0	64.728	5.234	< 0.001*	-26.623	2.438	< 0.001*	-10.898	0.898	< 0.001*	10.437	0.710	< 0.001*	155.230	9.231	< 0.001*
β_C	-7.434	3.912	0.058	6.349	1.643	< 0.001*									
β_{V_m}	-4.996	2.383	0.036	-1.380	0.888	0.120	0.559	0.586	0.341	-0.779	0.426	0.067	-14.753	6.249	0.019
β_{V_f}	-22.459	2.752	< 0.001*	-3.670	1.125	0.001*	1.794	0.600	0.003*	-0.146	0.659	0.825	-23.091	6.452	< 0.001*
β_{FSA}	1.399	0.260	< 0.001*	0.656	0.052	< 0.001*	0.355	0.035	< 0.001*	-0.176	0.027	< 0.001*	-1.993	0.530	< 0.001*
$\beta_{C:V_m}$	7.209	3.653	0.049	1.073	0.797	0.178									
$\beta_{C:V_f}$	14.472	3.748	< 0.001*	4.664	0.724	< 0.001*									
$\beta_{C:FSA}$	-0.736	0.319	0.021	-0.675	0.079	< 0.001*									
$\beta_{V_m:FSA}$	-0.020	0.325	0.950	-0.147	0.061	0.016*	-0.004	0.049	0.941	-0.014	0.038	0.712	1.611	0.776	0.039
$\beta_{V_f:FSA}$	0.716	0.337	0.034	-0.123	0.056	0.030	-0.070	0.046	0.125	-0.044	0.042	0.294	3.083	0.890	0.001*
$\beta_{C:V_m:FSA}$	-0.602	0.374	0.107	0.110	0.065	0.092									
$\beta_{C:V_f:FSA}$	-1.131	0.376	0.003*	0.313	0.055	< 0.001*									
Coeff.	Est.	Lower	Upper	Est.	Lower	Upper	Est.	Lower	Upper	Est.	Lower	Upper	Est.	Lower	Upper
σ_0	18.115	12.264	26.756	10.495	7.562	14.564	3.768	2.709	5.240	2.937	2.022	4.267	29.640	19.935	44.070
σ_C	5.744	3.346	9.859	5.546	3.961	7.766									
σ_{V_m}				3.317	2.338	4.707	2.100	1.491	2.958	1.404	0.919	2.145			
σ_{V_f}				4.482	3.195	6.287	2.204	1.527	3.183	2.484	1.705	3.618			
$\rho_{0:C}$	-0.437	-0.800	0.158	-0.202	-0.586	0.257									
$\rho_{0:V_m}$				-0.161	-0.563	0.303	-0.600†	-0.826	-0.209	-0.666†	-0.891	-0.180			
$\rho_{0:V_f}$				-0.118	-0.528	0.338	-0.674†	-0.865	-0.313	-0.503†	-0.782	-0.057			
$\rho_{C:V_m}$				-0.512†	-0.781	-0.081									
$\rho_{C:V_f}$				-0.242	-0.619	0.225									
$\rho_{V_m:V_f}$				0.613†	0.224	0.834	0.844†	0.606	0.944	0.611†	0.088	0.870			
ε_{ij}	12.034	11.541	12.548	3.067	2.972	3.164	1.339	1.279	1.401	0.977	0.931	1.024	15.518	14.193	16.967

Coeff.	Est.	Est.	Est.	Est.	Est.
R^2_{adj}	0.73	0.92	0.91	0.86	0.76

Table 7.3.1: Model coefficient (Coeff.) estimates for the mean crp(τ) during **impact phase**. Fixed-effects coefficient estimates (Est.) are calculated as described in Section 7.2.6, with standard error (S.E.) and p-value. * denotes significance at $\alpha_f = 0.05$, following a Bonferroni correction. Standard deviation of random coefficients σ, estimates of correlation coefficients ρ, and standard deviation of the residuals ε_{ij} are presented with 95% confidence intervals. † denotes a correlation parameter is significantly different from zero. The adjusted coefficient of determination R^2_{adj} quantifies the final model goodness of fit. Cells are shaded grey where the parameters were not part of the model.

	PelThi			**ThiTib**			**TibRft**			**RftFft**			**EVTIR**		
Coeff.	Est.	S.E.	p-value	Est.	S.E.	p-value	Est.	S.E.	p-value	Est.	S.E.	p-value	Est.	S.E.	p-value
β_0	12.432	1.561	< 0.001*	2.944	0.268	< 0.001*	1.402	0.151	< 0.001*	0.774	0.086	< 0.001*	15.642	3.553	< 0.001*
β_C	-2.436	2.163	0.157	-0.305	0.339	0.347									
β_{V_m}	-0.449	2.217	0.572	-0.778	0.249	0.002*	-0.075	0.144	0.606	-0.121	0.092	0.194	-9.946	5.048	0.064
β_{V_f}	-2.252	2.087	0.468	-0.683	0.244	0.004*	-0.199	0.141	0.165	0.017	0.091	0.852	-8.615	5.120	0.109
β_{FSA}	-0.149	0.167	0.268	0.004	0.022	0.821	0.005	0.015	0.718	0.011	0.009	0.222	-0.314	0.364	0.399
$\beta_{C:V_m}$	2.845	3.214	0.103	0.693	0.471	0.141									
$\beta_{C:V_f}$	1.263	3.071	0.686	0.020	0.450	0.916									
$\beta_{C:FSA}$	0.105	0.192	0.769	0.008	0.026	0.743									
$\beta_{V_m:FSA}$	0.010	0.297	0.987	0.036	0.029	0.209	-0.013	0.017	0.427	-0.001	0.011	0.916	1.168	0.542	0.044
$\beta_{V_f:FSA}$	0.140	0.260	0.964	-0.003	0.027	0.934	-0.002	0.015	0.898	-0.005	0.010	0.627	0.869	0.688	0.222
$\beta_{C:V_m:FSA}$	-0.144	0.333	0.478	-0.059	0.037	0.115									
$\beta_{C:V_f:FSA}$	-0.074	0.298	0.802	0.018	0.035	0.629									

Coeff.	Est.	Lower	Upper	Est.	Lower	Upper	Est.	Lower	Upper	Est.	Lower	Upper	Est.	Lower	Upper
σ_0	3.198	2.039	5.017	0.826	0.582	1.172	0.391	0.252	0.604	0.194	0.118	0.318	3.046	0.745	12.464
ε_{ij}	2.640	2.149	3.243	0.524	0.449	0.610	0.300	0.233	0.387	0.187	0.143	0.246	4.929	2.972	8.175

Coeff.	Est.	Est.	Est.	Est.	Est.
R^2_{adj}	0.52	0.75	0.66	0.53	0.40

Table 7.3.2: Model coefficient (Coeff.) estimates for the mean vcrp(τ) during **impact phase**. Fixed-effects coefficient estimates (Est.) are calculated as described in Section 7.2.6, with standard error (S.E.) and p-value. * denotes significance at $\alpha_f = 0.05$, following a Bonferroni correction. Standard deviations of the random intercept coefficient σ, and residuals ε_{ij} are reported with 95% confidence intervals. The adjusted coefficient of determination R^2_{adj} quantifies the final model goodness of fit. Cells are shaded grey where the parameters were not part of the model. Units are in degrees.

	PelThi			ThiTib			TibRft			RftFft			EVTIR		
Coeff.	Est.	S.E.	p-value	Est.	S.E.	p-value	Est.	S.E.	p-value	Est.	S.E.	p-value	Est.	S.E.	p-value
β_0	31.098	3.115	< 0.001*	-27.780	2.709	< 0.001*	-12.601	1.296	< 0.001*	13.921	1.118	< 0.001*	82.398	18.645	< 0.001*
β_C	0.587	2.908	0.840	2.305	1.473	0.118									
β_{V_m}	-3.410	1.840	0.064	-0.716	0.826	0.386	0.859	0.863	0.320	-1.324	0.502	0.009*	27.994	25.624	0.276
β_{V_f}	-1.929	2.702	0.475	-2.354	1.236	0.057	0.643	0.843	0.446	-0.619	0.568	0.277	-1.494	21.755	0.945
β_{FSA}	0.421	0.177	0.018	0.273	0.046	< 0.001*	0.069	0.038	0.074	-0.066	0.021	0.002*	-1.123	0.871	0.198
$\beta_{C:V_m}$	-3.291	2.415	0.173	-0.716	0.707	0.312									
$\beta_{C:V_f}$	-10.271	2.850	< 0.001*	-3.959	0.639	< 0.001*									
$\beta_{C:FSA}$	-0.591	0.229	0.010*	-0.287	0.071	< 0.001*									
$\beta_{V_m:FSA}$	0.366	0.220	0.096	-0.123	0.055	0.026	-0.041	0.060	0.493	0.039	0.037	0.295	-3.339	1.729	0.055
$\beta_{V_f:FSA}$	0.088	0.246	0.722	-0.147	0.050	0.003*	0.052	0.056	0.357	-0.063	0.033	0.054	2.864	1.702	0.094
$\beta_{C:V_m:FSA}$	0.011	0.245	0.965	0.147	0.058	0.012*									
$\beta_{C:V_f:FSA}$	0.497	0.268	0.064	0.420	0.048	< 0.001*									
Coeff.	Est.	Lower	Upper	Est.	Lower	Upper	Est.	Lower	Upper	Est.	Lower	Upper	Est.	Lower	Upper
σ_0	10.508	7.159	15.424	11.712	8.441	16.249	5.526	3.977	7.677	4.773	3.375	6.752	62.166	41.588	92.927
σ_C	4.859	2.966	7.962	5.004	3.596	6.963									
σ_{V_m}	3.536	1.942	6.438	3.125	2.201	4.436	3.304	2.357	4.630	1.751	1.058	2.899	56.91	29.900	108.320
σ_{V_f}	7.044	4.044	12.268	5.089	3.642	7.112	3.241	2.209	4.756	2.005	1.266	3.177	48.864	24.660	96.822
$\rho_{0:C}$	-0.194	-0.552	0.224	-0.348	-0.681	0.104									
$\rho_{0:V_m}$	0.609†	0.385	0.766	-0.404	-0.718	0.048	-0.525†	-0.785	-0.109	-0.700†	-0.926	-0.108	-0.311	-0.839	0.519
$\rho_{0:V_f}$	0.647†	0.437	0.791	-0.321	-0.664	0.134	-0.494†	-0.776	-0.046	-0.482	-0.857	0.226	-0.307	-0.853	0.560
$\rho_{C:V_m}$	-0.318	-0.666	0.144	-0.106	-0.529	0.360									
$\rho_{C:V_f}$	-0.304	-0.652	0.149	-0.067	-0.494	0.387									
$\rho_{V_m:V_f}$	0.999†	0.997	0.999	0.590†	0.193	0.821	0.805†	0.518	0.929	0.202	-0.437	0.706	0.982†	0.251	1.000
ε_{ij}	7.443	7.136	7.763	2.699	2.616	2.785	1.418	1.355	1.484	0.732	0.697	0.769	21.459	19.597	23.497

Coeff.	Est.	Est.	Est.	Est.	Est.
R^2_{adj}	0.76	0.94	0.93	0.96	0.90

Table 7.3.3: Model coefficient (Coeff.) estimates for the mean crp(τ) during **stance phase**. Fixed-effects coefficient estimates (Est.) are calculated as described in Section 7.2.6, with standard error (S.E.) and p-value. * denotes significance at $\alpha_f = 0.05$, following a Bonferroni correction. Standard deviation of random coefficients σ, estimates of correlation coefficients ρ, and standard deviation of the residuals ε_{ij} are presented with 95% confidence intervals. † denotes a correlation parameter is significantly different from zero. The adjusted coefficient of determination R^2_{adj} quantifies the final model goodness of fit. Cells are shaded grey where the parameters were not part of the model. Units are in degrees.

	PelThi			ThiTib			TibRft			RftFft			EVTIR		
Coeff.	Est.	S.E.	p-value	Est.	S.E.	p-value	Est.	S.E.	p-value	Est.	S.E.	p-value	Est.	S.E.	p-value
β_0	9.452	1.222	< 0.001*	3.044	0.202	< 0.001*	1.796	0.136	< 0.001*	0.961	0.091	< 0.001*	23.807	3.702	< 0.001*
β_C	0.538	1.800	0.766	-0.307	0.319	0.337									
β_{V_m}	1.494	1.691	0.381	-0.679	0.237	0.005*	-0.185	0.136	0.178	-0.088	0.075	0.250	-5.019	5.625	0.383
β_{V_f}	-1.019	1.759	0.565	-0.495	0.232	0.036	-0.393	0.133	0.005*	-0.107	0.074	0.155	-5.050	5.853	0.398
β_{FSA}	-0.065	0.138	0.639	-0.022	0.020	0.285	-0.001	0.014	0.960	0.011	0.009	0.234	-0.548	0.352	0.135
$\beta_{C:V_m}$	-2.923	2.605	0.266	0.419	0.447	0.351									
$\beta_{C:V_f}$	-0.711	2.605	0.786	-0.120	0.427	0.779									
$\beta_{C:FSA}$	-0.037	0.162	0.821	0.026	0.025	0.294									
$\beta_{V_m:FSA}$	-0.273	0.233	0.247	0.039	0.027	0.160	-0.010	0.016	0.518	-0.009	0.009	0.323	0.495	0.564	0.391
$\beta_{V_f:FSA}$	-0.025	0.219	0.911	-0.003	0.025	0.914	0.001	0.015	0.943	0.002	0.008	0.817	0.002	0.776	0.998
$\beta_{C:V_m:FSA}$	0.333	0.266	0.215	-0.051	0.035	0.155									
$\beta_{C:V_f:FSA}$	0.064	0.252	0.800	0.011	0.033	0.749									
Coeff.	Est.	Lower	Upper	Est.	Lower	Upper	Est.	Lower	Upper	Est.	Lower	Upper	Est.	Lower	Upper
σ_0	2.041	1.255	3.320	0.431	0.288	0.645	0.331	0.215	0.509	0.274	0.188	0.401			
ε_{ij}	2.250	1.838	2.755	0.498	0.428	0.580	0.283	0.222	0.362	0.152	0.116	0.200	0.699		

Coeff.	Est.	Est.	Est.	Est.	Est.
R^2_{adj}	0.52	0.75	0.62	0.82	0.00

Table 7.3.4: Model coefficient (Coeff.) estimates for the mean vcrp(τ) during **stance phase**. Fixed-effects coefficient estimates (Est.) are calculated as described in Section 7.2.6, with standard error (S.E.) and p-value. * denotes significance at $\alpha_f = 0.05$, following a Bonferroni correction. Standard deviations of the random intercept coefficient σ, and residuals ε_{ij} are reported with 95% confidence intervals. The adjusted coefficient of determination R^2_{adj} quantifies the final model goodness of fit. The fixed-effects model for EVTIR explains no variance in the data. Cells are shaded grey where the parameters were not part of the model. Units are in degrees.

	PelThi			ThiTib			TibRft			RftFft			EVTIR		
Coeff.	Est.	S.E.	p-value	Est.	S.E.	p-value	Est.	S.E.	p-value	Est.	S.E.	p-value	Est.	S.E.	p-value
β_0	4.725	8.268	0.568	-70.290	1.545	< 0.001*	7.213	0.719	< 0.001*	-0.476	0.461	0.303	163.700	11.338	< 0.001*
β_C	-8.200	9.393	0.383	-0.484	0.666	0.467									
β_{V_m}	-3.264	6.396	0.610	1.168	0.347	0.001*	-0.353	0.339	0.298	-0.369	0.218	0.090	0.812	9.384	0.931
β_{V_f}	-23.001	7.971	0.004*	2.670	0.428	< 0.001*	-0.891	0.443	0.045	-0.295	0.317	0.352	-18.467	17.444	0.292
β_{FSA}	-0.029	0.566	0.959	0.175	0.031	< 0.001*	0.117	0.024	< 0.001*	-0.041	0.015	0.005*	0.233	0.935	0.804
$\beta_{C:V_m}$	9.428	9.510	0.322	-1.174	0.512	0.022									
$\beta_{C:V_f}$	28.390	9.657	0.003*	-1.572	0.466	0.001*									
$\beta_{C:FSA}$	1.536	0.712	0.031	-0.202	0.042	< 0.001*									
$\beta_{V_m:FSA}$	0.990	0.816	0.225	-0.004	0.034	0.901	0.068	0.031	0.026	0.026	0.021	0.223	0.601	1.093	0.583
$\beta_{V_f:FSA}$	2.261	0.779	0.004*	-0.033	0.034	0.334	0.053	0.036	0.136	-0.015	0.024	0.533	1.488	1.673	0.376
$\beta_{C:V_m:FSA}$	-1.700	0.900	0.059	0.083	0.041	0.040									
$\beta_{C:V_f:FSA}$	-3.429	0.898	< 0.001*	0.154	0.036	< 0.001*									
Coeff.	Est.	Lower	Upper	Est.	Lower	Upper	Est.	Lower	Upper	Est.	Lower	Upper	Est.	Lower	Upper
σ_0	26.198	18.752	36.602	6.476	4.621	9.077	3.044	2.181	4.249	1.909	1.362	2.677	24.630	13.750	44.122
σ_C	16.815	10.962	25.795	1.654	1.151	2.375									
σ_{V_m}	10.102	5.282	19.320	0.847	0.522	1.374	1.174	0.770	1.790	0.679	0.454	1.016	8.195	2.727	24.623
σ_{V_f}	16.737	10.425	26.870	1.328	0.893	1.975	1.561	1.075	2.268	1.118	0.775	1.611	29.282	11.920	71.936
$\rho_{0:C}$	-0.131†	-0.164	-0.097	-0.594†	-0.829	-0.180									
$\rho_{0:V_m}$	-0.453†	-0.565	-0.323	-0.667†	-0.899	-0.142	-0.119	-0.560	0.374	-0.412	-0.741	0.076	-0.136	-0.661	0.478
$\rho_{0:V_f}$	-0.356†	-0.385	-0.326	-0.604†	-0.844	-0.162	-0.059	-0.518	0.426	-0.375	-0.711	0.101	0.999†	0.999	1.000
$\rho_{C:V_m}$	0.231†	0.047	0.400	0.406	-0.169	0.775									
$\rho_{C:V_f}$	-0.880†	-0.883	-0.877	-0.018	-0.500	0.474									
$\rho_{V_m:V_f}$	0.005	-0.182	0.191	0.442	-0.133	0.794	0.963†	0.779	0.994	0.612†	0.162	0.851	-0.103	-0.642	0.504
ε_{ij}	20.952	19.969	21.983	2.015	1.947	2.084	0.957	0.912	1.004	0.554	0.527	0.582	8.396	7.330	9.617

Coeff.	Est.	Est.	Est.	Est.	Est.
R^2_{adj}	0.53	0.89	0.89	0.92	0.94

Table 7.3.5: Model coefficient (Coeff.) estimates for the mean crp(τ) during **swing phase**. Fixed-effects coefficient estimates (Est.) are calculated as described in Section 7.2.6, with standard error (S.E.) and p-value. * denotes significance at $\alpha_f = 0.05$, following a Bonferroni correction. Standard deviation of random coefficients σ, estimates of correlation coefficients ρ, and standard deviation of the residuals ε_{ij} are presented with 95% confidence intervals. † denotes a correlation parameter is significantly different from zero. The adjusted coefficient of determination R^2_{adj} quantifies the final model goodness of fit. Cells are shaded grey where the parameters were not part of the model. Units are in degrees.

	PelThi			**ThiTib**			**TibRft**			**RftFft**			**EVTIR**		
Coeff.	Est.	S.E.	p-value	Est.	S.E.	p-value	Est.	S.E.	p-value	Est.	S.E.	p-value	Est.	S.E.	p-value
β_0	26.999	3.593	< 0.001*	10.557	0.441	< 0.001*	6.086	0.269	< 0.001*	3.695	0.310	< 0.001*	22.377	4.996	0.003*
β_C	-1.021	4.836	0.834	1.267	0.578	0.031									
β_{V_m}	-7.872	4.780	0.106	-0.595	0.458	0.198	-0.470	0.271	0.089	-0.155	0.220	0.486	7.479	3.625	0.078
β_{V_f}	-9.105	4.529	0.050	-1.123	0.440	0.012*	-0.456	0.261	0.087	-0.146	0.215	0.500	-13.145	6.732	0.092
β_{FSA}	-0.260	0.442	0.560	0.122	0.038	0.002*	-0.042	0.027	0.125	-0.010	0.026	0.705	-0.262	0.666	0.706
$\beta_{C:V_m}$	5.317	7.703	0.493	0.686	0.818	0.404									
$\beta_{C:V_f}$	2.091	7.070	0.769	-0.705	0.773	0.364									
$\beta_{C:FSA}$	0.062	0.497	0.901	-0.088	0.045	0.053									
$\beta_{V_m:FSA}$	0.749	0.632	0.242	-0.050	0.050	0.316	-0.013	0.031	0.670	-0.004	0.025	0.864	-1.123	0.450	0.041
$\beta_{V_f:FSA}$	0.357	0.575	0.538	-0.058	0.047	0.214	-0.015	0.029	0.594	0.005	0.023	0.837	-0.357	0.903	0.704
$\beta_{C:V_m:FSA}$	-0.787	0.745	0.296	-0.009	0.064	0.887									
$\beta_{C:V_f:FSA}$	-0.259	0.676	0.703	0.037	0.060	0.539									
Coeff.	Est.	Lower	Upper	Est.	Lower	Upper	Est.	Lower	Upper	Est.	Lower	Upper	Est.	Lower	Upper
σ_0	4.262	2.347	7.740	1.091	0.740	1.610	0.664	0.435	1.014	0.996	0.669	1.483	6.696	3.530	12.699
ε_{ij}	5.156	4.073	6.527	0.877	0.742	1.035	0.554	0.432	0.710	0.430	0.320	0.578	1.820	0.624	5.307

Coeff.	Est.	Est.	Est.	Est.	Est.
R^2_{adj}	0.44	0.74	0.72	0.85	0.98

Table 7.3.6: Model coefficient (Coeff.) estimates for the mean vcrp(τ) during **swing phase**. Fixed-effects coefficient estimates (Est.) are calculated as described in Section 7.2.6, with standard error (S.E.) and p-value. * denotes significance at $\alpha_f = 0.05$, following a Bonferroni correction. Standard deviations of the random intercept coefficient σ, and residuals ε_{ij} are reported with 95% confidence intervals. The adjusted coefficient of determination R^2_{adj} quantifies the final model goodness of fit. Cells are shaded grey where the parameters were not part of the model. Units are in degrees.

	PelThi			ThiTib			TibRft			RftFft			EVTIR		
Coeff.	Imp	St	Sw	Imp	St	Sw	Imp	St	Sw	Imp	St	Sw	Imp	St	Sw
β_C				⋆											
β_{V_m}				†	†	⋆					⋆				
β_{V_f}	⋆		⋆	⋆ †		⋆ †	⋆	†					⋆		
β_{FSA}	⋆			⋆	⋆	⋆ †	⋆		⋆	⋆	⋆	⋆	⋆		
$\beta_{C:V_m}$															
$\beta_{C:V_f}$	⋆	⋆	⋆	⋆	⋆	⋆									
$\beta_{C:FSA}$		⋆		⋆	⋆	⋆									
$\beta_{V_m:FSA}$				⋆											
$\beta_{V_f:FSA}$			⋆		⋆								⋆		
$\beta_{C:V_m:FSA}$					⋆										
$\beta_{C:V_f:FSA}$	⋆		⋆	⋆	⋆	⋆									

Table 7.3.7: Summary of the significant fixed-effects in all models for impact (Imp), stance (St), and swing (Sw) phases at $\alpha_f = 0.05$, following a Bonferroni correction. ⋆ denotes significant effects for crp(t) and † denotes significant effects for vcrp(t). Cells are shaded grey where the parameters were not part of the model. Units are in degrees.

effect depended on the segment coupling. For ThiTib and EVTIR coordination in particular, high velocity led to more out-of-phase coupling (Table 7.3.1, β_0 and β_{V_f}), directly contradicting the original hypotheses and the results of Stergiou *et al.* [194].

PelThi coupling was out of phase during impact, but became more in-phase at high velocity. Interactions show this change was largest for BF running. TibRft coupling was generally in phase during impact but also became more in-phase at high velocity. For both coupling relationships, high velocity was not a significant main effect of coordination for stance phase.

Velocity was associated with a reduction in vcrp(τ) for ThiTib coupling for all three time periods studied. There was also a significant decrease in TibRft vcrp(τ) at high velocity for stance phase.

7.3.6 Foot-strike angle

Foot-strike angle was a significant main effect on coordination during impact (five out of five cases), stance (two out of five cases) and swing phases (three out of five cases). A more dorsi-

flexed foot at FS was associated with more out-of-phase coordination during impact for EVTIR but no changes for stance or swing phase were identified, supporting the original hypotheses motivated by Pohl and Buckley [164].

For ThiTib, TibRft, and RftFft couplings during contact phases, more foot dorsiflexion at FS was associated with more in-phase coordination. The magnitude of TibRft and RftFft couplings (Tables 7.3.1 and 7.3.3, and Figure 7.3.1) suggest that the sagittal plane motion phase planes of the tibia and forefoot segments may be in-phase during impact and stance phase, and that variation with respect FSA is small.

For one case, ThiTib coupling during swing phase, FSA was a significant main effect for vcrp(τ) such that vcrp(τ) decreased with more foot plantarflexion at FS. Therefore, the hypothesis that vcrp(τ) reduces for RFS during impact phase was not supported.

7.3.7 Within-subject and between subject variation

The magnitude of the random effects in the crp(τ) and vcrp(τ) statistical analyses are typically comparable to the magnitude of the significant fixed effects.

7.4 Discussion

This chapter sought to analyze running biomechanics from a dynamical systems perspective with a view to defining the range of coordination and coordinative variability in an uninjured population of trained distance runners. For this, coordination and coordinative variability was quantified by crp(τ) and vcrp(τ) respectively, using a Hilbert transform construction of phase space [113, 175], in a manner consistent with the foundations of DST. Coordination was less sensitive to changes in velocity and FSA for SD running, and as velocity increased in the BF condition, rearfoot coronal plane dynamics adapted to synchronize with tibial rotation, possibly

to mitigate injury risk.

The need to run long distances for scavenging and hunting directed evolutionary adaptations of the *homo* [21]. Therefore, large knee joints compared to other mammals developed [21], and as with most other mammals that run or gallop, by concentrating mass proximally, the inertia of rapidly moving distal segments is minimized and efficiency is increased. With observations here, there is an association between more rapidly moving distal segments, proximally concentrated mass, and lower vcrp(τ) between associated adjacent segments. One question follows: Given a task, is the set of coordinative strategies for segments comprising a joint, quantified with vcrp(τ), a reflection of the function of the muscles associated with that joint? During walking and running, muscle groups across proximal joints operate at a lower level relative to their maximum compared to the muscle groups across distal joints [111]. Lower vcrp(τ) for segments comprising a joint may reflect that the associated muscles are working at a higher relative effort. Put another way, where muscles across a joint are working at a higher capacity of their maximum there may be fewer coordinative strategies between the segments involved. Movement patterns converge onto a progressively smaller set of 'solutions' as a function of relative effort.

7.4.1 Running-related injuries

The injury rate in the present running population six and twelve months after the data collection was 11% and 39% respectively (Table C.1.1). This is comparable with the recreational population and within previously observed bounds [204], in contradiction to the hypothesis.

In another study of collegiate male athletes [39], higher injury rates were higher than for those observed here. The retrospective study recorded more in-depth information on individuals' training data, quantified injury severity, and analysed possible covariates such as running volume and BMI. In the present study, whilst injuries were also diagnosed by medical profes-

sionals, running-related injury data were self-reported at six and twelve month intervals as a binary injured or not-injured. The sample of runners in this thesis was representative of a typical healthy population at the time of data collection and as such, it is likely that observations in this chapter relate to healthy coordination strategies. However, differences between the injury rates observed in this thesis and those from the study by Daoud *et al* [39] may be influenced by difference in the data collection methodology. Also, and importantly, discussions surrounding injury biomechanics are not directly attributable to the biomechanics here, but rather serve as avenues for future study.

7.4.2 Comparison with previous literature

Compared to previous studies, a larger sample size (19 subjects here versus 10 [194], 8 [142], and 6 [121]) and more gait cycles per trial (mean [st. dev.] 16 ± 3 here versus 10 [194], 7 [142], and 5 [121]) were collected, thus facilitating the application of LMM.

The magnitude of vcrp(τ) is smaller than previous studies [77,142,194], most likely because different segmental relations are considered and also because a LMM accounts for between-subject variability, giving more accurate coefficient estimates. Rearfoot coronal plane to tibial transverse plane vcrp(τ) is similar to Miller *et al.* [142], especially for swing phase. Miller *et al.*, with 95% confidence intervals, reported vcrp(τ) values of approximately $27^\circ \pm 2^\circ$ and $33 \pm 2^\circ$ for swing phase and stance phase respectively.

Miller argues that most differences in their study between the healthy and pathological groups were not significant because there was large between-subject variation. For EVTIR, in the analysis in this chapter, between-subject variation is accounted for during swing phase and no significant main effects of velocity or FSA are identified. A random intercept model accounted for 98% of the variation in this case. For stance phase, a random intercept model was not appropriate and more data may be needed to look at this further. Artefacts which arose

from applying a Hilbert transform were to the detriment of statistical analysis because of the necessary omission of data. The artefacts in the case were unphysical, limit-cycle oscillations. Whilst variation in the data may be accounted for when using certain statistical methods, the available methods are dependent on the properties of the data.

To the higher impact forces which arise from running over progressively higher obstacles, Stergiou *et al.* [194] suggest that ThiTib coupling adapts by becoming more in-phase. Comparing data to their results for the no-obstacle case suggest that the sample in this study is generally more in-phase. Discrepancies in magnitude arise from differences between traditional (x, v) versus Hilbert transform phase space constructions. Other, likely less important differences in methodology include 2D video analysis versus 3D motion capture, the definition of impact phase (for Stergiou, this is based on force plate data), overground versus treadmill running and different statistical analysis techniques. The different phase space constructions may also explain difference in EVTIR crp(τ) between results here and Miller *et al.* [142]. Furthermore, previous studies looked at SD running and foot segment movement, verses BF running and the rearfoot segment. A direct comparison to literature is difficult because of the different phase space construction methods. However, the traditional phase space construction is misleading, and the present Hilbert-transform-based construction should be considered the gold standard because of the more principled foundation (Section 7.2.3) and consistent interpretation.

Li *et al.* [121] studied crp(τ) for walking and running at 2.24 ms^{-1}. Although 2.24 ms^{-1} is far outside set of training speeds for the study group, traces of the ThiTib (*i.e.* thigh-leg) crp(τ) using the (x, v) method are comparable across the gait cycle, even though the phase planes are slightly different.

Apart from a reflection about the x-axis, one recent study of forwards and backwards running [138] produced similar results to this chapter. The reason for the reflection is that the Hilbert transform, compared to the phase planes from traditional methods, is reflected about the

x-axis. When this occurs for both phase planes, it manifests as a reflection in the crp(τ) values. This was accounted for in the present analysis to make a qualitative comparison to previous literature using traditional techniques. This does not appear to be the case for [138]. Additionally, and of concern, is that applying a Hilbert transform to individual strides necessarily means data from that stride must be omitted. This is because of the aforementioned edge effects associated with the signal processing procedure. In the work of Mehdisadeh *et al.* [138] edge effects are clearly visible in the crp(τ) traces, and necessarily, any analysis of vcrp(τ) is flawed.

7.4.3 Condition

Coordinative changes as a function of condition and velocity for PelThi and ThiTib are different because of the differences in their functional demands. High velocity causes PelThi coupling to be more in-phase during impact, with the effect being more pronounced for BF running, whereas ThiTib becomes more out-of-phase for BF running and more in-phase for SD running. PelThi coordination during impact serves to decouple the two segments in order to stabilize the pelvis and minimize the transfer of angular momentum from the lower limb to the torso. This appears to become less effective at high velocity, particularly for BF running. This may be because of the unfamiliarity of BF running, or changes in impact forces. ThiTib coordination during impact is related to force dissipation normal to the surface and in-phase coordination is desirable [194]. Available lower leg muscle capacity, which exists because of the presence of shoes, may allow more in-phase behaviour for SD running. Matched for velocity, SD running is always more in-phase than BF running.

By removing shoes the foot is afforded more mechanical degrees of freedom. Coordination changes exist as a function of FSA but are dependent on foot condition, such that coordination does not change with FSA for SD running. The quadricep and hamstring muscle groups are primarily responsible for influencing TibThi coordination but the *gastrocnemius*, which also

crosses the knee joint may play a minor role. Elevated stance phase *gastrocnemius* EMG activity for BF running may be part of the mechanism by which ThiTib coordination changes as a function of FSA for BF running. Quadricep and hamstring muscle group EMG data and ground reaction force data is necessary to verify this claim.

The body reduces ThiTib vcrp(τ) in preparation for FS for BF running. De Wit *et al.* [43] found that joint configuration of the leg at touchdown is prepared in free flight, arguing that there exists an actively induced adaptation strategy to BF running. This strategy was observed at the level of joint kinematics and was explained by a functional demand to lower local pressure at the heel pad and potentially reduce shear forces acting at the heel. Whilst swing phase PelThi and ThiTib crp(τ) is independent of condition, there is a reduction in ThiTib vcrp(τ), which may be associated with an increased coordinative demand when adapting to BF running. This may have implications for an underlying increase in injury risk for BF running given that populations with a history of knee injury have more repeatable ThiTib crp(τ) [77, 142]. Miller [142] argue that changes in vcrp(τ) during swing phase reflect historical pathological biomechanics, since movement patterns have not needed to adapt because the leg is not under load, and therefore it is less likely to be in pain. The results here may reflect that BF running predisposes uninjured runners to knee (re-)injury.

Given the interaction between FSA and condition for ThiTib segment vcrp(τ), a $+1^{\circ}$ change in FSA for BF running may have greater implications for running injury than for SD running. Whilst runners naturally run with a more plantarflexed foot at FS in the BF condition [43], an elevated sensitivity to injury risk may exist for BF running in runners with more foot plantarflexion at FS. To affirm this a prospective study focused on specific knee injuries as a function of FSA is necessary. Nevertheless studies with minimalist shoes, which sought to emulate a 'BF running' technique [125], by encouraging FFS running as a means to minimize injury risk, have demonstrated that a transition to BF running in this manner is associated with injury [171]. At

the first attempt of BF running there is a potentially observable marker of injury risk associated with BF FFS running in habitually SD runners. It is not yet clear if a transition to BF running with a RFS strategy is definitively more injurious than FFS running. Forefoot impact forces cause edema because the repeated impacts are sufficient to cross the injury threshold. At the knee and in the absence of the edema, there may be other repetitive loading behaviours which could potentially lead to injury. Three runners (MC: Hamstring strain; MH: ITBS; and MN: PFPS) developed a knee-related injury within twelve months of the data collection but, none ran BF after the data collection. Therefore the reduction in vcrp(τ) for BF running is not necessarily responsible for the subsequent knee injuries.

The general observation that for SD running, coordination changes less as a function of velocity and condition may reflect that habituation manifest as coordination patterns which do not typically change with smaller interventions.

7.4.4 Velocity

The results for coordination changes with velocity contradict the hypotheses in this chapter. The hypothesis for the ThiTib coupling was motivated by a study of running over obstacles [194]. Coordinative adaptions to increases in running velocity are different to those for running over obstacles.

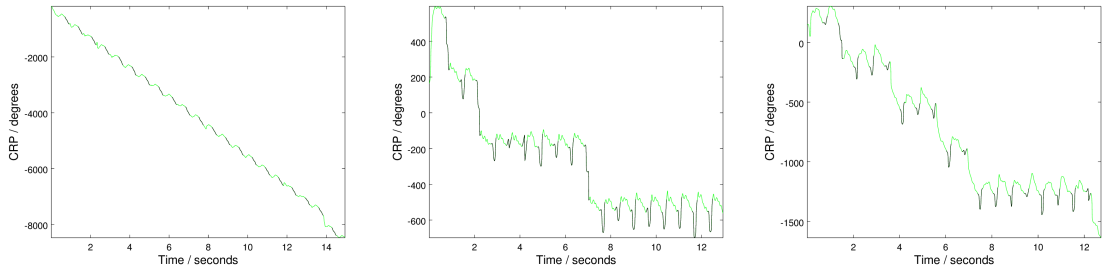
Without ground reaction force data, it is not possible to study impact forces as a function of velocity. Furthermore, any change in impact force may not be sufficient to alter ThiTib coordination which mirrors the results of Stergiou *et al*. [194]. A qualitatively new ThiTib coordination pattern emerged for obstacle running whereas the same is not true for fast versus slow running in the present study. It is not clear what causes the observations for ThiTib crp(τ) here. There are changes with high velocity during impact for three out of the four sagittal plane couplings and only the ThiTib coupling moves out-of-phase. An interaction between segments

may be complicated by the small incremental changes in velocity, and a wider selection of running speeds may provide a valuable insight.

Lower variability of ThiTib coupling is consistent with the concept that an increase in relative effort of the muscles crossing the knee joint is associated with a reduction in vcrp(τ). Whilst changes in impact force with velocity cannot be verified, it is plausable that impulse increases as a function of increased velocity. Accordingly, decreases in ThiTib vcrp(τ) with velocity are observed for both impact phase and stance phase. An alternative explanation is that more out-of-phase coordination, which occurs simultaneously with decreases in vcrp(τ), demonstrates that the out-of-phase ThiTib coordination which occurs at higher velocities is by itself an at-risk running modality.

From the entire crp(t) times series for EVTIR there is qualitatively different behaviour for different velocities. At low velocity, tibia and rearfoot segments are desynchronized (Figure 7.4.1a) but, for medium and high velocity there are periods of phase locking, and thus synchronicity between segments (Figure 7.4.1b and 7.4.1c). The resonant interaction arises from changes in the phase plane of the rearfoot during stance phase as a function of velocity whilst the phase plane of the tibia remains invariant (Figure 7.4.2). It is likely that the underlying coupling between segments changes with time for medium and high velocity, leading to periods of synchronous and desynchronous behaviour [175]. The phase locked crp(τ) from 10-30% of the gait cycle is associated with an increase in vcrp(τ) (Figure 7.3.2), which may indicate that the new coordinative pattern is a healthy adaptation to faster running, whilst from an overuse injury risk perspective, this synchronous movement is desirable, mitigating adverse effects at the foot and ankle which arise from high speed BF running. A relatively small dataset was used for this particular analysis and therefore further study with larger groups is encouraged. Bone pin studies have shown consistency in tibio-calcaneal kinematics (with respect to joint kinematics) between BF and SD running [190] but, changes in joint kinematics do not necessarily reflect

changes in segment coordination [140,142]. Therefore, it is not possible to ascertain if the lower leg coordinative changes with velocity for BF running necessarily extend to SD running.



(a) Slow (b) Medium (c) Fast

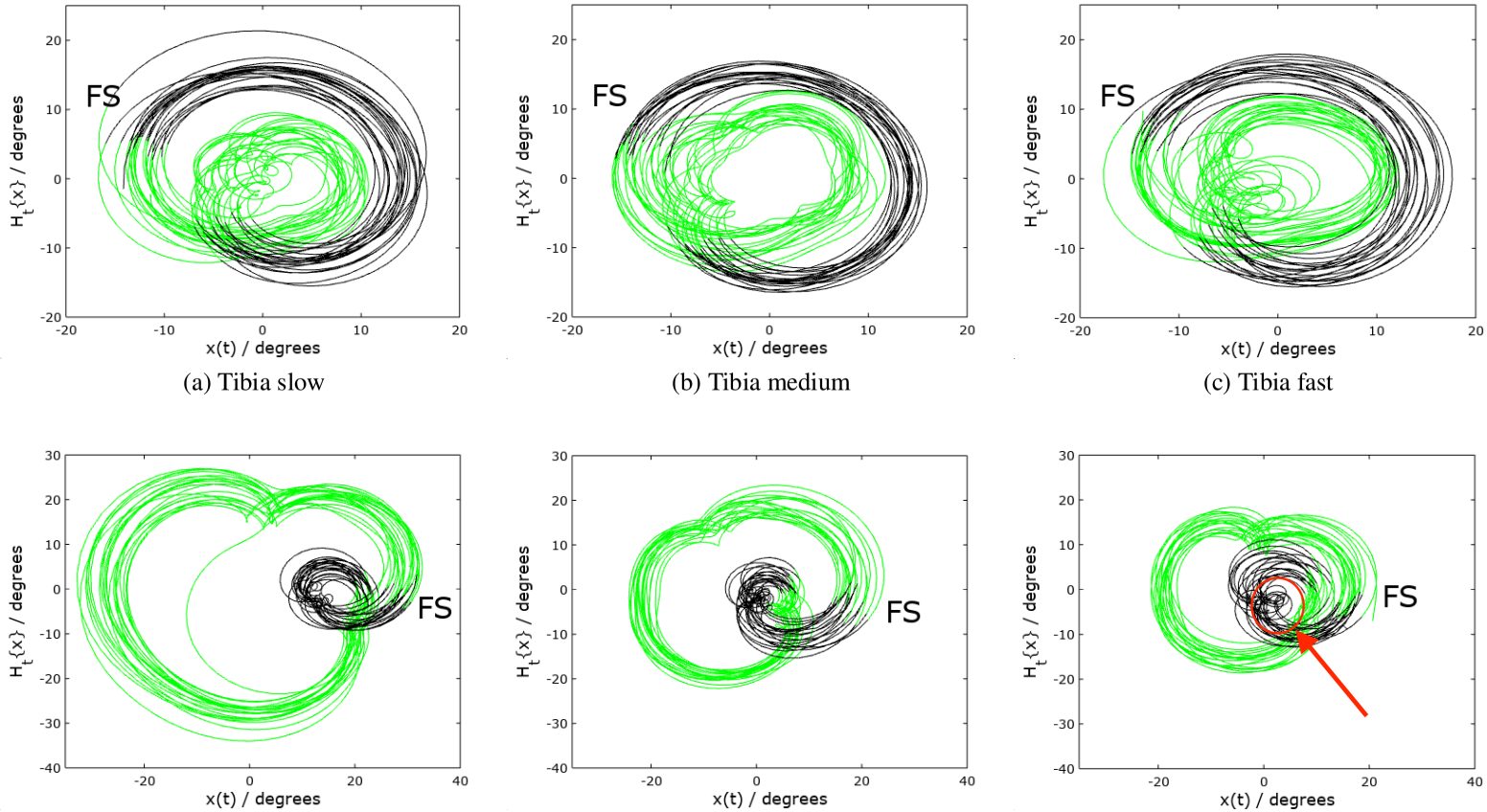
Figure 7.4.1: Time evolution of EVTIR crp(t) data (green) for subject MN. Successive stance phases are in black. Medium and fast velocity running shows periods of synchronicity.

7.4.5 Foot-strike angle

Differences in FSA are associated with changes in crp(τ). The observations for EVTIR corroborate previous work, but inferences interpreted from an overuse injury perspective contradict a recent prominent study [39]. It is likely that the coordinative changes are of little biomechanical significance with respect to injury and simply provide healthy bounds of the coordinative changes with respect to FSA for a sample of healthy trained distance runners.

The results for EVTIR corroborate the observations Pohl and Buckley [164]. They argue that during RFS running the rearfoot is in a dorsiflexed position, and that this is inefficient for the transfer of motion from the calcaneus to the tibia via the talus. Pohl and Buckley used VC and studied joint angles and although comparison to their results is cautioned against because of a general lack of consistency between methodology [141], in this case there appears to be a correspondence in the results across the two methods. As vcrp(τ) for EVTIR is independent of FSA, although crp(τ) changes with FSA during impact phase, it is unlikely that these changes affect injury risk.

In one case changes in crp(τ) and vcrp(τ) occured simultaneously. Lower vcrp(τ) ThiTib



(a) Tibia slow (b) Tibia medium (c) Tibia fast

(d) Rearfoot slow (e) Rearfoot medium (f) Rearfoot fast

Figure 7.4.2: Phase plane dynamics as a function of velocity for the tibia in the transverse plane and rearfoot in the coronal plane, constructed using the Hilbert transform. Data for a representative subject (MN) are presented in green, where stance phase data is in black and 'FS' denotes foot strike. Tibia dynamics (7.4.2a to 7.4.2c) are invariant, whilst rearfoot dynamics (7.4.2d to 7.4.2f) change as a function of velocity. With higher velocity, an extra cycle emerges in the rearfoot phase plane during stance phase (see red circle and arrow), such that rearfoot and tibia dynamics become more synchronous (Figure 7.4.1). A smaller state space is sampled during swing phase for the rearfoot.

was observed during swing phase in preparation for more FFS-like running. This may reflect that the FFS technique puts a greater coordinative demand on the knee joint, and that there may also be an elevated knee related injury risk for FFS running [142]. This idea directly contradicts the observations of Daoud *et al.* [39], who found an elevated knee-related injury risk with RFS running. Whilst the sample in the Daoud study matches the present sample of college athletes with respect to performance ability and age, there are several differences. First, the yearly injury rate was far lower for the present group (42% in one year versus 79%) even through the running volume was comparable (mean [std. error]: 54 [7] here versus 45 [6] mpw). Second, the study here collected 200 Hz 3D data and measured FSA, whereas Daoud *et al.* [39] used a single 500 Hz video camera and assigned subjects to a FFS or RFS group. The reported injury rates in the Daoud study are high compared to previous literature [204], whilst the rate reported in the present study lies within previously observed boundaries. It is likely therefore, that differences in training methodology contribute to the differences in injury rate between studies. It is also likely that the reduction in ThiTib vcrp(τ), whilst statistically significant, is not biomechanically significant with respect to injury and rather, represents a healthy, natural reduction in the vcrp(τ) during swing phase. The observed differences in injury rate between RFS and FFS running appear to be dependent on training methodology.

7.4.6 Within-subject and between-subject variation

In the statistical analysis of crp(τ), the coefficient for ε_{ij} is an estimate of unexplained variance in the data. The coefficient β_0 in vcrp(τ) analysis is a direct estimate of the within-subject vcrp(τ) by way of the pointwise standard deviation for slow barefoot running. The estimate of within-subject vcrp(τ) is not the same as the unexplained variation in the crp(τ). The unexplained variance in crp(τ) is derived from the difference between observed values of crp(τ) and the estimated mean crp(τ) for a subject, whereas β_0 for the vcrp(τ) is a specific measure of

coordinative variability with its foundations in DST.

It is still possible to consider between-subject variability in the context of the fixed effects. The magnitude of the random effects for crp(τ) is typically comparable to the magnitude of the significant fixed effects. Therefore, it is possible that the fixed effects, whilst statistically significant, are not biomechanically significant. For example, it is possible that for one subject, there is no change with velocity and for another there is. For the case of vcrp(τ), unexplained variance is similar in magnitude to the between-subject variation, and these two coefficients similar in magnitude to any significant fixed effects (for FSA, consider the case for a 10° change in FSA). This suggests that a change in velocity would elicit a change in vcrp(τ) for one subject, but not for another, again potentially precluding the possibility that the statistical effects are biomechanically significant.

7.5 Limitations

This chapter is not without limitations. First, a record of injuries which developed in subjects after data collection is presented in this chapter. To provide a direct link between the biomechanics presented in this chapter and subsequent injury development, follow-up gait analyses are necessary. Owing to practical considerations this was not possible, neither at six month intervals or when injuries occured.

Global segment angles were calculated in a reverse engineered process from joint angles (Equation 7.2.4). This is undesirable because, in general, matrix rotations are not commutative and therefore consistency in the rotation sequence between studies is necessary. At the time of calculation, it was practically unfeasable to extract segment angles from the original data capture. Despite this, data analysed compared favourably to previous studies.

Condition effects were studied for two coupling relationships. It was not possible to use

the OFM for three coupling relationships because subjects used their own shoes. Therefore, making incisions in the shoes to measure foot motion, at the expense of the subjects' shoes, was impracticable even though the direct study in-shoe foot motion is valuable.

When applying the Hilbert transform it is desirable to have a long time series ($O(10^3)$) since data is naturally lost at the ends of the times series because of edge effects. To apply the Hilbert transform and calculate vcrp(τ), a trial must comprise at least seven continuous gait cycles at a sufficient sample rate. The Hilbert transformer is an infinite impulse response filter [175] and therefore in principle, edge effects can extend over the entire times series. However, a 256-point filter can provide 1% precision and times series here are typically $O(10^3)$ data points. A sample rate which allows for at least 20 points per oscillation must also be chosen [175]. Whilst there are $O(10^2)$ data points per gait cycle for this study, the sample rate requirement sets a lower limit on the data capture rate of approximately 33 Hz, assuming that a typical running gait cycle lasts 60 ms.

Artefacts were observed both from applying the Hilbert transform [113] and from resampling the data to 51 data points. Although the method gives more accurate results, data were lost due to artefacts arising from the signal processing procedures. Whilst this was not typically a problem, owing to the large pool of data collected, the EVTIR results were adversely affected by the aforementioned limit cycle oscillations (Section 7.4.2). and therefore require further study. In general, the flexibility of mixed model analysis over ANOVA based methods mitigates small datasets by being more robust to problems associated with missing data.

When calculating a summary statistic over a given time period for the crp(τ), it can be misleading if the time series for the crp(τ) is highly variable across the time period because important time dependent structure may be lost (Figure 7.3.2). To avoid this, an initial observation of the crp(τ) time series is necessary before any summary statistics are calculated.

As a general comment on LMM, attention must be paid to outliers because the method

is sensitive to outliers. To guard against this, a thorough understanding and application of diagnostic tools is crucial.

7.6 Conclusion

In general, the results contradicted the hypotheses of this chapter. Nevertheless, the primary objective of presenting coordination and coordinative variability, quantified using crp(τ) and vcrp(τ), for uninjured, trained distance runners was achieved. This was conducted in a manner consistent with the foundations of DST because phase planes for segment angle data in a global coordinate system were generated using the Hilbert transform. Thus a foundation exists, upon which future studies can build, with the focused study of pathological populations.

Coordination is generally more robust to changes in velocity and differences in FSA for SD running, possibly reflecting habituation or that more muscle capacity is available for SD running, and coordinative variability is independent of FSA. Further study of EVTIR with a larger population is encouraged, given what appears to be the emergence of transient phase locking between segments at high velocity. This may be a mechanism utilized by the foot to address an increased functional demand of pronation. Finally and tentatively, given a specific task, low coordinative variability between segments comprising a joint may be related to the higher relative effort of the muscles crossing the joint.

Chapter 8

Conclusion and future work

8.1 Conclusion

This cross-sectional study of nineteen uninjured trained male distance runners considered the effects of velocity and condition on running biomechanics. Foot-strike angle was studied and incorporated into statistical models, on a stride-by-stride basis, in the analysis of muscle activity and inter-segment coordination in three dimensions.

Foot-strike angle variability may reflect subjective comfort because of sensory feedback related to the heel pad deformation [43]. In Chapter 4, data for eight female runners were added to data collected for the nineteen male runners in an investigation of a discrete versus continuous classification of FSS, and of anatomical factors influencing gait. Classifying individuals by FSS does not acknowledge the variation from stride-to-stride which occurs naturally [124], and a continuous, stride-specific parametrization is desirable because it avoids this restriction. Also in this Chapter 4, differences in hip anatomy between genders were associated with kinematic differences which relate to injury, corroborating and adding credence to previous studies [60, 93, 209].

A logistic regression model investigated the probability of sustaining a running-related in-

jury rate as a function of FSA and FSA variability for slow BF running. The model used the representative trial FSA and the standard deviation of FSA per subject. The injury rate was lower than in a previous retrospective study of the same population [39] but comparable to the running populations as a whole [203, 204]. A main effect of increasing FSA variability correlated with the probability of developing a running-related injury, and an interaction with FSA existed. High variability in the habitually SD population, which manifests during BF running, may demonstrate a propensitity for injury development. Additionally, those who ran with more plantarflexion at FS were at highest risk of injury, contradicting a previous observation which linked RFS running to a higher absolute risk of running-related injury [39]. A study of variability in Kenyan habitually SD versus BF runners [124] identified higher variability in FSA for the habitually BF population. The authors suggested higher variability, because it was observed for the habitually BF runners, is more natural and therefore beneficial. Additionally, they suggested that higher variability demonstrates higher skill. The results here contradict the idea of higher variability, in and of itself, being more beneficial. The results here motivate further study of the interactions between variability, habituation, and injury.

Extrinsic factors such as training techniques and fatigue may be particularly relevant for the population studied here and in [39]. Running in the limit of no external cushioning may place demands on runners' kinematics which are sufficient to elicit anomalous running kinematics, in the form of high variability. This explains how novice BF running in the habitually SD population may have use as a diagnostic tool (Sections 4.3.2 and 4.4.1) for running-related injury risk, taking a form analagous to a cardiac stress test. It is reiterated here that limitations exist (Section 4.4.6), particularly in regard to the number of injuries observed, and further work exploring this idea is necessary. It is noted that a study of the effects of FSA and FSA variability on injury rate was not conducted for the SD condition, and such information would be valuable. Also, using SD running for habitually BF runners may also provide valuable insights for the

biomechanics of habitually BF population especially because whilst BF running is the limit of no external cushioning for a habitually SD runner, the same is not true for an habitually BF runner.

The concept of BF running as a diagnostic tool is separate to a discussion of the implications surrounding the general practice of BF running. Following the description of fixed-velocity BF running kinematics, the investigation focused on the effects of velocity and condition on FSA. As previously described, novice BF running causes runners to adopt a more anterior foot placement at FS [43] such that a different FSS may occur [2, 85]. In Chapter 5 the magnitude of within-subject variation (assumed to be equal to the unexplained variance) was measured to be more than half the magnitude of between-subject variability. This allowed for a discussion of the probability of observing an individual FS which is different to the majority of those observed. The probability of a 'misrepresentative FS' was low for SD running but not for BF running (Section 5.4.3).

Foot-strike angle was not affected by velocity for BF running. Therefore for BF running, actions which relate to FS mechanics are amplified because they occur independent of velocity. This, coupled with higher lower-leg *gastrocnemius* muscle activity observed in Chapter 6, and potentially higher Achilles tendon strain and *gastrocnemius medialis* force for FFS running [4], is a cause for caution for novice BF runners. These observations help explain why novice BF runners experience Achilles tendon pain in the period following a transition to BF running [94]. Observations of increasingly dorsiflexed FSA with faster velocity for SD running may appear counter intuitive [22, 151]. However, the statistical methodology allowed for more accurate estimates of fixed effects, because the random variation of fixed effects at the subject level (where valid) was accounted for.

A recent study of SD running which also used LMM corroborated the observations here [131]. Restrictions in FSA as a function of velocity, which exist possibly because of comfort,

may not exist in the SD condition. This is hypothesized because the maximal deformation of the heel pad, which occurs for BF heel striking, does not occur for SD heel striking [42]. Therefore the practice of increasing FSA dorsiflexion with velocity in the range of speeds studied is not painful for SD running. It is acknowledged that stride length is related to FSA [19, 199] but that this covariate was not included along with the effects of condition and velocity. Including two strongly correlated predictors (velocity and stride length) in the statistical model would be undesirable because the order the predictors are introduced to account for variation would strongly influence whether they were statistcally significant or not.

Chapter 6 was a detailed study of lower-leg EMG. The interaction effect between velocity and condition on FSA, observed in Chapter 5, motivated the inclusion of second-order interactions in the final statistical models. The two heads of the *gastrocnemius* muscle may serve different functions around FS. A simulation study [80] identified that the *soleus* and *gastrocnemius* muscle both contribute to forward acceleration. The observations in Chapter 6 provided evidence that of the two *gastrocnemius* heads, the *gastrocnemius medialis* may have a role in foot stability around FS, whilst the *gastrocnemius lateralis* is involved primarily in increasing in forward acceleration. A direct study of muscle fatigue for BF running, which includes a musculoskeletal model, would be a valuable extension to help understand *gastsrocnemius medialis* and *gastrocnemius lateralis* function.

Chapter 7 provided an analysis of coordination and coordinative variability and served as a description of uninjured runners, upon which future studies may build. This work was motivated by recent advances in analysis methods [113,175] and work which inappropriately applied these new techniques [138] (for discussion, see Section 7.4.2 and 7.5). Shod running was more robust to changes in velocity than BF running; whilst FSA changed with velocity for SD running, inter-segment coordination did not. This reinforces the need to distinguish between traditional joint kinematic analysis and inter-segment coordination. For BF running, rearfoot coronal and tibial

transverse phase plane dynamics demonstrated transisent phase locking as velocity increased. Coupled with an increase in coordinative variability, this may reflect the emergence of a new coordinative structure for EVTIR coupling in response to an increase in the functional demand on the talocrucal and subtalar joints.

8.2 Future work

At a small scale, a particular research laboratory may conceivably leverage more of their collected data by combining it and taking a population modeling approach similar to the one demonstrated in this thesis. Mixed-effects models may be progressively developed as more data are added. Whilst this approach is not without limitation in regard to the homogeneity in study design and protocol, the practice of updating mixed-effects model as more data are collected is typical in settings where data are collected in batches and over a period of years, such as in population pharmacokinetic and pharmacodynamic modeling. Biomechanics at the individual research-laboratory level, and even across research sites, is well placed to take advantage of this modeling technique because, in general, data collection and data analysis methods are standardized.

Random effects in the models presented here reflect unexplained between-subject variability in response. One covariate (FSA) was considered in this thesis when describing muscle activity and coordination. However, future work should include a more comprehensive set of covariates to explain the currently unexplained variability. With more comprehensive covariate models, a better appreciation of how individual characteristics explain the unexplained between-subject variability in experimentally controlled effects is possible. As a purely hypothetical example, the Froude number for each individual may be a covariate effect which explains the between-subject variability in the effect of velocity on FSA. This would manifest as follows: once this

covariate effect was added, there would be no remaining bias in the residuals within a subject as a function of velocity and thus there would be no unexplained variability remaining as a function of velocity. The random effect of velocity may conceivably be removed from the model assuming the model was statistically more significant. An assessment of model predictive power could then validate such models [16].

The approach outlined above requires that biomechanists develop a deep understanding in the statistical techniques required for population modeling and the diagnostic tools required for robust model building. Combining subject-level data for habitually BF and habitually SD subjects across more than one study would faciliate more meaningful insights into the two populations if mixed-effects models are employed. Because data are leveraged, there is also less of a need for rich sampling in every individual.

More immediately, a study with the same interventions for matched habitually BF runners would be valuable. Recreational athletes in the developed world do not typically train at volumes or with intensities comparable to the present study group. Additionally, they typically complete less than 25% of their running volume BF or in minimalist shoes [94]. Thus, it is conceivable to suggest that they do not reflect a complementary group of 'highly trained habitually BF runners'. Studies of the Kalenjin tribe in Kenya comprise research into habitually BF runners who are also typically competitive distance runners [124, 125]. Thus, this population of 'highly trained habitually BF runners' is of interest for comparison.

For habitually SD competitive athletes spiked shoes and 'racing flats', for the purpose of high intensity training or competition, would typically replace their standard training shoes. Studying biomechanics in spiked-shoe running would be interesting, because the modality still represents a relevant condition. In addition, competitive athletes from the Kalenjin tribe typically race on the track in spiked shoes, whether they were habitually BF or SD originally.

Studying variability in recreational and untrained populations in developed nations is a nat-

ural extension to the work here and to [124]. For the same stride length, a study of BF and SD running found no differences in kinematic or kinetic parameters [199]. In this thesis stride length was longer for SD running and moreover velocity, and the interaction between condition and velocity, were significant. In addition to accounting for stride-specific FSA, future work on BF and SD running should also account for stride length, in light of recent research highlighting the dependence of FSA on stride length and stride width [19, 199]. The addition of stride length would be valuable if incorporated into the analysis in Chapter 6, but without stride length being experimentally controlled this is inadvisable, owing to strong correlations between velocity and stride length. The valid inclusion of condition as a random effect in hypothesis tests may reflect only that subjects used different shoes to each other. However, studies have long since shown that subject-shoe interactions are complicated [12]. Future studies where a single shoe is used for SD running would benefit from the application mixed-models because more accurate and less biased analysis of subject-shoe interactions is possible. This would be useful also for studies of orthotic intervention.

Velocity was modeled as an ordinal variable. A useful extension for future research would be to use a wider range of velocities such that velocity could be modeled as a continuous variable and cover the set of relevant velocities for all runners. The velocities of 8:15 min mile^{-1} and 5:15 min mile^{-1} are recommended for study, because they are relevant aerobic training velocities which may be sustained for over 30 minutes for the population of interest in this thesis, but also cover the relevant velocity range for recreational runners.

In light of the observations for EVTIR crp(t), further work is encouraged for SD running using skin mounted foot markers. Can the results for BF running be reproduced and does similar behaviour exist for SD running? What are the behaviours over a wider range of velocities? Foot and ankle phase plane dynamics presents an interesting area of future study using DST techniques. Applying the methods from Chapter 7 to revisit previous studies of inter-segment

coordination would constitute an improvement on those studies and clarify if coordinative variability is associated with running-related injury.

The distinction between FSS is made based on physical characteristics. It would be interesting to see how a clustering algorithm partitions groups using FSA as an input, compared with classification via strike index.

Subjects in the present study are motivated by performance and running-related injuries limit performance. Further study of variability and the role is plays in injury-risk assessment would be valuable. A study comparing variability as a function of velocity and in racing shoes may validate (or not) the idea that there is a link between FSA variability and injury risk and elaborate on any potential mechanisms. If so, there may be cases where a meaningful physiological response and a minimal injury risk is identified at a subject-level.

References

[1] A. Agresti. *An introduction to categorical data analysis*. Wiley, Hoboken, New Jersey, second edition, 2007.

[2] A. N. Ahn, C. Brayton, T. Bhatia, and P. Martin. Muscle activity and kinematics of forefoot and rearfoot strike runners. *Journal of Sport and Health Science*, 3:102–112, 2014.

[3] H. Akaike. Information theory and an extension of the maximum likelihood principle. In B. N. Petrov and F. Csaki, editors, *Second International Symposium on Information Theory*, pages 267–281, Budapest, 1973.

[4] T. Almonroeder, J. D. Willson, and T. W. Kernozek. The effect of foot-strike pattern on Achilles tendon load during running. *Ann. Biomed. Eng.*, 41(8):1758–1766, 8 2013.

[5] A. R. Altman and I. S. Davis. Barefoot running: biomechanics and implicatons for running injuries. *Curr. Sports Med. Rep.*, 11(5):244–250, 2012.

[6] A. R. Altman and I. S. Davis. A kinematic method for footstrike pattern detection in barefoot and shod runners. *Gait Posture*, 35(2):298–300, 2 2012.

[7] J. Arbanas, G. S. Klasan, M. Nikolic, R. Jerkovic, I. Miljanovic, and D. Malnar. Fibre type composition of the human psoas major muscle with regard to the level of its origin. *J. Anat.*, 215(6):636–641, 12 2009.

[8] G. A. Arutyunyan, V. S. Gurfinkel, and M. L. Mirskii. Investigating aiming at a target. *Biofizica*, 13(3):536–538, 1968.

[9] R. Baker, L. Finney, and J. Orr. A new approach to determine the rotation profile from clinical gait analysis data. *Hum. Mov. Sci.*, 18(5):655–667, 1999.

[10] W. R. Barfield, D. T. Kirkendall, and B. Yu. Kinematic instep kicking differences between elite female and male soccer players. 1(72-9), 2002.

[11] R. Bartlett, J. Wheat, and M. Robins. Is movement variability important for sports biomechanists? *Sports Biomech.*, 6(2):224–243, 2007.

[12] B. T. Bates, L. R. Osternig, J. A. Sawhill, and S. L. James. An assessment of subject variability, subject-shoe interaction, and the evaluation of running shoes using ground reaction force data. *J. Biomech.*, 16(3):181–191, 1983.

[13] A. Baudet, C. Morriset, P. d'Athis, J. Maillefert, J. Casillas, P. Ornetti, and D. Laroche. Cross-talk correction method for knee kinematics in gait analysis using principle component analysis (PCA): A new proposal. *PLoS One*, 9(7):e102098, 7 2014.

[14] A. Belli, J. R. Lacour, R. Komi, and C. D. Candau. Mechanical step variability during treadmill running. *Eur. J. Appl. Physiol.*, 70:510–517, 1995.

[15] P. Berens. CircStat: A MATLAB toolbox for circular statistics. *Journal of Statistical Software*, 31(10), 2009.

[16] M. Bergstrand, A. C. Hooker, J. E. Wallin, and M. O. Karlsson. Prediction-corrected visual predictive checks for diagnosing nonlinear mixed-effects models. 13(2):143–151, 2011.

[17] L. Blankevoort, R. Huiskes, and A. de Lange. The envelope of passive knee joint motion. *J. Biomech.*, 21(9):705–709 711–720, 1988.

[18] J. Bonacci, P. U. Saunders, A. Hicks, T. Rantalainen, G. T. Vicenzino, and W. Spratford. Running in a minimalist and lightweight shoe is not the same as running barefoot: a biomechanical study. *Br. J. Sports Med.*, 47(6):387–392, 4 2013.

[19] E. R. Boyer and T. R. Derrick. Select injury-related variables are affected by stride length and foot strike style during running. *Am. J. Sports Med.*, 43(9):2310–2317, 9 2015.

[20] E. R. Boyer, B. D. Rooney, and T. R. Derrick. Rearfoot and midfoot or forefoot impacts in habitually shod runners. *Med. Sci. Sports Exerc.*, 46(7):1384–1391, 11 2014.

[21] D. M. Bramble and D. E. Lieberman. Endurance running and the evolution of the *Homo*. *Nature*, 432:345–352, 11 2004.

[22] B. Briene, P. Malcolm, E. C. Frederick, and D. De Clercq. Relationship between running speed and initial foot contact patterns. *Med. Sci. Sports Exerc.*, 46(8):1595–1603, 2014.

[23] F. Buchtal and H. Schmalbruch. Motor unit of mammalian muscle. *Physiol. Rev.*, 60(1):90–142, 1 1980.

[24] R. Burgess-Limerick, B. Abernethy, and R. J. Neal. Relative phase quantifies interjoint coordination. *J. Biomech.*, 26(1):91–94, 1993.

[25] T. D. Bushnell. A biomechanical analysis of sprinters vs distance runners at equal and maximal speeds. Master's thesis, 2004.

[26] G. E. Calancie, B. Needham-Shropshire, P. Jacobs, K. Willer, G. Zych, and B. A. Green. Involuntary stepping after chronic spinal injury. evidence for a central pattern generator for locomotion in man. *Brain*, 117(5):1143–1159, 1994.

[27] G. Cappellini, Y. P. Ivanenko, R. E. Poppele, and F. Lacquanti. Motor patterns in human walking and running. *J. Neurophysiol.*, 95:3426–3437, 2006.

[28] A. Cappozzo, F. Catani, U. Della Croce, and A. Leardini. Position and orientation in space of bones during movement: anatomical frame definition and determination. *Clin. Biomech.*, 10(4):171–178, 1995.

[29] A. Cappozzo, U. Della Croce, A. Leardini, and L. Chiari. Human movement analysis using stereophotogrammetry: Part 1: Theoretical background. *Gait Posture*, 21(2):186–196, 2005.

[30] M.C. Carson, M.E. Harrington, N. Thompson, J.J. O'Connor, and T.N. Theologis. Kinematic analysis of a multi-segment foot model for research and clinical applications: a repeatability analysis. *J. Biomech.*, 34:1299–1307, 2001.

[31] P. R. Cavanagh and M. A. Lafortune. Ground reaction forces in distance running. *J. Biomech.*, 13:397–406, 1980.

[32] D. Cazzola, G. Pavei, and E. Preatoni. Can coordination variability identify performance factors and skill level in competitive sport? the case of race walking. *Journal of Sport and Health Science*, 5:35–43, 2016.

[33] M. Christophy, N. A. Faruk Senan, J. Lotz, and O. O'Reilly. A musculoskeletal model for the lumbar spine. *Biomech. Model. Mechanobiol.*, 11:19–34, 2012.

[34] J. E. Clark and S. J. Phillips. A longitudinal study of intralimb coordination in the first year of independent walking: a dynamical systems analysis. *Child Dev.*, 64:1143–1157, 1993.

[35] J. Close, V. Inman, P. Poor, and F. Tood. The function of the subtalar joint. *Clin. Orthop.*, 1:159–179, 1967.

[36] R. Cook. Influential observations in linear regression. *J. Am. Stat. Assoc.*, 74:169–174, 1979.

[37] G. Courtine, S. J. Harkema, C. J. Dy, Y. P. Gerasimenko, and P. Dyhre-Poulsen. Modulation of multisegmental monosynaptic responses in a variety of leg muscles during walking and running in humans. *J. Physiol. (Lond.)*, 582(Pt 3):1125–1139, 8 2007.

[38] T. J. Cunningham, D. R. Mullineaux, B. Noehren, R. Shapiro, and T. L. Uhl. Coupling angle variability in healthy and patellofemoral pain runners. *Clin. Biomech.*, 29:317–322, 2014.

[39] A. I. Daoud, G. J. Geissler, F. Wang, J. Saretsky, Y. A. Daoud, and D. E. Lieberman. Foot strike and injury rates in endurance runners: a retrospective study. *Med. Sci. Sports Exerc.*, 44(7):1325–1334, 2012.

[40] K. Davids, S. Bennett, and K. Newell. *Movement system variability*. Human Kinetics, Champaign, Illinois, 2006.

[41] R. Davis, S. Ounpuu, D. Tyburski, and J. Gage. A gait analysis data collection and reduction technique. *Hum. Mov. Sci.*, 10:575–587, 1991.

[42] D. De Clercq, P. Aerts, and M. Kunnen. The mechanical characteristics of the human heel pad during foot strike in running: an *in vivo* cineradiographic study. *J. Biomech.*, 27(10):1213–1222, 1994.

[43] B. De Wit, D. De Clercq, and P. Aerts. Biomechanical analysis of the stance phase during barefoot and shod running. *J. Biomech.*, 33:269–278, 2000.

[44] U. Della Croce, A. Cappozzo, and D. Kerrigan. Pelvis and lower limb anatomical landmark calibration precision and its propagation to bone geometry and joint angles. *Med. Biol. Eng. Comput.*, 37(2):155–161, 1999.

[45] U. Della Croce, A. Leardini, L. Chiari, and A. Cappozza. Human movement analysis using stereophotogrammetry: Part 4: Assessment of anatomical landmark misplacement and its effect on joint kinematics. *Gait Posture*, 21(2):226–237, 2005.

[46] J. A. Dickinson, S. D. Cook, and T. M. Leinhardt. The measurement of shock waves following heel strike while running. *J. Biomech.*, 18(6):415–22, 1985.

[47] F. Y. Diedrich and W. H. Warren. Why change gaits? dynamics of the walk-run transition. *J. Exp. Psychol. Hum. Percept. Perform.*, 21:183–202, 1995.

[48] T A. Dierks, K. T. Manal, J. Hamill, and I. S. Davis. Proximal and distal influences on hip and knee kinematics in runners with patellofemoral pain during a prolonged run. *J. Orthop. Sports Phys. Ther.*, 38(8):448–456, 2008.

[49] M. R. Dimitijevic, Y. Gerasimenko, and M. M. Pinter. Evidence for a spinal central pattern generator in humans. *Ann. N.Y. Acad. Sci.*, 800:360–376, 1998.

[50] C. Divert, G. Mornieux, H. Baur, F. Mayer, and A. Belli. Mechanical comparison of barefoot and shod running. *Int. J. Sports Med.*, 26(59):3–8, 2005.

[51] A. J. Dobson. *An introduction to generalized linear models*. Chapman and Hall/CRC, Boca Raton, FL, second edition, 2002.

[52] D. Domkin, J. Laczko, S. Jaric, H. Johansson, and M. L. Latash. Structure of joint variability in bimanual pointing tasks. *Exp. Brain Res.*, 143:11–23, 2002.

[53] R. Dubbledam, C. Nester, A. V. Nene, H. J. Hermens, and J. H. Buurke. Kinematic coupling relationships exist between non-adjacent segments of the foot and ankle of healthy subjects. *Gait Posture*, 37:159–164, 2013.

[54] O. Dunn. Confidence intervals for the means of dependent, normally distributed variables. *J. Am. Stat. Assoc.*, 54:613–621, 1959.

[55] J. Duysens and H. W. A. A. Van de Crommert. Neural control of locomotion: Part 1: The central pattern generator from cats to humans. *Gait Posture*, 7:131–141, 1998.

[56] W. B. Edwards. Internal structure loading of the lower extremity during running: Implications for skeletal injury, 2009.

[57] W. B. Edwards, D. Taylor, T. J. Rudolphi, J. C. Gillette, and T. R. Derrick. Effects of stride length and running mileage on a probabilistic stress fracture model. *Med. Sci. Sports Exerc.*, 41(12):2177–2184, 2009.

[58] W.B. Edwards, J. C. Gilette, J. M. Thomas, and T.R. Derrick. Internal femoral force and moments during running: implications for stress fracture development. 23(10):1269–78, 2008.

[59] M. Eslami, M. Begon, N. Farahpour, and P. Allard. Forefoot-rearfoot coupling patterns and tibial internal rotation during stance phase of barefoot versus shod running. *Clin. Biomech.*, 22:74–80, 2007.

[60] R. Ferber, I. McClay Davis, and D. S. Williams III. Gender differences in lower extremity mechanics during running. *Clin. Biomech.*, 18:350–357, 2003.

[61] R. Ferber, I. McClay Davis, and D. S. Williams III. Effects of foot orthotic on rearfoot and tibia joint coupling patterns and variability. *J. Biomech.*, 38:477–483, 2005.

[62] D. P. Ferris, M. Louie, and C. T. Farley. Running in the real world: adjusting leg stiffness for different surface. *Proceedings of the Royal Society of London, Series B*, 265(1400):989–994, 6 1998.

[63] S. Fioretti, A. Cappozzo, and L. Luchetti. *Three-dimensional analysis of human locomotion*. Wiley, New York, 1997. p. 173-189.

[64] N. I. Fisher. *Statistical analysis of circular data*. Cambridge University Press, 1995.

[65] W. Fredericks, S. Swank, M. Teisberg, B. Hampton, L Ridpath, and J. B. Hanna. Lower extremity biomechanical relationships with different speeds in traditional, minimalist, and barefoot footwear. *Journal of Sports Science and Medicine*, 14:276–283, 2015.

[66] K. S. Fu, R. C. Gonzalez, and C. S. G. Lee. *Robotics: control, sensing, vision and intelligence.* McGraw-Hill, New York, 1988.

[67] A. Fuchs, V. Jirsa, H. Haken, and J. S. Kelso. Extending the HKB model of coordinated movements to oscillators with different eigenfrequencies. *Biol. Cybern.*, 74:21–30, 1996.

[68] D. Gabor. Theory of communication. *J. Inst. Electr. Eng.*, 93:429–457, 1946.

[69] M. Giandolini, P. J. Arnal, G. Y. Millet, N. Peyrot, P. Samozino, B. Dubois, and J.-B. Morin. Impact reduction during running: efficiency of simple acute interventions in recreational runners. *Eur. J. Appl. Physiol.*, 113(3):599–609, 3 2013.

[70] M. Giandolini, S. Pavailler, P. Samozino, J.-B. Morin, and N. Horvais. Foot strike pattern and impact continuous measurements during a trail running race: proof of concept in a world-class athlete. *Footwear Sci.*, 7(2):127–137, Mar 2015.

[71] G. B. Gillis and A. A. Biewener. Hindlimb muscle function in relation to speed and gait: in vivo patterns of strain and activation in a hip and knee extensor of the rat (*Rattus norvegicus*). *J. Exp. Biol.*, 204:2717–2731, 2001.

[72] L. Glass and M. C. Mackey. *From clocks to chaos*. Princeton University Press, Princeton, NJ, 1988.

[73] P. S. Glazier, K. Davids, and R. Bartlett. Dynamics systems theory: a relevant framework for performance-orientated sports biomechanics research. *Sportscience*, 7, 1 2003.

[74] E. S. Grood and W. J. Suntay. A joint coordinate system for the clinical description of three-dimensional motions: applications to the knee. *J. Biomech. Eng.*, 105:136–144, 1983.

[75] A. H. Gruber, B. R. Umberger, B. Braun, and J Hamill. Economy and rate of carbohydrate oxidation during running with rearfoot and forefoot strike patterns. *J. Appl. Physiol.*, 115:194–201, 2013.

[76] H. Haken, J. A. S. Kelso, and H. Bunz. A theoretical model of phase transitions in human hand movements. *Biol. Cybern.*, 51:347–356, 1985.

[77] J. Hamill, R. E. Emmerik, B. C. Heiderscheit, and L Li. A dynamical systems approach to lower extremity running injuries. *Clin. Biomech.*, 14:297–308, 1999.

[78] J. Hamill, C. Palmer, and R. E. A. van Emmerik. Coordinative variability and overuse injury. *Sports Medicine, Anthroscopy, Rehabilitation, Therapy and Technology*, 4:45, 2012.

[79] J. Hamill, E. M. Russell, A. H. Gruber, and R. Miller. Impact characteristics in shod and barefoot running. *Footwear Sci.*, 3:33–40, 2011.

[80] S. R. Hamner and S. L. Delp. Muscle contributions to fore-aft and vertical body mass center accelerations over a range of running speeds. *J. Biomech.*, 46:780–787, 2013.

[81] S. R. Hamner, A. Seth, and S. L. Delp. Muscle contributions to propulsion and support during running. *J. Biomech.*, 43(14):2709–2716, 10 2010.

[82] C. Hanon, C. Thépaut-Mathieu, C. Hausswirth, and J. M. Le Chevalier. Electromyogram as an indicator of neuromuscular fatigue during incremental exercise. *Eur. J. Appl. Physiol.*, 78(4):315–323, Sep 1998.

[83] C. Hanon, C. Thépaut-Mathieu, and H. Vandewalle. Determination of muscular fatigue in elite runners. *Eur. J. Appl. Physiol.*, 94:118–125, 2005.

[84] H. Hasegawa, T. Yamauchi, and W. J. Kraemer. Foot strike patterns of runners at the 15-km point during an elite-level half marathon. *The Journal of Strength and Conditioning Research*, 21(3):888–893, 2007.

[85] R. Hashish, S. D. Samarawickrame, C. M. Power, and G. J. Salem. Lower limb dynamics vary in shod runners who acutely transition to barefoot running. *J. Biomech.*, 49(2):284–288, 2016.

[86] T. Hastie, R. Tibshirani, and J. Friedman. *The elements of statistical learning: data mining, inference, and prediction*. Springer, New York, second edition, 2009.

[87] K. G. Hatala, H. L. Dingwall, R. E. Wunderlich, and B. G. Richmond. Variations in foot strike patterns during running among habitually barefoot populations. *PLoS One*, 8(1):e52548, 2013.

[88] J. M. Hausdorff. Gait dynamics, fractals and falls: finding meaning in the stride-to-stride fluctuations of human walking. *Hum. Mov. Sci.*, 26:555–589, 2007.

[89] B. C. Heiderscheit, E. S. Chumanov, M. P. Michalski, C. M. Wille, and M. B. Ryan. Effects of step rate manipulation on joint mechanics during running. *Med. Sci. Sports Exerc.*, 43(2):296–302, 2011.

[90] B. C. Heiderscheit, J. Hamill, and R. E. A. van Emmerik. Variability of stride characteristics and joint coordination amond individuals with unilateral patellofemoral pain. *Journal of Applied Biomechanics*, 18(2):110–121, 2002.

[91] J. Hicks. The mechanics of the foot: (1) the joints. *J. Anat.*, 87(3):345–357, 1953.

[92] H. Hobura, M. Sato, T. Sakaguchi, and K. Nakazawa. Step frequency and lower extremity loading during running. *Int. J. Sports Med.*, 33:310–313, 2012.

[93] M. Horton and T. Hall. Quadriceps femoris muscle angle: normal values and relationships with gender and selected skeletal measures. *Phys. Ther.*, 69:897–901, 1989.

[94] D. Hryvniak, J. Dicharry, and R Wilder. Barefoot running survey: Evidence from the field. *Journal of Sport and Health Science*, 3:131–136, 2014.

[95] http://www.seniam.org. Recommendations for sensor locations on individual muscles, Accessed 30^{th} August 2012.

[96] F. Hug, N. A. Turpin, A. Guével, and S. Dorel. Is interindividual variability of emg patterns in trained cyclists related to different muscle synergies? *J. Appl. Physiol.*, 108(6):1727–1736, 2010.

[97] V. Inman. *The joints of the ankle*. The Williams and Wilkins Company, Baltimore, 1976.

[98] M. L. Ireland, J. D. Willson, B. T. Ballantyne, and I. McClay Davis. Hip strength in females with and without patellofemoral pain. *J. Orthop. Sports Phys. Ther.*, 33(11):671–676, 2003.

[99] R. Isman and V. Inman. Anthropometric studies of the human foot and ankle. *Bull. Prosthet. Res.*, 10-11:97–129, 1969.

[100] M. Kadaba, H. Ramakrishnan, and M. Wooten. Measurement of lower extremity kinematics during level walking. *J. Orthop. Res.*, 8(3):383–392, 1990.

[101] M. P. Kadaba, J. Wootten, M. E. Gainey, G. Gorton, and G. V. Cochran. Repeatability of phasic muscle activity: performance of surface and intramuscular wire electrodes in gait analysis. *J. Orthop. Res.*, 3:350–359, 1985.

[102] K. Kamm, E. Thelen, and J. L. Jensen. A dynamical systems approach to motor development. *Phys. Ther.*, 70:763–775, 1990.

[103] T. R. Kane, P. W. Likins, and D. A. Levinson. *Spacecraft dynamics*. McGraw-Hill, New York, 1983.

[104] J. A. S. Kelso. *Dynamic patterns: the self-organization of brain and behaviour*. MIT Press, Cambridge, MA, 1995.

[105] J. A. S. Kelso, K. G. Holt, P. Rubin, and P. N. Kugler. Patterns of human intralimb coordination emerge form the properties of nonlinear limit cycle oscillatory processes. *Journal of Motor Behaviour*, 13:226–261, 1981.

[106] W. Kim, A. S. Voloshin, and S. H. Johnson. Modeling of heel strike transients during running. *Hum. Mov. Sci.*, 13:221–244, 1994.

[107] G. G. Koch. *Intraclass correlation coefficient*, volume 4, pages 213–217. John Wiley & Sons, New York, first edition, 1982.

[108] P. E. Komi, A. Gollhofer, D. Schmidtbleicher, and D. Frick. Interaction between man and shoe in running: considerations for a more comprehensive measurement approach. *Int. J. Sports Med.*, 8(3):196–202, 1987.

[109] P. Konrad. *The ABC of EMG: A practical introduction to kinesiological electromyography*. Noraxon U. S. A. Inc., Scottsdale, Arizona, 1.4 edition, 3 2006.

[110] C. Krueger and L. Tian. A comparison of the general linear mixed model and repeated measures ANOVA using a data with multiple missing data points. *Biol. Res. Nurs.*, 6(2):151–157, 2004.

[111] J.P. Kulmala, M. T. Korhonen, L. Ruggiero, S. Kuitunen, H. Suominen, Heinonen A., A. Mikkola, and J Avela. Walking and running require greater effort from the ankle and the knee extensor muscles. *Med. Sci. Sports Exerc.*, 48(11):2181–2189, 2016.

[112] M. Kurz and N. Stergiou. The spanning set indicates that variability during the stance period of running is affected by footwear. *Gait Posture*, 17(2):132–135, 2003.

[113] P. F. Lamb and M. Stöckl. On the use of continuous relative phase: Review of current approach and outline for a new standard. *Clin. Biomech.*, 29(5):484–493, 2014.

[114] P. Larson. Comparison of foot strike patterns of barefoot and minimally shod runners in a recreational road race. *Journal of Sport and Health Science*, 3:137–142, 2014.

[115] P. Larson, E. Higgins, J. Kaminski, T. Decker, J. Preble, D. Lyons, K. McIntyre, and A. Normile. Foot strike patterns of recreational and sub-elite runners in a long-distance road race. *J. Sports Sci.*, 29(15):1665–1673, 12 2011.

[116] M. L. Latash, J. P. Scholz, and G. Schoner. Motor control strategies revealed in the structure of motor variability. *Exerc. Sport Sci. Rev.*, 30:25–31, 2002.

[117] V. Lavanksa, N. F. Taylor, and A. G. Schache. Familiarization to treadmill running in young unimpaired adults. *Hum. Mov. Sci.*, 24:544–557, 2005.

[118] D. Le Ray, L. Juvin, D. Ryczko, and R. Dubuc. Chapter 4–supraspinal control of locomotion: the mesencephalic locomotor region. *Prog. Brain Res.*, 188:51–70, 2011.

[119] Y. Lee, J. A. Nelder, and Y. Pawitan. *Generalized linear models with random effects: Unified analysis via H-likelihood*. Chapman and Hall/CRC, Boca Raton, FL, 2006.

[120] J. Leitch. *The biomechanics of patellofemoral pain syndrome in distance runners*. DPhil Thesis, University of Oxford, 2011.

[121] L. Li, E. C. H. van den Bogert, G. E. Caldwell, R. E. A. van Emmerik, and J. Hamill. Coordination patterns of walking and running at similar speed and stride frequency. *Hum. Mov. Sci.*, 18:67–85, 1999.

[122] D. E. Lieberman. What we can learn about running from barefoot running: and evolution medical perspective. *Exerc. Sport Sci. Rev.*, 40(2):63–72, Apr 2012.

[123] D. E. Lieberman. Strike type variation among Tarahumara indians in minimal sandals versus conventional running shoes. *Journal of Sport and Health Sciences*, 3:86–94, 2014.

[124] D. E. Lieberman, E. R. Castillo, E. Otarola-Castilla, M. K. Sang, T. K. Sigei, R. Ojiambo, P. Okutoyi, and Pitsiladis Y. Variation in foot strike patterns among habitually barefoot and shod runners in Kenya. *PLoS One*, page e0131354, 2015.

[125] D. E. Lieberman, M. Venkadesan, W. A. Werbel, A. I. Daoud, S. D'Andrea, R. O. Davis, I.S. Mang'Eni, and Y. Pitsiladis. Foot strike patterns and collision forces in habitually barefoot versus shod runners. *Nature*, 463:531–535, 2010.

[126] L. A. Lipsitz. Dynamics of stability: the physiological basis of function health and frailty. *The Journals of Gerontology: Series A, Biological science and medical sciences*, 57:B115–B125, 2002.

[127] V. Lun, W. H. Meeuwisse, P. Stergiou, and D. Stefanyshyn. Relation between running injury and static lower limb alignment in recreational runners. *Br. J. Sports Med.*, 38(5):576–580, 2004.

[128] A. Lundberg, O. Svensson, C. Bylund, and G. Selvik. Kinematics of the ankle/foot complex - part 3: Influence of leg rotation. *Foot Ankle*, 9(6):304–309, 1989.

[129] C. A. Macera, P. R. Pate, K. E. Powell, K. L. Jackson, J. S. Kendrick, and T. E. Craven. Predicting lower-extremity injuries among habitual runners. *Arch. Intern. Med.*, 149(11):2565–2568, 11 1989.

[130] C. Maiwald, T. Sterzing, T. Mayer, and T.L. Milani. Detecting gait events in running from kinematic data. In *Proc 22nd Congr Int Soc Biomech*, Cape Town, South Africa, 2009.

[131] R. Mann, L. Malisoux, C. Nührenbörger, A. Urhausen, K. Meijer, and D. Theisen. Association of previous injury and speed with running style and stride-to-stride fluctuations. *Scand. J. Med. Sci. Sports*, 25(6):e638–e645, 2015.

[132] R. A. Mann and J. Hagy. Biomechanics of walking, running, and sprinting. *Am. J. Sports Med.*, 8(5):345–350, 1980.

[133] R. A. Mann, G. T. Moran, and S. E. Dougherty. Comparative electromyography of the lower extremity in jogging, running, and sprinting. *Am. J. Sports Med.*, 14(6):501–510, 1986.

[134] J. T. Manter. Movements of the subtalar and transverse tarsal joints. *The Anatomical Record*, 80(4):397–410, 1941.

[135] F. Marin, H. Mannel, L. Claes, and L. Dürselen. Correction of axis misalignment in the analysis of knee rotations. *Hum. Mov. Sci.*, 22(3):285–296, 8 2003.

[136] J. N. Maykut, J. A. Taylor-Haas, M. V. Paterno, C. A. DiCesare, and K. R. Ford. Concurrent validity and reliability of 2d kinematic analysis of frontal plane motion during running. *International Journal of Sports Physical Therapy*, 10(2):136–146, 2015.

[137] P. McCullagh and J. A. Nelder. *Generalized linear models*. Chapman and Hall/CRC, second edition, 8 1989.

[138] S. Mehdisadeh, A. R. Arshi, and K. Davids. Quantifying coordination and coordination variability in backward versus forward running: implications for control of motion. *Gait Posture*, 42:172–177, 2015.

[139] E. E. Miller, K. K. Whitcome, D. E. Lieberman, H. L. Norton, and R. E. Dyer. The effect of minimal shoes on arch structure and intrinsic foot muscle strength. *Journal of Sport and Health Sciences*, 3:74–85, 2014.

[140] R. Miller, J. L. Lowry, S. A. Meardon, and J. C. Gillette. Lower extremity mechanics of iliotibial band syndrome during an exhaustive run. *Gait Posture*, 26:407–413, 2007.

[141] R. H. Miller, R. Chang, J. L. Baird, R. E. A. van Emmerik, and J. Hamill. Variability in kinematic coupling assessed by vector coding and continuous relative phase. *J. Biomech.*, 43(17):2554–2560, 2010.

[142] R. H. Miller, S. A. Meardon, T. R. Derrick, and J. C. Gillette. Continuous relative phase variability during an exhaustive run in runners with a history of iliotibial band syndrome. *Journal of Applied Biomechanics*, 24:262–270, 2008.

[143] S. Mori, T. Sakamoto, Y. Ohta, K. Takakusaki, and K. Matsuyama. Site-specific postural and locomotor changes evoked in awake, freely moving intact cats by stimulating the brain stem. *Brain Res.*, 505:66–74, 1989.

[144] Mosby. *Mosby's dictionary of medicine, nursing and health professions*. Mosby/Elsevier, St. Louis, MO, 8th edition, 12 2008.

[145] K. E. Muller and C. N. Barton. Approximate power for repeated-measures ANOVA lacking sphericity. *J. Am. Stat. Assoc.*, 84(406):549–555, 1989.

[146] R. Mundry and C. Nunn. Stepwise model fitting and statistical inference: turning noise into signal pollution. *Am. Nat.*, 173(1):119–123, 2009.

[147] M. P. Murray, L. A. Mollinger, G. M. Gardner, and S. B. Sepic. Kinematic and emg patterns during slow, free and fast walking. *J. Orthop. Res.*, 2:272–280, 1984.

[148] Y. Nakayama, K. Kudo, and T. Ohtsuki. Variability and fluctuations in running gait cycle of trained runners and non-runners. *Gait Posture*, 31(3):331–335, 3 2010.

[149] F. H. Netter. *Atlas of human anatomy*. Saunders, Philadelphia, USA, sixth edition, 2014.

[150] B. M. Nigg, R. W. de Boer, and V. Fisher. A kinematic comparison of overground and treadmill running. *Med. Sci. Sports Exerc.*, 27(1):98–105, 1995.

[151] T. F. Novacheck. The biomechanics of running. *Gait Posture*, 7(1):77–95, 1 1998.

[152] M. Nunns, C. House, J. Fallowfield, A. Allsopp, and S Dixon. Biomechanical characteristics of barefoot footstrike modalities. *J. Biomech.*, 46:2603–2610, 2013.

[153] C.M. O'Connor, S.K. Thorpe, M.J. O'Malley, and C.L. Vaughan. Automatic detection of gait events using kinematic data. *Gait Posture*, 25(3):469–474, 2007.

[154] A. Ogueta-Alday, J. A. Rodrìguez-Marroyo, and J. Garcìa-Lòpez. Rearfoot striking runners are more economical than midfoot strikers. *Med. Sci. Sports Exerc.*, 46(3):580–585, 2014.

[155] E. D. Olin and G. M. Gutierrez. EMG and tibial shock upon the first attempt at barefoot running. *Hum. Mov. Sci.*, 32:343–352, 5 2013.

[156] G.N. Orlovsky, Deliagina T. G., and Grillner S. *Neuronal Control of Locomotion: From Mollusc to Man*. Oxford University Press, 1999.

[157] T. Pavlidis. *Biological oscillators: their mathematical analysis*. Academic Press, New York, 1973.

[158] K. G. Pearson. Generating the walking gait: role of sensor feedback. *Prog. Brain Res.*, 143:123–129, 2004.

[159] D. P. Perl, A. I. Daoud, and D. E. Lieberman. Effects of footwear and strike type on running economy. *Med. Sci. Sports Exerc.*, 44(7):1335–1343, 2012.

[160] B. T. Peters, J. M. Haddad, B. C. Heiderscheit, R. E. A. van Emmerik, and J. Hamill. Limitations in the use and interpretation of continuous relative phase. *J. Biomech.*, 36:217–238, 2003.

[161] S. J. Piazza and P. R. Cavanagh. Measurement of the screw-home motion of the knee is sensitive to errors in axis alignment. *J. Biomech.*, 33(8):1029–1034, 2000.

[162] J. Pinheiro, D. Bates, S. DebRoy, D. Sarkar, and R Core Team. *nlme: Linear and Nonlinear Mixed Effects Models*, 2016. R package version 3.1-128.

[163] J. C. Pinheiro and D. M. Bates. *Mixed-effects models in S and S-Plus*. Springer-Verlag, New York, 2000.

[164] M. B. Pohl and J. G. Buckley. Changes in foot and shank coupling due to alterations in foot strike pattern during running. *Clin. Biomech.*, 23:334–341, 2008.

[165] H. Poincaré. Sur le problème des trois corps et les équations de la dynamique. *Acta Mathematica*, 13:1–270, 1890.

[166] H. Pontzer, K. Suchman, Raichlen D. A., B. M. Wood, A. Z. P. Mabulla, and F. W. Marlowe. Foot strike patterns and hind limb joint angles during running in Hadza hunter-gatherers. *Journal of Sport and Health Sciences*, 3:95–101, 2014.

[167] R Core Team. *R: A Language and Environment for Statistical Computing*. R Foundation for Statistical Computing, Vienna, Austria, 2016.

[168] M. E. Raabe and A. M. W. Chaudhari. An investigation of jogging biomechanics using the full-body lumbar spine model: Model development and validation. *J. Biomech.*, 49(7):1238–1243, 5 2016.

[169] H. K. Ramakrishnan and M. P. Kadaba. On the estimation of join kinematics during gait. *J. Biomech.*, 24(10):969–977, 1991.

[170] L. Reber, J. Perry, and M. Pink. Muscular control of the ankle in running. *Am. J. Sports Med.*, 21(6):805–810, 1993.

[171] S. T. Ridge, A. W. Johnson, U. H. Mitchell, I. Hunter, E. Robinson, B. S. E. Rich, and S. D. Brown. Foot bone marrow edema after a 10-wk transition to minimalist running shoes. *Med. Sci. Sports Exerc.*, 45(7):1363–1368, 2013.

[172] P. O. Riley, J. Dicharry, J. Franz, U. Della Croce, R. P. Wilder, and D. C. Kerrigan. A kinematics and kinetics comparison of overground and treadmill running. *Med. Sci. Sports Exerc.*, 40(6):1093–1100, 2008.

[173] B. D. Rooney and T. R. Derrick. Joint contact loading in forefoot and rearfoot strike patterns during running. *J. Biomech.*, 46:2201–2206, 2013.

[174] M. Root, J. Weed, T. Sgarlato, and D. Bluth. Axis of motion of the subtalar joint. *J. Am. Podiatr. Med. Assoc.*, 56(4):149–155, 1966.

[175] M. Rosenblum and J. Kurths. Analysing synchonization phenomena from bivariate data by means of the Hilbert transform. In H. Kantz, J. Kurths, and G. Mayer-Kress, editors, *Nonlinear analysis of physiological data*, pages 91–99. Springer, Berlin, 1998.

[176] C. D. Samaan, M. J. Rainbow, and I. S. Davis. Reduction in ground reaction force variables with instructed barefoot running. *Journal of Health and Sport Science*, 3:143–151, 2014.

[177] L. Samuel. Anatomical planes and spatial relationships in the human body. `www.interactive-biology.com/2681/064-anatomical-planes-and-spatial-relationships-in-the-human-body/`, 8 2011. Accessed: 2016-07-04.

[178] A.G. Schache, R. Baker, and Lamoreux L.W. Defining the knee joint flexion-extension axis for purposes of quantitative gait analysis: An evaluation of methods. *Gait Posture*, 24:100–109, 2006.

[179] J. P. Scholz, Schöner G., and Latash M. L. Identifying the control structure of multi-joint coordination during pistol shooting. *Exp. Brain Res.*, 135:382–404, 2000.

[180] G. Schöner and J. A. S. Kelso. Dynamics patterns generation in behavioral and neural systems. *Science*, 239:1513–1520, 1988.

[181] K. Schweizer, P. C. Cattin, R. Brunner, B. Müller, C. Huber, and J. Romkes. Automatic selection of a representative trial from multiple measurements using principle component analysis. *J. Biomech.*, 45(13):2306–2309, 8 2012.

[182] R. Shiavi, C. Frigo, and A. Pedotti. Electromyographic signals during gait: criteria for envelope filtering and number of strides. *Med. Biol. Eng. Comput.*, 35:171–178, 3 1998.

[183] Y. Shih, K. L. Lin, and T. Y. Shiang. Is the foot striking pattern more important than barefoot or shod conditions in running? *Gait Posture*, 38(3):490–494, 7 2013.

[184] M. L. Shik. *Action of the brainstem locomotor region on spinal stepping generators via propriospinal pathways*, pages 421–434. Raven Press, New York, 1983.

[185] M. L. Shik, F. V. Severin, and G. N. Orlovsky. Control of walking and running by means of electrical stimulation of the midbrain. *Biofizika*, 11(4):659–666, 1 1966. In Russian.

[186] J. L. Smith, S. H. Chung, and R. F. Zernicke. Gait-related motor patterns and hindlimb kinetics for the cat trot and gallop. *Exp. Brain Res.*, 94:308–322, 1993.

[187] R. W. Soutas-Little. The use of 'virtual markers' in human movement analysis. *Gait Posture*, 4(2):176–177, 1996.

[188] R. Squadrone and C. Gallozzi. Biomechanical and physiological comparison of barefoot and two shod conditions in experienced barefoot runners. *J. Sports Med. Phys. Fitness*, 49(1):6–13, 3 2009.

[189] C. L. Stackhouse, I. M. Davis, and J. Hamill. Orthotic intervention in forefoot and rearfoot strike running patterns. *Clin. Biomech.*, 19:64–70, 2004.

[190] A. Stacoff, B. M. Nigg, C. Reinschmidt, A. J. van den Bogart, and A. Lundberg. Tibiocalcaneal kinematics of barefoot versus shod running. *J. Biomech.*, 33(11):1387–1395, 11 2000.

[191] J. Stebbins, N. Harrington, M. Thompson, N. Zavatsky, and T. Theologis. Repeatability of a model for measuring multi-segment foot kinematics in children. *Gait Posture*, 23(4):401–410, 2006.

[192] N. Stergiou and L. M. Decker. Human movement variability, nonlinear dynamics, and pathology: Is there a connection? *Hum. Mov. Sci.*, 30(5):869–888, 2011.

[193] N. Stergiou, R. T. Harbourne, and J. T. Cavanaugh. Optimal movement variability: A new theoretical perspective for neurologic physical therapy. *J. Neurol. Phys. Ther.*, 30:120–129, 2006.

[194] N. Stergiou, J. L. Jensen, B. T. Bates, and G. Tzetzis. A dynamical systems investigation of lower extremity coordination during running over obstacles. *Clin. Biomech.*, (16):213–221, 4 2001.

[195] N. Tam, J. L. Astephen Wilson, T. D. Noakes, and Tucker R. Barefoot running: an evaluation of the current hypothesis, future research and clinical applications. *Br. J. Sports Med.*, 48:349–355, 2013.

[196] E. Thelen. Motor development. a new synthesis. *The American Psychologist*, 50:79–95, 1995.

[197] E. Thelen and B. D. Ulrich. Hidden skills: A dynamic systems analysis of treadmill stepping during the first year. *Monogr. Soc. Res. Child Dev.*, 56:1–98, discussion 99–104, 1991.

[198] J. M. T. Thompson and H. B. Stewart. *Nonlinear dynamics and chaos*. Wiley, New York, 1986.

[199] M. A. Thompson, A. Gutmann, J. Seegmiller, and C. P. McGowan. The effect of stride length on the dynamics of barefoot and shod running. *J. Biomech.*, 47(11):2745–2750, 2014.

[200] M. T. Turvey. Coordination. *Am. Psychol.*, 45(8):938–953, 8 1990.

[201] U. C. Ubgolue, E. Papi, K. T. Kaliarntas, A. Kerr, L. Earl, V. M. Pomeroy, and P. J. Rowe. The evaluation of an inexpensive, 2D, video based gait assessment system for clinical use. *Gait Posture*, 38(3):483–489, 7 2013.

[202] K. A. Valenzuela, S. K. Lynn, L. R. Mikelson, G. J. Noffal, and D. A. Judelson. Effect of acute alterations in foot strike patterns during running on sagittal plane lower limb kinematics and kinetics. *Journal of Sports Science and Medicine*, 14:224–232, 2015.

[203] R. N. van Gent, D. Siem, M. van Middlekoop, A. G. van Os, S. M. A. Bierma-Zeinstra, and B. W. Koes. Incidence and determinants of lower extremity running injuries in long distance runner: a systematic review. *Br. J. Sports Med.*, 41(8):469–480, 8 2007.

[204] W. van Mechelen. Running injuries: A review of the epidemiological literature. *J. Sports Med.*, 14(5):320–335, 11 1992.

[205] V. von Tscharner, B. Goepfert, and B. M. Nigg. Changes in EMG signals for the muscle tibialis anterior while running barefoot and with shoes resolved by non-linearly scaled wavelets. *J. Biomech.*, 36(8):1169–1176, 8 2003.

[206] S. D. Walter, L. E. Hart, J. M. McIntosh, and J. R. Sutton. The Ontario cohort study of running-related injuries. *Arch. Intern. Med.*, 149(11):2561–2564, 11 1989.

[207] K. R. Williams. Biomechanics of running. *Exerc. Sport Sci. Rev.*, 13:389–441, 1985.

[208] D. S. B. Williams III, D. H. Green, and B. Wurzinger. Changes in lower extremity movement and power absorption during forefoot striking and barefoot running. *International Journal of Sports Physical Therapy*, 7(5):525–532, 10 2012.

[209] J. D. Willson, T. W. Kernozek, R. L. Arndt, D. A. Reznichek, and J. S. Straker. Gluteal muscle activation during running in females with and without patellofemoral pain syndrome. *Clin. Biomech.*, 26(7):735–740, 8 2011.

[210] D. G. Wright. Action of the subtalar and ankle-joint complex during the stance phase of walking. *J. Bone Joint Surg. Am.*, 46(2):361–382, 1964.

[211] G. Wu, S. Seigler, P. Allard, C. Kirtley, A. Leardini, D. Rosenbaum, M. Whittle, D. D'Lama, L. Cristofilini, H. Witte, O. Schmid, and I. Stokes. ISB recommendation on definitions of joint coordinate systems of various joints for the reporting of human joint motion-part i: ankle, hip, and spine. *J. Biomech.*, 35(4):543–548, 2002.

[212] G. Wu, F. C. T. van der Helm, H. E. J. Veeger, M. Makhsous, P. Van Roy, C. Anglin, J. Nagels, A. R. Karduna, K. McQuade, X. Wang, F. W. Wener, and B. Buchholz. ISB recommendation on definitions of joint coordinate systems of various joints for the reporting of human joint motion-part ii: shoulder, elbow, wrist and hand. *J. Biomech.*, 38(5):981–992, 2005.

[213] S. L. Zeger, K-Y. Liang, and P. S. Albert. Models for longitudinal data: A generalized estimating equation approach. *Biometrics*, 44(4):1049–1060, December 1988.

Appendix A

Calculating joint kinematics

This section presents a method for calculating joint kinematics, favoured by the International Society of Biomechanics [120, 211, 212] and outlined in detail by Cappozzo *et al*. [29]. Definitions of global and local frames are given followed by an outline of the transformations used to calculate joint segment orientation. The global (photogrammetric) frame is a static frame [29] arbitrarily defined using a calibration object in the capture volume. The set of axes are used to give marker position coordinates. Typically, in the global frame the mean direction of progression is defined to coincide with a motor task and a plumb line, perpendicular to the mean direction of progression, is defined as the direction of gravity. A local frame is embedded in a body segment and referred to as a technical frame (TF). These frames are reconstructed at each time step using the position of (at least) three non-collinear skin mounted markers (TFs) and tracked by the stereophotogrammetry system. Thus, this marker technical frame (MTF) describes the position in space of the body segment under analysis. These technical markers do not necessarily coincide with anatomical landmarks (ALs) as the MTF is arbitrary. Therefore clusters of markers may also be used. An anatomical frame (AF), defined to meet the requirements for within- and between-subject repeatability, is a TF constructed from surface mounted markers typically placed on ALs. The AF is defined using a transformation from the MTF dur-

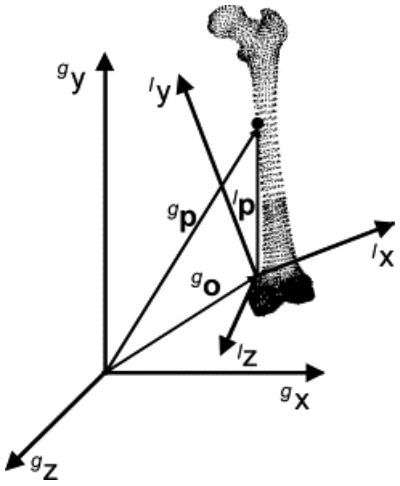


Figure A.0.1: The position vector ($\mathbf{p}$) of a particle in a global frame (${}^{g}x, {}^{g}y, {}^{g}z$) and local frame $\left({}^{l}x, {}^{l}y, {}^{l}z\right)$. The position vector (${}^{g}\mathbf{o}$) defines the origin of the local frame with respect to the origin of global frame. Reprinted from [29].

ing an anatomical calibration (static trial). Because the planes of the AF typically approximate the sagittal, coronal and transverse plane of a segment, markers may be placed on bony prominences or along anatomical planes. Internal ALs are estimated using the positions of surface landmarks, predictive models or even functional tasks. Joint kinematics are the description of the relative orientation of body segments, typically calculated as orientation of the distal segment relative to proximal segment. The position vector $\mathbf{p}$ of a point in the global frame ${}^{g}\mathbf{p}$ may be written in terms of its position vector in the local frame ${}^{l}\mathbf{p}$, a 3-by-3 orientation matrix ${}^{g}\mathbf{R}_{l}$, which describes orientation of the local frame relative to the global frame, and a translation ${}^{g}\mathbf{o}$, which describes the position of the origin of the local frame relative to the origin of the global frame (Figure A.0.1).

Algebraically,

$$ {}^{g}\mathbf{p} = {}^{g}\mathbf{R}_{l}{}^{l}\mathbf{p} + {}^{g}\mathbf{o} \tag{A.0.1} $$

Thus for a given point, take the position vector in the local frame, rotate it onto axes aligned with the global frame and then translate it some distance corresponding to the relative distance between the origin of the local frame and global frame. Given the orientation of the local with

respect to global frames for the proximal ${}^{\mathrm{g}}\mathbf{R}_{\mathrm{p}}$ and distal ${}^{\mathrm{g}}\mathbf{R}_{\mathrm{d}}$ segments and the relative positions of their origins ${}^{\mathrm{g}}\mathbf{o}_{\mathrm{p}}$ and ${}^{\mathrm{g}}\mathbf{o}_{\mathrm{d}}$, it is possible to calculate the joint orientation matrix, $\mathbf{R}_{\mathrm{j}}$, and joint position vector $\mathbf{t}_{\mathrm{j}}$ as

$$\mathbf{R}_{\mathrm{j}} = {}^{\mathrm{g}}\mathbf{R}_{\mathrm{p}}^{\mathrm{T}\,\mathrm{g}}\mathbf{R}_{\mathrm{d}} = {}^{\mathrm{p}}\mathbf{R}_{\mathrm{d}} \tag{A.0.2}$$

and

$$\mathbf{t}_{\mathrm{j}} = {}^{\mathrm{g}}\mathbf{R}_{\mathrm{p}}^{\mathrm{T}}\left({}^{\mathrm{g}}\mathbf{o}_{\mathrm{d}} - {}^{\mathrm{g}}\mathbf{o}_{\mathrm{p}}\right) = \mathbf{o}_{\mathrm{d/p}} \tag{A.0.3}$$

leading to six degrees of freedom (three rotational, three translational) between segments. The joint orientation matrix may be represented as three independent rotations, $\mathbf{R}_{\mathrm{j}\alpha}$, $\mathbf{R}_{\mathrm{j}\beta}$ and $\mathbf{R}_{\mathrm{j}\gamma}$ and the orientation of the distal segment may be mapped onto that of the proximal segment by performing three successive rotations, each about one of the six possible axes. Calling $\{x_{\mathrm{p}}y_{\mathrm{p}}z_{\mathrm{p}}\}$ the proximal and $\{x_{\mathrm{d}}y_{\mathrm{d}}z_{\mathrm{d}}\}$ the distal set of axes, if $\{x_{\mathrm{d}}y_{\mathrm{d}}z_{\mathrm{d}}\}$ is rotated some angle α about the axis x_{p} or x_{d}, the relevant independent orientation matrix is

$$\mathbf{R}_{\mathrm{j}\alpha} = \begin{bmatrix} 1 & 0 & 0 \\ 0 & \cos\alpha & -\sin\alpha \\ 0 & \sin\alpha & \cos\alpha \end{bmatrix}$$

By extension, the matrices corresponding to rotation some angle β about y_{p} or y_{d} and some angle γ about z_{p} or z_{d} are

$$\mathbf{R}_{\mathrm{j}\beta} = \begin{bmatrix} \cos\beta & 0 & \sin\beta \\ 0 & 1 & 0 \\ -\sin\beta & 0 & \cos\beta \end{bmatrix}$$

and

$$\mathbf{R}_{j\gamma} = \begin{bmatrix} \cos\gamma & -\sin\gamma & 0 \\ \sin\gamma & \cos\gamma & 0 \\ 0 & 0 & 1 \end{bmatrix}$$

respectively [63, 66, 103]. A rotation about an axis in the proximal segment requires multiplication from the left, whereas a rotation about an axis in the distal segment requires multiplication from the right [29]. For example for three rotations: first about z_{p}; second about by x_{d}; and third about y_{d}, the orientation matrix would be

$$\mathbf{R}_{\mathrm{j}} = \mathbf{R}_{j\gamma}\mathbf{R}_{j\alpha}\mathbf{R}_{j\beta}$$

which may be explicitly written as

$$\begin{bmatrix} r_{11} & r_{12} & r_{13} \\ r_{21} & r_{22} & r_{23} \\ r_{31} & r_{32} & r_{33} \end{bmatrix} = \begin{bmatrix} \cos\beta\cos\gamma - \sin\alpha\sin\beta\sin\gamma & -\sin\gamma\cos\alpha & \sin\beta\cos\gamma + \sin\alpha\sin\gamma\cos\beta \\ \sin\gamma\cos\beta + \sin\alpha\sin\beta\cos\gamma & \cos\alpha\cos\gamma & \sin\beta\sin\gamma - \sin\alpha\cos\beta\cos\gamma \\ -\sin\beta\cos\alpha & \sin\alpha & \cos\alpha\cos\beta \end{bmatrix}$$

From this, we may obtain α, β and γ as

$$\alpha = \sin^{-1} r_{32}$$

$$\beta = \sin^{-1}\left(\frac{-r_{31}}{\cos\alpha}\right)$$

$$\gamma = \sin^{-1}\left(\frac{-r_{12}}{\cos\alpha}\right)$$

The specific rotations given above are consistent with the convention of Grood and Suntay [74]. A standardized sequence of rotations is necessary because matrix multiplications are not commutative. Through the proper selection of anatomical frames, it is possible for the given rotations to correspond to functional anatomy. If relative to the bony segment and in the AF, the x, y, and z axes are defined as the antero-posterior, longitudinal and medio-lateral directions respectively: z_{p} describes flexion-extension of the distal segment relative to the proximal segment; x_{d} describes abduction-adduction of the distal segment relative to the proximal segment; y_{d} describes internal-external rotation of the distal segment relative to the proximal segment. These three rotations are often described as occurring about three non-orthogonal axes, known as a joint coordinate system: The z_{p} axis, a floating axis and the y_{d} axis. The floating axis is orthogonal to both the the z_{p} and y_{d} axes and thus, the second rotation evidently coincides with the floating axis.

Appendix B

Anatomical frame misalignment affects joint kinematics

As previously noted (Section 3.3.1), by defining an AF within- and between-subject repeatability of joint kinematics is theoretically possible. However, when defining AFs using skin mounted markers, marker misplacement and therefore AF axis misalignment may affect joint kinematics. Bony landmarks may be large irregular areas rather than points and are occasionally difficult to palpate due to excess tissue.

Precision errors between 13 and 25 mm have been reported when six examiners located ALs on two subjects [45], leading to precision errors in the anatomical frame axes of up to 9° [28] for the hip, knee and ankle. Following the convention of Grood and Suntay [74] for calculating joint kinematics, internal-external rotation angles were least precise with reported precision errors of 4° to 10°. Also, the precision of knee abduction-adduction and internal-external rotation angles were dependent on knee flexion angle. Misalignment of a chosen joint coordinate system with the axes about which rotation is assumed to occur means one joint rotation (*e.g.* flexion) may be interpreted as another (*e.g.* rotation). This error, known as kinematic crosstalk, is particularly relevant when describing the knee joint because of challenges estimating the flexion-extension

axis [9, 17, 44, 100, 135, 161, 169].

Kadaba *et al.* [100] performed a sensitivity analysis of lower limb kinematics for level walking among normal adults, in which transverse plane orientation of the flexion-extension axis at the hip, knee and ankle was analytically varied from -15° to +15° in increments of 5°. The authors presented results only for the knee. Whilst knee flexion angle error remained unaffected, as knee flexion angle increased the error in knee abduction-adduction angle increased and error in knee rotation angle remained roughly constant with a magnitude similar to that of the perturbation imposed. For a 10° perturbation, knee flexion angles between 10° and 40° (values comparable to knee flexion during the stance phase of running) induced errors in knee abduction-adduction angle from 2° and 6°. Further studies [169] have found similar tendencies for hip, where following perturbation in the flexion-extension axis, increases in hip flexion angle are coupled with larger errors in the abduction-adduction and internal-external rotation angles.

Knee extension is coupled with tibial rotation in a normal knee owing to asymmetry in the femoral condyles. Specifically, the medial condyle has been reported to be larger than the lateral condyle [161]. This mechanism, known as the 'screw home' mechanism, was investigated by Piazza and Cavanagh [161] and its observation is sensitive to errors is AF misalignment because of kinematic crosstalk. The study considered two different two-segment mechanical linkages; first, a hinge joint and second, a joint incorporating a gearing to induce 15° of screw-home rotation with 90° of knee flexion. Misalignment of the flexion-extension axis in the hinge joint allowed it to exhibit 'screw-home' rotation, whilst misalignment of the geared joint flexion-extension axis allowed it to exhibit pure flexion, implying the measurement of screw-home rotation may be influenced by precision errors when identifying the knee flexion-extension axis. Furthermore, the marker placement precision errors which led to these observations were comparable to the between-observer variability of five experienced observers placing markers on

the medial and lateral femoral epicondyles. The work of Piazza and Cavanagh stresses the need for care when interpreting small rotations and abduction-adduction angles to ensure they are not artefacts of kinematic crosstalk.

Whilst work has shown correction methods using principle component analysis can minimize kinematic crosstalk [13], as these methods have not been integrated into this study, it is still necessary to acknowledge the limits of interpretability of joint kinematics. Additionally, by relying on few (preferably one) trained observer to place markers may be help minimize variability and thus maximize between-subject repeatability in this study.

Appendix C

Subject information

C.1 A summary of injury developments

Follow-up data on injury development is summarized in Table C.1.1.

Subject	six months	twelve months
MC	Hamstring strain	Hamstring strain
MH		ITBS
ML		Stress fracture* (right foot)
MN		PFPS†
MO	Achilles tendon strain (right foot)	
MP		Bone bruise (right foot)
MR		Calf strain

Table C.1.1: Follow-up interviews six and twelve months after data collection pertaining to the development of running-related injuries. Note that motion capture data were analysed for the left foot only. Eleven subjects out of eighteen did not develop a running-related injury in the twelve months following data collection. One subject (MQ) did not have follow-up data. * Triple stress fracture to the 3^{rd} and 4^{th} metatarsals, and navicular. † From running on a twisted ankle.

C.2 Anthropometric data and running history

Data from the anthropometric assessment and running history is summarize in Table C.2.1.

Subject	Age	Mass (kg)	Height (cm)	MPW	SPW	Training shoe	Orthotics	1500 PB	Squats	Notes
MA	26	68.4	188	48	7	Saucony Fast-twitch	N	4:07	P	
MB	27	68.2	184	78	8	Brooks Switch	N	-	P	
MC	31	67.2	180	28	6	Adidas Supernova Glide	Y A 24 M	3:56	F	‘tight quadriceps’
MD	26	63.4	174	50	7	Adidas Nimbus	Y A 121 M	3:59	P	
MF	20	59.1	166	45	5	Nike Lunar Swift	N	4:12	P	‘tight L hamstring’
MG	24	56.0	169	85	13	Nike Pegasus	N	4:02	P	
MH	20	52.7	173	48	6	Brooks Launch	N	4:05	P	
MI	21	79.8	188	40	6	Asics Gel Cumulus	N	4:06	P	
MJ	20	59.0	180	63	10	Adidas Supernova Cushion	N	3:46	P	
MK	20	66.9	186	38	6	Asics Gel Cumulus	N	-	P	
ML	20	62.1	180	60	9	Brooks Racer ST 5	Y R 37 M	-	P	
MM	20	60.1	178	68	8	Mizuno Wave Rider	N	3:47	P	
MN	19	61.2	175	50	6	Asics GT 2160	Y R 4 M	3:47	P	
MO	22	65.0	182	50	10	Nike Lunar Glide	N	4:08	F	
MP	21	64.6	178	50	6	Asics DS Trainer 16	Y A 25 M	4:21	P	
MQ	21	66.7	179	35	5	Saucony Mirage	Y R 7 M	3:46	P	
MR	23	64.1	170	50	8	Saucony Pro Gride Guide 3	Y W 8 M	3:54	P	
MS	26	76.9	182	70	10	Nike Free 3.0	N	3:56	P	
MT	23	70.5	180	65	9	Nike Lunar Elite 2	N	4:05	P	

Table C.2.1: A selection of data from the anthropometric assessment and running history. All subjects successfully completed ten calf raises on each leg. MPW = running volume in miles per week. SPW = running session per week. Y = Yes. N = No. A = Always. R = Running only. W = Walking only. M = Months. P = Pass. F = Fail. PB = Personal best. L = Notes were recorded as comments from a physiotherapist.